Tesis Doctoral

PROCESOS DE REVALORIZACIÓN CATALIZADA DE XILOSA VÍA FURFURAL SOBRE SISTEMAS BASADOS EN MgO, ZrO_2 Y TiO_2

CATALYTIC VALORIZATION OF XYLOSE VIA FURFURAL ON MgO, ZrO_2 AND TiO_2 SYSTEMS

Almudena Parejas Barranco

Directores:

Dr. Alberto Marinas Aramendía
Dr. Jesús Hidalgo Carrillo

Universidad de Córdoba
Facultad de Ciencias
Departamento de Química Orgánica

Córdoba, 2019

TITULO: *Procesos de revalorización catalizada de xilosa vía furfural sobre sistemas basados en MgO, ZrO2 y TiO2.*

AUTOR: *Almudena Parejas Barranco*

© Edita: UCOPress. 2019
Campus de Rabanales
Ctra. Nacional IV, Km. 396 A
14071 Córdoba

https://www.uco.es/ucopress/index.php/es/
ucopress@uco.es

D. José Rafael Ruiz Arrebola, Director del Departamento de Química Orgánica de la Universidad de Córdoba.

CERTIFICA:

Que el presente Trabajo de Investigación, titulado **"PROCESOS DE REVALORIZACIÓN CATALIZADA DE XILOSA VÍA FURFURAL SOBRE SISTEMAS BASADOS EN MgO, ZrO_2 Y TiO_2"**, que constituye la Memoria presentada por Almudena Parejas Barranco para optar al título de Doctor en Química Orgánica de la Universidad de Córdoba, bajo la dirección de los profesores D. Alberto Marinas Aramendía y D. Jesús Hidalgo Carrillo.

Y para que conste, firmo el presente certificado en Córdoba, a 27 de Mayo de 2019.

Fdo. D. José Rafael Ruiz Arrebola

TÍTULO DE LA TESIS: PROCESOS DE REVALORIZACIÓN CATALIZADA DE XILOSA VÍA FURFURAL SOBRE SISTEMAS BASADOS EN MgO, ZrO_2 y TiO_2.

DOCTORANDO/A: ALMUDENA PAREJAS BARRANCO

INFORME RAZONADO DEL/DE LOS DIRECTOR/ES DE LA TESIS

(se hará mención a la evolución y desarrollo de la tesis, así como a trabajos y publicaciones derivados de la misma).

Como Directores de esta Tesis Doctoral consideramos que durante el desarrollo de la misma, la doctoranda ha adquirido las habilidades y competencias necesarias para obtener el título de Doctor y que el trabajo desarrollado constituye una aportación relevante en el campo de la revalorización de la biomasa. Estas afirmaciones se apoyan en los siguientes puntos:

1. La doctoranda ha superado con buen aprovechamiento los créditos correspondientes a la formación teórico-práctica de la parte formativa del Programa de Doctorado en Química Fina (Máster Interuniversitario en Química).

2. La doctoranda ha adquirido una sólida formación en la gran variedad de técnicas instrumentales y metodologías que han sido utilizadas durante el desarrollo de la extensa labor experimental asociada a esta Tesis.

3. Los resultados obtenidos han puesto de manifiesto la necesidad de diseñar un catalizador a medida para cada tipo de proceso de interés. Asimismo, la

doctoranda ha establecido interesantes relaciones estructura-actividad que han arrojado más luz acerca de los procesos estudiados. Así, por ejemplo, se ha relacionado la actividad en la reacción MPV del furfural a alcohol furfurílico con la presencia de pares ácido-base en el catalizador, los cuales fueron determinados mediante la reacción modelo del MBOH. También se ha demostrado la influencia que tiene el método de síntesis del catalizador, así como los diferentes parámetros experimentales, en la condensación aldólica entre el furfural y la acetona utilizando óxidos laminares mixtos de Mg-Al. Además, las investigaciones llevadas a cabo, han mostrado la importancia del circonio superficial en el proceso de deshidratación de xilosa llevado a cabo mediante óxidos mixtos de Zr-Mg.

4. Como resultado de la labor desarrollada directamente relacionada con la presente Tesis, se han presentado 10 comunicaciones a congresos nacionales y 2 a internacionales y publicado tres artículos científicos en revistas indexadas de prestigio.

I. Parejas, A.; Cosano, D.; Hidalgo-Carrillo, J.; Ruiz, J.R.; Marinas, A.; Jiménez-Sanchidrián, C.; Urbano, F.J. *Aldol Condensation of Furfural with Acetone Over Mg/Al Mixed Oxides. Influence of Water and Synthesis Method*. **Catalysts** 2019, 9, 203.

II. Hidalgo-Carrillo, J.; Parejas, A.; Cuesta-Rioboo, M.J.; Marinas, A.; Urbano, F.J. *MPV Reduction of Furfural to Furfuryl Alcohol on Mg, Zr, Ti, Zr–Ti, and Mg–Ti Solids: Influence of Acid–Base Properties*. **Catalysts** 2018, 8, 539.

III. Parejas, A.; Montes, V.; Hidalgo-Carrillo, J.; Sánchez-López, E.; Marinas, A.; Urbano, F.J. *Microemulsion and Sol-Gel Synthesized ZrO2-MgO Catalysts for the Liquid-Phase Dehydration of Xylose to Furfural*. **Molecules** 2017, 22, 2257.

5. La doctoranda ha realizado una estancia de 3 meses en la University of Chemistry and Technology (Praga) bajo la supervisión del Dr. David Kubička. Fruto de dicha estancia, se ha familiarizado con la síntesis de catalizadores mesoporosos multifuncionales, así como con su caracterización mediante diferentes técnicas. Dicho grupo de investigación posee amplia experiencia en este campo, así como en procesos catalizados, más concretamente en la condensación aldólica utilizando catalizadores básicos. De esta manera, la estancia le ha permitido obtener y ampliar el conocimiento necesario para la realización de los trabajos de investigación aquí recogidos. Por otra parte, esto le ha permitido presentar la presente Memoria como Doctorado Internacional.

Por todo ello, se autoriza la presentación de la tesis doctoral.

Córdoba, 27 de Mayo de 2019

Firma del/de los director/es

Fdo.: Alberto Marinas Aramendía

Fdo.: Jesús Hidalgo Carrillo

Las investigaciones realizadas en la presente Memoria de Tesis Doctoral forman parte de un Plan de Investigación desarrollado por el grupo de investigación FQM-162. Este Plan de Investigación ha sido subvencionado con cargo al Proyecto de Investigación ENE2016-81013-R concedido por el Ministerio de Economía y Competitividad y Proyecto de Investigación F.ARECES CONV. 2014 concedido por la Fundación Ramón Areces.

Por otra parte, el Instituto de Estudios de Postgrado de la Universidad de Córdoba (IDEP) proporcionó una ayuda para la realización de una estancia de tres meses en el "Technopark Kralupy VŠCHT Praha" de la Universidad de Química y Tecnología de Praga (República Checa).

Mediante la defensa de esta Memoria de Tesis Doctoral se pretende optar a la Mención de Doctorado Internacional, habida cuenta de que el doctorando reúne los requisitos para tal mención, según el artículo 35 de la Normativa Reguladora de los Estudios de Doctorado de la Universidad de Córdoba:

1. El doctorando ha realizado una estancia de tres meses de duración en el "Technopark Kralupy VŠCHT Praha" de la Universidad de Química y Tecnología de Praga (República Checa).

2. Parte de la Memoria de la Tesis Doctoral se ha redactado en una lengua distinta de las lenguas oficiales de España.

3. Cuenta con los informes favorables de dos doctores expertos con experiencia acreditada, pertenecientes a una institución no española de Educación Superior:

   Dr. Ali Khalilov (Baku State University, Azerbaijan)
   Dr. Antonio Rafael Montoro Bustos (National Institute of Standards and Technology, Maryland, USA)

4. Un miembro del tribunal que ha de evaluar la Tesis es un doctor experto con experiencia acreditada, perteneciente a una institución no española de Educación Superior, y es distinto del responsable de la estancia mencionada en el primer apartado:

   Dr. Ángel Caravaca Huertas (University of Lyon I, Lyon, France)

5. La presentación de parte de la Tesis Doctoral se realizará en una lengua distinta de las lenguas oficiales de España.

ÍNDICE GENERAL

Resumen/Summary

Resumen de la Tesis Doctoral "Procesos de revalorización catalizada de xilosa vía furfural sobre sistemas basados en MgO, ZrO_2 y TiO_2"

1. Introducción o motivación de la Tesis Doctoral

Los problemas relacionados con la necesidad de producir combustibles y productos químicos, el crecimiento de la industria, el aumento de las emisiones de los gases de efecto invernadero, la disminución de las reservas de los combustibles fósiles, etc. han provocado la necesidad de cambiar de una economía basada en energías no renovables y contaminantes a otra más fundamentada en energías renovables.

Una solución es el empleo de la biomasa como fuente de obtención de energía al ser abundante, neutra en emisiones de carbono y todavía poco aprovechada [1]. En concreto, la producción mundial estimada de biomasa es de unas 10^{11} toneladas/año, siendo un 60% terrestre y un 40% acuática. De ella, sólo el 3% es empleado para el consumo humano (como alimento y otras aplicaciones), por lo que resulta útil su aplicación [2].

Dentro de la biomasa, se encuentra la biomasa lignocelulósica, constituyente de la pared celular de las plantas, a partir de la cual se pueden obtener diversas moléculas plataforma. Estas moléculas poseen múltiples grupos funcionales, por lo que a partir de ellas mediante reacciones químicas se puede obtener una amplia variedad de moléculas [3,4].

En el marco de un proyecto financiado por la Fundación Ramón Areces, nos centramos en una molécula plataforma (el furfural) incluida en la lista creada por J.J. Bozell y G.R. Petersen, conocida como "*10 principales*

productos químicos a partir de la bio-refinería de carbohidratos" [3,5]. Se trata de una molécula muy versátil, pudiendo ser empleada en reacciones típicas de aldehídos, como adiciones nucleófilas, reacciones de condensación, oxidaciones o reducciones; y reacciones típicas de un anillo furánico, como la sustitución electrófila aromática [6].

Actualmente, la revalorización de la biomasa en productos de interés, mediante catálisis heterogénea, es un importante campo de investigación dentro de la llamada química sostenible.

El objetivo de la presente memoria de Tesis Doctoral es la síntesis de nuevos catalizadores heterogéneos con la finalidad de ser empleados en procesos de revalorización de la biomasa a través del furfural, obteniéndose productos y compuestos químicos de interés.

2. Contenido de la investigación

En esta memoria de Tesis Doctoral se han sintetizado y caracterizado nuevos catalizadores heterogéneos para ser utilizados en diferentes procesos como: i) la transformación de D-xilosa en furfural, mediante la reacción de deshidratación y ii) la síntesis de productos de interés a partir del furfural, como la 1,5-bis-(2-furanil)-1,4-pentadien-3-ona y el alcohol furfurílico, mediante la reacción de condensación aldólica con acetona y la reacción de reducción Meerwein-Ponndorf-Verley con propan-2-ol, respectivamente.

- En el trabajo **"Microemulsion and sol-gel synthesized ZrO_2-MgO catalysts for the liquid-phase dehydration of xylose to furfural"** se han sintetizado y caracterizado catalizadores de óxido de zirconio, óxido de magnesio y sistemas mixtos de zirconio y magnesio, utilizando el método de sol-gel y de microemulsión, siendo la temperatura de calcinación de 200 ºC.

Los sólidos fueron probados en la reacción de deshidratación de la xilosa para la obtención de furfural, estudiando diferentes variables de reacción como el tipo de disolvente orgánico (butan-2-ol o tolueno) en sistemas bifásicos (agua/medio orgánico) o el dispositivo experimental empleado (a presión atmosférica o en autoclave).

- En el trabajo **"Aldol condensation of furfural with acetone over Mg/Al mixed oxides. Influence of water and synthesis method"** se ha partido de hidróxidos dobles laminares sintetizados mediante el método de co-precipitación, los cuales tras un proceso de calcinación a 450 ºC se han convertido en óxidos mixtos de Mg/Al. Estos sólidos se han sometido a diferentes condiciones durante su síntesis tanto en lo que se refiere al modo de calentamiento (convencional o microondas) como a la presencia o ausencia de un surfactante (Pluronic 123). Además, se ha llevado a cabo un estudio de la actividad catalítica de los sólidos en la reacción de condensación aldólica del furfural con la acetona para la obtención de 1,5-bis-(2-furanil)-1,4-pentadien-3-ona, abordando la influencia de la temperatura de reacción y el efecto del agua (bien prehidratando los sólidos antes de su empleo como catalizadores o añadiendo agua al medio de reacción en mezclas agua/tolueno).

- En el trabajo **"MPV reduction of furfural to furfuryl alcohol on Mg, Zr, Ti, Zr-Ti, and Mg-Ti solids: influence of acid-base properties"** se han sintetizado catalizadores de ZrO_x, TiO_x, MgO_x, sistemas mixtos de Mg-Ti y sistemas mixtos de Zr-Ti y se han probado en la reducción de Meerwein-Ponndorf-Verley (MPV), para poder conocer cuál es la naturaleza de los centros activos responsables de la actividad catalítica conseguida. En la reacción MPV, el furfural fue reducido a alcohol furfurílico con la ayuda de propan-2-ol que actuó como fuente de hidrógeno. También, se ha estudiado la influencia que

tiene en el proceso el sistema de calefacción empleado (convencional o por microondas).

3. Conclusiones

- En el trabajo **"Microemulsion and sol-gel synthesized ZrO_2-MgO catalysts for the liquid-phase dehydration of xylose to furfural"**, se prepararon dos series de catalizadores mediante el método sol-gel y un procedimiento sintético de microemulsión (SG y ME, respectivamente). Cada serie incluye sólidos puros de Mg y Zr, así como óxidos mixtos de Mg-Zr con un contenido atómico nominal de Zr del 25%, 50% y 75%. El sólido MgZr-SG presentó la mayor acidez superficial, mientras que el Mg3Zr-SG mostró la mayor basicidad superficial entre los sistemas mixtos. En cuanto a la deshidratación de la xilosa, el uso de tolueno como disolvente orgánico en la mezcla de reacción bifásica (agua/tolueno) conduce a un mejor rendimiento del furfural que el uso de butan-1-ol, lo que puede deberse a la mayor capacidad de extracción del furfural por parte del tolueno, evitando así la formación de huminas que tienen lugar principalmente en la fase acuosa.

El rendimiento a furfural aumenta con el contenido de Zr del catalizador y, por lo tanto, los catalizadores constituidos por ZrO_2 puro son los más adecuados para llevar a cabo el proceso (conversión del 98%, rendimiento del 40%, tras 24 horas), aunque los sólidos mixtos de MgZr también podrían ser adecuados para procesos generales con etapas de reacción adicionales que precisen tanto de centros ácidos como de básicos.

- En el trabajo **"Aldol condensation of furfural with acetone over Mg/Al mixed oxides. Influence of water and synthesis method"** se han sintetizado cuatro óxidos mixtos de Mg/Al mediante el método de co-precipitación con modificaciones durante la síntesis como el empleo del

calentamiento convencional o microondas y la presencia o ausencia de Pluronic 123. Se observó, a partir de los difractogramas de rayos X, que todos los sólidos calcinados presentaban las reflexiones típicas de la periclasa $MgAlO_x$. Las isotermas de los sólidos fueron tipo IV y aquellos que sufrieron alguna modificación en la síntesis (microondas y/o surfactante) mostraron un aumento en el área BET. Además, al utilizar el calentamiento por microondas y/o Pluronic 123, los sólidos presentaron una disminución en la basicidad total y un aumento en la acidez total.

Cuando los sólidos fueron probados en la reacción de condensación aldólica del furfural con acetona durante 3h, el valor más alto de conversión obtenido (35,0%), fue cuando se utilizó el sólido HTCON-450 (calentamiento convencional, sin surfactante). Mientras que cuando el tiempo aumenta, hasta las 16h, los sólidos que fueron sintetizados con Pluronic 123 consiguieron valores de rendimiento a 1,5-bis-(2-furanil)-1,4-pentadien-3-ona más altos, sobresaliendo el sólido HTMWP-450 (sintetizado en microondas) con un valor de rendimiento del 44,5%. Así, se puede concluir que la presencia de ambas modificaciones en la síntesis de los sólidos, calentamiento por microondas y Pluronic 123, favorecen la transformación del furfural al producto de interés, lo que podría ser debido al aumento del tamaño de poro y el aumento de la acidez total producido en los sólidos. Respecto a la influencia del agua, se ha observado cómo los sólidos que sufrieron una rehidratación previa a la reacción presentaron una peor actividad, probablemente debido a la solvatación de los centros activos. Mientras que, por el contrario, el aumento del porcentaje de agua añadido al medio de reacción (agua/tolueno) consiguió un aumento en la conversión de furfural, pero una disminución de la selectividad a 1,5-bis-(2-furanil)-1,4-pentadien-3-ona. Una posible explicación es que el agua debilita el enlace C=O del furfural favoreciendo su transformación, pero al mismo tiempo el primer producto de condensación del furfural con una molécula de acetona

(FAc, 4-(2-furanil)-3-buten-2-ona) es retirado de la fase orgánica una vez formado, dada su mayor solubilidad en agua, por lo que no puede reaccionar con otra molécula de furfural y originar el producto deseado (F_2Ac).

- En el trabajo **"MPV reduction of furfural to furfuryl alcohol on Mg, Zr, Ti, Zr-Ti, and Mg-Ti solids: influence of acid-base properties"** se sintetizaron catalizadores a base de MgO_x, ZrO_x y TiO_x puros, así como los sistemas mixtos Mg-Ti y Zr-Ti mediante el método sol-gel. Los sólidos fueron caracterizados, obteniéndose valores de superficies específicas (S_{BET}) de 219-263 m^2/g en aquellos que contienen Zr y/o Ti, mientras que para los sólidos compuestos por Mg fueron de 42-81 m^2/g. Comparando los perfiles termogravimétricos obtenidos, se pudo observar cómo la presencia de titanio retarda la cristalización del ZrO_2, pero favorece la transformación de $Mg(OH)_2$ a MgO. Los sólidos fueron probados en la reacción de reducción de MPV del furfural a alcohol furfurílico bajo calentamiento convencional y por microondas. Cuando se emplea el primer tipo de calentamiento, analizando los sólidos puros, el ZrO_x demostró ser el más activo, con un 90,4 % de selectividad a alcohol furfurílico (a 50.1% conversión, t=20h), seguido del TiO_x, con un 68,7% (16.2% conv.), y el MgO_x con un 56% (15.2% conv). Por otro lado, en los sólidos mixtos, la selectividad obtenida a alcohol furfurílico disminuye con el contenido en titanio. Cuando se emplea el calentamiento por microondas, las actividades catalíticas aumentaron (conversiones del orden de 4 veces mayores respecto al calentamiento convencional), manteniendo las selectividades en valores similares o superiores, como el caso del catalizador ZrO_x, con el que se obtuvo un 96,8% de selectividad a alcohol furfurílico, a 27,6% de conversión (t=2h).

La reacción test del metilbutinol (MBOH) evidenció la presencia de pares de centros ácido-base en el ZrO_x, y los estudios DRIFT con piridina mostraron que los centros ácidos del ZrO_x eran principalmente de Lewis

mientras que los sitios de Brönsted y Lewis estaban presentes en los sólidos mixtos de TiO_x y Zr-Ti. El catalizador más activo y selectivo en la reducción de MPV de furfural a alcohol furfurílico fue el ZrO_x, mientras que ambos parámetros disminuyeron en los sólidos de Zr-Ti a medida que aumentaba el contenido de titanio. Estos resultados sugieren que pares ácido-base son particularmente activos en la reducción de MPV y que los sitios de ácidos de Lewis son más activos que los de Brönsted.

4. Referencias

1. Stocker, M. Biofuels and biomass-to-liquid fuels in the biorefinery: catalytic conversion of lignocellulosic biomass using porous materials. *Angewandte Chemie International Edition* **2008**, *47*, 9200-9211, doi:10.1002/anie.200801476.
2. Sheldon, R.A. Green and sustainable manufacture of chemicals from biomass: state of the art. *Green Chemistry* **2014**, *16*, 950-963, doi:10.1039/c3gc41935e.
3. Bozell, J.J.; Petersen, G.R. Technology development for the production of biobased products from biorefinery carbohydrates-the US Department of Energy's "Top 10" revisited. *Green Chemistry* **2010**, *12*, 539-554, doi:10.1039/b922014c.
4. Werpy, T.; Petersen, G. Editores. *Top value added chemicals from biomass. Volume 1-Results of screening for potential candidates from sugars and synthesis gas*. 2004. Disponible en: https://www.nrel.gov/docs/fy04osti/35523.pdf (accesible a 21/04/2019).
5. Serrano-Ruiz, J.C.; Luque, R.; Sepulveda-Escribano, A. Transformations of biomass-derived platform molecules: from high added-value chemicals to fuels via aqueous-phase processing. *Chemical Society Reviews* **2011**, *40*, 5266-5281, doi:10.1039/c1cs15131b.
6. Hidalgo-Carrillo, J.; Marinas, A.; Urbano, F.J. Chemistry of Furfural and Furanic Derivates. En *Furfural: an entry point of lignocellulose in biorefineries to produce renewable chemicals, polymers, and biofuels*, López-Granados, M., Martín-Alonso, D., Eds. World Scientific, 2018.

Summary of the Doctoral Thesis "Catalytic valorization of xylose via furfural on MgO, ZrO_2 and TiO_2 systems"

1. Introduction or motivation of the Doctoral Thesis

Problems related with the need to produce chemicals and fuels, industrial growth, the increase in the emissions of greenhouse gases, the reduction of fossil fuel reserves, etc. have resulted in the necessity to change from one economy based on non-renewable energies to other more based on renewables.

One solution is the use of biomass to produce energy, since it is neutral as regards carbon emissions and still underused [1]. In fact, the estimated global production of biomass is ca. 10^{11} tonnes per annum (60% terrestrial and 40% aquatic). Only 3% is used in food and non-food applications, its more extensive utilization thus being particularly interesting [2].

Whithin biomass, *Lignocellulose* is the primary building block of plant cell wall and can be converted into several platform molecules. These molecules possess multiple functional groups and can be transformed into a wide variety of molecules by different chemical reactions [3,4].

In the framework of a project funded by "Fundación Ramón Areces", we focused on a platform molecule (furfural), which is included in the list of "Top 10 Chemicals from biorefinery carbohydrates" created by J.J. Bozell and G.R. Petersen [3,5]. Furfural is a versatile molecule which can undergo typical aldehyde reactions, such as nucleophilic additions, condensation reactions, oxidations or reductions; as well as others associated to the furan ring such as electrophilic aromatic substitution [6].

Currently, biomass valorization to desired products through heterogeneous catalysts is an important research line in the context of sustainable chemistry.

The final goal of the present Doctoral Thesis is the synthesis of some new heterogeneous catalysts to use them in several valorization processes of biomass through furfural, thus yielding chemicals of interest.

2. Content of the research

Some new heterogeneous catalysts were synthesized and characterized in this Doctoral Thesis to be used in different process such as: i) transformation of D-xilose to furfural by dehydration and ii) conversion of furfural into 1,5-bis-(2-furnyl)-1,4-pentadien-3-one and furfuryl alcohol, by aldol condensation with acetone and Meerwein-Ponndorf-Verley reduction with propan-2-ol, respectively.

- In the paper entitled **"Microemulsion and sol-gel synthesized ZrO_2-MgO catalysts for the liquid-phase dehydration of xylose to furfural"**, pure ZrO_2, MgO and several MgO-ZrO_2 mixed catalysts were synthesized through sol-gel and microemulsion methods, the calcination temperature being set at 200 ºC. The solids were tested for dehydration of xylose to furfural studying different variables such as the organic solvent (butan-2-ol or toluene) in biphasic systems (water/organic mixture) or different reaction systems (atmospheric-pressure multi-reactor or high-pressure autoclave).

- In the paper entitled **"Aldol condensation of furfural with acetone over Mg/Al mixed oxides. Influence of water and synthesis method"**, different Mg/Al mixed oxides were obtained through calcination at 450ºC of layered double hydroxides. These solids were synthesized modifying two variables: conventional or microwave heating in the presence or absence of a

surfactant (Pluronic 123). Furthermore, they were tested for aldol condensation of furfural to 1,5-bis-(2-furanyl)-1,4-pentadien-3-one, studying the influence of temperature and the effect of water (either pre-hydrating the solids before catalytic studies or in water/toluene mixtures as the reaction medium) over catalytic results.

- In the paper entitled **"MPV reduction of furfural to furfuryl alcohol on Mg, Zr, Ti, Zr-Ti, and Mg-Ti solids: influence of acid-base properties"** pure ZrO_x, TiO_x and MgO_x, as well as several Mg-Ti and Zr-Ti mixed systems were synthesized and tested in the Meerwein-Ponndorf-Verley (MPV) reduction, to try to cast further light on the nature of the active sites responsible for the catalytic activity. In the MPV reaction, the transformation of furfural to furfuryl alcohol was carried out through the hydrogen transfer from propan-2-ol, as a donor. The influence of conventional or microwave irradiation heating on catalytic results was also studied.

3. Conclusions

- In the paper entitled **"Microemulsion and sol-gel synthesized ZrO_2-MgO catalysts for the liquid-phase dehydration of xylose to furfural",** two series of catalysts were prepared by sol-gel and microemulsion synthetic procedures (SG and ME series, respectively). Each series includes both pure Mg and Zr solids as well as Mg-Zr mixed solids with 25%, 50% and 75% atomic nominal Zr content. The MgZr-SG solid presented the highest surface acidity while the Mg3Zr-SG exhibited the highest surface basicity among mixed systems. As for xylose dehydration, the use of toluene as organic solvent in the biphasic reaction mixture (toluene/water) led to higher furfural yields than the use of butan-1-ol which could be associated with the ability of toluene

to extract the furfural formed, thus avoiding the formation of humins that takes place mainly in the aqueous phase.

The yield to furfural increases with the Zr content of the catalysts and, therefore, the catalysts constituted by pure ZrO_2 are the most suitable to carry out the process (98% conversion, 40% yield, 24h), although MgZr mixed solids could also be suitable for overall processes with additional reaction steps requiring both acid and basic sites.

- In the paper entitled **"Aldol condensation of furfural with acetone over Mg/Al mixed oxides. Influence of water and synthesis method"**, four Mg/Al mixed oxides were synthesized by co-precipitation synthetic procedure with two synthetic variables: conventional or microwave heating with the presence or in the absence of Pluronic 123. All XRD diffractograms of the calcined solids exhibited the typical reflections ascribed to periclase $MgAlO_x$. Moreover, isotherms were type IV and the solids with modification of conventional synthesis (use of microwaves and/or surfactant) led to an increase in BET area. Furthermore, microwave irradiation and/or the use of Pluronic 123 resulted in a decrease in total basicity and an increase in total acidity.

When the solids were tested for aldol condensation with acetone for 3h, the highest conversion value (35.0%) was achieved for HTCON-450 (Conventional heating, no surfactant). For longer reaction times (16h), the yield obtained to 1,5-bis-(2-furanyl)-1,4-pentadien-3-one on the systems synthesized using Pluronic 123 is higher, the best results (44.5% yield) being obtained for HTMWP-450 (synthesized using microwaves). Therefore, it can be concluded that the combined use of Pluronic 123 and microwaves in the reaction medium during the synthesis improves the transformation of furfural to desired product of condensation. The increase in pore size and total acidity could account for that. As for the influence of water, re-hydration of the solid prior to catalytic

test was detrimental to activity, probably as a result of the solvation of active sites. On the contrary, the increase in water percentage in the reaction medium (water/toluene) resulted in higher furfural conversions, though selectivity to 1,5-bis-(2-furanyl)-1,4-pentadien-3-one decreased. A plausible explanation is that water weakens the C=O bond in furfural, this favoring its transformation. However, at the same time the first condensation product with one molecule of acetone (FAc, 4-(2-furanyl)-3-buten-2-one) is retired from the aqueous phase once formed, due to its higher solubility in water, thus avoiding its subsequent reaction with another furfural molecule to obtain the desired product (F_2Ac).

- In the paper entitled **"MPV reduction of furfural to furfuryl alcohol on Mg, Zr, Ti, Zr-Ti, and Mg-Ti solids: influence of acid-base properties"** several catalysts consisting of pure MgO_x, ZrO_x and TiO_x, as well as Mg-Ti and Zr-Ti mixed systems, were synthesized by the sol-gel method. BET surface values are in the 219-263 m^2/g range for the solids consisting of Zr and/or Ti, whereas for the solids containing Mg are in the 42-81 m^2/g range. Thermogravimetric profiles evidenced that the presence of titanium retards ZrO_2 crystallization but favors the transformation of $Mg(OH)_2$ to MgO. The solids were tested in the MPV reduction of furfural to furfuryl alcohol under conventional and microwave heating. When the solids were tested under conventional heating, ZrO_x was the most active, (selectivity to furfuryl alcohol of 90.4% at 50.1% conversion, t=20h), followed by TiO_x (68.7% selectivity, 16.2% conversion) and MgO_x (56.0% selectivity, 15.2% conversion). The selectivity to furfuryl alcohol dropped upon the introduction of titanium in the mixed systems. When the microwave heating was tested, catalytic activities increased (conversions 4 times higher than the conventional heating), while the selectivity values were similar or higher; for instance, conversion of 27.6% and selectivity to furfuryl alcohol of 96.8% was achieved on ZrO_x.

The methylbutynol (MBOH) test reaction evidenced the presence of acid-base pair sites in ZrO_x, and pyridine DRIFT studies showed that acid sites in ZrO_x were mainly of the Lewis type whereas both Brönsted and Lewis sites were present in TiO_x and Zr-Ti mixed solids. The most active and selective catalysts in the MPV reduction of furfural to furfuryl alcohol was ZrO_x whereas both parameters decreased in Zr-Ti solids as the titanium content increased. These results suggest that acid-base pair sites are particularly active in MPV reduction and that Lewis acid sites are more active than Brönsted ones.

4. References

1. Stocker, M. Biofuels and biomass-to-liquid fuels in the biorefinery: catalytic conversion of lignocellulosic biomass using porous materials. *Angewandte Chemie-International Edition* **2008**, *47*, 9200-9211, doi:10.1002/anie.200801476.
2. Sheldon, R.A. Green and sustainable manufacture of chemicals from biomass: state of the art. *Green Chemistry* **2014**, *16*, 950-963, doi:10.1039/c3gc41935e.
3. Bozell, J.J.; Petersen, G.R. Technology development for the production of biobased products from biorefinery carbohydrates-the US Department of Energy's "Top 10" revisited. *Green Chemistry* **2010**, *12*, 539-554, doi:10.1039/b922014c.
4. Werpy, T.; Petersen, G. Editores. *Top value added chemicals from biomass. Volume 1-Results of screening for potential candidates from sugars and synthesis gas*. 2004. Available at: https://www.nrel.gov/docs/fy04osti/35523.pdf (accessed April 21st, 2019).
5. Serrano-Ruiz, J.C.; Luque, R.; Sepulveda-Escribano, A. Transformations of biomass-derived platform molecules: from high added-value chemicals to fuels via aqueous-phase processing. *Chemical Society Reviews* **2011**, *40*, 5266-5281, doi:10.1039/c1cs15131b.
6. Hidalgo-Carrillo, J.; Marinas, A.; Urbano, F.J. Chemistry of Furfural and Furanic Derivates. In *Furfural: an entry point of lignocellulose in biorefineries to produce renewable chemicals, polymers, and biofuels*, López-Granados, M., Martín-Alonso, D., Eds. World Scientific, 2018.

Capítulo I.

Introducción

CAPÍTULO I. INTRODUCCIÓN

I.1. Preámbulo – Antecedentes de la Investigación

Una necesidad que presenta la sociedad hoy en día, es encontrar alternativas para el desarrollo de procesos económicos y energéticamente eficientes para la producción sostenible de combustibles y productos químicos. En este sentido, resulta imprescindible encontrar alternativas a las energías no renovables debido al crecimiento de la industria, la disminución de las reservas de combustibles fósiles, el efecto del calentamiento global, etc.

Entre las alternativas renovables a los llamados combustibles fósiles, se encuentran la energía solar, eólica, geotérmica, biomasa, etc. De estas formas de energía destaca la biomasa por ser la única fuente de producción de productos químicos y biocombustibles abundante y neutra en emisiones de carbono (como se muestra en el ciclo de la biomasa, Figura I.1). Así, cuando es convertida a productos químicos o empleada en combustibles se genera dióxido de carbono, que es consumido posteriormente en su recrecimiento a través de la fotosíntesis de las plantas. Asimismo, se consigue una reducción en la

producción de las emisiones de gases de efecto invernadero al compararlas con el empleo de combustibles fósiles [1,2].

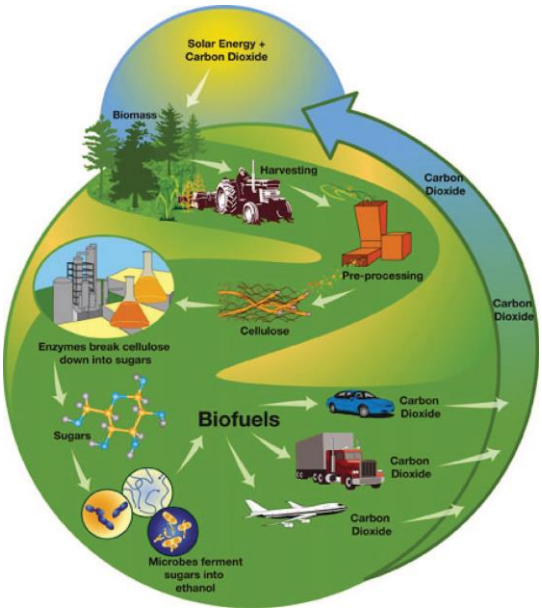

Figura I.1. Ciclo de la biomasa [2]. Adaptado de M. Stöcker.

Con el empleo de los biocombustibles es posible perseguir una sostenibilidad energética y mitigar las preocupaciones sobre la disponibilidad limitada de los combustibles fósiles. Además, muchos de los materiales empleados para su obtención se tratan de materias primas de bajo costo, no aprovechables para la alimentación humana o subproductos en la producción de otros productos capaces de ser transformados en biocombustibles con un costo final del proceso bajo [3].

En 1992, en la Cumbre de la Tierra de Río de Janeiro (Agenda 21) [4,5] se planteó el desarrollo sostenible para conseguir un cuidado del medio ambiente adecuado y a largo plazo, pudiendo avanzar hacia una sociedad sostenible. Posteriormente, en 1997 fue suscrito el Protocolo de Kioto, teniendo como objetivo reducir seis gases causantes del calentamiento global: gas metano (CH_4), dióxido de carbono (CO_2), óxido nitroso (N_2O),

hidrofluorocarbonos (HFC), perfluorocarbonos (PFC) y hexafluoruro de azufre (SF_6). Aunque no entró en vigor hasta 2005.

Por su parte, la Unión Europea aprobó una nueva directiva (Directiva 2009/28/CE) donde se estableció un conjunto común de normas para reducir las emisiones de gases de efecto invernadero y promover un transporte más limpio, pretendiéndose así, alcanzar en 2020 una cuota del 20% de energía procedente de fuentes renovables en el consumo de energía y una cuota del 10% de energía procedente de fuentes renovables en el consumo de combustibles para el transporte [6]. En 2012, tuvo lugar la Conferencia de las Naciones Unidas sobre el Desarrollo Sostenible (Río+20) con el título "El Futuro que queremos" y se centró en dos temas principalmente con la finalidad de conseguir ese desarrollo sostenible comentado anteriormente: la construcción de una economía verde, liberando a la población de la pobreza; y buscar mejorar las relaciones y cooperación internacional [7]. Recientemente, en 2015, se aprobó el Acuerdo de París que estableció un plan de acción mundial poniendo el límite del aumento de la temperatura global muy por debajo de 2 ºC con el fin de reducir las emisiones mundiales [8].

Sin embargo, la sostenibilidad no sólo se basa en lo ya comentado, sino que también se encuentra relacionada con un factor económico, como puede ser el modelo de economía circular, cuyo principal objetivo es la reducción, la reutilización y el reciclaje de los materiales, los productos y los recursos [9]. Así, se conseguiría reducir la producción de estos al mínimo necesario, luego hacer uso de ellos y posteriormente, reutilizarlos [10].

Teniendo todo esto como referente, cada vez son más los investigadores que participan en el campo de la búsqueda de alternativas, adoptando estos criterios de sostenibilidad para la producción de compuestos químicos empleando catalizadores.

Aproximadamente un 80% de los productos químicos sintetizados requieren un catalizador para su obtención. Pudiéndose decir que la catálisis es un campo imprescindible para que se den procesos químicos y se obtenga una amplia variedad de productos [11].

Dentro de la catálisis, se pueden distinguir varios tipos dependiendo de si el catalizador y el sistema reactivo se encuentran en la misma fase (catálisis homogénea), en diferentes (catálisis heterogénea) o si el aumento de la velocidad es causada por la acción de una enzima (catálisis enzimática). En esta memoria de Tesis Doctoral nos centraremos en la catálisis heterogénea.

Los catalizadores heterogéneos se emplean como una alternativa a los catalizadores homogéneos, los cuales son muy empleados a nivel industrial, pero necesitan un paso adicional para separarlos del medio de reacción, siendo más difícil su reutilización. Los catalizadores heterogéneos pueden ser diseñados para poseer las características necesarias para el correcto desarrollo de una reacción, por ejemplo resistentes a temperaturas elevadas y presiones superiores a la atmosférica; y actuando como sustitutos de ácidos o bases [12,13]. En la tabla I.1 aparecen algunas características diferenciales de ambos tipos de catálisis atendiendo a diferentes factores.

Aunque, en concreto, algunas de las ventajas que presentan los catalizadores heterogéneos son:

- Se separan fácilmente de los reactivos y/o productos.
- Se pueden reciclar con facilidad.
- Menor contaminación del producto con el catalizador.
- Son fácilmente adaptables a un proceso en flujo continuo.

Tabla I.1. Características diferenciales de las catálisis homogénea y heterogénea atendiendo a diferentes factores, adaptado de A. Brown [14].

Factores	Catálisis homogénea	Catálisis heterogénea
Selectividad	Alta	Variable
Actividad	Alta	Variable
Condiciones de reacciones	Moderadas	Alta
Tiempo de uso de catalizador	Variable	Prolongado
Mecanismo	Posiblemente bajo determinadas condiciones	Muy complejo
Impacto económico	Menor	Mayor

En esta memoria de Tesis Doctoral los catalizadores van a ser empleados en la transformación de D-xilosa en furfural y éste en productos de interés, como la 1,5-bis-(2-furanil)-1,4-pentadien-3-ona y el alcohol furfurílico.

I.2. Química Verde

La química verde se define como *el diseño de productos y procesos químicos que reducen o eliminan el uso y la generación de sustancias peligrosas* [15]. Fueron Anastas y Warner, considerados como los padres de la Química, quienes enunciaron sus 12 principios.

Estos principios son una categorización de los enfoques fundamentales para alcanzar una química verde de productos y procesos benignos para la salud humana y el medio ambiente. Así pues, se podría establecer y analizar cómo de "verde" puede ser una reacción química, un proceso o un producto [16]. Los 12 principios establecen:

1. Es preferible evitar la formación de un residuo que tratar de limpiarlo después de ser formado.
2. Los métodos de síntesis deben ser diseñados para maximizar la incorporación de todos los materiales utilizados en el proceso al producto final.

3. Cuando sea posible, las metodologías de síntesis deben de ser diseñadas para utilizar y generar sustancias que presenten poca o ninguna toxicidad para la salud humana y el medio ambiente.
4. Los productos químicos deben ser diseñados para mantener su eficacia mientras reducen su toxicidad.
5. El uso de sustancias auxiliares (por ejemplo, agentes de separación, disolventes, etc.) debe evitarse cuando sea posible y si se han de utilizar, que sean inocuas.
6. Los requerimientos energéticos deben ser reconocidos por su impacto ambiental y económico, y deben ser minimizados. Los métodos de síntesis deben ser llevados a cabo a temperatura y presión ambiente.
7. La materia prima debe ser renovable en lugar de agotable, mientras sea viable técnica y económicamente.
8. La derivatización innecesaria (grupos de bloqueo, de protección/desprotección, modificación temporal de procesos físico/químicos) debería ser evitada siempre que sea posible.
9. Los reactivos catalíticos (tan selectivos como sea posible) se utilizarán con prioridad a los reactivos estequiométricos.
10. Los productos deben diseñarse para mantener su función mientras se reduce su toxicidad.
11. Es necesario desarrollar metodologías analíticas que permitan la monitorización y el control en tiempo real del proceso antes de la formación de sustancias peligrosas.
12. Las sustancias y la forma de una sustancia utilizada en un proceso químico, debe ser elegidas para minimizar el riesgo de accidentes químicos, incluidos emisiones, explosiones e incendios [17,18].

Teniendo presente los 12 principios, se podría decir que el concepto de química verde no incluye un elemento económico, de lo que podría depender la

aplicabilidad de los procesos a escala industrial. Por ello es importante nombrar la química sostenible, la cual se basa en tres pilares fundamentalmente: la población (elementos sociales), el planeta (medio ambiente) y las ganancias (economía). Por consiguiente, reconoce la necesidad de satisfacer a la sociedad actual sin comprometer las necesidades de la sociedad futura. Así, los recursos naturales que empleamos deben usarse pero sin finalizar sus reservas y evitar su agotamiento, y los residuos generados no deben exceder las cantidades que el medio ambiente puede asimilar. Por lo que se podría decir, a modo resumen, que para que una tecnología sea sostenible a largo plazo, debe estar basada en los criterios de los tres pilares y cumplir lo más posible con los principios de la química verde [19].

I.3. Valorización de la Biomasa

I.3.1. Biorrefinería

La biorrefinería es *"una industria que, usando biomasa como materia prima y una variedad de tecnologías diferentes, produce energía y/o biocombustibles, a la par que productos químicos, materiales, alimentos y piensos"* [20].

Las biorrefinerías pueden dividirse en varios tipos dependiendo del criterio que se emplee para su clasificación, así podemos hablar de:

- El tipo de desarrollo tecnológico (biorrefinerías avanzadas vs. convencionales).
- El tipo de biomasa empleada (biorrefinerías de 1ª, 2ª, 3ª y 4ª generación).
- El proceso de conversión que predomina (biorrefinerías termoquímicas).
- La creación de varias plataformas para el desarrollo de productos (biorrefinerías con dos plataformas) [20].

Por consiguiente, centrándonos en el tipo de biomasa utilizada como materia prima se pueden diferenciar cuatro tipos de biorrefinerías:

- Primera generación: emplea biomasa de cultivos (maíz, soja, palma, etc.).
- Segunda generación: incluye una amplia variedad de materias primas derivadas de plantas o de residuos vegetales no aprovechables para la alimentación humana, desde la biomasa lignocelulósica hasta residuos sólidos urbanos.
- Tercera generación: emplea biomasa proveniente de algas y permite mejorar el proceso desde la selección de la materia prima hasta la propia producción del combustible.
- Cuarta generación: trabaja con materia prima genéticamente modificada para producir combustibles de forma eficiente [21].

En lo que se refiere a los biocombustibles obtenidos en las biorrefinerías de primera generación, algunos llevan comercializándose desde hace varias décadas, como el bioetanol y el biodiésel. No obstante, este tipo de combustibles se trata de una energía de transición, ya que presentan problemas de abastecimiento de sus materias primas de partida y no son capaces de sustituir por completo a los combustibles derivados del petróleo. Además, presentan el problema causado por la competencia de las materias primas necesarias para su producción, las cuales son necesarias en el mercado energético y en el mercado alimenticio, pudiendo tener repercusiones en la subida de sus precios.

Por ese motivo, la industria ha encontrado como una alternativa energética real, los combustibles y productos químicos obtenidos a partir de biorrefinerías de segunda generación que utilizan productos ecológicos y

sostenibles de cultivos con mayor productividad, menores costes de producción y no destinados al mercado alimenticio [22].

En consecuencia, lo más beneficioso sería conseguir una biorrefinería integrada (Figura I.2), capaz de aprovechar los productos y subproductos de la biomasa para la producción de biocombustibles, bioenergía y biomateriales, buscando una sostenibilidad a largo plazo [23].

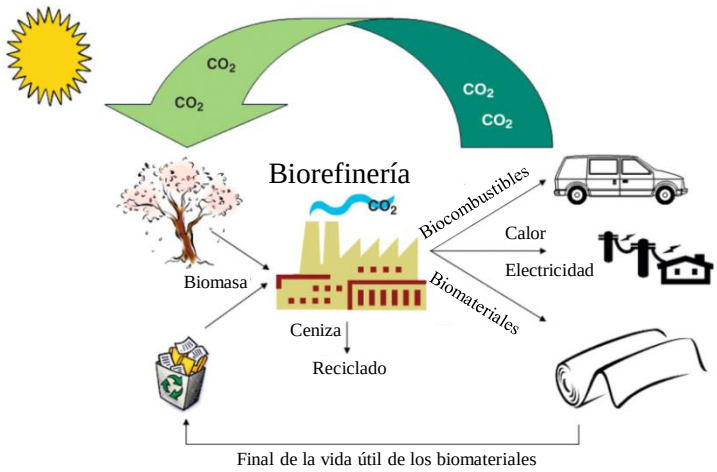

Figura I.2. El ciclo de una biorrefinería integrada para tecnologías sostenibles, adaptado de A. J. Ragauskas et al. [23].

I.3.2. Aplicación de la Biomasa

La producción mundial estimada de biomasa es de una 10^{11} toneladas/año, siendo dividida en un 60% terrestre y un 40% acuática. Sólo el 3% es empleado para el consumo humano (como alimento y otras aplicaciones), siendo útil su valorización [19,24].

La biomasa está constituida por hidratos de carbono (lignocelulosa), triglicéridos, proteínas y terpenos [19]. La biomasa lignocelulósica (Figura I.3) es muy abundante, se localiza en la pared celular de las plantas y está compuesta por: celulosa (40-50%), hemicelulosa (25-35%), lignina (15-20%),

pectina (2-20%) y otros (10%). Los porcentajes varían según la especie de planta en estudio [23,25]. A continuación se explicarán con mayor detalle los tres componentes principales.

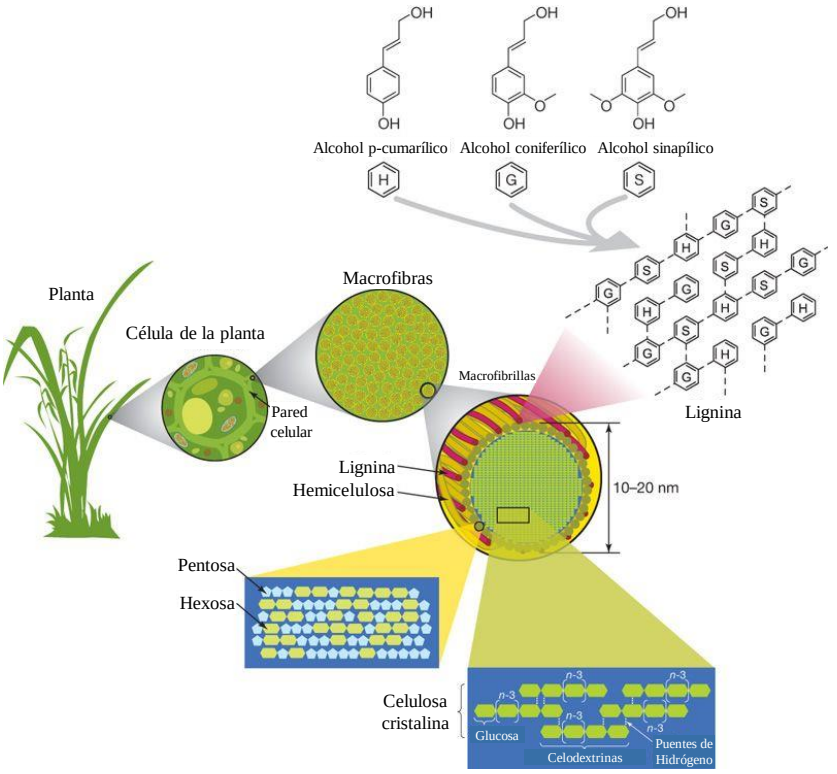

Figura I.3. Estructura de la biomasa lignocelulósica con sus tres componentes principales, adaptado de E. M. Rubin [26].

La **celulosa** se trata del principal material de la pared celular, es un polímero formado por la unión de moléculas de β-D-glucosa mediante enlaces β-1,4-O-glucosídicos. Posee una estructura lineal, conocida como microfibrillas, unidas entre sí por puentes de hidrógeno y fuerzas de Van der Waals, formando una estructura resistente a la hidrólisis y susceptible a la degradación enzimática [27-29].

La **hemicelulosa** se trata de un polímero con una estructura ramificada constituida por la unión de diferentes azúcares como pentosas (D-xilosa, L-

arabinosa), hexosas (D-glucosa, D-manosa y D-galactosa) y ácidos de estos azúcares mediante enlaces β-1,4 y β-1,3. Su componente principal es el xilano, el polisacárido hemicelulósico más abundante en la pared celular de las plantas (30-35% del total de peso seco), formado por una cadena principal de β-(1,4)-xilopiranosa (xilosa). La hemicelulosa se encuentra recubriendo las microfibrillas de la celulosa y permite su unión con las pectinas [28,30].

La **lignina** se trata de un polímero ramificado, amorfo, formado por unidades de fenilpropanoides, principalmente, alcohol p-cumarílico, alcohol coniferílico y alcohol sinapílico [31]. Estas unidades pueden variar, no repitiéndose de manera regular, dependiendo del origen de la lignina. Su principal función es mantener unidas entre sí, la celulosa y la hemicelulosa [19,32,33].

Para la conversión de la biomasa lignocelulósica en combustibles y productos químicos, esta tiene que dividirse en sus diferentes componentes [34], mediante unos procesos de separación. De manera general se pueden separar mediante dos vías [35-38]:

1. **Vía hidrolítica:** se producirá la extracción de los azúcares presentes en la lignocelulosa en presencia de catalizadores, como ácidos minerales (se utilizan temperaturas elevadas) o enzimas (se emplean temperaturas suaves).
2. **Vía termoquímica:** se realizan procesos de pirólisis para la obtención de "biochar" y biocrudos; y procesos de gasificación transformándose a gas de síntesis.

Ambas opciones presentan ventajas e inconvenientes, por lo que se elegirá una de las dos dependiendo del objetivo que se quiera conseguir. La vía hidrolítica permite obtener los monómeros, utilizables como moléculas

plataforma [39]; mientras que la vía termoquímica produce una mayor ruptura de las moléculas, si bien, a su favor, presenta la amplia diversidad de materias primas que se pueden utilizar [38,40].

En la Figura I.4 aparecen los productos obtenidos a partir de biomasa lignocelulósica en una biorrefinería. Se observa cómo la lignina se emplea para la producción de adhesivo natural, carbón bituminoso y combustible sólido sin azufre. La hemicelulosa tiene diferentes aplicaciones como la obtención de resina furánica, productos químicos, etc. Y la celulosa se utiliza en la generación de compuestos empleados como disolventes, lubricantes, etc. y, vía fermentación, la producción de ácidos orgánicos, bioetanol, etc. De entre los diferentes compuestos que se pueden generar a partir de lignocelulosa, cabe destacar las llamadas moléculas plataforma (ver apartado siguiente) como el xilitol, el furfural, el 5-hidroximetilfurfural y el ácido levulínico que aparecen en el esquema, por la amplia variedad de compuestos que pueden ser obtenidos a partir de ellos. Por ejemplo, el furfural se trata de un material de partida para la producción de Nylon 6 y Nylon 6,6, siendo un mercado muy grande y explotado; y a partir del ácido levulínico se pueden obtener derivados de alto valor añadido como pirrolidonas, aditivos para combustibles (levulinato de etilo) y monómeros para la síntesis de polímeros amorfos [41].

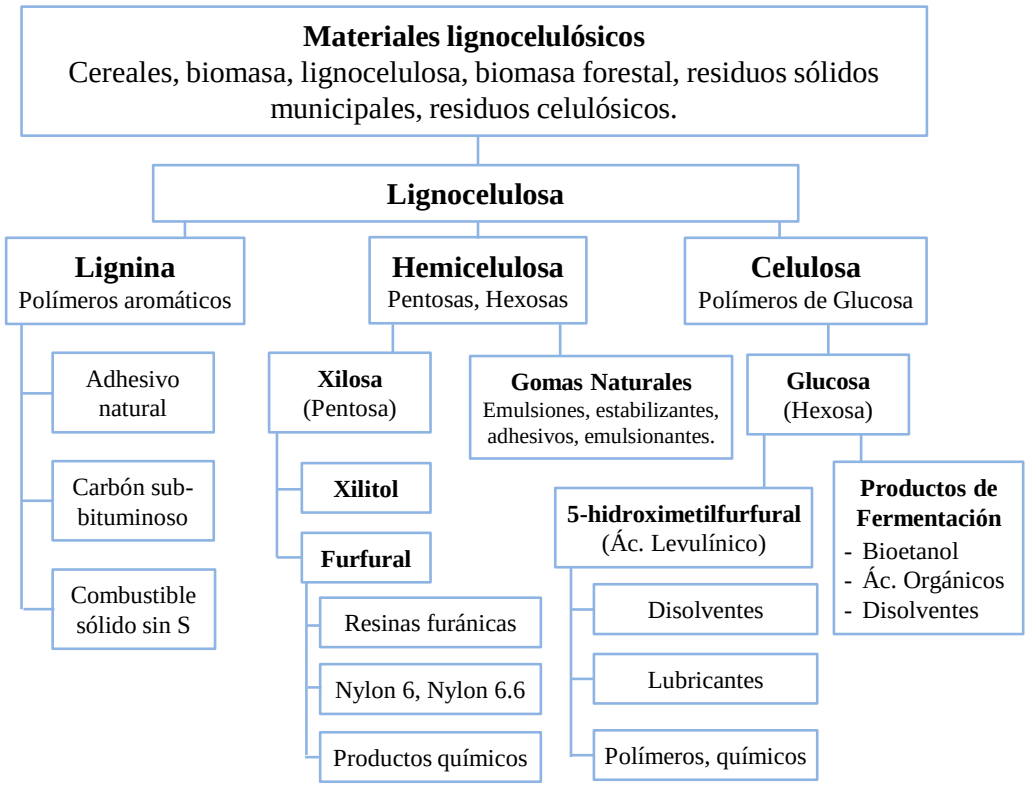

Figura I.4. Productos obtenidos de una biorrefinería empleando biomasa lignocelulósica, adaptado de B. Kamm et al. [41].

I.3.2.1. Moléculas plataforma

La definición de moléculas plataforma es "*materiales de partida o bloques de construcción capaces de producir productos químicos por medio de rutas catalíticas*" [42]. Estas moléculas poseen múltiples grupos funcionales por lo que muestran una gran aplicabilidad en la formación de materiales y productos químicos, sobresaliendo por ser capaces de obtener varios compuestos químicos a partir de una sola molécula con cierta facilidad [43,44]. Ellas se sintetizan a partir de la biomasa lignocelulósica empleando una de las vías anteriormente comentadas (vía hidrolítica o termoquímica).

Este concepto comenzó a conocerse a finales del siglo XX, bajo el nombre de moléculas plataforma de base biológica, y se pensaba que moléculas

pequeñas y simples derivadas de la biomasa se podrían emplear como bloques de construcción. Pero, no fue hasta 2004, en el Departamento de Energía de los Estados Unidos (DOE), cuando T. Werpy y G. Petersen, crean una lista de 12 compuestos (ver Tabla I.2) capaces de ser utilizados como moléculas plataforma. Entre ellos destacaron a los diácidos de cuatro carbonos (ácido málico, fumárico y ácido succínico), los cuales recibieron una gran atención por parte de Myriant, BioAmber, BASF-Purac (empresa asociada de Succinity) y DSM-Roquette (empresa asociada de Reverdia) que buscaban su producción a escala comercial. Las capacidades de producción de las plantas industriales para estos diácidos varían entre 10.000 y 100.000 toneladas por año debido a su uso en aplicaciones de polímeros [43,45,46].

Posteriormente en 2010, fueron J.J. Bozell y G.R. Petersen, quienes establecieron una nueva lista revisada de compuestos en base a su potencial actual y futuro, conocida como "*Top 10 Chemicals*" (ver Tabla I.2). Esta lista elimina algunos compuestos incluidos en la lista anterior, como el ácido 2,5-furanodicarboxílico que se obtiene a partir del 5-hidroximetilfurfural (HMF). Además, incluye nuevos, como el etanol y furanos (derivados de la biomasa lignocelulósica) [44,47].

Tabla I.2. Moléculas plataforma: 2004 vs 2010.

Moléculas plataforma (Werpy y Petersen, 2004)	**Moléculas plataforma** (Bozell y Petersen, 2010)
Diácidos de cuatro carbonos: 1. Ácido succínico 2. Ácido fumárico 3. Ácido Málico	Furanos: 1. Furfural 2. 5-hidroximetilfurfural
Ácido 2,5 furanodicarboxílico	Etanol
Ácido 3-hidroxipropanoico	Glicerol
Ácido aspártico	Ácido láctico
Ácido glucárico	Ácido succínico
Ácido glutámico	Ácido 3-hidroxipropanoico
Ácido itacónico	Ácido Levulínico
Ácido levulínico	Sorbitol
3-Hydroxibutirolactona	Xilitol
Glicerol	
Sorbitol	
Xilitol/Arabinitol	

I.3.3. Compuestos derivados de la Biomasa objeto de estudio: xilosa, furfural y derivados.

Seguidamente, pasamos a describir las diferentes moléculas objeto de estudio en la presente memoria de Tesis Doctoral. Comenzaremos con la xilosa, centrándonos luego en especial en el furfural y, posteriormente en los productos obtenidos a partir del furfural, como el alcohol furfurílico y el 1,5-bis-(2-furanil)-1,4-pentadien-3-ona.

La **xilosa** es una aldopentosa, un monosacárido que posee un grupo aldehído y cinco átomos de carbono. Puede ser obtenida a partir del xilano de la hemicelulosa de la biomasa lignocelulósica mediante una hidrólisis ácida, separándose la hemicelulosa de la celulosa. La hemicelulosa contiene aproximadamente un 30% de polisacáridos de xilosa. Es conocida como azúcar de madera, debido a su distribución en diferentes materiales, el tronco del cerezo, paja, etc. Destaca por ser barata y fácilmente accesible [48]. Sus principales derivados son el xilitol, obtenido mediante hidrogenación catalítica a alta presión y alta temperatura en contacto con un catalizador de níquel; y el furfural, obtenido mediante deshidratación (ambas moléculas plataforma) [49,50].

El **furfural** es un compuesto orgánico con un grupo funcional aldehído y un anillo aromático (perteneciente a la familia de los furanos), convirtiéndose en una molécula muy versátil, y pudiendo ser empleado en reacciones típicas de aldehídos, como adiciones nucleófilas, reacciones de condensación, oxidaciones o reducciones; y reacciones típicas de una anillo furánico como sustitución electrófila aromática [51]. En estado puro es un líquido aceitoso, incoloro con olor a almendras, pero en presencia de aire se oxida tornándose rápidamente a amarillo y luego de marrón a negro, por lo que deben de tomarse

precauciones durante su manejo [52]. Presenta una polaridad intermedia, siendo parcialmente soluble en sustancias altamente polares y no polares [53,54].

En 1832, el furfural fue aislado por primera vez por Johann Wolgang Dobereiner como subproducto de la síntesis del ácido fórmico. Aunque no fue hasta 1840 por Juan Stenhouse cuando se obtuvo el furfural al destilar productos de la cosecha, como avena, maíz, etc. determinando su fórmula empírica $C_5H_4O_2$ [55]. Actualmente, se sintetiza a partir de la deshidratación de la xilosa en un medio acuoso y ácido, con relativas altas presiones y altas temperaturas (su proceso será explicado más adelante).

Centrándonos en la estructura del furfural, en concreto en su grupo carbonilo, habría que comentar dos características principalmente:

- La geometría plana: esta característica se encuentra relacionada con la hibridación sp_2 de los átomos de carbono y oxígeno del grupo C=O, portándole a este grupo ángulos de enlace de 120 º.
- La polaridad: esta característica puede observarse en las dos formas resonantes del furfural que se muestran en la Figura I.5. El grupo carbonilo posee una estructura polar como consecuencia del desplazamiento del par de electrones π del doble enlace C=O al átomo de oxígeno. Así, el átomo de carbono tendrá densidad de carga positiva (y susceptible a ser atacado por reactivos nucleófilos), mientras que el átomo de oxígeno poseerá densidad de carga negativa [51].

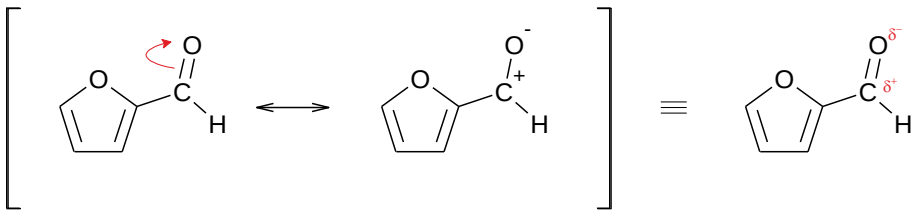

Figura I.5. Formas resonantes del grupo carbonilo del furfural, adaptado de J. Hidalgo-Carrillo et al. [51].

Los principales productores de furfural y sus derivados son China, Sudáfrica y República Dominicana. Para su síntesis emplean residuos agrícolas como materia prima, en concreto en China utilizan mazorcas de maíz y en Sudáfrica y Republica Dominicana, bagazo. La producción mundial de furfural es aproximadamente 300.000 toneladas anuales y la planta de producción más grande se encuentra en República Dominicana con una capacidad de 35.000 toneladas anuales [56].

La principal aplicación del furfural es actuar como material de partida de productos de interés y precursor natural de compuestos [50] como metiltetrahidrofurano, tetrahidrofurano, alcohol tetrahidrofurfurílico, ácido furoico, etc. mediante reacciones químicas simples. En la Figura I.6 aparecen los principales productos químicos obtenidos a partir del furfural. Los productos que aparecen recuadrados (furfural, furano, ácido furoico, alcohol furfurílico, alcohol tetrahidrofurfurílico y dihidropirano (DHP)) son comerciales. Pero hay otros productos (aparecen señalados con un círculo) que se obtienen en la industria petroquímica actualmente, pero pueden ser obtenidos a partir del furfural, permitiendo la síntesis de poliamida, Nylon 6,6, Nylon 6, Nylon 7,7, caucho, etc. y empleándose en industrias como la farmacéutica, agroquímica, plásticos, lubricantes, resinas, agentes blanqueadores, fungicidas, etc.

El **alcohol furfurílico** puede ser considerado el producto más importante, ya que aproximadamente un 65 % de la producción del furfural es empleada para su síntesis [57]. Este compuesto está formado por un anillo furánico y un grupo hidroximetilo en la posición 2 (Figura I.7). Es sintetizado mediante la hidrogenación del furfural en un medio en fase líquida o vapor, siendo el más empleado en fase líquida. Es soluble en disolventes orgánicos, como etanol, metanol, propanol, cloroformo, etc. y parcialmente en agua, ya que apenas es miscible en ella. Resulta ser un compuesto químico muy

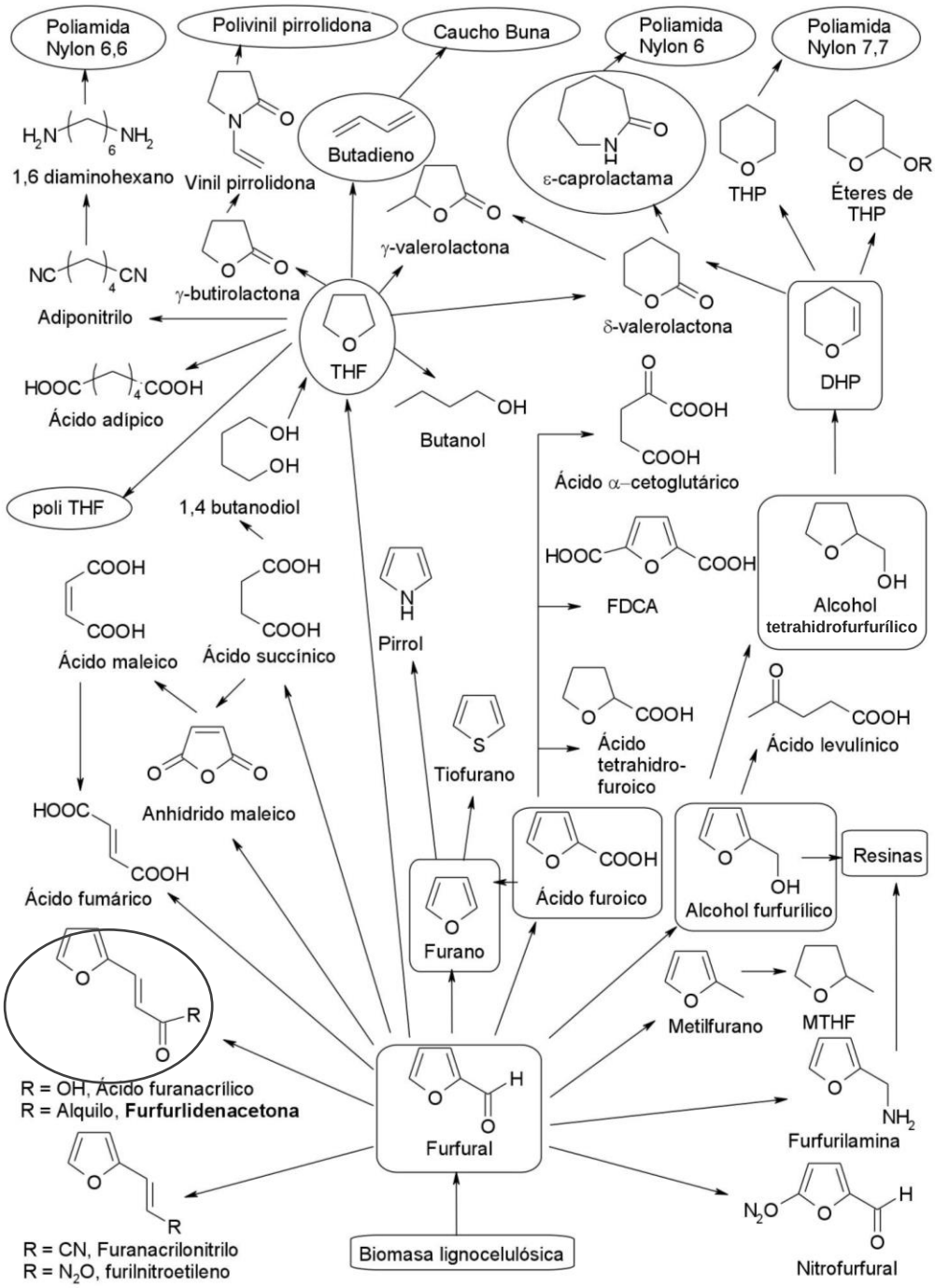

Figura I.6. Productos químicos derivados del furfural, adaptado de I. Sádaba [58].

relevante, debido a su amplia aplicabilidad en la industria química. Se puede emplear como material de partida para la síntesis de otros compuestos y como intermediario para la fabricación de fragancias, vitamina C y lisina. También puede ser utilizado para la producción de resinas y disolventes, la elaboración de fibras sintéticas, la modificación de fenoles, la síntesis de fármacos, la fabricación de espumas de poliuretano y poliésteres, decapantes de pintura, modificación de madera, etc. [59-61].

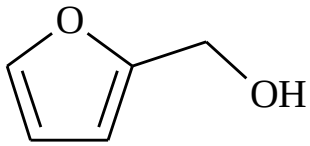

Figura I.7. Estructura del alcohol furfurílico.

En los últimos años, viene despertando interés el empleo del furfural como fuente renovable para la producción de diésel, mediante la combinación de procesos de hidrogenación /condensación aldólica/ deshidratación [62-65]. En un primer momento se obtendrá la molécula de furfurlidenacetona (4-(2-furanil)-3-buten-2-ona) al reaccionar mediante una condensación aldólica una molécula de furfural y una molécula de acetona, pero al añadirle otra molécula de furfural se obtendrá la **1,5-bis-(2-furanil)-1,4-pentadien-3-ona** (F2Ac) (ver Figura I.8). Este es un compuesto poco soluble en agua y mediante un proceso de hidrodeoxigenación se obtendrá un alcano líquido con longitud de cadena de 13 átomos de carbono que tiene las propiedades de diésel.

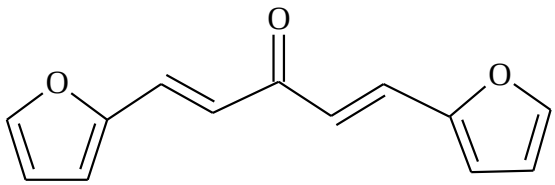

Figura I.8. Estructura de la 1,5-bis-(2-furanil)-1,4-pentadien-3-ona.

I.4.Reacciones Estudiadas

Las reacciones estudiadas en la presente memoria de Tesis Doctoral son la deshidratación de la xilosa para la obtención de furfural, la condensación aldólica del furfural con acetona para la obtención de 1,5-bis-(2-furanil)-1,4-pentadien-3-ona y la reacción de reducción de Meerwein-Ponndorf-Verley del furfural para la obtención de alcohol furfurílico.

I.4.1. Deshidratación de Xilosa a Furfural

La reacción de deshidratación de la xilosa permite la obtención de una molécula plataforma como es el furfural, a partir de los pentosanos (xilano) de la hemicelulosa procedente de la biomasa lignocelulósica. Como material de partida, se suelen utilizar compuestos con alto contenido en xilanos, mazorca de maíz (23%), copos de avena (22%), salvado de algodón (19%), residuos de caña (17%) y copos de arroz (22%) [51].

La reacción que tiene lugar es la que se muestra en la Figura I.9, donde los pentosanos (xilosanos o xilanos) extraídos de la biomasa se hidrolizan a pentosas (xilosas) y posteriormente, mediante una ciclodeshidratación inducida

por ácido, se obtienen disoluciones acuosas de furfural [53,66,67]. Por último, se destila y purifica el furfural para poder obtener una pureza superior al 98%.

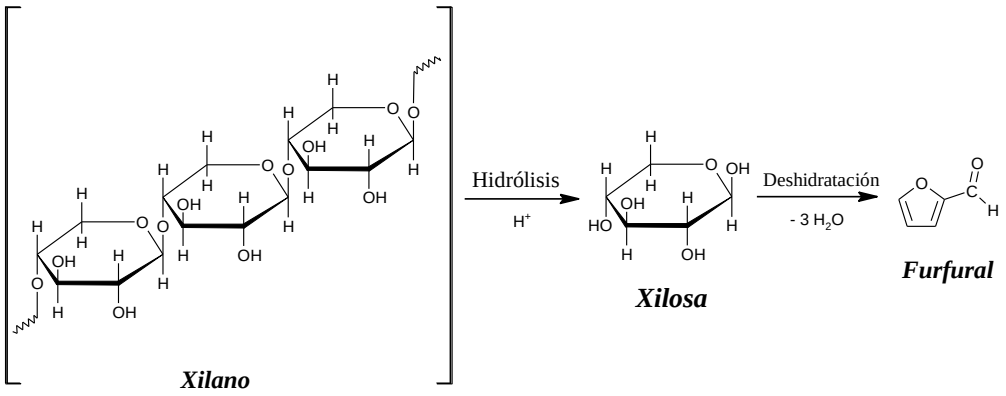

Figura I.9. Reacción de obtención del furfural a partir de biomasa lignocelulósica, adaptado de J. Hidalgo-Carrillo et al. [51].

Existen diferentes procesos industriales para la obtención de furfural, siendo el más antiguo el de QUAKER OATS en 1921 [68-70]. Se empleaba ácido sulfúrico diluido como catalizador y presión de vapor, obteniéndose un rendimiento molar de furfural del 50% a partir de xilano.

En bibliografía se pueden encontrar numerosos procesos sobre este tipo de reacción como el proceso Escher Wyss, el proceso Rosenlew, el proceso Stake, el proceso Wastpro modificado, etc. Aunque el más reciente, 2003, es el desarrollado por Arnold y Buzzard, denominado SupraYield®, consiguiendo obtener furfural con una alta pureza, evitando su degradación, estando libre de subproductos y con una mayor eficiencia energética [71].

I.4.1.1. Mecanismo de reacción de la deshidratación de xilosa

En esta memoria de Tesis Doctoral se ha partido de la D-xilosa para la obtención del furfural. Para ello, se produjo la deshidratación de la D-xilosa, dando lugar a tres moléculas de agua y el correspondiente furfural. Actualmente

existen diferentes propuestas de mecanismo de esta reacción, siendo las dos principales: mediante apertura del anillo de la xilosa propuesto por K.J. Zeitsch [52] (Figura I.10) y sin apertura de este anillo por M.J. Antal et al. [72] (Figura I.11).

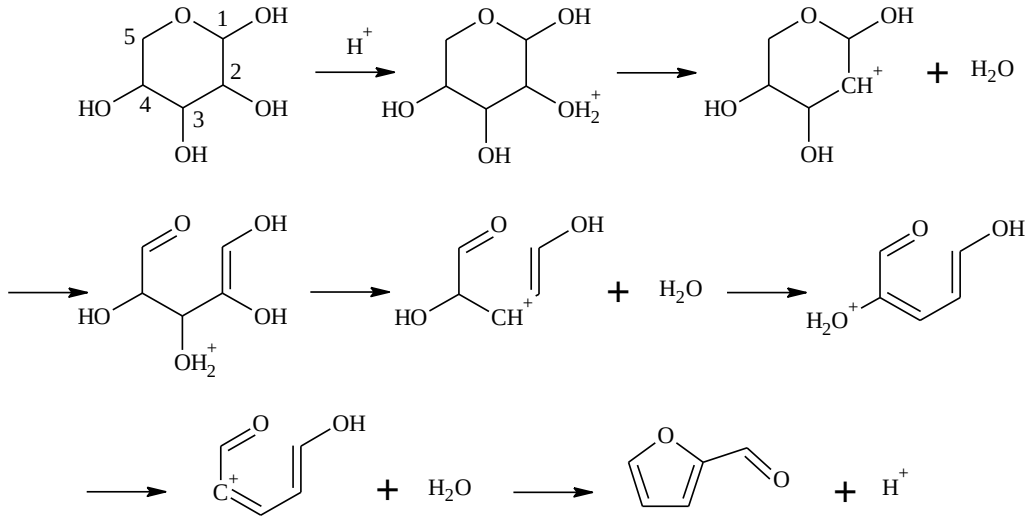

Figura I.10. Mecanismo de la xilosa a furfural propuesto por K.J. Zeitsch [52].

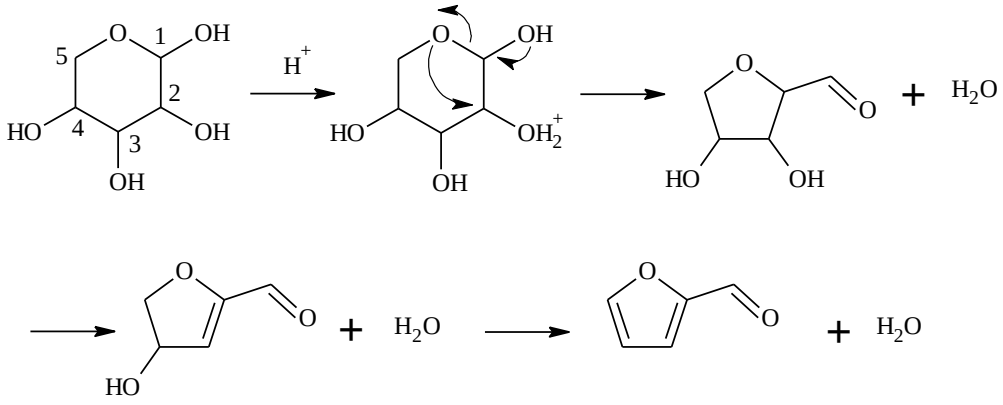

Figura I.11. Mecanismo de la xilosa a furfural propuesto por M.J. Antal et al. [72].

Ambos mecanismos fueron estudiados en fase homogénea y parten de la D-xilopiranosa comenzando con una protonación en el grupo hidroxilo del carbono 2 de la xilosa [73].

En el mecanismo propuesto por K.J. Zeitsch, primero se producen dos eliminaciones en posición 1,2 de agua y luego una eliminación 1,4 de agua. Las eliminaciones 1,2 necesitan la participación de dos átomos de carbono vecinos, permitiendo la formación de un doble enlace entre ellos, mientras que la eliminación 1,4 requiere dos átomos de carbono separados por otros dos átomos, formando el anillo furánico. En resumen, este mecanismo propuesto se basa en la transformación de los grupos hidroxilo de la pentosa a grupos H_2O^+, conduciendo a la formación de carbocationes a través de las eliminaciones de las moléculas de agua.

El mecanismo propuesto por M.J. Antal et al. sugiere que la primera protonación del grupo hidroxilo puede tener lugar en el carbono 1 o 2, pero en la Figura I.11 aparece protonado en el carbono 2 ya que en 2006 se demostró que la protonación se encuentra favorecida en esta posición [74]. En el mecanismo se puede observar que una vez protonado el grupo hidroxilo del carbono 2 se produce la transformación de D-xilopiranosa a D-xilofuranosa, creándose una molécula de agua. Luego, se produce la eliminación de los grupos hidroxilos formándose sus correspondientes doble enlaces y moléculas de agua respectivamente, hasta obtener la molécula de furfural [75].

Para finalizar, al comparar ambas propuestas, M.R. Nimlos et al. han demostrado mediante mecánica cuántica que el mecanismo propuesto por M.J. Antal es el más probable debido a que la barrera energética producida por la apertura del anillo es mayor en el mecanismo propuesto por K.J. Zeitsch [74].

I.4.1.2. Factores a tener en cuenta durante la deshidratación de la xilosa

Durante la reacción de deshidratación pueden tener lugar otras reacciones secundarias (Figura I.12), siendo las causantes de los bajos rendimientos a furfural observados en bibliografía [76,77]. Algunas de estas

reacciones son: la fragmentación de la xilosa (Figura I.12a) y la descomposición del furfural (Figura I.12c) a otros compuestos como acetol, ácido láctico, gliceraldehído formaldehído, crotonaldehído, piruvaldehído, etc. [78]; la condensación del furfural consigo mismo (resinificación del furfural) (Figura I.12d) y con intermedios de la xilosa (Figura I.12e) obteniéndose polímeros y oligómeros [79].

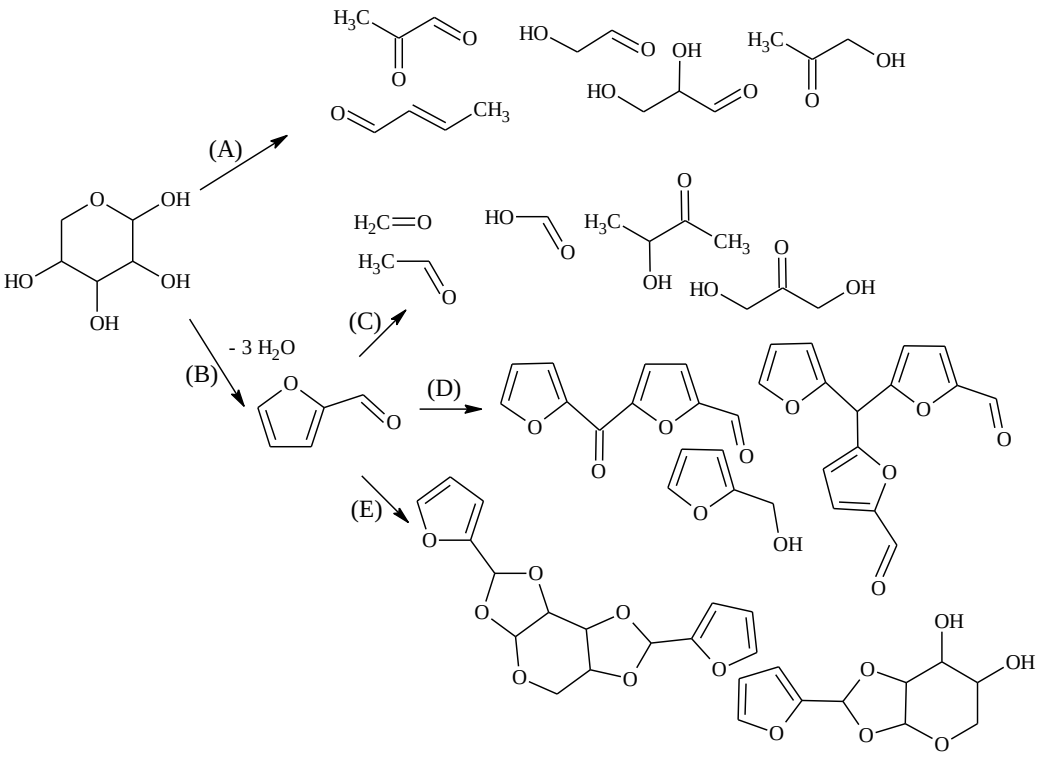

Figura I.12. Esquema de reacción para la deshidratación de la xilosa, incluyéndose algunas reacciones secundarias. (A) Fragmentación de la xilosa, (B) Deshidratación de la xilosa a furfural, (C) Descomposición del furfural, (D) Resinificación del furfural, (E) Condensación entre el furfural e intermedios de la xilosa. Adaptado de R. Karinen et al. [78].

Una solución para evitar estas reacciones podría ser el empleo de un disolvente adecuado. Como primera opción, se podría pensar en emplear el agua, ya que es barato y no contaminante, pero cuando el furfural se encuentra

en presencia de ésta se favorece la generación de huminas [80-82]. Por lo que, algunas de las alternativas que se han estudiado son el empleo de líquidos iónicos (siendo un problema su alto coste) [83], CO_2 supercrítico (necesitando una tecnología compleja) [84], dimetilsulfóxido (pudiendo provocar contaminación con azufre) [66], disolvente orgánicos [85] y/o sistemas bifásicos [86,87], empleando agua y un disolvente orgánico (aproximación empleada en la reacción llevada a cabo en el Capítulo 3). Los disolventes orgánicos más empleados en los sistemas bifásicos son el tolueno, el butan-1-ol o el butirato de etilo [88,89].

Otra solución, siendo útil cuando se van a realizar varias reacciones en cadena (por ejemplo, si después de la deshidratación de la xilosa se va a emplear el furfural obtenido como material de partida para otra reacción), es el empleo de catalizadores multifuncionales, permitiendo llevar a cabo procesos conocidos como "one-pot" o en cascada. El objetivo de este tipo de procesos es reducir los procesos de separación, abaratando los costes y realizando el proceso en una sola operación [90-92].

I.4.1.3. Catalizadores empleados en la deshidratación de la xilosa

Los catalizadores homogéneos industrialmente empleados, comentados anteriormente, son ácidos minerales como el ácido sulfúrico o el ácido clorhídrico. El empleo de ellos causa corrosión en los reactores, genera residuos tóxicos y dificulta la reutilización del catalizador empleado. Por ello, actualmente se buscan alternativas, empleando catalizadores heterogéneos sólidos, que puedan reducir costes de reactores y disminuyan el impacto medioambiental producido por el proceso.

Los catalizadores más estudiados en bibliografía son materiales que presentan propiedades ácidas, como resinas de intercambio iónico [93], óxidos

metálicos de zirconio y titanio [94], sílices mesoporosas sin modificar [95] y funcionalizadas con grupos ácidos (sulfónicos) [66,96,97], hidrotalcitas [98], fosfatos metálicos [99], titanatos y niobatos [100] y polímeros sulfónicos [101].

En la tabla I.3 aparecen los catalizadores más recientemente descritos en bibliografía en la reacción de deshidratación de xilosa a furfural con sus condiciones de reacción y los resultados obtenidos. De manera general, sobresale la complejidad de los métodos de síntesis utilizados para la obtención de los catalizadores, empleando materiales como grafeno, ácidos (H_2SO_4, H_3PO_4 o HF), así como metales caros (W o Ta). En las reacciones, se puede observar el empleo de un sistema bifásico, siendo predominante el uso de tolueno como fase orgánica. Las temperaturas y los tiempos utilizados se encuentran en el rango de 160-175 ºC y 2-20h, respectivamente, las relaciones en peso sustrato/catalizador están en el intervalo de 0,1-5,0% y las conversiones de xilosa obtenida se encuentran entre 90-100%. El mayor rendimiento a furfural, 88%, ha sido obtenido empleando KIT-6-SO_3H (sílice mesoporosa tipo KIT-6 funcionalizada con un grupo sulfónico), con tolueno y un tiempo de 2h. Al emplear la SBA-15-SO_3H (sílice mesoporosa SBA-15 funcionalizada con un grupo sulfónico), el rendimiento a furfural también es elevado siendo 82%, pero el tiempo empleado para llegar a ese valor de rendimiento es muy alto, siendo 20h.

Tabla I.3. Comparación de la actividad catalítica de los catalizadores más recientemente descritos en la bibliografía en la reacción de deshidratación de xilosa a furfural: temperatura, relación en peso sustrato/catalizador ($R_{sus./cat.}$), tiempo de reacción (en horas), disolvente empleado, presión (en MPa), conversión de xilosa (Con. Xil.) y rendimiento a furfural (Rend. Furf.).

Catalizador	Tª (ºC)	R sus./cat. (peso)	t (h)	Disolvente	Presión (MPa)	Con. Xil. (%)	Rend. Furf. (%)	Ref.
KIT-6-SO_3H [a]	170	4,0	2,0	Tolueno	-	98	88	[102]
TA-P-300 [b]	160	1,0	3,0	Agua/ butan-1-ol	2,0	90	48	[103]
SBA-15-SO_3H	160	1,7	20,0	Agua/ tolueno	1,5	98	82	[104]
SO_4^{2-}/ZrO_2-TiO_2	170	0,1	2,0	Agua/ butan-1-ol	-	98	48	[105]
MgF_2-71% (p/p) [c]	160	5,0	20,0	Agua/ tolueno	1,5	94	78	[106]
ZrWAl-MP [d]	170	1,5	6,0	Agua/ tolueno	-	100	50	[107]
TiO_2-grafeno	175	3,0	3,5	Agua/ tolueno	-	97	69	[108]

[a] Sílice mesoporosa tipo KIT-6 funcionalizada con un grupo sulfónico.
[b] Hidróxido de tantalio con el 10% de H_3PO_4 y calcinado a 300 ºC.
[c] 71% (p/p) de HF en una solución de Mg.
[d] Sólido mesoporoso de hidróxido de zirconio impregnado por W y Al.

Los catalizadores que se han empleado en la deshidratación de la xilosa del Capítulo 3 han sido óxido de zirconio, óxido de magnesio y sistemas mixtos de MgO-ZrO_2 (con una relación nominal Mg:Zr de 75:25, 50:50 y 25:75).

I.4.2. Condensación Aldólica del Furfural y la Acetona

La reacción de condensación aldólica, también conocida como adición aldólica consiste en la formación de enlaces C-C [34,63,109,110], transformando moléculas de bajo peso molecular en moléculas de mayor

tamaño. La reacción se produce entre dos compuestos carbonílicos, por ejemplo, un furfural y una acetona (Figura I.13.). Para que tenga lugar la reacción es necesaria la presencia de un protón reactivo en α [111] en uno de los dos compuestos carbonílicos (aportado en este caso por la acetona) que reaccionará con el otro compuesto formando un enol. Posteriormente, se formará su enona conjugada tras un proceso de deshidratación. Además, requiere la presencia de un catalizador ácido o básico [63,109,111-114], siendo utilizados generalmente catalizadores básicos.

I.4.2.1. Mecanismo de reacción de la condensación aldólica del furfural y la acetona para la obtención de 1,5-bis-(2-furanil)-1,4-pentadien-3-ona

La reacción de condensación aldólica del furfural y la acetona para la obtención de 1,5-bis-(2-furanil)-1,4-pentadien-3-ona aparece representada en la Figura I.13a. Se puede observar cómo la reacción comienza con una primera condensación aldólica, donde se produce la abstracción de un protón en α de la acetona por el catalizador empleado, creando un ion enolato estabilizado que atacará al grupo carbonilo del furfural mediante un ataque nucleofílico, formando su aducto aldólico correspondiente, 4-(2-furanil)-4-hidroxi-butan-2-ona. Este aducto, se deshidrata, perdiendo una molécula de agua y formando una cetona α,β-insaturada, 4-(2-furanil)-3-buten-2-ona (FAc). Seguidamente, se producirá una segunda condensación aldólica donde una molécula de FAc (previamente formado su carbanión con la presencia del catalizador) atacará (ataque nucleofílico) al grupo carbonilo de una molécula de furfural, deshidratándose y formándose un segundo producto 1,5-bis-(2-furanil)-1,4-pentadien-3-ona (F2Ac), el producto deseado que se quiere obtener [115-117].

Durante el proceso se pueden dar algunas reacciones secundarias, no deseadas, como la autocondensación de la acetona formando la diacetona alcohol y el óxido de mesitilo (Figura I.13b), la condensación entre FAc y

acetona (Figura I.13c), y múltiples condensaciones aldólicas entre diferentes compuestos carbonílicos, formando polímeros (Figura I.13d).

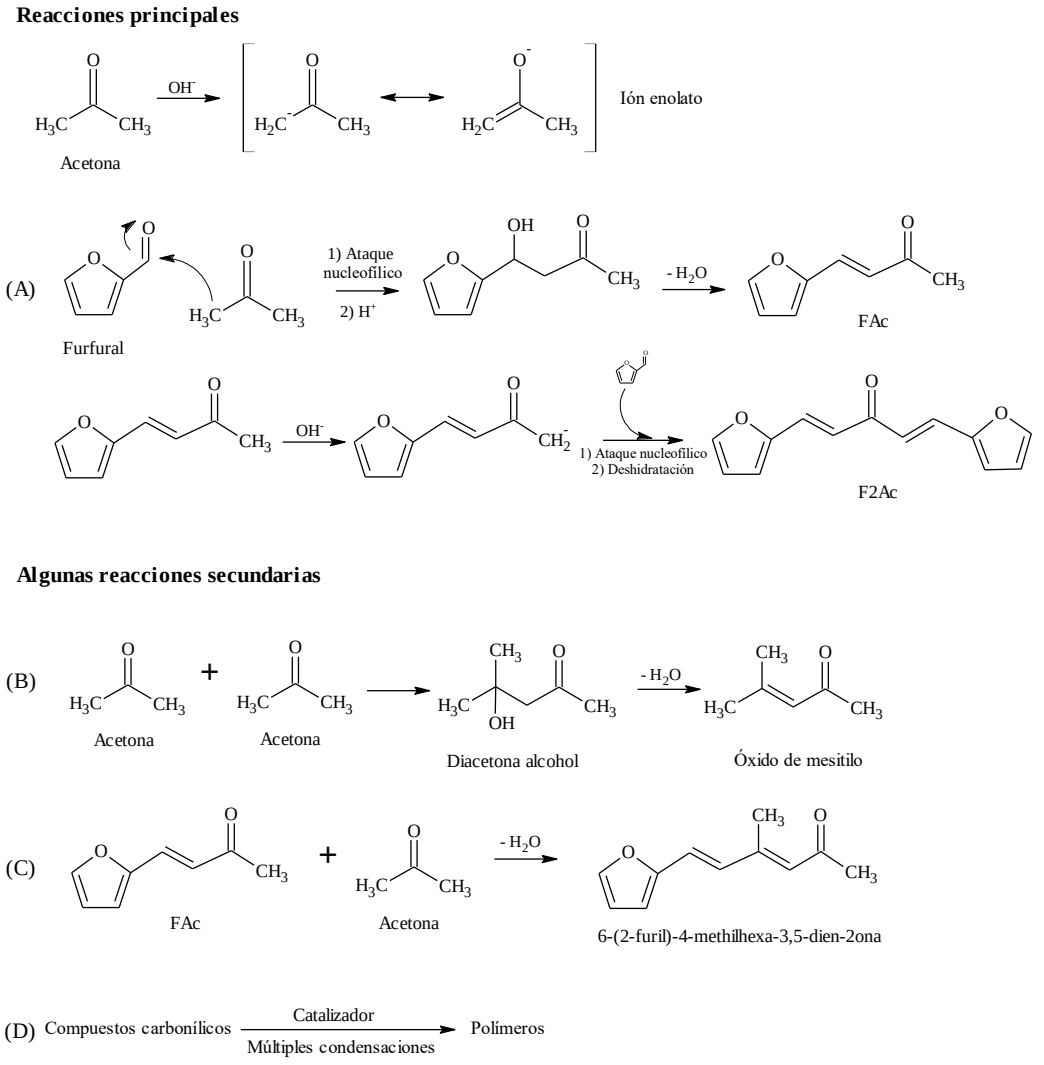

Figura I.13. Esquema de reacción para la condensación aldólica del furfural y la acetona, incluyéndose algunas reacciones secundarias: (A) Condensación aldólica del furfural y la acetona, (B) autocondensación de la acetona, (C) condensación entre el FAc y la acetona y (D) múltiples condensaciones aldólicas entre diferentes compuestos carbonílicos. Adaptado de A. Parejas et al. [118].

I.4.2.2. Factores a tener en cuenta durante la condensación aldólica

De manera general, durante una reacción de condensación aldólica influyen diferentes factores que hay que tener en cuenta para evitar posibles reacciones secundarias, entre las que se pueden incluir las anteriormente comentadas, y así obtener el producto que se desea conseguir. Entre estos factores se encuentran:

- El catalizador. Debe de poseer características que favorezcan la reacción, así como conocer cuál es su concentración más favorable a emplear durante el proceso.
- El disolvente. Los reactivos de partida no son solubles en todos los disolventes, por lo que se debe escoger un disolvente, en el cual sean solubles los reactivos, los productos y el catalizador. Los más usados son el etanol, el etanol acuoso y el agua.
- La temperatura y el tiempo de reacción. La reacción de condensación aldólica normalmente es reversible y exotérmica, obteniéndose altos rendimientos cuando se emplean temperaturas en el rango de 5-25 ºC en un tiempo de 12 a 24 h, aunque depende de los reactivos de partida a emplear. Pero en el caso de la reacción de condensación aldólica del furfural y la acetona, es necesario el uso de altas temperaturas para favorecer la formación de compuestos carbonilos α,β-insaturados.
- La proporción de los compuestos de partida. Es importante conocer cuál es la relación más adecuada de ambos reactivos, siendo las cantidades estequiométricas las más empleadas. En la condensación aldólica del furfural y la acetona ocurre una excepción, ya que se suele emplear un exceso de acetona para minimizar la autocondensación del furfural y favorecer la formación del segundo producto de condensación [119].

I.4.2.3. Catalizadores empleados en la condensación aldólica del furfural y la acetona para la obtención de 1,5-bis-(2-furanil)-1,4-pentadien-3-ona

En la industria, las condensaciones aldólicas suelen tener lugar en presencia de un disolvente orgánico y catalizadores homogéneos básicos, como el hidróxido de sodio [62,115]. Pero, este tipo de catalizadores presentan varios inconvenientes anteriormente comentados (corrosión, difícil reutilización, etc). Por este motivo se han estudiado otras alternativas, empleando catalizadores heterogéneos, como puede ser metales alcalinos [120,121], óxidos mixtos derivados de hidrotalcitas [122,123], zeolitas [124-126], sólidos mesoporosos [127], óxidos metálicos[114,128-131], etc.

En la tabla I.4 aparecen los catalizadores más recientemente descritos en la bibliografía en la reacción de condensación aldólica, las condiciones de reacción empleadas y los resultados obtenidos. Se puede observar el empleo de catalizadores básicos como las hidrotalcitas MgAl (relación molar Mg/Al=1) y Mg_2Al (relación molar Mg/Al=2), la dolomita y el sólido Mg-Zr/HGSA300 (óxido mixto de MgO-ZrO_2 soportado por grafito y con un área superficial de 300 m^2/g, siendo la relación molar Mg/Zr=4); y catalizadores ácidos como MCM-22, H-BEA (zeolita transformada de la forma NH_4 a forma H) y 0,7K-N-BEA (BEA con un 0,7 M de KNO_3 y sin lavar después de la filtración.). La temperatura utilizada se encuentra en el rango de 50-140 ºC, siendo la más utilizada 100 ºC. De manera general, la relación en peso sustrato/catalizador empleada es alta, encontrándose en el intervalo de 3,3-11,0%. La relación molar acetona/furfural también es alta, siendo normalmente 10%, excepto en aquellas reacciones en las que se ha empleado Mg-Zr/HGSA300 y dolomita como catalizadores. El mejor valor de rendimiento a F2Ac obtenido ha sido al utilizar como catalizador la dolomita, 72%, en 1h; aunque es difícil comparar las condiciones. Por ejemplo, en este catalizador, la temperatura (140 ºC) y el contenido en peso del furfural (11,0%) son los mayores de todos de la Tabla I.4.

Tabla I.4. Comparación de la actividad catalítica de los catalizadores más recientemente descritos en la bibliografía en la reacción de condensación aldólica del furfural con acetona: temperatura, contenido de furfural en peso, relación en peso sustrato/catalizador ($R_{sus./cat.}$), relación molar acetona/furfural ($R_{ac./fur.}$), tiempo de reacción (en horas), presión (en MPa), conversión de furfural (Con. Furf.), rendimiento a 4-(2-furanil)-3-buten-2-ona (Ren. FAc) y rendimiento a 1,5-bis-(2-furanil)-1,4-pentadien-3-ona (Rend. F2Ac).

Catalizador	Tª (ºC)	Furf. (p/p) (%)	$R_{sus./cat.}$ (peso)	$R_{ac./fur.}$ (molar)	t (h)	Presión (MPa)	Con. Fur. (%)	Rend. FAc (%)	Rend. F2Ac (%)	Ref.
Hidrotalcita MgAl	100	3,3	3,3	10,1	2	Aut. P	95	67	22	[122]
Mg-Zr/ HSAG300 [a]	50	1,5	7,5	1,0	24	1	97	37	53	[132]
Dolomita	140	11,0	11,0	1,0	1	Aut. P	90	20	72	[117]
MCM-22	100	6,5	6,5	10,0	2	Aut. P	60	49	4	[133]
H-BEA[b]	100	3,3	3,3	10,0	8	Aut. P	39	31	1	[125]
0,7K-N-BEA[c]	100	14,1	3,3	10,0	2	Aut. P	78	65	9	[124]
Hidrotalcita Mg_2Al [d]	50	14,1	3,3	10,0	6	Aut. P	100	60	35	[65]

[a] óxido mixto de MgO-ZrO_2 soportado por grafito y con un área superficial de 300 m^2/g, siendo la relación molar Mg/Zr=4)

[b] H-BEA: transformación de la forma NH_4 de la zeolita a forma H.

[c] 0,7 K-N-BEA: BEA con un 0,7 M de KNO_3 y no fue lavada después de la filtración.

[d] Mg_2Al hidrotalcita: hidrotalcita con un relación molar de Mg/Al=2/1.

A este valor de rendimiento a F2Ac le sigue 53%, obtenido al emplear Mg-Zr/HGSA300 en un tiempo de 24h (el tiempo más alto). Los resultados de F2Ac obtenidos al utilizar catalizadores ácidos MCM-22, H-BEA y 0,7K-N-BEA son los más bajos siendo 4%, 1% y 9%, respectivamente, por ello generalmente se emplean catalizadores básicos en la reacción de condensación aldólica del furfural y la acetona.

Los catalizadores que se han empleado en la reacción de condensación aldólica del Capítulo 4 han sido óxidos mixtos de Mg/Al derivados de hidrotalcita, sintetizados modificando dos variables durante la síntesis (calentamiento convencional o microondas con la presencia o ausencia de Pluronic 123 como surfactante).

I.4.3. Reducción Meerwein-Ponndorf-Verley (MPV) del Furfural

La reacción de Meerwein-Ponndorf-Verley (MPV) es un proceso de reducción de compuestos carbonílicos por transferencia de hidrógeno, utilizando un alcohol de sacrificio como fuente de hidrógeno [134-137]. Este alcohol de sacrificio normalmente es un alcohol secundario. Durante la reacción, al existir esa transferencia de hidrógeno, el alcohol secundario se transformará en una cetona, mientras que el compuesto carbonílico se reducirá a su correspondiente alcohol.

Esta reacción presenta grandes ventajas a escala industrial, algunas de ellas son la simplicidad del proceso de MPV, la gran quimioselectividad de la transformación, los catalizadores empleados no son metales nobles (Pt, Pd, etc.) soportados, al no emplearse hidrógeno (H_2) se evitan problemas relacionados con su almacenamiento y las condiciones de reacción empleadas son bajas, por lo que se consiguen grandes rendimientos con un bajo costo del proceso [138,139].

I.4.3.1. Mecanismo de reacción de la reducción MPV del furfural

La reacción de reducción MPV del furfural y el propan-2-ol para la obtención de alcohol furfurílico, aparece representada en la Figura I.14. Para ello, el grupo carbonilo del furfural y el grupo alcóxido del propan-2-ol reaccionan con un catalizador óxido metálico (ácido de Lewis) [140], formando un complejo y dándose una reacción concertada en la cual se forma un estado de transición de seis miembros [141,142]. Así, el grupo carbonilo se activa al producirse un enlace de coordinación con el centro ácido de Lewis, quedándose con una densidad de carga positiva. Mientras, se produce la transferencia de un hidruro del grupo alcóxido al grupo carbonilo y da lugar al alcohol furfurílico y la acetona correspondiente.

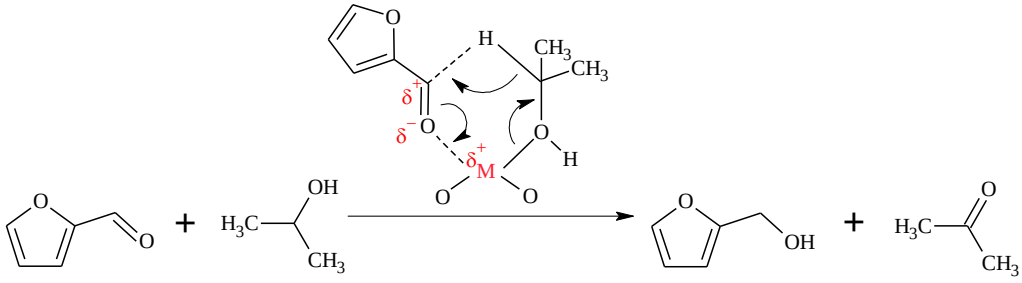

Figura I.14. Mecanismo de la reacción de reducción MPV, siendo M el catalizador metálico. Adaptado de V.J. Shiner Jr et al. [143].

I.4.3.2. Factores a tener en cuenta durante la reducción MPV del furfural

Durante la reducción MPV del furfural es importante tener en cuenta una serie de factores para conocer el mecanismo de la reacción, y son:

- Qué tipos de centros están involucrados en la reacción, centros ácidos (Lewis o Brönsted) y/o básicos.
- Cómo se ha formado el estado de transición entre los reactivos de partida y el catalizador, pudiendo ser de seis o siete miembros [144].

I.4.3.3. Catalizadores empleados en la reducción MPV del furfural

Los catalizadores homogéneos que se emplean en esta reacción se basan en alcóxidos metálicos, algunos de ellos son el aluminio [145], el boro [146] y el zirconio [135,142,147]. Aunque estos catalizadores presentan grandes ventajas, se han desarrollado investigaciones probando diferentes catalizadores heterogéneos para poder conseguir resultados equivalentes y sustituirlos. Algunos de los catalizadores heterogéneos que se utilizan son zeolitas con zirconio [148,149], óxidos metálicos [150,151] e hidrotalcitas [152-154].

En la tabla I.5 aparecen los catalizadores más recientemente descritos en bibliografía en la reacción de reducción MPV del furfural a alcohol furfurílico, las condiciones de reacción empleadas y los resultados obtenidos. En todas las reacciones se ha empleado como alcohol de sacrificio el propan-2-ol. La mayoría de los catalizadores han sido sintetizados con un precursor de zirconio y métodos de síntesis complejos, e incluso algunos con ácidos caros como el ácido húmico y el ácido trimésico. También se han utilizado catalizadores de óxido de aluminio como el B-Al_2O_3 calc. (550 ºC) (alúmina comercial) y el Al_2O_3–S(7) (catalizador de alúmina y carbono). Las relaciones en peso sustrato/catalizador se encuentran en el intervalo de 1,0-9,6%, siendo mayoritario el uso de 4,8%. Respecto a las relaciones molar furfural/alcohol, la más utilizada ha sido 0,02%, aunque también se ha empleado 0,01% y 0,05%. La temperatura y el tiempo se encuentran en el rango de 70-140 ºC y 1-9h, respectivamente. El mayor valor obtenido de conversión a furfural (97,5%) y rendimiento a alcohol furfurílico (96,0%) ha sido al utilizar el catalizador Zr-LS (catalizador $ZrCl_4$ y lignosulfato de sodio), donde sobresale la alta relación en peso sustrato/catalizador, 9,6%, utilizada.

Tabla I.5. Comparación de la actividad catalítica de los catalizadores más recientemente descritos en bibliografía en la reacción de reducción MPV del furfural a alcohol furfurílico: temperatura, relación en peso sustrato/catalizador ($R_{sus./cat.}$), relación molar furfural/alcohol ($R_{fur./alc.}$), tiempo de reacción (en horas), alcohol empleado (donador de H_2), conversión de furfural (Con. Furf.), rendimiento a alcohol furfurílico (Rend. FUOL).

Catalizador	T[a] (ºC)	R sus./cat. (peso)	R fur./alc. (molar)	t (h)	Alcohol (Donador de H_2)	Con. Fur. (%)	Rend. FUOL (%)	Ref.
Zr-LS [a)]	100	9,6	0,01	1	Propan-2-ol	97,5	96,0	[155]
Zr-RLS [b)]	90	4,8	0,02	6	Propan-2-ol	93,4	80,9	[156]
B-Al_2O_3 calc. (550 ºC) [c)]	150	1,0	0,02	5	Propan-2-ol	93,0	87	[60]
Al_2O_3 – S(7) [d)]	160	1,0	0,05	6	Propan-2-ol	96,9	95,5	[157]
Zr-HAs [e)]	70	4,8	0,02	9	Propan-2-ol	98,0	80	[158]
Zr-TMSA [f)]	70	4,8	0,02	5	Propan-2-ol	93,6	89,5	[159]
Zr-PN [g)]	100	2,4	0,02	15	Propan-2-ol	93,0	90	[160]

a) Catalizador de $ZrCl_4$ y lignosulfato de sodio.
b) Catalizador basado en Zr y lignita como ligando orgánico.
c) Alúmina básica comercial (γ-Al_2O_3).
d) Catalizador de alúmina y carbono (relación en peso surfactante/precursor=7).
e) Catalizador de ácido húmico y Zr.
f) Catalizador de ácido trimésico y Zr.
g) Catalizador híbrido organotrifosfato-zirconio.

Los catalizadores que se han empleado en la reacción de reducción MPV del furfural del Capítulo 5 han sido ZrO_x, TiO_x, MgO_x, sistemas mixtos de Mg-Ti y sistemas mixtos de Zr-Ti (los sistemas mixtos presentan una relación nominal de X/Ti de 75:25, 50:50 y 25:75, siendo X: Zr o Mg).

I.5. Referencias

1. Chheda, J.N.; Huber, G.W.; Dumesic, J.A. Liquid-phase catalytic processing of biomass-derived oxygenated hydrocarbons to fuels and chemicals. *Angewandte Chemie-International Edition* **2007**, *46*, 7164-7183, doi:10.1002/anie.200604274.
2. Stocker, M. Biofuels and biomass-to-liquid fuels in the biorefinery: catalytic conversion of lignocellulosic biomass using porous materials. *Angewandte Chemie-International Edition* **2008**, *47*, 9200-9211, doi:10.1002/anie.200801476.
3. Serna, F.; Barrera, L.; Montiel, H. Impacto Social y Económico en el uso de Biocombustibles. *Journal of technology management & innovation* **2011**, *6*, 100-114, doi:10.4067/s0718-27242011000100009.
4. Declaración de Río sobre el medio ambiente y el desarrollo. Disponible en: http://portal.uned.es/pls/portal/docs/PAGE/UNED_MAIN/LAUNIVERSIDAD/DEPARTAMENTOS/0614/ASIGNAT/MEDIOAMBIENTE/TEM

A%201/%20%20%20%20%20DECLARACI%C3%93N%20DE%20R%C3%8DO%201992.PDF (accesible a 20/04/2019).

5. Agenda 21. Disponible en: https://sustainabledevelopment.un.org/content/documents/Agenda21.pdf (accesible a 20/04/2019).
6. DIRECTIVA 2009/28/CE. Disponible en: https://www.boe.es/doue/2009/140/L00016-00062.pdf (accesible a 20/04/2019).
7. Documento final de la Conferencia - El futuro que queremos. Disponible en: https://rio20.un.org/sites/rio20.un.org/files/a-conf.216-l-1_spanish.pdf.pdf (accesible a 20/04/2019).
8. Acuerdo de París. Disponible en: https://ec.europa.eu/clima/policies/international/negotiations/paris_es (accesible a 20/04/2019).
9. Ghisellini, P.; Cialani, C.; Ulgiati, S. A review on circular economy: the expected transition to a balanced interplay of environmental and economic systems. *Journal of Cleaner Production* **2016**, *114*, 11-32, doi:10.1016/j.jclepro.2015.09.007.
10. ¿En qué consiste la economía circular? Disponible en: https://www.sostenibilidad.com/desarrollo-sostenible/en-que-consiste-la-economia-circular/ (accesible a 20/04/2019).
11. Polshettiwar, V.; Varma, R.S. Green chemistry by nano-catalysis. *Green Chemistry* **2010**, *12*, 743-754, doi:10.1039/b921171c.
12. Argyle, M.D.; Bartholomew, C.H. Heterogeneous catalyst deactivation and regeneration: a review. *Catalysts* **2015**, *5*, 145-269, doi:10.3390/catal5010145.
13. Sun, L.-B.; Liu, X.-Q.; Zhou, H.C. Design and fabrication of mesoporous heterogeneous basic catalysts. *Chemical Society Reviews* **2015**, *44*, 5092-5147, doi:10.1039/c5cs00090d.

14. Brown, A. Consideraciones sobre el estudio de catálisis homogénea y heterogénea. En *Instituto Cubano de Investigaciones sobre Derivados de la Caña de Azucar, ICIDCA. Sobre los Derivados de la Caña de Azúcar*, 2005; Vol. 39, pág. 10-14. Disponible en: http://www.redalyc.org/articulo.oa?id=223120659002 (accesible a 20/04/2019).
15. Anastas, P.T.; Heine, L.G.; Williamson, T.C. *Green Chemical: syntheses and processes*, American Chemical Society, Washington DC, 2000.
16. Anastas, P.T.; Kirchhoff, M.M. Origins, current status, and future challenges of green chemistry. *Accounts of Chemical Research* **2002**, *35*, 686-694, doi:10.1021/ar010065m.
17. Anastas, P.T.; Warner, J.C. *Green Chemistry: theory and practise*; New York, Oxford University Press, 2000.
18. Anastas, P.T.; Bartlett, L.B.; Kirchhoff, M.M.; Williamson, T.C. The role of catalysis in the design, development, and implementation of green chemistry. *Catalysis Today* **2000**, *55*, 11-22, doi:10.1016/s0920-5861(99)00222-9.
19. Sheldon, R.A. Green and sustainable manufacture of chemicals from biomass: state of the art. *Green Chemistry* **2014**, *16*, 950-963, doi:10.1039/c3gc41935e.
20. Manual sobre las biorrefinerías en España. Disponible en: http://www.suschem-es.org/docum/pb/2017/publicaciones/Manual_de_Biorrefinerias_en_Espana_feb_2017.pdf (accesible a 20/04/2019).
21. Gomez Millan, G. Desarrollo de biorrefinerías en el mundo (Biorefineries development: a worldwide review). *Ciencia y desarrollo* **2015**, *1*, 13.
22. Fernández González, J.; al., *Tecnologías para el uso y transformación de biomasa energética*; Paraninfo, SA, Madrid, 2015.

23. Ragauskas, A.J.; et al. The path forward for biofuels and biomaterials. *Science* **2006**, *311*, 484-489, doi:10.1126/science.1114736.
24. Lenk, F.; Broring, S.; Herzog, P.; Leker, J. On the usage of agricultural raw materials-energy or food? An assessment from an economics perspective. *Biotechnology Journal* **2007**, *2*, 1497-1504, doi:10.1002/biot.200700153.
25. Alonso, D.M.; Bond, J.Q.; Dumesic, J.A. Catalytic conversion of biomass to biofuels. *Green Chemistry* **2010**, *12*, 1493-1513, doi:10.1039/c004654j.
26. Rubin, E.M. Genomics of cellulosic biofuels. *Nature* **2008**, *454*, 841-845, doi:10.1038/nature07190.
27. Cuervo, L.; Folch, J.L.; Quiroz, R.E. Lignocelulosa como fuente de azúcares para la producción de etanol. *BioTecnología* **2009**, *13*, 11-25.
28. Franco, A.G.; Yépes, P.N.M.; Sánchez, H.A.V. Pretratamientos de la celulosa y biomasa para la sacarificación. *Scientia et Technica* **2009**, *15*, 284-289.
29. Baldovín, F.L.; García, J.C.; Zamudio, M.A.M.; Muñoz, A.P. Biorrefinería de materiales lignocelulósicos: Eucalyptus globulus. *Boletín Informativo CIDEU* **2010**, *8*, 75-82.
30. Cooper Bribiesca, B.L. Enzimas xilanolíticas bacterianas y sus aplicaciones industriales. *Vertientes. Revista Especializada en Ciencias de la Salud* 2013.
31. Sifontes, M.C.; Domine, M.E. Lignina, estructura y aplicaciones: métodos de despolimerización para la obtención de derivados aromáticos de interés industrial. *Avances en ciencias e Ingeniería* **2013**, *4*, 15-46.
32. Ragauskas, A.J.; et al. Lignin valorization: improving lignin processing in the biorefinery. *Science* **2014**, *344*, 1246843, doi:10.1126/science.1246843.

33. Saha, B.C. Hemicellulose bioconversion. *Journal of Industrial Microbiology & Biotechnology* **2003**, *30*, 279-291, doi:10.1007/s10295-003-0049-x.
34. Climent, M.J.; Corma, A.; Iborra, S. Conversion of biomass platform molecules into fuel additives and liquid hydrocarbon fuels. *Green Chemistry* **2014**, *16*, 516-547, doi:10.1039/c3gc41492b.
35. Lange, J.-P. Lignocellulose conversion: an introduction to chemistry, process and economics. *Biofuels Bioproducts & Biorefining-Biofpr* **2007**, *1*, 39-48, doi:10.1002/bbb.7.
36. Leisch, H.; Grosse, S.; Morley, K.; Abokitse, K.; Perrin, F.; Denault, J.; Lau, P.C.K. Chemicals from agricultural biomass: chemoenzymatic approach for production of vinylphenols and polyvinylphenols from phenolic acids. *Green Processing and Synthesis* **2013**, *2*, 7-17, doi:10.1515/gps-2012-0082.
37. Kosa, M.; Ragauskas, A.J. Lignin to lipid bioconversion by oleaginous Rhodococci. *Green Chemistry* **2013**, *15*, 2070-2074, doi:10.1039/c3gc40434j.
38. Sheldon, R.A. *Chemicals from synthesis gas: catalytic reactions of CO and. H2 (Vol. 2)*; Springer Science & Business Media: 1983.
39. Himmel, M.E.; Ding, S.Y.; Johnson, D.K.; Adney, W.S.; Nimlos, M.R.; Brady, J.W.; Foust, T.D. Biomass recalcitrance: Engineering plants and enzymes for biofuels production. *Science* **2007**, *315*, 804-807, doi:10.1126/science.1137016.
40. Machado, C. Situación de los biocombustibles de 2ª y 3ª generación en América Latina y Caribe. *Organización latinoamericana de energía-IICA . Brasilia (Brasil)*, 2010.
41. Kamm, B.; Kamm, M. Principles of biorefineries. *Applied Microbiology and Biotechnology* **2004**, *64*, 137-145, doi:10.1007/s00253-003-1537-7.

42. Vidal Castro, J.D. Valorización de moléculas plataforma derivadas de biomasa mediante aminación reductiva utilizando nanopartículas metálicas como catalizadores heterogéneos. Tesis Doctoral Universidad Politécnica de Valencia, 2017.
43. Werpy, T.; Petersen, G. Editores *Top value added chemicals from biomass. Volume 1-Results of screening for potential candidates from sugars and synthesis gas*. 2004. Disponible en: https://www.nrel.gov/docs/fy04osti/35523.pdf (accesible a 21/04/2019).
44. Bozell, J.J.; Petersen, G.R. Technology development for the production of biobased products from biorefinery carbohydrates-the US Department of Energy's "Top 10" revisited. *Green Chemistry* **2010**, *12*, 539-554, doi:10.1039/b922014c.
45. Farmer, T.J.; Mascal, M. Platform molecules. En I*ntroduction to chemicals from biomass,* Vol. 2. Clarj, J.; Deswarte, F.; Editores. Wiley 2015.
46. Gallezot, P. Conversion of biomass to selected chemical products. *Chemical Society Reviews* **2012**, *41*, 1538-1558, doi:10.1039/c1cs15147a.
47. Carlos Serrano-Ruiz, J.; Luque, R.; Sepulveda-Escribano, A. Transformations of biomass-derived platform molecules: from high added-value chemicals to fuels via aqueous-phase processing. *Chemical Society Reviews* **2011**, *40*, 5266-5281, doi:10.1039/c1cs15131b.
48. Kamm, B.; Gruber, P.R.; Kamm, M. Editores, Biorefineries - Industrial Processes and Products Status Quo and Future Directions **2006**.
49. Chheda, J.N.; Roman-Leshkov, Y.; Dumesic, J.A. Production of 5-hydroxymethylfurfural and furfural by dehydration of biomass-derived mono- and poly-saccharides. *Green Chemistry* **2007**, *9*, 342-350, doi:10.1039/b611568c.
50. Zhang, L.; Yu, H.; Wang, P.; Li, Y. Production of furfural from xylose, xylan and corncob in gamma-valerolactone using $FeCl_3.6H_2O$ as catalyst.

Bioresource Technology **2014**, *151*, 355-360, doi:10.1016/j.biortech.2013.10.099.

51. Hidalgo-Carrillo, J.; Marinas, A.; Urbano, F.J. Chemistry of Furfural and Furanic Derivates. En *Furfural: an entry point of lignocellulose in biorefineries to produce renewable chemicals, polymers, and biofuels*, López-Granados, M., Martín-Alonso, D., Eds. World Scientific, 2018.
52. Zeitsch, K.J. The chemistry and technology of furfural and its many by-products - Introduction. Sugar Series, Elsevier, *vol.13*, **2000**, pág. 1-2.
53. Mariscal, R.; Maireles-Torres, P.; Ojeda, M.; Sadaba, I.; Lopez Granados, M. Furfural: a renewable and versatile platform molecule for the synthesis of chemicals and fuels. *Energy & Environmental Science* **2016**, *9*, 1144-1189, doi:10.1039/c5ee02666k.
54. Hoydonckx, H.E.; Van Rhijn, W.M.; Van Rhijn, W.; De Vos, D.; Jacobs, P.A.; Furfural and Derivatives Wiley-VCH Verlag Weinheim 2007; Ullmann's Encyclopedia of Industrial Chemistry, pág. 1-25.
55. Da Costa Lopes, A.M.; Morais, A.R.C.; Lukasik, R.M. Sustainable catalytic strategies for C5-sugars and biomass hemicellulose conversion towards furfural production. En *Production of platform chemicals from sustainable resources*, Springer, 2017.
56. Dashtban, M.; Gilbert, A.; Fatehi, P. Production of furfural: overview and challenges. *J-for-Journal of Science & Technology for Forest Products and Processes* **2012**, *2*, 44-53.
57. Maireles-Torres, P.; L. Arias, P. Furfuryl Alcohol and Derivatives. En *Furfural: an entry point of lignocellulose in biorefineries to produce renewable chemicals, polymers, and biofuels*, López-Granados, M., Martín-Alonso, D., Eds. World Scientific, 2018; pág. 55-78.
58. Sádaba Zubiri, I. Catalizadores para biorrefinería: obtención de furfural y su transformación a productos de condensación aldólica. Tesis Doctoral. Universidad Autonómica de Madrid, 2012.

59. Zhang, Z.; Dong, K.; Zhao, Z. Efficient conversion of furfuryl alcohol into alkyl levulinates catalyzed by an organic-inorganic hybrid solid acid catalyst. *ChemSusChem* **2011**, *4*, 112-118, doi:10.1002/cssc.201000231.
60. Lopez-Asensio, R.; Cecilia, J.A.; Jimenez-Gomez, C.P.; Garcia-Sancho, C.; Moreno-Tost, R.; Maireles-Torres, P. Selective production of furfuryl alcohol from furfural by catalytic transfer hydrogenation over commercial aluminas. *Applied Catalysis A: General* **2018**, *556*, 1-9, doi:10.1016/j.apcata.2018.02.022.
61. Huang, W.; Li, H.; Zhu, B.; feng, Y.F.; Wang, S.; Zhang, S. Selective hydrogenation of furfural to furfuryl alcohol over catalysts prepared via sonochemistry. *Ultrasonics Sonochemistry* **2007**, *14*, 67-74, doi:10.1016/j.ultsonch.2006.03.002.
62. Barrett, C.J.; Chheda, J.N.; Huber, G.W.; Dumesic, J.A. Single-reactor process for sequential aldol-condensation and hydrogenation of biomass-derived compounds in water. *Applied Catalysis B: Environmental* **2006**, *66*, 111-118, doi:10.1016/j.apcatb.2006.03.001
63. Chheda, J.N.; Dumesic, J.A. An overview of dehydration, aldol-condensation and hydrogenation processes for production of liquid alkanes from biomass-derived carbohydrates. *Catalysis Today* **2007**, *123*, 59-70, doi:10.1016/j.cattod.2006.12.006.
64. Corma, A.; de la Torre, O.; Renz, M. High-quality diesel from hexose- and pentose-derived biomass platform molecules. *ChemSusChem* **2011**, *4*, 1574-1577, doi:10.1002/cssc.201100296.
65. Smolakova, L.; Frolich, K.; Kocik, J.; Kikhtyanin, O.; Capek, L. Surface properties of hydrotalcite-based Zn(Mg)Al oxides and their catalytic activity in aldol condensation of furfural with acetone. *Industrial & Engineering Chemistry Research* **2017**, *56*, 4638-4648, doi:10.1021/acs.iecr.6b04927.

66. Dias, A.S.; Pillinger, M.; Valente, A.A. Dehydration of xylose into furfural over micro-mesoporous sulfonic acid catalysts. *Journal of Catalysis* **2005**, *229*, 414-423, doi:10.1016/j.jcat.2004.11.016.
67. Zhang, L.X.; Yu, H.B.; Wang, P.; Dong, H.; Peng, X.H. Conversion of xylan, D-xylose and lignocellulosic biomass into furfural using $AlCl_3$ as catalyst in ionic liquid. *Bioresource Technology* **2013**, *130*, 110-116, doi:10.1016/j.biortech.2012.12.018.
68. Brownlee, H.J.; Miner, C.S. Industrial development of furfural. *Industrial and Engineering Chemistry* **1948**, *40*, 201-204, doi:10.1021/ie50458a005.
69. Zhang, Y.; Chen, M.; Wang, J.; Hu, Q. Synthesis of furfural from D-xylose and corncob with chromium chloride as catalyst in biphasic system. *Asian Journal of Chemistry* **2014**, *26*, 1717-1720, doi:10.14233/ajchem.2014.17333.
70. Binder, J.B.; Blank, J.J.; Cefali, A.V.; Raines, R.T. Synthesis of furfural from xylose and xylan. *ChemSusChem* **2010**, *3*, 1268-1272, doi:10.1002/cssc.201000181.
71. Arnold, D.R.; Buzzard, J.L. A novel process for furfural production. En *Proceedings of South African Chemical Engineering Congress*, 2003. Disponible en: http://ift.co.za/media/mediafiles/archive/SAIChE%20Congress%202003%20Arnold%20and%20Buzzard%20paper.pdf. (accesible a 21/04/2019).
72. Antal, M.J.; Leesomboon, T.; Mok, W.S.; Richards, G.N. Kinetic-studies of the reactions of ketoses and aldoses in water at high-temperature. 3. Mechanism of formation of 2-furaldehyde from d-xylose. *Carbohydrate Research* **1991**, *217*, 71-85, doi:10.1016/0008-6215(91)84118-x.
73. Dias, A.S.; Lima, S.; Pillinger, M.; Valente, A.A. Furfural and furfural-based industrial chemicals. En *Ideas in Chemistry and Molecular Sciences: Advances in Synthetic Chemistry*, Pignataro, B. Ed, Wiley, 2010.

74. Nimlos, M.R.; Qian, X.; Davis, M.; Himmel, M.E.; Johnson, D.K. Energetics of xylose decomposition as determined using quantum mechanics modeling. *Journal of Physical Chemistry A* **2006**, *110*, 11824-11838, doi:10.1021/jp0626770.
75. Imhof, P.; Van der Waal, J.C. *Catalytic process development for renewable materials*; John Wiley & Sons, 2013.
76. Lucas, N.; Kokate, G.; Nagpure, A.; Chilukuri, S. Dehydration of fructose to 5-hydroxymethyl furfural over ordered AlSBA-15 catalysts. *Microporous and Mesoporous Materials* **2013**, *181*, 38-46, doi:10.1016/j.micromeso.2013.07.015.
77. Grande, P.M.; Bergs, C.; de Maria, P.D. Chemo-enzymatic conversion of glucose into 5-hydroxymethylfurfural in seawater. *ChemSusChem* **2012**, *5*, 1203-1206, doi:10.1002/cssc.201200065.
78. Karinen, R.; Vilonen, K.; Niemela, M. Biorefining: heterogeneously catalyzed reactions of carbohydrates for the production of furfural and hydroxymethylfurfural. *ChemSusChem* **2011**, *4*, 1002-1016, doi:10.1002/cssc.201000375.
79. Dee, S.J.; Bell, A.T. A study of the acid-catalyzed hydrolysis of cellulose dissolved in ionic liquids and the factors influencing the dehydration of glucose and the formation of humins. *ChemSusChem* **2011**, *4*, 1166-1173, doi:10.1002/cssc.201000426.
80. van Zandvoort, I.; Wang, Y.; Rasrendra, C.B.; van Eck, E.R.H.; Bruijnincx, P.C.A.; Heeres, H.J.; Weckhuysen, B.M. Formation, molecular structure, and morphology of humins in biomass conversion: influence of feedstock and processing conditions. *ChemSusChem* **2013**, *6*, 1745-1758, doi:10.1002/cssc.201300332.
81. Patil, S.K.R.; Heltzel, J.; Lund, C.R.F. Comparison of structural features of humins formed catalytically from glucose, fructose, and 5-

hydroxymethylfurfuraldehyde. *Energy & Fuels* **2012**, *26*, 5281-5293, doi:10.1021/ef3007454.

82. Patil, S.K.R.; Lund, C.R.F. Formation and growth of humins via aldol addition and condensation during acid-catalyzed conversion of 5-hydroxymethylfurfural. *Energy & Fuels* **2011**, *25*, 4745-4755, doi:10.1021/ef2010157.
83. Sievers, C.; Musin, I.; Marzialetti, T.; Olarte, M.B.V.; Agrawal, P.K.; Jones, C.W. Acid-catalyzed conversion of sugars and furfurals in an ionic-liquid phase. *ChemSusChem* **2009**, *2*, 665-671, doi:10.1002/cssc.200900092.
84. Kim, Y.C.; Lee, H.S. Selective synthesis of furfural from xylose with supercritical carbon dioxide and solid acid catalyst. *Journal of Industrial and Engineering Chemistry* **2001**, *7*, 424-429.
85. Campos Molina, M.J.; Mariscal, R.; Ojeda, M.; Lopez Granados, M. Cyclopentyl methyl ether: a green co-solvent for the selective dehydration of lignocellulosic pentoses to furfural. *Bioresource Technology* **2012**, *126*, 321-327, doi:10.1016/j.biortech.2012.09.049.
86. Dumesic, J.A.; Roman-Leshkov, Y.; Dumesic, J. Production of liquid alkanes in the jet fuel range (c8-c15) from biomass-derived carbohydrates. WO2008151178-A1; US2009124839-A1; EP2164928-A1; US7880049-B2.
87. Parejas, A.; Montes, V.; Hidalgo-Carrillo, J.; Sanchez-Lopez, E.; Marinas, A.; Urbano, F.J. Microemulsion and sol-gel synthesized ZrO_2-MgO catalysts for the liquid-phase dehydration of xylose to furfural. *Molecules* **2017**, *22*, doi:10.3390/molecules22122257.
88. Hua, D.R.; Wu, Y.L.; Liu, Y.F.; Chen, Y.; Yang, M.D.; Lu, X.N.; Li, J. Preparation of furfural and reaction kinetics of xylose dehydration to furfural in high-temperature water. *Petroleum Science* **2016**, *13*, 167-172, doi:10.1007/s12182-015-0069-y.

89. Hu, X.; Westerhof, R.J.M.; Dong, D.; Wu, L.; Li, C.-Z. Acid-catalyzed conversion of xylose in 20 solvents: insight into interactions of the solvents with xylose, furfural, and the acid catalyst. *ACS Sustainable Chemistry & Engineering* **2014**, *2*, 2562-2575, doi:10.1021/sc5004659.
90. Fogg, D.E.; dos Santos, E.N. Tandem catalysis: a taxonomy and illustrative review. *Coordination Chemistry Reviews* **2004**, *248*, 2365-2379, doi:10.1016/j.ccr.2004.05.012.
91. Climent, M.J.; Corma, A.; Iborra, S. Heterogeneous catalysts for the one-pot synthesis of chemicals and fine chemicals. *Chemical Reviews* **2011**, *111*, 1072-1133, doi:10.1021/cr1002084.
92. Climent, M.J.; Corma, A.; Hernandez, J.C.; Hungria, A.B.; Iborra, S.; Martinez-Silvestre, S. Biomass into chemicals: One-pot two- and three-step synthesis of quinoxalines from biomass-derived glycols and 1,2-dinitrobenzene derivatives using supported gold nanoparticles as catalysts. *Journal of Catalysis* **2012**, *292*, 118-129, doi:10.1016/j.jcat.2012.05.002.
93. Agirrezabal-Telleria, I.; Larreategui, A.; Requies, J.; Guemez, M.B.; Arias, P.L. Furfural production from xylose using sulfonic ion-exchange resins (Amberlyst) and simultaneous stripping with nitrogen. *Bioresource Technology* **2011**, *102*, 7478-7485, doi:10.1016/j.biortech.2011.05.015.
94. Chareonlimkun, A.; Champreda, V.; Shotipruk, A.; Laosiripojana, N. Catalytic conversion of sugarcane bagasse, rice husk and corncob in the presence of TiO_2, ZrO_2 and mixed-oxide TiO_2-ZrO_2 under hot compressed water (HCW) condition. *Bioresource Technology* **2010**, *101*, 4179-4186, doi:10.1016/j.biortech.2010.01.037.
95. Zhang, J.; Zhuang, J.; Lin, L.; Liu, S.; Zhang, Z. Conversion of D-xylose into furfural with mesoporous molecular sieve MCM-41 as catalyst and butanol as the extraction phase. *Biomass & Bioenergy* **2012**, *39*, 73-77, doi:10.1016/j.biombioe.2010.07.028.

96. Shi, X.J.; Wu, Y.L.; Li, P.P.; Yi, H.F.; Yang, M.D.; Wang, G.H. Catalytic conversion of xylose to furfural over the solid acid SO_4^{2-}/ZrO_2-Al_2O_3/SBA-15 catalysts. *Carbohydrate Research* **2011**, *346*, 480-487, doi:10.1016/j.carres.2011.01.001.

97. Jeong, G.H.; Kim, E.G.; Kim, S.B.; Park, E.D.; Kim, S.W. Fabrication of sulfonic acid modified mesoporous silica shells and their catalytic performance with dehydration reaction of D-xylose into furfural. *Microporous and Mesoporous Materials* **2011**, *144*, 134-139, doi:10.1016/j.micromeso.2011.04.002.

98. Shirotori, M.; Nishimura, S.; Ebitani, K. One-pot synthesis of furfural derivatives from pentoses using solid acid and base catalysts. *Catalysis Science & Technology* **2014**, *4*, 971-978, doi:10.1039/c3cy00980g.

99. Pholjaroen, B.; Li, N.; Wang, Z.; Wang, A.; Zhang, T. Dehydration of xylose to furfural over niobium phosphate catalyst in biphasic solvent system. *Journal of Energy Chemistry* **2013**, *22*, 826-832.

100. Dias, A.S.; Lima, S.; Carriazo, D.; Rives, V.; Pillinger, M.; Valente, A.A. Exfoliated titanate, niobate and titanoniobate nanosheets as solid acid catalysts for the liquid-phase dehydration of D-xylose into furfural. *Journal of Catalysis* **2006**, *244*, 230-237, doi:10.1016/j.jcat.2006.09.010.

101. Sadaba, I.; Ojeda, M.; Mariscal, R.; Granados, M.L. Silica-poly(styrenesulphonic acid) nanocomposites for the catalytic dehydration of xylose to furfural. *Applied Catalysis B: Environmental* **2014**, *150*, 421-431, doi:10.1016/j.apcatb.2013.12.025.

102. Thi Tuong Vi, T.; Kongparakul, S.; Karnjanakom, S.; Reubroycharoen, P.; Guan, G.; Chanlek, N.; Samart, C. Highly productive xylose dehydration using a sulfonic acid functionalized KIT-6 catalyst. *Fuel* **2019**, *236*, 1156-1163, doi:10.1016/j.fuel.2018.09.089.

103. Li, X.-L.; Pan, T.; Deng, J.; Fu, Y.; Xu, H.-J. Catalytic dehydration of D-xylose to furfural over a tantalum-based catalyst in batch and continuous process. *RSC Advances* **2015**, *5*, 70139-70146, doi:10.1039/c5ra11411j.
104. Agirrezabal-Telleria, I.; Requies, J.; Gueemez, M.B.; Arias, P.L. Dehydration of D-xylose to furfural using selective and hydrothermally stable arenesulfonic SBA-15 catalysts. *Applied Catalysis B: Environmental* **2014**, *145*, 34-42, doi:10.1016/j.apcatb.2012.11.010.
105. Zhang, J.; Li, J.; Lin, L. Dehydration of Sugar Mixture to HMF and Furfural over SO42-/ZrO2-TiO2 Catalyst. *Bioresources* **2014**, *9*, 4194-4204.
106. Agirrezabal-Telleria, I.; Hemmann, F.; Jaeger, C.; Arias, P.L.; Kemnitz, E. Functionalized partially hydroxylated MgF_2 as catalysts for the dehydration of d-xylose to furfural. *Journal of Catalysis* **2013**, *305*, 81-91, doi:10.1016/j.jcat.2013.05.005.
107. Antunes, M.M.; Lima, S.; Fernandes, A.; Candeias, J.; Pillinger, M.; Rocha, S.M.; Ribeiro, M.F.; Valente, A.A. Catalytic dehydration of D-xylose to 2-furfuraldehyde in the presence of Zr-(W,Al) mixed oxides. Tracing by-products using two-dimensional gas chromatography-time-of-flight mass spectrometry. *Catalysis Today* **2012**, *195*, 127-135, doi:10.1016/j.cattod.2012.03.066.
108. Russo, P.A.; Lima, S.; Rebuttini, V.; Pillinger, M.; Willinger, M.-G.; Pinna, N.; Valente, A.A. Microwave-assisted coating of carbon nanostructures with titanium dioxide for the catalytic dehydration of D-xylose into furfural. *RSC Advances* **2013**, *3*, 2595-2603, doi:10.1039/c2ra22874b.
109. Shen, W.Q.; Tompsett, G.A.; Hammond, K.D.; Xing, R.; Dogan, F.; Grey, C.P.; Conner, W.C.; Auerbach, S.M.; Huber, G.W. Liquid phase aldol condensation reactions with $MgO\text{-}ZrO_2$ and shape-selective

nitrogen-substituted NaY. *Applied Catalysis A: General* **2011**, *392*, 57-68, doi:10.1016/j.apcata.2010.10.023.

110. Cota, I.; Ramirez, E.; Medina, F.; Sueiras, J.E.; Layrac, G.; Tichit, D. New synthesis route of hydrocalumite-type materials and their application as basic catalysts for aldol condensation. *Applied Clay Science* **2010**, *50*, 498-502, doi:10.1016/j.clay.2010.09.019.
111. Resasco, D.E.; Sitthisa, S.; Faria, J.; Prasomsri; T.; Ruiz, .M.P. Furfurals as chemical platform forbiofuels production. En *Heterogeneous Catalysis in Biomass to Chemicals and Fuels*, Kubičková, D.; Kubička, D. Editores, Research Signpost, 2011.
112. West, R.M.; Liu, Z.Y.; Peter, M.; Gaertner, C.A.; Dumesic, J.A. Carbon-carbon bond formation for biomass-derived furfurals and ketones by aldol condensation in a biphasic system. *Journal of Molecular Catalysis A: Chemical* **2008**, *296*, 18-27, doi:10.1016/j.molcata.2008.09.001.
113. Climent, M.J.; Corma, A.; Fornes, V.; Guil-Lopez, R.; Iborra, S. Aldol condensations on solid catalysts: A cooperative effect between weak acid and base sites. *Advanced Synthesis & Catalysis* **2002**, *344*, 1090-1096, doi:10.1002/1615-4169(200212)344:10<1090::aid-adsc1090>3.0.co;2-x.
114. Sadaba, I.; Ojeda, M.; Mariscal, R.; Richards, R.; Lopez Granados, M. Mg-Zr mixed oxides for aqueous aldol condensation of furfural with acetone: Effect of preparation method and activation temperature. *Catalysis Today* **2011**, *167*, 77-83, doi:10.1016/j.cattod.2010.11.059.
115. Fakhfakh, N.; Cognet, P.; Cabassud, M.; Lucchese, Y.; Días de los Rios, M.. Stoichio-kinetic modeling and optimization of chemical synthesis: Application to the aldolic condensation of furfural on acetone. *Chemical Engineering and Processing* **2008**, *47*, 349-362, doi:10.1016/j.cep.2007.01.015.
116. Xing, R.; Subrahmanyam, A.V.; Olcay, H.; Qi, W.; van Walsum, G.P.; Pendse, H.; Huber, G.W. Production of jet and diesel fuel range alkanes

from waste hemicellulose-derived aqueous solutions. *Green Chemistry* **2010**, *12*, 1933-1946, doi:10.1039/c0gc00263a.

117. O'Neill, R.E.; Vanoye, L.; De Bellefon, C.; Aiouache, F. Aldol-condensation of furfural by activated dolomite catalyst. *Applied Catalysis B: Environmental* **2014**, *144*, 46-56, doi:10.1016/j.apcatb.2013.07.006.
118. Parejas, A.; Cosano, D.; Hidalgo-Carrillo, J.; Ruiz, J.R.; Marinas, A.; Jiménez-Sanchidrián, C.; Urbano, F.J. Aldol condensation of furfural with acetone over Mg/Al mixed oxides. Influence of water and synthesis method. *Catalysts* **2019**, *9*, doi:10.3390/cata9020203.
119. Nielsen, A.T.; Houlihan, W.J. The aldol condensation. *Organic reactions* **2004**, 1-438, doi: 10.1002/0471264180.or016.01.
120. Zhang, Z.; Dong, Y.W.; Wang, G.W. Efficient and clean aldol condensation catalyzed by sodium carbonate in water. *Chemistry Letters* **2003**, *32*, 966-967, doi:10.1246/cl.2003.966.
121. Wang, G.W.; Zhang, Z.; Dong, Y.W. Environmentally friendly and efficient process for the preparation of beta-hydroxyl ketones. *Organic Process Research & Development* **2004**, *8*, 18-21, doi:10.1021/op0341263.
122. Hora, L.; Kelbichova, V.; Kikhtyanin, O.; Bortnovskiy, O.; Kubicka, D. Aldol condensation of furfural and acetone over Mg-Al layered double hydroxides and mixed oxides. *Catalysis Today* **2014**, *223*, 138-147, doi:10.1016/j.cattod.2013.09.022.
123. Ordonez, S.; Diaz, E.; Leon, M.; Faba, L. Hydrotalcite-derived mixed oxides as catalysts for different C-C bond formation reactions from bioorganic materials. *Catalysis Today* **2011**, *167*, 71-76, doi:10.1016/j.cattod.2010.11.056.
124. Kikhtyanin, O.; Bulanek, R.; Frolich, K.; Cejka, J.; Kubicka, D. Aldol condensation of furfural with acetone over ion-exchanged and

impregnated potassium BEA zeolites. *Journal of Molecular Catalysis A: Chemical* **2016**, *424*, 358-368, doi:10.1016/j.molcata.2016.09.014.

125. Kikhtyanin, O.; Kelbichova, V.; Vitvarova, D.; Kubu, M.; Kubicka, D. Aldol condensation of furfural and acetone on zeolites. *Catalysis Today* **2014**, *227*, 154-162, doi:10.1016/j.cattod.2013.10.059.
126. Su, M.; Li, W.; Zhang, T.; Xin, H.; Li, S.; Fan, W.; Ma, L. Production of liquid fuel intermediates from furfural via aldol condensation over Lewis acid zeolite catalysts. *Catalysis Science & Technology* **2017**, *7*, 3555-3561, doi:10.1039/c7cy01028a.
127. Fujita, S.-I.; Segawa, S.; Kawashima, K.; Nie, X.; Erata, T.; Arai, M. One-pot room-temperature synthesis of mg containing mcm-41 mesoporous silica for aldol reactions. *Journal of Materials Science & Technology* **2016**, doi:10.1016/j.jmst.2016.08.025.
128. Ramos, R.; Tisler, Z.; Kikhtyanin, O.; Kubicka, D. Solvent effects in hydrodeoxygenation of furfural-acetone aldol condensation products over Pt/TiO_2 catalyst. *Applied Catalysis A: General* **2017**, *530*, 174-183, doi:10.1016/j.apcata.2016.11.023.
129. Ulfa, S.M.; Mahfud, A.; Nabilah, S.; Rahman, M.F.; Influence of solvent on liquid phase hydrodeoxygenation of furfural-acetone condensation adduct using Ni/Al_2O_3-ZrO_2 catalysts. IOP Conference Series: Materials Science and Engineering. 172, 012053.
130. Dong Nguyen, T.; Kikhtyanin, O.; Ramos, R.; Kothari, M.; Ulbrich, P.; Munshi, T.; Kubicka, D. Nanosized TiO_2: A promising catalyst for the aldol condensation of furfural with acetone in biomass upgrading. *Catalysis Today* **2016**, *277*, 97-107, doi:10.1016/j.cattod.2015.11.027.
131. Sadaba, I.; Ojeda, M.; Mariscal, R.; Fierro, J.L.G.; Granados, M.L. Catalytic and structural properties of co-precipitated Mg-Zr mixed oxides for furfural valorization via aqueous aldol condensation with acetone.

Applied Catalysis B: Environmental **2011**, *101*, 638-648, doi:10.1016/j.apcatb.2010.11.005.

132. Faba, L.; Diaz, E.; Ordonez, S. Improvement on the catalytic performance of MgZr mixed oxides for furfuralacetone aldol condensation by supporting on mesoporous carbons. *ChemSusChem* **2013**, *6*, 463-473, doi:10.1002/cssc.201200710.
133. Kikhtyanin, O.; Chlubna, P.; Jindrova, T.; Kubicka, D. Peculiar behavior of MWW materials in aldol condensation of furfural and acetone. *Dalton Transactions* **2014**, *43*, 10628-10641, doi:10.1039/c4dt00184b.
134. Leyrit, P.; McGill, C.; Quignard, F.; Choplin, A. A novel heterogeneous molecular catalyst for the Meerwein-Ponndorf-Verley and Oppenauer reactions. *Journal of Molecular Catalysis A: Chemical* **1996**, *112*, 395-400, doi:10.1016/1381-1169(96)00234-8.
135. Axpuac, S.; Aramendia, M.A.; Hidalgo-Carrillo, J.; Marinas, A.; Marinas, J.M.; Montes-Jimenez, V.; Urbano, F.J.; Borau, V. Study of structure-performance relationships in Meerwein-Ponndorf-Verley reduction of crotonaldehyde on several magnesium and zirconium-based systems. *Catalysis Today* **2012**, *187*, 183-190, doi:10.1016/j.cattod.2011.10.004.
136. Aramendia, M.A.; Borau, V.; Jimenez, C.; Marinas, J.M.; Ruiz, J.R.; Urbano, F. Reduction of alpha,beta-unsaturated aldehydes with basic MgO/M_2O_3 catalysts (M=Al, Ga, In). *Applied Catalysis A: General* **2003**, *249*, 1-9, doi:10.1016/s0926-860x(03)00163-7.
137. Meerwein, H.; Schmidt, R. Ein neues Verfahren zur Reduktion von Aldehyden und Ketonen. *Justus Liebigs Annalen der Chemie* **1925**, *444*, 221-238, doi:10.1002/jlac.19254440112.
138. Iglesias, J.; Antonio Melero, J.; Morales, G.; Moreno, J.; Segura, Y.; Paniagua, M.; Cambra, A.; Hernandez, B. Zr-SBA-15 Lewis acid catalyst: activity in Meerwein Ponndorf Verley reduction. *Catalysts* **2015**, *5*, 1911-1927, doi:10.3390/catal5041911.

139. Polshettiwar, V.; Varma, R.S. Revisiting the Meerwein-Ponndorf-Verley reduction: a sustainable protocol for transfer hydrogenation of aldehydes and ketones. *Green Chemistry* **2009**, *11*, 1313-1316, doi:10.1039/b913079a.
140. Corma, A.; Domine, M.E.; Valencia, S. Water-resistant solid Lewis acid catalysts: Meerwein-Ponndorf-Verley and Oppenauer reactions catalyzed by tin-beta zeolite. *Journal of Catalysis* **2003**, *215*, 294-304, doi:10.1016/s0021-9517(03)00014-9.
141. Huber, G.W.; Iborra, S.; Corma, A. Synthesis of transportation fuels from biomass: Chemistry, catalysts, and engineering. *Chemical Reviews* **2006**, *106*, 4044-4098, doi:10.1021/cr068360d.
142. Chuah, G.K.; Jaenicke, S.; Zhu, Y.Z.; Liu, S.H. Meerwein-Ponndorf-Verley reduction over heterogeneous catalysts. *Current Organic Chemistry* **2006**, *10*, 1639-1654, doi:10.2174/138527206778249621.
143. Shiner Jr, V.J.; Whittaker, D. Kinetics of the Meerwein-Ponndorf-Verley reaction. *Journal of the American Chemical Society* **1969**, *91*, 394-398, doi: 10.1021/ja01030a031.
144. Gonell, F.; Boronat, M.; Corma, A. Structure-reactivity relationship in isolated Zr sites present in Zr-zeolite and ZrO_2 for the Meerwein-Ponndorf-Verley reaction. *Catalysis Science & Technology* **2017**, *7*, 2865-2873, doi:10.1039/c7cy00567a.
145. Cha, J.S. Recent developments in Meerwein-Ponndorf-Verley and related reactions for the reduction of organic functional groups using aluminum, boron, and other metal reagents: A review. *Organic Process Research & Development* **2006**, *10*, 1032-1053, doi:10.1021/op068002c.
146. Uysal, B.; Aksu, Y.; Oksal, B.S. Chemoselective reduction of alpha,beta-unsaturated aldehydes and ketones over mesoporous $B(OiPr)_3$-MCM-41 catalyst via MPV reduction process: preparation, characterization and

catalytic application. *Journal of Porous Materials* **2013**, *20*, 115-127, doi:10.1007/s10934-012-9580-3.

147. Ooi, T.; Miura, T.; Takaya, K.; Ichikawa, H.; Maruoka, K. $Zr(OBut)_4$ as an effective promoter for the Meerwein-Ponndorf-Verley alkynylation and cyanation of aldehydes: development of new asymmetric cyanohydrin synthesis. *Tetrahedron* **2001**, *57*, 867-873, doi:10.1016/s0040-4020(00)01040-1.
148. Zhu, Y.Z.; Chuah, G.; Jaenicke, S. Chemo- and regioselective Meerwein-Ponndorf-Verley and Oppenauer reactions catalyzed by Al-free Zr-zeolite beta. *Journal of Catalysis* **2004**, *227*, 1-10, doi:10.1016/j.jcat.2004.05.037.
149. Zhu, Y.; Chuah, G.-K.; Jaenicke, S. Selective Meerwein-Ponndorf-Verley reduction of alpha, beta-unsaturated aldehydes over Zr-zeolite beta. *Journal of Catalysis* **2006**, *241*, 25-33, doi:10.1016/j.jcat.2006.04.008.
150. Aramendia, M.A.; Borau, V.; Jimenez, C.; Marinas, J.M.; Ruiz, J.R.; Urbano, F.J. Influence of the preparation method on the structural and surface properties of various magnesium oxides and their catalytic activity in the Meerwein-Ponndorf-Verley reaction. *Applied Catalysis A: General* **2003**, *244*, 207-215, doi:10.1016/s0926-860x(02)00213-2.
151. Komanoya, T.; Nakajima, K.; Kitano, M.; Hara, M. Synergistic catalysis by lewis acid and base sites on ZrO_2 for Meerwein-Ponndorf-Verley reduction. *Journal of Physical Chemistry C* **2015**, *119*, 26540-26546, doi:10.1021/acs.jpcc.5b08355.
152. Jimenez-Sanchidrian, C.; Ruiz, J.R. Tin-containing hydrotalcite-like compounds as catalysts for the Meerwein-Ponndorf-Verley reaction. *Applied Catalysis A: General* **2014**, *469*, 367-372, doi:10.1016/j.apcata.2013.09.049.
153. Kumbhar, P.S.; Sanchez-Valente, J.; Lopez, J.; Figueras, F. Meerwein-Ponndorf-Verley reduction of carbonyl compounds catalysed by Mg-Al

hydrotalcite. *Chemical Communications* **1998**, 535-536, doi:10.1039/a708431e.

154. Hidalgo, J.M.; Jimenez-Sanchidrian, C.; Rafael Ruiz, J. Delaminated layered double hydroxides as catalysts for the Meerwein-Ponndorf-Verley reaction. *Applied Catalysis A: General* **2014**, *470*, 311-317, doi:10.1016/j.apcata.2013.11.007.
155. Zhou, S.; Dai, F.; Xiang, Z.; Song, T.; Liu, D.; Lu, F.; Qi, H. Zirconium-lignosulfonate polyphenolic polymer for highly efficient hydrogen transfer of biomass-derived oxygenates under mild conditions. *Applied Catalysis B: Environmental* **2019**, *248*, 31-43, doi:10.1016/j.apcatb.2019.02.011.
156. Hao, J.; Han, L.; Sha, Y.; Yu, X.; Liu, H.; Ma, X.; Yang, Y.; Zhou, H.; Liu, Q. Facile use of lignite as robust organic ligands to construct Zr-based catalysts for the conversion of biomass derived carbonyl platforms into alcohols. *Fuel* **2019**, *239*, 1304-1314, doi:10.1016/j.fuel.2018.11.129.
157. Kim, M.S.; Simanjuntak, F.S.H.; Lim, S.; Jae, J.; Ha, J.-M.; Lee, H. Synthesis of alumina-carbon composite material for the catalytic conversion of furfural to furfuryl alcohol. *Journal of Industrial and Engineering Chemistry* **2017**, *52*, 59-65, doi:10.1016/j.jiec.2017.03.024.
158. Sha, Y.; Xiao, Z.; Zhou, H.; Yang, K.; Song, Y.; Li, N.; He, R.; Zhi, K.; Liu, Q. Direct use of humic acid mixtures to construct efficient Zr-containing catalysts for Meerwein-Ponndorf-Verley reactions. *Green Chemistry* **2017**, *19*, 1829-1837, doi:10.1039/c7gc01925d.
159. Zhou, H.; Xiaoo, Z.; Li, L.; Hao, J.; Yang, K.; Li, N.; He, R.; Liu, Q. Using benzene carboxylic acids to prepare zirconium-based catalysts for the conversion of biomass-derived furfural. *International Journal of Coal Science & Technology* **2017**, 1-9, doi:10.1007/s40789-017-0181-2.
160. Li, H.; He, J.; Riisager, A.; Saravanamurugan, S.; Song, B.; Yang, S. Acid-base bifunctional zirconium N-alkyltriphosphate nanohybrid for

hydrogen transfer of biomass-derived carboxides. *ACS Catalysis* **2016**, *6*, 7722-7727, doi:10.1021/acscatal.6b02431.

Capítulo II.

Hipótesis y Objetivos

Hipótesis y objetivos

A continuación se exponen las hipótesis y los objetivos que se han conseguido en esta Tesis Doctoral.

Hipótesis 1

El furfural es una de las principales moléculas plataforma obtenidas a partir de la biomasa, pudiéndo ser transformada en una amplia variedad de compuestos y productos químicos. Se trata de un material de partida y precursor natural para la obtención de compuestos furánicos como tetrahidrofurano, ácido furoico, metiltetrahidrofurano, entre otros. Además puede ser utilizado en industrias como la agroquímica, resinas, farmaceútica, etc.

El aumento de la demanda del furfural ha provocado la búsqueda de rutas sintéticas alternativas a las actualmente empleadas. Así, se conseguiría evitar el empleo de catalizadores homogéneos ácidos para la transformación de xilosa (procedente de la biomasa lignocelulósica) a furfural, los cuales aumentan los costes procedentes del deterioro de reactores y las emisiones contaminantes provenientes del proceso. Por lo que, una solución para mejorar la reacción es el uso de catalizadores heterogéneos. Además, debido a la alta reactividad de la molécula de furfural pueden darse reacciones secundarias que se podrían impedir con la correcta elección de un disolvente durante la reacción, como el uso de sistemas bifásicos con los que puede ser extraído fácilmente el furfural obtenido tras la síntesis, mediante una extracción en fase líquida.

Objetivo 1

El objetivo ha sido llevar a cabo la reacción de deshidratación de xilosa para obtener furfural, empleando catalizadores heterogéneos de óxido de

zirconio y magnesio y óxidos mixtos de ellos con características ácido-básicas, sintetizados mediante el método de sol-gel y de microemulsión. Como disolvente, se ha utilizado un sistema bifásico compuestos por agua/tolueno o agua/butan-2-ol. Los resultados obtenidos se encuentran recogidos en el Capítulo 3, en el artículo **"Microemulsion and sol-gel synthesized ZrO_2-MgO catalysts for the liquid-phase dehydration of xylose to furfural"**.

Hipótesis 2

Un tema actual es la búsqueda de alternativas renovables al empleo de combustibles fósiles siendo la biomasa una solución. El furfural como se ha comentado en la hipótesis 1, se trata de un compuesto de partida para la obtención de otros compuestos. En concreto, puede ser empleado como energía renovable para la producción de diésel a través de la reacción de condensación aldólica del furfural y la acetona para la obtención de 1,5-bis-(2-furanil)-1,4-pendien-3-ona. Posteriormente, este compuesto mediante una deshidratación/deshidrogenación puede ser convertido a alcanos líquidos con longitud de cadena de 13 átomos de carbono (diésel).

La reacción de condensación aldólica es un proceso de formación de enlaces C-C, con la finalidad de convertir moléculas con un bajo peso molecular en moléculas de mayor peso. El proceso tiene lugar entre dos compuestos carbonílicos en presencia de un catalizador ácido o básico, siendo más empleado los catalizadores básicos. Para que se pueda dar el proceso es necesaria la presencia de un protón reactivo en α en al menos uno de los dos compuestos carbonílicos. Así, se formaría su correspondiente enol y luego, tras una reacción de deshidratación, su enona conjugada.

Por lo tanto, es recomendable utilizar un catalizador heterogéneo con las características necesarias para poder obtener una actividad catalítica con altas

conversiones y selectividades al producto de interés, mediante un proceso no contaminante con el medio ambiente y con una aplicabilidad industrial.

Objetivo 2

El objetivo ha sido emplear como catalizadores heterogéneos óxidos mixtos de Mg/Al, obtenidos a partir de la calcinación de hidróxidos dobles laminares, en la reacción de condensación aldólica del furfural y la acetona para la formación de 1,5-bis-(2-furanil)-1,4-pendien-3-ona. Durante la actividad catalítica de los óxidos mixtos de Mg/Al se ha estudiado la influencia de dos variables que se modificaron en su síntesis (calentamiento convencional o microondas con la presencia o ausencia de Pluronic 123 como surfactante), la influencia de la temperatura de reacción y el efecto del agua (tanto prehidratando los sólidos antes de los estudios catalíticos como añadiendo agua en el medio de reacción en mezclas agua/tolueno). Los resultados obtenidos se encuentran recogidos en el Capítulo 4, en el artículo **"Aldol condensation of furfural with acetone over Mg/Al oxides. Influence of water and synthesis method".**

Hipótesis 3

El alcohol furfurílico es el principal producto obtenido del furfural, debido a que un 65% del furfural producido es empleado para su síntesis. Es sintetizado mediante la hidrogenación del furfural, normalmente, en fase líquida y utilizando catalizadores basados en Ni, Co, Cu, Pt y Pd. Destaca por sus aplicaciones en la industria química para la producción de resinas y disolventes, la elaboración de fibras sintéticas, la modificación de fenoles, la síntesis de fármacos, etc.

La transformación de furfural a alcohol furfurílico también puede tener lugar en presencia de un donador de hidrógeno, normalmente un alcohol

secundario como puede ser el propan-2-ol, y un catalizador óxido metálico (ácido de Lewis). Esta reacción recibe el nombre de reducción de Meerwein-Ponndorf-Verley (MPV) y durante ella se formará un estado de transición de seis miembros, para que el propan-2-ol se transforme a acetona y el furfural a alcohol furfurílico.

Algunos de los catalizadores heterogéneos que han sido estudiados son zeolitas de zirconio, óxidos metálicos e hidrotalcitas.

Objetivo 3

El objetivo ha sido llevar a cabo la reducción MPV de furfural para la obtención de alcohol furfurílico en presencia de catalizadores de ZrO_x, TiO_x, MgO_x, sistemas mixtos de Mg-Ti y sistemas mixtos de Zr-Ti calcinados a 200 ºC y conocer cuál es la naturaleza de los centros activos responsables de la actividad catalítica conseguida. Se ha escogido esta temperatura porque en investigaciones previas se ha comprobado que los sólidos de zirconio calcinados a estas temperaturas mostraron una mayor selectividad a la obtención de alcohol furfurílico en esta reacción.

Además, se ha estudiado la influencia de la reacción MPV al variar el dispositivo experimental, utilizándose calefacción convencional y por microondas. Los resultados obtenidos se encuentran recogidos en el Capítulo 5, en el artículo **"MPV reduction of furfural to furfuryl alcohol on Mg, Zr, Ti, Zr-Ti, and Mg-Ti solids: influence of acid-base properties".**

Capítulo III.

Resultados y discusión (Paper 1)

CHAPTER III. RESULTS AND DISCUSSION: MICROEMULSION AND SOL-GEL SYNTHESIZED ZrO_2-MgO CATALYSTS FOR THE LIQUID-PHASE DEHYDRATION OF XYLOSE TO FURFURAL

PAPER 1

Microemulsion and sol-gel synthesized ZrO_2-MgO catalysts for the liquid-phase dehydration of xylose to furfural

*Almudena Parejas, Vicente Montes, Jesús Hidalgo-Carrillo, Elena Sánchez-López, Alberto Marinas and Francisco J. Urbano **

Department of Organic Chemistry, Institute for Research in Fine Chemistry and Nanochemistry, IUIQFN, Universidad de Córdoba, Campus de Rabanales, Marie Curie Building, E-14014 Córdoba, Spain.

q12pabaa@uco.es (A.P.); vicente.montesjimenez@ucalgary.ca (V.M.); q12hicaj@uco.es (J.H.C.); g02saloe@uco.es (E.S.L.).

* Correspondence: alberto.marinas@uco.es (A.M.); fj.urbano@uco.es (F.J.U.); Tel.: +34957218638.

Published in *Molecules* **2017**, 22, 2257; doi: 10.3390/molecules22122257.

Abstract

Two series of catalysts were prepared by sol-gel and microemulsion synthetic procedure (SG and ME, respectively). Each series includes both pure Mg and Zr solids as well as Mg-Zr mixed solids with 25%, 50% and 75% nominal Zr content. The whole set of catalysts was characterized from thermal, structural and surface chemical points of view and subsequently applied to the liquid-phase xylose dehydration to furfural. Reactions were carried out in either a high-pressure autoclave or in an atmospheric pressure multi-reactor under a biphasic (organic/water) reaction mixture. Butan-2-ol and toluene were essayed as organic solvents. Catalysts prepared by microemulsion retained part of the surfactant used in the synthetic procedure, mainly associated with the Zr part of the solid. The MgZr-SG solid presented the highest surface acidity while the Mg3Zr-SG one exhibited the highest surface basicity among mixed systems. Xylose dehydration in the high-pressure system and with toluene/water solvent mixture led to the highest furfural yield. Moreover, the yield of furfural increases with the Zr content of the catalyst. Therefore, the catalysts constituted of pure ZrO_2 (especially Zr-SG) are the most suitable to carry out the process under study although MgZr mixed solids could be also suitable for overall processes with additional reaction steps.

Keywords: xylose dehydration; furfural; MgO-ZrO_2 mixed catalysts; microemulsion synthesis; sol-gel synthesis; solvent effect.

III.1. Introduction

Nowadays, one of the priorities of scientists is the search for alternatives to non-renewable energies. A renewable solution for this challenge is biomass, which can provide both energy [1] and useful chemicals compounds for industry [2].

The estimated biomass production is about 10^{11} ton per year whose 60% is terrestrial and 40% aquatic. However, only 3% of the produced biomass is utilized for human-derived applications [3]. Therefore, the transformation of biomass into platform molecules that can be further converted into high-added value chemicals is a hot topic nowadays [4,5].

Biomass is composed by carbohydrates (75%), lignin (20%) and a mixture of triglycerides, proteins and terpenes (5%) [5] Lignocellulose is the main constituent of plant cell walls whose hydrolysis yields a mixture of C5 and C6 sugars as well as aromatic compounds (lignin). Therefore, valorization of pentoses and hexoses, such as xylose or glucose, is very interesting from the chemical point of view [4].

Furfural is one of the top platform molecules that can be obtained from biomass [6,7] and that is able to be further transformed into a wide range of chemicals by chemo and /or enzymatic transformations. It is a natural precursor to a range of furan-based chemicals and solvents such as methyltetrahydrofuran, tetrahydrofuran, tetrahydrofurfuryl alcohol and furoic acid, among others. Compounds derived from furfural are used in the pharmaceutical industry, and as plastics, agricultural fungicides or nematocides, lubricants, resins, bleaching agents, food and beverage additives, wood modifiers or book preservatives, among other uses. Moreover, within the last decade the conversion of furfural into diesel by means of a combination of

dehydration, aldol condensation and hydrogenation reactions have been described [8-12].

Due to the continuous demand for furfural, the search for alternative synthetic routes or the improvement of the existing ones is still an active research area. The classic industrial furfural production process is based on the treatment of pentose-containing lignocellulosic biomass with mineral acids (H_2SO_4, HCl) [13]. However, mineral acids cause corrosion of the reactors and generate toxic effluents; therefore, the design of active, selective and stable heterogeneous solid acid catalysts is a key point to reduce costs of reactors as well as the environmental impact of the process. An additional effort should be made to improve the process sustainability by designing water resistant and recyclable solid acid catalysts. Furthermore, if a chemical process is to be coupled following the synthesis of furfural in the so-called cascade processes, it may be necessary to synthesize catalysts which, in addition to acidic properties, have a second functionality which may be basic sites (e.g., for condensation reactions) or metal centers (for redox processes) [14].

During the process, due to the high reactivity of furfural molecule, several side reactions such as condensation or acetalyzation can take place leading to hemiacetals and oligomers (humines) [15-17]. Additionally, xylose fragmentation reactions can occur producing acetol, lactic acid, glyceraldehyde, etc. [18]. Water is typically the solvent of choice for sugar transformation reactions due to solubility, economic and environmental aspects. However, water favors the formation of humines thus lowering the selectivity to the desired product. An adequate solvent mixture (biphasic systems) can help to reduce these by-products since formed furfural could be rapidly extracted to a second liquid phase thus avoiding further transformation [19-21]. Toluene, n-butanol or ethyl butyrate [22,23] can be found among the secondary solvents (extracting agents) reported in the literature. Alternative described solutions

such as the use of ionic liquids [24] or supercritical carbon dioxide [25] are expensive or technologically demanding.

This piece of research deals with the synthesis and characterization of zirconium/magnesium mixed oxides in order to obtain bifunctional acid/base solids. Two series of catalysts were synthesized using the sol-gel or microemulsion processes (SG and ME series, respectively). The solids were subsequently tested for xylose dehydration to furfural. The final goal was to obtain some robust and water-resistant acid-base catalysts that can be active not only for xylose dehydration to furfural but also able to carry out one-pot or cascade reactions for further transformation of furfural [26].

III.2. Results

III.2.1. Catalysts Characterization

Thermogravimetric analysis (TGA) was carried out for the dried gels before thermal treatment at 200 ºC, the obtained results being presented in Figure 1. The TGA profiles obtained for both series of solids were quite similar. As for pure systems, the weight loss for both Mg-SG and Mg-ME systems was around 29% with a single weight loss starting at temperatures around 325 ºC. This weight loss is consistent with the transformation from $Mg(OH)_2$ to MgO (theoretical weight loss around 31%). For pure Zr-SG and Zr-ME solids a more complex profile was obtained with several weight loss spreading over 100-500 ºC temperature range. Overall, the weight loss was 13.9% and 20.8% for Zr-SG and Zr-ME, respectively. Taking into account that the theoretical weight loss associated to the transformation of $ZrO(OH)_2$ into ZrO_2 is around 13%, the weight loss of 20.8% obtained for the Zr-ME gel has to be also ascribed to the burning of the surfactant remaining on the surface of the solid. On the other hand, the fact that the weight loss for Mg-ME and Mg-SG solids is very similar and close to the theoretical value suggests that no surfactant is remaining on the

surface of pure Mg-ME solid. Finally, mixed MgZr solids in both series exhibited an intermediate behavior between both pure Zr and Mg solids.

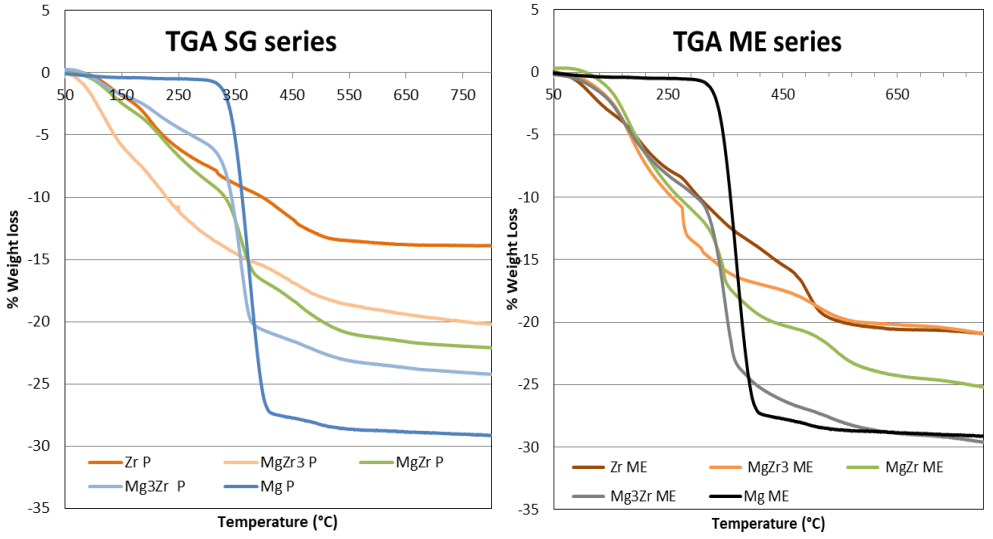

(**a**) (**b**)

Figure 1. Thermogravimetric analysis (TGA) of the dried gels corresponding to both series of solids synthesized: (**a**) Sol-Gel and (**b**) Microemulsion.

Differential thermal analysis (DSC) of the solids is presented in Figure 2 where it can be observed that for pure Mg-based solids there is a single endothermic signal at 375 ºC associated to the transition from $Mg(OH)_2$ to MgO [27]. No differences were observed between Mg-SG and Mg-ME solids in DSC profiles, in agreement with the TGA data. On the contrary, Zr-SG and Zr-ME exhibited very different DSC profiles. The first one only presents an exothermic peak (glow exotherm) centered at 450 °C associated to the crystallization of the low-temperature tetragonal metastable phase of ZrO_2 [28]. For mixed solids in the SG series, the glow exotherm is also observed but is weaker and shifted to higher temperatures (up to 650°C for Mg3Zr-SG), indicating that crystallization is somehow inhibited or retarded by the presence of Mg species [29].

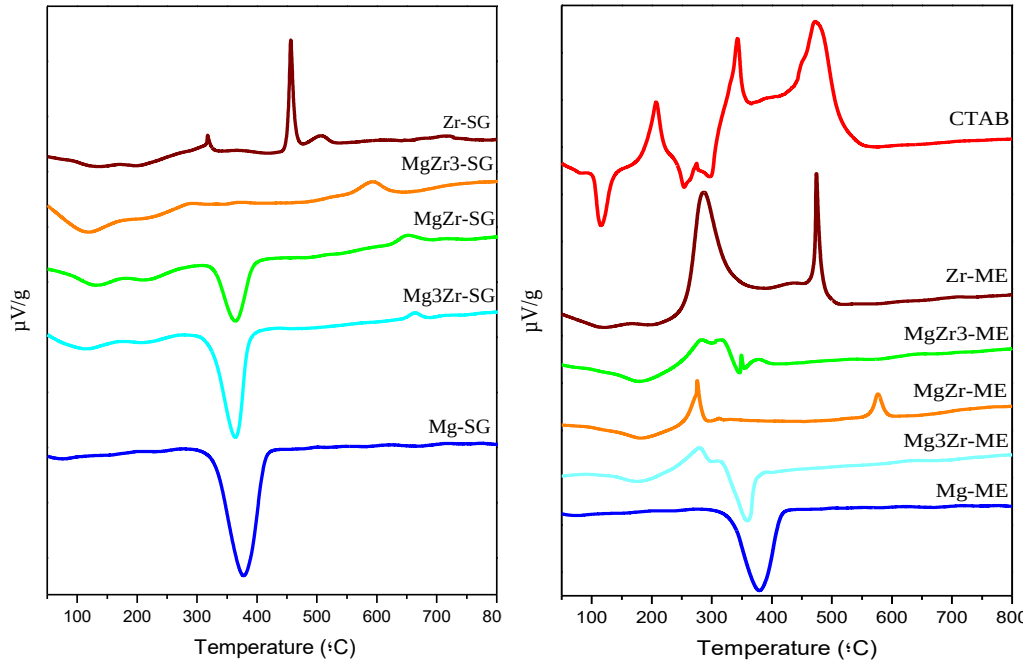

Figure 2. Differential thermal analysis (DSC) profiles obtained for the dried gels corresponding to both series of solids synthesized: (**a**) Sol-Gel and (**b**) Microemulsion.

As far as the ME series is concerned, Zr-ME solid presents a DSC profile with two exothermic peaks; the above commented glow exotherm at 475 ºC and another one at lower temperature (around 300 ºC) associated to the combustion of the organic part of the surfactant remaining on the catalyst surface. This peak is smaller as the magnesium content increases, until complete disappearance for Mg-ME. Again, it seems that the amount of surfactant retained on the surface of the solids is greater for the systems containing the highest Zr content. The DSC profile for pure surfactant, CTAB, is included in Figure 2 for comparison. It is assumed that the CTAB combustion takes place at lower temperatures on the surface of the solids.

As far as the chemical composition of the solids is concerned, it was obtained from SEM-EDX and XPS measurements, the results being presented in Table 1. EDX and XPS atomic concentration values are somehow different

to each other and, in this sense, it has to be taken into account that XPS penetration is lower than the EDX one. Therefore, XPS data have to be assumed as a surface composition meanwhile EDX values are associated to bulk chemical composition of the mixed solids. Thus, EDX data indicate that the magnesium content is somehow higher than the nominal value except for the MgZr3-ME solid which is the mixed solid with the lowest magnesium content. It seems that either the precipitation at pH 10 is more efficient for $Mg(OH)_2$ or, more likely, precipitated $ZrO(OH)_2$ species re-dissolve at the precipitating pH.

Table 1. Nominal, EDX and XPS chemical composition (%mol) and textural properties of the catalytic systems synthesized in this work.

	Chemical Composition (Nominal)		**Chemical Composition (EDX)**		**Chemical Composition (XPS)**		**Surface Area**
Catalyst	**Mg**	**Zr**	**Mg**	**Zr**	**Mg**	**Zr**	**BET (m^2/g)**
Mg-SG	100	0.0	100	0.0	100	0.0	41
Mg3Zr- SG	75	25	94.2	5.8	69.4	30.6	119
MgZr- SG	50	50	67.7	32.3	60.3	39.7	173
MgZr3- SG	25	75	32.6	67.4	10.4	89.6	169
Zr- SG	0.0	100	0.0	100	0.0	100	239
Mg-ME	100	0.0	100	0.0	100	0.0	31
Mg3Zr-ME	75	25	90.5	9.5	74.2	25.8	196
MgZr-ME	50	50	70.6	29.4	27.4	72.6	197
MgZr3-ME	25	75	22.2	77.8	3.5	96.5	192
Zr-ME	0.0	100	0.0	100	0.0	100	222

On the other hand, XPS data revealed an opposite behavior, i.e., the Zr content is higher than the nominal value for the mixed solids, except for the MgZr3-ME. This finding implies that ZrO_2 particles are localized on the outer

part of the aggregates while the MgO ones are located within the inner part of the agglomerated particles.

SEM-EDX measurements have revealed that in the solids prepared through the microemulsion technique, in spite they were washed 5 times with chloroform/ethanol, a small amount of bromine coming from surfactant molecules was detected on the solids surface (Supplementary Figure S1). In addition, as the zirconium content increases in ME series, the amount of detected Br is higher (from 0.9% for Mg-ME to 4.3% for Zr-ME), thus pointing out the higher affinity of the surfactant for the ZrO_2 particles.

Nitrogen adsorption-desorption isotherms for the solids calcined at 200 ºC were obtained (file. Red arrow marks Br signal, Supplementary Figure S2) and the BET surface area presented in Table 1. The largest surface area was obtained for pure Zr-SG solid (239 $m^2 \cdot g^{-1}$) while Zr-ME exhibited a somehow lower surface area (222 $m^2 \cdot g^{-1}$), revealing that the surfactant remaining on the catalyst negatively affects its surface area. On the other hand, pure Mg-SG and Mg-ME solids present the lowest surface area (41 and 31 $m^2 \cdot g^{-1}$ respectively) indicating that the porous structure is still absent on these solids after calcination at 200 ºC. As far as the mixed solids are concerned, the higher the Zr content the higher the surface area. It is, however, relevant to indicate that the Mg3Zr-ME solid with a scarce 9.5% Zr (EDX, Table 1) presents a BET surface area as high as 196 $m^2 \cdot g^{-1}$.

Transmission electron microscopy (TEM) images obtained for the solids are presented in Figure 3-5. Irrespective of the synthetic procedure, pure Zr solids are constituted by agglomerated small particles (2-5 nm) (Figure 3) while pure Mg-SG and Mg-ME solids are based on larger hexagonal particles of around 200 nm in diameter (Figure 4). Moreover, mixed MgZr-SG and MgZr-ME solids are formed by large MgO particles surrounded by small ZrO_2

nanoparticles (Figure 5), in agreement to the higher Zr content observed in the surface XPS measurements (Table 1).

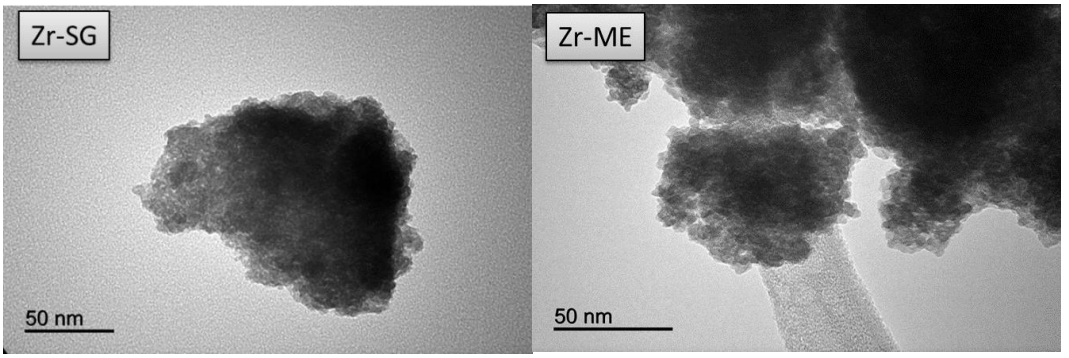

(**a**) (**b**)

Figure 3. TEM images corresponding to pure (**a**) Zr-SG and (**b**) Zr-ME solids.

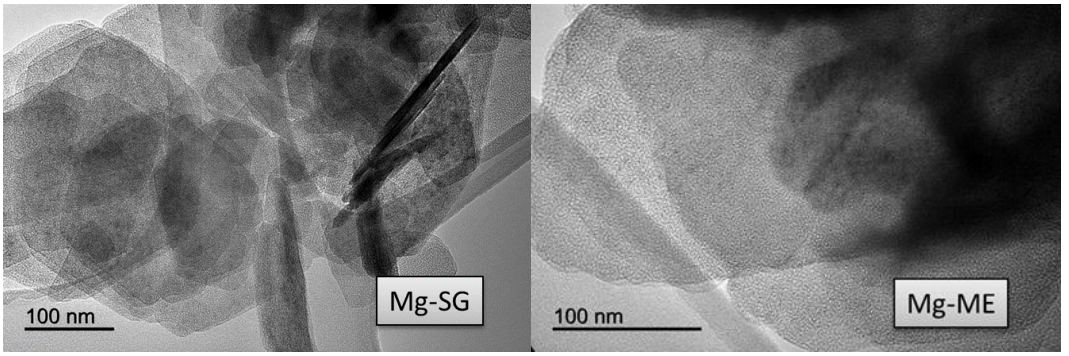

(**a**) (**b**)

Figure 4. TEM images corresponding to pure (**a**) Mg-SG and (**b**) Mg-ME solids.

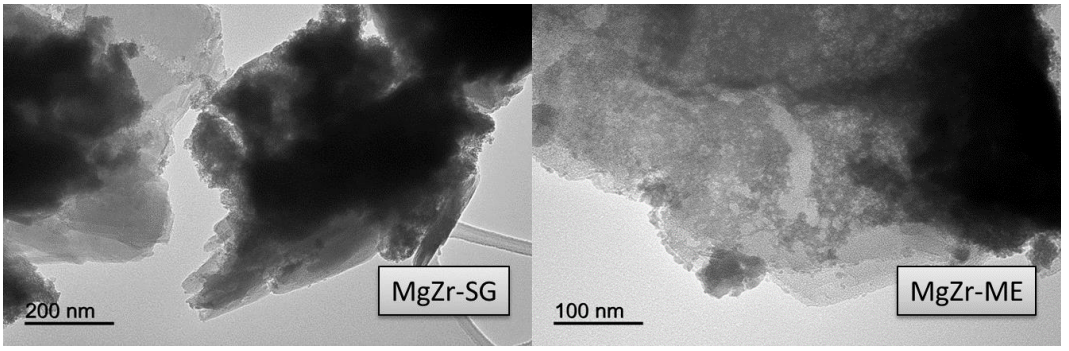

(**a**) (**b**)

Figure 5. TEM images corresponding to (**a**) MgZr-SG and (**b**) MgZr-ME solids.

III.2.2. Catalysts Surface Acid-Base Properties

Catalysts surface acidity was determined from temperature programmed desorption of pre-adsorbed pyridine (TPD-PY), the results being presented in Table 2 and Supplementary Figure S3. Values obtained for pyridine desorbed per gram of catalyst indicate that, as expected, pure Zr solids are much more acidic than pure Mg ones. Thus, Zr-SG and Zr-ME desorbed 748 and 871 μmol PY/g while Mg-SG and Mg-ME only desorbed 176 and 115 μmol/g, respectively. On the other hand, Mg-Zr mixed solids present a surface acidity in the 444-991 μmol/g range, with some interesting features that will be presented below. First of all, those mixed solids obtained from microemulsion present similar acidity, irrespective of its chemical composition —856, 885 and 788 μmol/g for Mg3Zr-ME, MgZr-ME and MgZr3-ME, respectively, while, on the contrary, sol-gel Mg-Zr mixed solids exhibit large differences in acidity, depending on its chemical composition: 444, 991 and 766 μmol/g for Mg3Zr-ME, MgZr-ME and MgZr3-ME, respectively. As a rule, surface acidity for ME solids is higher than that obtained for SG series. Finally, it is relevant to note that, in both series, the MgZr solids (with the nominal ratio Mg/Zr = 1) are the most acidic among the whole set of synthesized solids with 991 and 885 μmol/g for MgZr-SG and MgZr-ME, respectively. Moreover, the density of surface acid sites is also the highest for MgZr-SG and Mg-Zr-ME solids with 5.73 and 4.49 μmol PY/m^2, respectively.

Table 2. Catalysts Surface acid-base properties obtained from temperature programmed desorption of pyridine (TPD-PY) and carbon dioxide (TPD-CO_2) experiments.

	Catalyst Acidity (TPD-PY)		**Catalysts Basicity (TPD-CO_2)**	
Catalyst	**µmol Py/g**	**µmol Py/m^2**	**µmol CO_2/g**	**µmol CO_2/m^2**
Mg-SG	176	4.36	457	11.29
Mg3Zr- SG	444	3.73	918	7.71
MgZr- SG	991	5.73	526	3.04
MgZr3- SG	766	4.53	517	3.06
Zr- SG	748	3.13	441	1.84
Mg-ME	115	3.69	354	11.42
Mg3Zr-ME	856	4.37	448	2.28
MgZr-ME	885	4.49	292	1.48
MgZr3-ME	788	4.11	368	1.91
Zr-ME	871	3.92	199	0.90

As far as the surface basicity is concerned, it was determined by means of carbon dioxide temperature programmed desorption, the results being presented in Table 2 and Supplementary Figure S4 and S5. Regarding the TPD profile, all catalysts except Mg-ME exhibited a similar TPD-CO_2 profile with a desorption peak centered at 100 ºC and a second, truncated, peak associated to the carbon dioxide desorbed during the isothermal period at 200 ºC. The Mg-ME solid, however, only presented an intense second peak while the first one is absent for this catalyst.

As a general rule for the surface basicity per gram of catalyst, ME catalysts present lower basicity than the SG- ones, probably due do the surfactant residues still adsorbed on the catalyst surface. Moreover, it is interesting to point out the low basicity of both pure Mg-SG and Mg-ME solids as compared to the Mg-Zr mixed ones in both series, but especially in the SG-derived catalysts. It has to be assumed that, when calcined at high temperature, MgO is a strongly basic solid that desorbs CO_2 at temperatures higher than 600

ºC. Therefore, since our pure Mg-SG and Mg-ME solids were calcined at 200 ºC, they do not present the expected basicity for a pure MgO solid.

If surface basicity per square meter is considered (density of surface basic sites), for both series the obtained results indicate that, as a rule, the higher the amount of magnesium in the solid, the higher the surface basicity (Supplementary Figure S4). In this case, surface basic sites density is higher for Mg-SG and Mg-ME dues to the low surface area of theses solids (41 and 31 $m^2 \cdot g^{-1}$, respectively) indicative of a deficient porous structure as a consequence of the low calcination temperature.

Moreover, it is also relevant to indicate that Mg3Zr-SG presents a relatively high basicity (7.7 μmol CO_2/m^2) when compared with the Mg3Zr-ME solid (2.3 μmol CO_2/m^2). For the rest of the catalysts, SG solids exhibit similar surface base properties than their ME counterparts.

In addition to the temperature-programmed desorption experiments, surface acid-base properties of all solids were determined through the gas-phase propan-2-ol decomposition test reaction. This reaction allows us to determine acid and basic properties of the catalysts by analyzing the products distribution formed upon propan-2-ol transformation. When the reaction takes place over acid sites, dehydration products (propene and/or diisopropyl ether) are produced, while if basic or redox sites are involved, acetone and/or diacetone alcohol (resulting from acetone self-condensation) are obtained [30-32]. Since the catalysts were calcined at 200 ºC, initially the reaction was carried out at such temperature observing that there was no propan-2-ol conversion. Therefore, 250 ºC was selected as reaction temperature obtaining a propan-2-ol conversion in the 1-7% range. No experiments were carried out at higher temperatures in order to avoid further changes in catalysts structure. Figure 6 shows the result obtained for both series of catalysts.

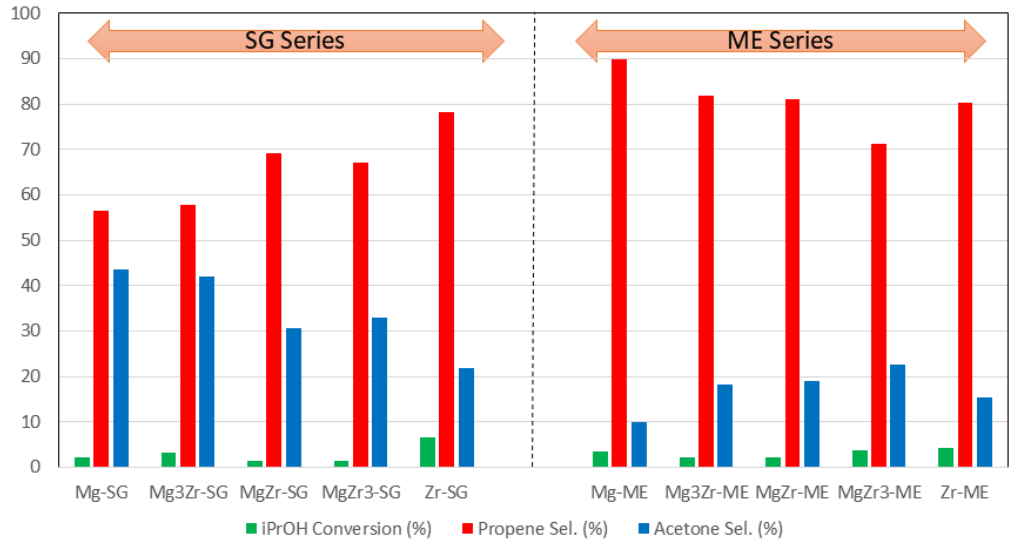

Figure 6. Catalytic activity in the gas-phase propanl-2-ol test reaction for the catalysts prepared in this work. Propan-2-ol conversion and selectivity to propene and acetone obtained at 250 ºC.

Despite the low conversion levels obtained, some interesting conclusions could be drawn from these experiments. First of all, for both series of catalysts, pure Zr-SG and Zr-ME catalysts exhibited the highest propan-2-ol conversion with 6.6 and 4.2%, respectively. Pure Mg and mixed Mg-Zr catalysts presented a catalytic conversion in the 1-4% range, irrespective of its composition and synthetic procedure.

The results concerning the selectivity to propene, formed over acid sites, or to acetone, formed over basic ones, seem to be more relevant. Thus, although propene is the major reaction product for all solids with selectivity in the 56-90% range, there are, however, significant differences. In general, in agreement with the TPD-PY results presented above (Table 2 and Supplementary Figure S3), selectivity to propene is higher for the ME- than for the SG series. In this line, the catalysts exhibiting the highest propene selectivity of the whole set of catalysts was Mg-ME (90% selectivity), an unexpected result since this solid was the less acidic (from TPD-PY, Table 2). Probably, the remaining surfactant

on the surface of the solids in the ME series accounts for this unexpected result. As for the SG series, propene selectivity results are somehow in good agreement with the TPD-PY data. Thus, pure Zr-SG catalyst presented a 78% selectivity to propene followed by MgZr-SG and MgZr3-SG solids with 69% and 67% selectivity respectively. These were also the most acidic catalysts in the SG series from pyridine temperature-programmed desorption experiments.

On the other hand, as far as the selectivity to basic sites-derived products is concerned, SG series gives the best results for the selectivity to acetone (22-44% sel.), being the solids with the highest magnesium content those giving the highest values: Mg-SG and Mg3Zr-SG with 44% and 42% sel., respectively. These results agree with catalysts basicity (TPD-CO_2, Table 2) where Mg-SG and especially Mg3Zr-SG present the highest basicity among the SG series catalysts. In contrast, for the catalysts corresponding to the ME series, the selectivity to acetone is in the range of 10-23%, even for those solids constituted mostly by Mg species (Mg-ME, 10% sel. to acetone). This fact, together with the unexpectedly high propene selectivity shown by the ME series catalysts, seems to indicate that surfactant molecules still remaining on the catalysts surface after calcination at 200 ºC affect its surface chemical properties.

III.2.3. Catalytic Activity

The above described catalysts were tested in the liquid-phase xylose dehydration to furfural in either a high-pressure autoclave or in an atmospheric pressure multi-reactor. The reaction medium in both cases was a biphasic system consisting of an organic/water (1:1 *v/v*) mixture, butan-1-ol or toluene being used as the organic solvent. The selected reaction temperature was 150 ºC. An initial set of reactions was performed to select the most appropriate reaction system to maximize the furfural yield. Figure 7 shows the catalytic

activity obtained for both series of catalysts in a butan-1-ol/water biphasic mixture in a multi-reactor and high-pressure autoclave reactors after 24h of reaction.

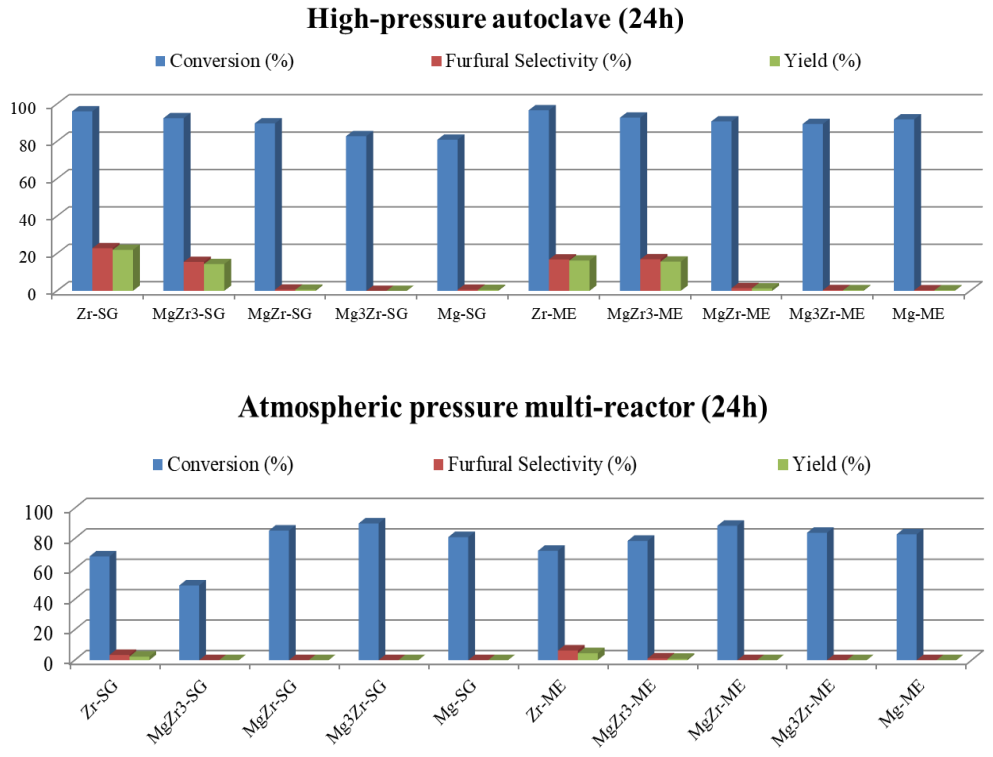

Figure 7. Catalytic activity for both series of catalysts in xylose dehydration in an atmospheric pressure multi-reactor (**upper**) and a high-pressure autoclave (**lower**) in a butan-1-ol/water biphasic media at 150 ºC. Xylose conversion and furfural selectivity and yield.

As can be observed, in both reaction systems xylose conversion is higher than 50%, being in most cases close to 90-100%. However, in spite of the above-described high xylose conversion, the selectivity for furfural is quite low (less than 25% at the best). Moreover, as a general trend, xylose conversion as well as furfural selectivity obtained in the high-pressure autoclave are both higher than those obtained in the multi-reactor system. Focusing on the autoclave reactions, Zr-SG and Zr-ME (pure zirconia solids) presented 23% and 17% selectivity to furfural, followed by MgZr3-SG and MgZr3-ME catalysts

with 16% selectivity in both cases. As could be expected, the higher the zirconium content, the higher the dehydrating activity for the catalysts.

Based on the above presented results, additional experiments were carried out with the high-pressure autoclave in order to increase the selectivity to furfural. Therefore, toluene was essayed as organic solvent in the biphasic reaction media, the obtained results being presented in Figure 8. The general trend observed in toluene/water medium is similar to that already reported by using butan-1-ol/water, that is, xylose conversions higher than 90% but, in this case, selectivity values to furfural practically doubled those obtained for the butan-1-ol/water mixture. Thus, Zr-SG presents a 41% selectivity to furfural, followed by Zr-ME (32% sel.), MgZr3-ME (29% sel.) and MgZr3-SG (17% sel.). The rest of the catalysts presented furfural selectivity lower than 5%.

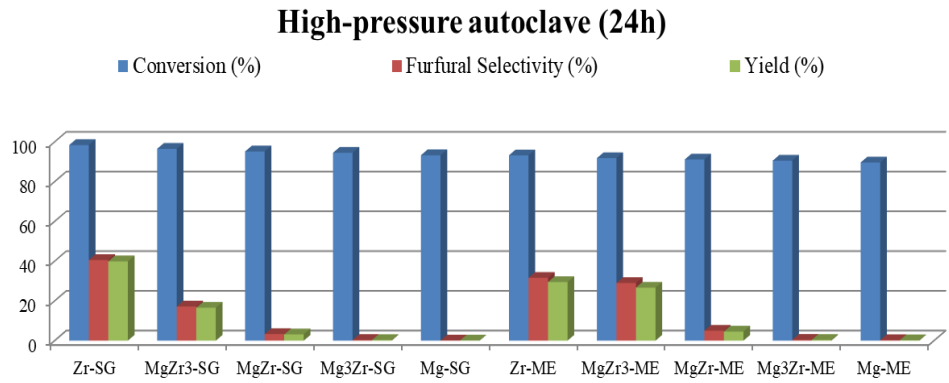

Figure 8. Catalytic activity for both series of catalysts in xylose dehydration in a high-pressure autoclave in a toluene/water biphasic media at 150 ºC. Xylose conversion and furfural selectivity and yield.

According to Hu et al. [23], with aromatic solvents, the formation of furfural from xylose is quick but so is its degradation. Therefore, additional experiments were carried out at shorter reaction times (3 and 5h) to analyze the influence of reaction time on both xylose conversion and furfural selectivity (Figure 9). Surprisingly, after 3h of reaction xylose conversion was already higher than 80% indicating that xylose was converted at the very beginning of

the reaction process. Moreover, furfural selectivity obtained at shorter reaction time was lower than that reported at 24h suggesting that xylose was converted to partially dehydrated intermediates during the initial stages of the process. It is interesting to note here that the transformation of xylose into furfural implies the loss of 3 water molecules and, therefore, longer reaction times facilitate furfural formation.

Since the time dependence of xylose conversion and furfural selectivity are opposite, it seems to be relevant to focus the discussion on the yield to furfural for all reaction times and catalytic systems. Moreover, as discussed above, the higher the zirconium content in the catalysts the better the furfural yield achieved. To illustrate this, Figure 10 presents the yield to furfural as a function of zirconium content for all reaction times essayed. It can be observed that irrespective of the reaction time, the yield to furfural depends mainly on the Zr content on the catalyst, being Zr-SG the solid yielding 40% to furfural as the better value after 24h of reaction. Zr-ME (29% yield), MgZr3-ME (27%) and MgZr3-SG (17%) catalysts showed a reasonably high yield to furfural. On the contrary, solids with high proportion of Mg yielded low amounts of furfural.

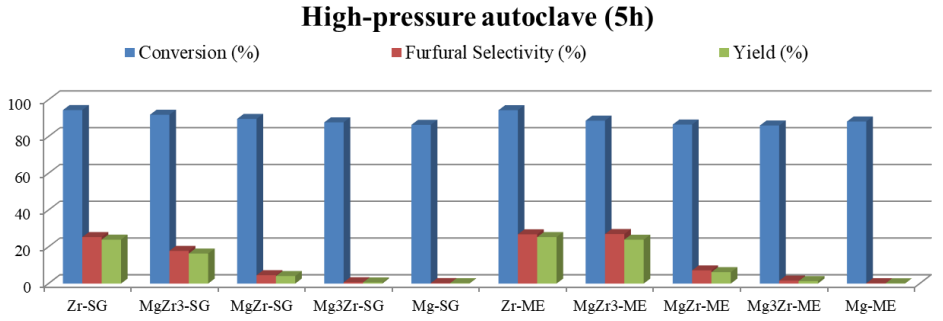

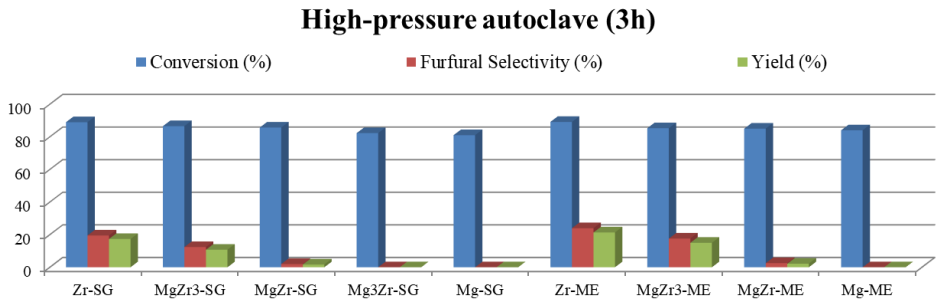

Figure 9. Catalytic activity in xylose dehydration in a high-pressure autoclave in a toluene/water biphasic media at 3 and 5h of reaction, and 150 ºC.

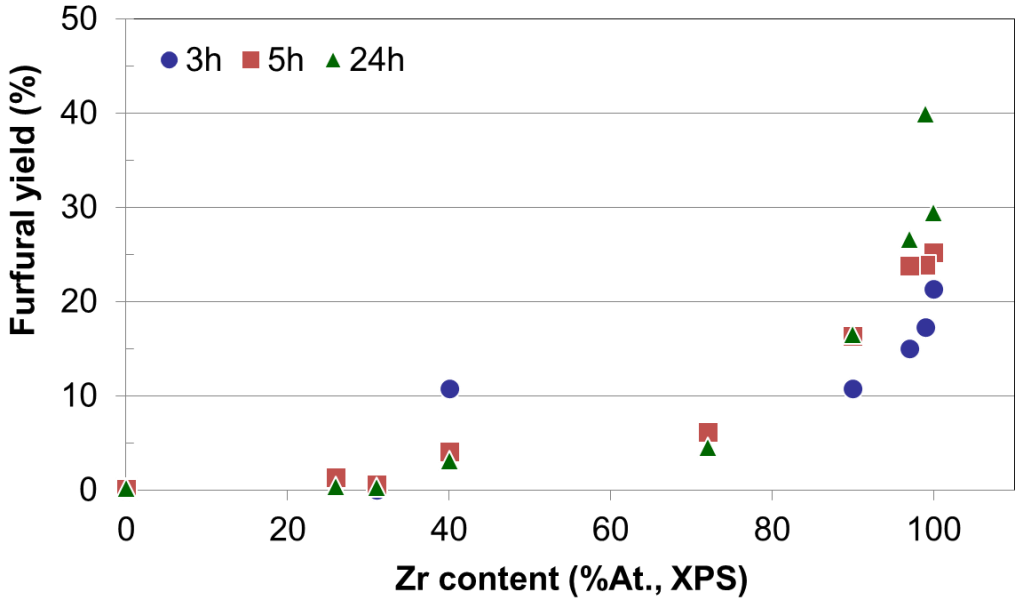

Figure 10. Furfural yield in xylose dehydration as a function of zirconium content (XPS) obtained after 3, 5 and 24h of reaction at 150 ºC in toluene/water reaction medium.

The results described above point out that the Zr sites are responsible for the dehydration of xylose to furfural, whereas the Mg related sites are not active at this point. However, in order to extend the scope of the research to cascade (one-pot) reactions, where both acid and base sites are needed, MgZr3 and MgZr catalysts may be interesting solids. Catalysts based on pure MgO, however, appear to be unsuitable for a reaction sequence including a dehydration step, as might reasonably be expected.

Finally, additional experiments were designed to rule out any homogeneous catalytic process due to the possibly lixiviated zirconium species under hydrothermal reaction conditions. Thus, Zr-SG catalyst was added to toluene/water (without xylose) solution and put under reaction condition (6 bar initial N_2 pressure, 150 ºC) for 5h. Then, the solid was removed by vacuum filtration and the appropriate amount of xylose was added to the filtrated, and put again under reaction conditions for another 5h of reaction. The xylose conversion obtained in this experiment was similar to that obtained in blank experiments, without any catalyst (less than 7%).

Additional experiments were carried out to verify the recyclability of our catalysts. Several reactions were performed using the MgZr3-SG catalyst; the reactions were stopped after 3 hours and the catalyst was recovered by vacuum filtration, washed with distilled water, dried in an oven at 110 ºC overnight and calcined at 200 ºC before being re-tested in a new reaction.

Figure 11 shows the results obtained after two reuses of the MgZr3-SG catalyst. With regard to the conversion of xylose (87% conversion in the first reaction), the conversion fell to 81% (a reduction of 7%) while after the second reuse, the conversion obtained was 78%, which represents a reduction of 10% with respect to the initial one. On the contrary, during the reuse tests, the selectivity to furfural increases slightly from the initial 12% to the 17-18% obtained in the reuses and, therefore, the furfural yield increases from 11% to 14%.

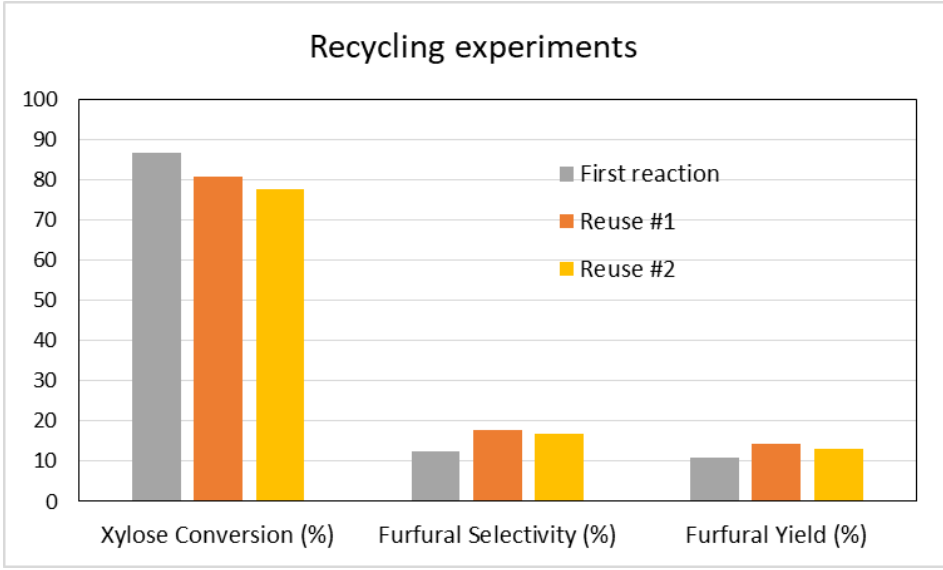

Figure 11. Conversion, selectivity and yield to furfural obtained during the dehydration of xylose on MgZr3-SG catalyst and two subsequent reuses. Reaction conditions: 0.1 g of catalyst, 20 mL of biphasic reaction mixture (water / toluene), 150 ºC, 3 h reaction.

In line with the reuse experiments, after 3 hours of reaction on MgZr3-SG catalyst, the aqueous phase of the reaction medium was analyzed by ICP-MS to verify the existence of leaching of the component species of the catalyst.

Results indicated the existence of magnesium at a level of 500 ppm while detected amount of zirconium was less than 20 ppb. According to the EDX composition of MgZr3-SG catalyst (Table 1), MgO molar content in the solid was 32.6% and, therefore, 65% of magnesium species were leached to the liquid-phase. However, zirconium species were resistant to leaching under reaction conditions.

In any case, as reported above, the loss in catalytic activity after the first reuse was only of 7%, while furfural selectivity slightly increases. These results reinforce the conclusion that ZrO_2 is the catalytically active component of the mixed catalyst.

III.3. Discussion

Two series of catalysts were prepared by sol-gel (SG series) and microemulsion (ME series) synthetic procedure. Each series includes both pure Mg and Zr solids as well as Mg-Zr mixed solids with 25%, 50% and 75% nominal Zr content.

Thermal TGA-DSC experiments carried out to the precursor ME-derived gels of the solids indicate that although the precipitated solid was washed five times with a mixture of chloroform/ethanol, part of the surfactant is retained on the surface of the solid. Moreover, results indicate that the surfactant is retained mainly on the Zr component of the solids, as confirmed by the detection of Br from the surfactant by SEM-EDX.

Due to the low calcination temperature (200 ºC), the porous structure of pure MgO-based catalysts has not been adequately developed as evidenced by the low surface area of the Mg-SG and Mg-ME catalysts. This lack of porous structure is reflected in the low surface basicity of these solids. In addition, the catalysts synthesized by ME retain surfactant in their structure which makes them less basic. TEM micrographs indicate that pure Zr-based catalysts are formed by agglomerated of small particles (2-5 nm) while pure Mg-SG and Mg-ME solids are based on larger hexagonal particles of around 200 nm in diameter. In addition, mixed Mg-Zr solids are formed by large MgO particles surrounded by small ZrO_2 nanoparticles.

In terms of acidity, it is possible that Bromide, coming from the surfactant, is adsorbed on the solids creating Lewis acid sites responsible for relatively higher acidity in the solids of the ME series than in those of the series SG.

The above results clearly indicate that the ME series catalysts retain surfactant adsorbed on their surface after calcination at 200 ºC which determines their surface chemical properties. In any case, the catalyst MgZr-SG has the best surface acidic properties, either per gram or per square meter of catalyst. As far as basicity is concerned, the solid with the most promising basic properties is Mg3Zr-SG, although MgZr-SG also shows interesting basic surface properties.

These results are reflected in the propan-2-ol decomposition test reaction since the Mg3Zr-SG catalyst exhibits comparable selectivities to propene and acetone, as a consequence of equilibrium balance between surface acid and basic properties.

The synthesized catalysts were tested for the xylose dehydration reaction in two different reaction systems (high-pressure autoclave and atmospheric-pressure multi-reactor) and using different reaction mixtures (solvents). For both reaction systems and using butan-1-ol /water as solvent, the obtained xylose conversions after 24 hours of reaction were high, although the furfural selectivity obtained was quite low (less than 25% sel.). In any case, the yields to furfural were higher in the high-pressure autoclave, so the multi-reactor at atmospheric pressure was ruled out for further testing. Similar yields were reported in the literature for monosaccharides dehydration on acid-base heterogeneous catalysts such as CoAl-hydrotalcite (22% yield to hydroxymethylfurfural) [33].

As regards the solvent effect, the change from butan-1-ol to toluene as the organic solvent in the biphasic reaction mixture led to better yields to furfural after 24h of reaction. According to the literature, compared with water, alcohols can promote the formation of furfural and slow down its degradation at prolonged reaction times. Moreover, when using aromatics as organic solvent,

the formation of furfural is quick but so is the degradation of furfural due to the aprotic properties of these solvents [23]. This behavior is, however, contrary to that observed in our case since with toluene better yield to furfural is obtained as compared to butan-1-ol (Zr-SG, toluene/water, 24h, 40% yield *vs* Zr-SG, butan-2-ol/water, 24h, 22% yield). This could be due to the fact that toluene is a good organic solvent that can extract furfural as it is formed, thus avoiding the formation of humins which takes place mainly in the aqueous phase [23].

Additional tests conducted with toluene/water at shorter reaction times (3 and 5h) still led to high xylose conversions but associated with even lower furfural selectivities. This behavior could be associated with a rapid dehydration of xylose to partially dehydrated intermediates which, along the reaction course, slowly culminate in the formation of furfural.

When we study the influence of the catalyst on the yield to furfural it is observed that the higher the zirconium content, the higher the dehydrating activity for the catalysts. That is, irrespective of the reaction time, the yield to furfural depends on the Zr content on the catalyst, while, on the contrary, solids with high proportion of Mg yielded low amounts of furfural (0% yield for Mg-SG and Mg-ME catalysts).

Finally, the reuse experiments of the catalysts, together with the analysis of leached species, indicated that while ZrO_2 component is practically not leached, a large part of the MgO component of the solids is leached to the reaction medium under the hydrothermal reaction conditions. However, this only implies a slight reduction in the conversion of xylose because, as mentioned, it is the ZrO_2 component that is responsible for the catalytic activity of the MgO-ZrO_2 mixed oxides.

All in all, from the point of view of the xylose dehydration to furfural, the catalysts constituted by pure ZrO_2 (especially Zr-SG) are the most suitable to carry out the process under study.

However, if a second process that occurs with the participation of surface basic sites is to be coupled to it in the so-called one-pot or cascade reactions, the MgZr mixed solids could be suitable for the overall process. Thus, the MgZr-SG and MgZr3-SG catalysts present a balance of acid and base centers that could be adequate for this type of processes. Leaching of the MgO component, however, is an issue that has to be solved in order to carry out the process in an effective way.

Finally, although some catalysts of the series ME present results that could be interesting, the problems associated to the surfactant that remains adsorbed on them seem to advise its use in more complex processes.

III.4. Materials and Methods

III.4.1. Materials

Chloroform anhydrous ≥99% (ref. 288306), 2,2,4-trimethylpentane anhydrous 99.8% (ref. 360066), hexadecyltrimethylammonium bromide ≥ 98% (CTAB) (ref. H5882), butan-1-ol ≥ 99% (ref. B7906), ethanol (ref. 652261), zirconium (IV) oxynitrate hydrate (ref. 346462), magnesium nitrate hexahydrate (ref. 203696), D-(+)-xylose ≥ 99% (ref. X1500) and toluene (ref. 244511) were purchased from Sigma-Aldrich. Ammonium hydroxide solution 5.0N (ref. 318612) and hydrochloric acid solution 1.0M (ref. 318949) were obtained from Honeywell Fluka. MilliQ water was used for preparation of the aqueous solutions.

III.4.2. Catalysts synthesis

Pure MgO and ZrO2 as well as several mixed MgO-ZrO2 systems (in an atomic Mg:Zr nominal ratio of 75:25, 50:50 and 25:75) were synthesized through both microemulsion (ME series) and sol-gel (SG series) methods. In both synthetic methods, magnesium and zirconyl nitrates were used as the precursors and aqueous NH_4OH (pH 10) as precipitating agent.

III.4.2.1.Sol-gel method

MgO was prepared from a 0.4M aqueous solution of magnesium nitrate hexahydrate which was introduced at controlled rate (0.56 mL/min) into a reactor containing 0.4L of ammonium hydroxide solution at pH 10. The process was carried out under magnetic stirring (700 rpm) and maintaining the initial pH level of 10 with help of a Syrris Atlas pump (Syrris Ltd., Hertforshire, UK) that introduced NH_4OH 5N or HCl 0.2M as needed. The gel was aged for 24h and the precipitate was then vacuum filtered and washed with water to obtain a white solid which was dried overnight at 120 ºC. The dried solid was calcined at 200 ºC for 6h under air flow. Finally, the solid was ground and sieved (0.149 µm light sieve). Similar procedure was followed for the rest of catalysts in the SG series just adjusting the appropriate amounts of magnesium and zirconium precursors to obtain solids with Mg:Zr atomic ratio of 100:0 (Mg-SG), 75:25 (Mg3Zr-SG), 50:50 (MgZr-SG), 25:75 (MgZr3-SG) and 0:100 (Zr-SG).

III.4.2.2.Microemulsion method

As for the solids prepared through microemulsion technique (ME series), two different microemulsions were prepared to include Mg and Zr precursors (ME1) and the precipitating agent, NH_4OH (ME2). Under optimized conditions, the composition of microemulsions was: 2,2,4-trimethylpentane anhydrous (oil, 53 wt%), hexadecyltrimethylammonium bromide (surfactant, 15

wt%), 1-butanol (co-surfactant, 12 wt%) and 0.4M aqueous solution of Mg and Zr precursors (ME1) or NH_4OH aqueous solutions of pH=10 (ME2) (20 wt%).

As a standard procedure ME1 was slowly added to ME2 under constant stirring (700 rpm) and the resulting mixture aged overnight under stirring. The white precipitate was then filtered and washed five times with 80 mL of a chloroform/ethanol mixture (1:1 *v/v*) to remove surfactant and oil remaining on the solid surface. The solid was dried, calcined and sieved in a similar way to the SG series. Catalysts in the ME series were prepared just adjusting the appropriate amounts of magnesium and zirconium precursors to obtain solids with Mg:Zr atomic ratio of 100:0 (Mg-ME), 75:25 (Mg3Zr-ME), 50:50 (MgZr-ME), 25:75 (MgZr3-ME) and 0:100 (Zr-ME).

III.4.3.Catalysts Characterization

Both series of catalysts were thoroughly characterized from textural, structural and chemical point of view.

Thermogravimetric analyses (TGA) were performed on a Setaram SetSys 12 instrument (Caluire, France). An amount of 20 mg of sample was placed in an alumina crucible and heated at temperatures ranging from 30 to 600 ºC (heating rate of 10 $ºC \cdot min^{-1}$) under synthetic air stream (50 $mL \cdot min^{-1}$) in order to measure weight loss, heat flow and derivative weight loss.

Surface areas of solids were obtained from nitrogen adsorption-desorption isotherms obtained at liquid nitrogen temperature on a Micromeritics ASAP-2010 instrument, following the Brunnauer-Emmett-Teller (BET) method. All samples were degassed to 0.1 Pa at 120 ºC before measurement.

Scanning electron microscopy (SEM-EDX) measurements were obtained on a JEOL JSM-6300 scanning electron microscope (Jeol, Tokyo,

Japan) equipped with an energy-dispersive X-ray (EDX) detector (Oxford Instruments, Abingdon, United Kingdom), available at the Central Service for Research Support (SCAI) of the University of Córdoba. It was operated at an acceleration voltage of 20 keV with a resolution of 65 eV. Transmission electron microscopy (TEM) images were obtained at the Central Service for Research Support (SCAI) of the University of Córdoba using a JEOL JEM 1400 microscope (Jeol, Tokyo, Japan). All samples were mounted on 3 mm holey carbon copper grids.

X-ray photoelectron spectroscopy (XPS) data were recorded at the Central Service for Research Support (SCAI) of the University of Córdoba on 4 mm x 4 mm pellets, 0.5 mm thick that were obtained by gently pressing the powered materials. Samples were outgassed to a pressure below about 2 x 10^{-8} Torr at 150 ºC in the instrument pre-chamber to remove chemisorbed volatile species. The main chamber of the Leibol-Heraeus LHS10 spectrometer used (Leibold, Cologne, Germany), capable of operating down to less than 2 x 10^{-9} Torr, was equipped with a EA-200MCD hemispherical electron analyzer with a dual X-ray source using Al Kα (hυ=1486.6 eV) at 120 W and 30 mA. C (1s) was used as energy reference (284.6 eV).

Surface acidity of the catalysts was determined by thermal programmed desorption of pre-absorbed pyridine (TPD-PY) with TCD detection. An amount of 20 mg of sample was introduced in a 10 mm ID reactor that was placed inside an oven. Solids were cleaned under He flow (75mL·min^{-1}) by heating to 200 ºC at a rate of 10 ºC·min^{-1} and then cooled down to 50 ºC. At that temperature, the solids were exposed for 30 min to a pyridine saturated Helium flow. After saturation, physisorbed pyridine was removed by flowing a pure He stream for 60 min (75 mL·min^{-1}). Then, the temperature-programmed desorption of chemisorbed pyridine was carried out by ramping the temperature from 50 to 200 ºC (heating rate 10 ºC·min^{-1}) and holding the final temperature

for 30 min. Desorbed pyridine was quantified against a calibration graph constructed from variable volumes of pyridine injected.

Surface basicity of the catalysts was determined on a Micromeritics Autochem II instrument (Micromeritics, Norcross, GA, USA) by thermal programmed desorption of pre-absorbed CO_2 (TPD-CO_2) with TCD detection. An amount of 100 mg of each catalyst was loaded into a reactor 10 mm ID and placed in a furnace. Solids were cleaned with an Ar stream (20mL·min^{-1}) by heating to 200 ºC at a rate of 10 ºC·min^{-1} for 60 min and then cooled down to 40 ºC. At that temperature, the catalysts were saturated with the probe molecule, using 5% CO_2/Ar flow at 20 mL·min^{-1} for 60 min. After saturation, physisorbed CO_2 was removed by flowing Ar stream for 30 min (20 mL·min^{-1}). Then, the temperature-programmed desorption of chemisorbed CO_2 was carried out by ramping the temperature from 40 to 200 ºC (heating rate 5 ºC·min^{-1}) and holding the final temperature for 60 min. The amount of CO_2 adsorbed was determined from a calibration graph constructed from the injection of variable volumes of 5% CO_2/Ar.

Propan-2-ol transformation test reaction was also used to confirm the surface chemical properties of the prepared catalysts. This reaction, widely described as a model process, can provide valuable information on surface acid-base properties of the catalyst as a function of its products distribution: surface acid sites yield propene or diisopropyl ether while basic or redox properties lead to acetone [30-32,34,35].

The gas-phase propan-2-ol transformation was carried out in a stainless-steel reactor (1/8 inch OD) that was loaded with 100 mg of catalyst and 1 g of inert SiO_2. Prior to the reaction, the catalyst was cleaned with a N_2 flow (20 mL·min^{-1}) while increasing the temperature until 200°C (rate, 2 ºC·min^{-1}). The reaction was started by introducing propan-2-ol by passing a nitrogen flow of

10 mL·min^{-1} through a saturator filled with propan-2-ol at room temperature. Analyses were carried out on-line by connecting the effluent to a gas chromatograph (HP 5890 series II) equipped with a capillary column Supelcowax-10 (60 m long, 0.25 mm ID, 0.25 μm film thickness).

III.4.4.Catalytic tests

The solids were tested for dehydration of xylose to furfural using a biphasic reaction medium on two different reaction systems.

III.4.4.1.Multi-reactor under Conventional Thermal Heating

A Carousel 12 Reaction StationTM multi-reactor (Radley Discovery Technologies, Essex, UK) furnished with twelve reaction glass tubes with a maximum reaction volume of 20mL. The reaction mixture consisted of 75 mg xylose, 6 mL milliQ water, 6 mL organic solvent (1-butanol or toluene) and 30 mg catalyst. The reaction mixture was purged with N_2 before reaction to work under controlled atmosphere. Temperature and stirring rate were adjusted at 150 ºC and 750 rpm, respectively, and the reaction time extended to 24h. The upper part of the reaction tubes was always refrigerated at 5 ºC thus preventing loss of the reaction mixture by evaporation.

III.4.4.2.High-Pressure Autoclave

A Berghof HR-100 stainless steel high-pressure autoclave (Berghof Products and Instruments GmbH, Eningen, Germany) equipped with a 75 mL PTFE insert vessel was also used in xylose dehydration to furfural. Under standard conditions, 250 mg xylose, 10 mL milliQ water, 10 mL organic solvent (1-butanol or toluene) and 100 mg catalyst were introduced in the vessel (i.e., same substrate/catalyst ratio as in multi-reactor). Reactor was purged with nitrogen and pressurized to 5 bar of N_2. The reaction temperature was set to 150

ºC and the reaction started by switching on the stirring at 750 rpm. Reaction was stopped by introducing the vessel in an ice bath at selected times (3, 5 and 24h).

III.4.4.3. Product Analysis

Once finished the reactions, the aqueous and organic phases were separated by centrifugation and filtered through a nylon syringe filter (0.22 µm). The aqueous phase was analysed by high-performance liquid chromatography (Water 2695 HPLC) with refraction index detection (IR detector) on a Fortis amino 5 µm (250 x 4.6 mm) column. 5 mM of H_2SO_4 was employed as the eluent with a 0.7 µL/min flow rate at 50 ºC. The volume of injection was 5µL. The organic phase was analysed by gas chromatography (Agilent 7890, Santa Clara, CA, USA) with flame ionization detector (GC-FID) using a Supelco Nukol™ capillary column. No xylose was detected in the organic phase and furfural detected in the aqueous phase was negligible. Quantification of xylose and furfural was performed using the appropriate calibration curves.

Blank experiments (without catalyst) were carried for both reaction systems being the xylose conversion obtained less than 7% at the best.

Xylose conversion and furfural selectivity and yield were defined by Eqs. (1), (2) and (3):

$$\text{Xylose conversion (\%)}: \frac{\text{initial xylose concentration-final xylose concentration}}{\text{initial xylose concentration}} \text{ x } 100 \quad (1)$$

$$\text{Furfural selectivity (\%)}: \frac{\text{furfural concentration}}{\text{initial xylose concentration-final xylose concentration}} \text{ x } 100 \quad (2)$$

$$\text{Furfural yield (\%)}: \frac{\text{furfural concentration}}{\text{initial xylose concentration}} \text{ x } 100 \quad (3)$$

III.5. Conclusions

Two series of catalysts were prepared (by sol-gel and microemulsion synthetic procedures), characterized and applied to the liquid-phase xylose dehydration to furfural. Catalysts prepared by microemulsion retained part of the surfactant used in the synthetic procedure, mainly associated to the Zr part of the solid.

As for xylose dehydration, the use of toluene as organic solvent in the biphasic reaction mixture (toluene/water) leads to better performance to furfural than the use of alcohols (1-butanol) which is associated with the ability of toluene to extract the furfural formed, thus avoiding the formation of humins that take place mainly in the aqueous phase.

The yield to furfural increases with the Zr content of the catalyst and, therefore, the catalysts constituted by pure ZrO_2 (especially Zr-SG) are the most suitable to carry out the process (98% conversion, 40% yield, 24 hours). The results described above point out that the Zr sites are responsible for the dehydration of xylose to furfural, whereas the Mg related sites are not active at this point.

The reuse experiments of the catalysts, together with the analysis of leached species, indicated that while ZrO_2 component is practically not leached, a large part of the MgO component of the solids is leached to the reaction medium under the hydrothermal reaction conditions. However, this only implies a slight reduction in the conversion of xylose because, as mentioned, it is the ZrO_2 component that is responsible for the catalytic activity of the MgO-ZrO_2 mixed oxides.

Supplementary Materials

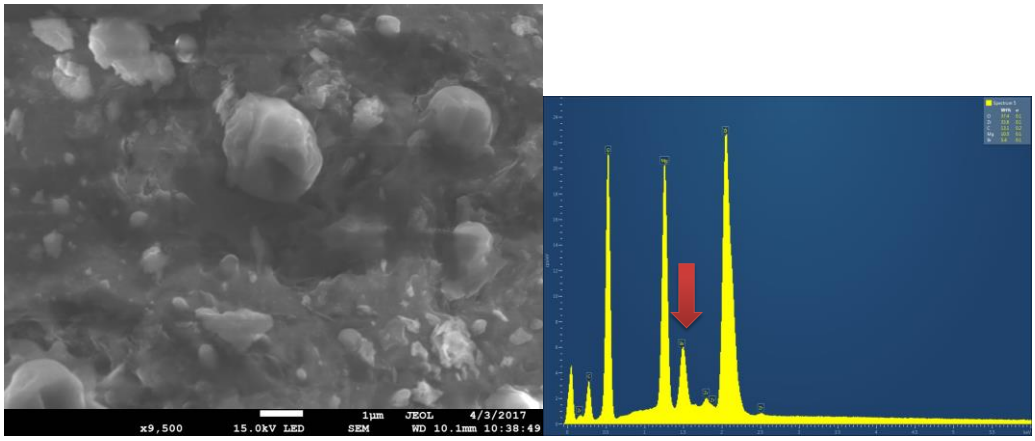

Supplementary Figure S1: SEM-EDX measurements for the MgZr-ME catalysts, including EDX profiles for the whole image area. Red arrow marks Br signal (2.1% atomic).

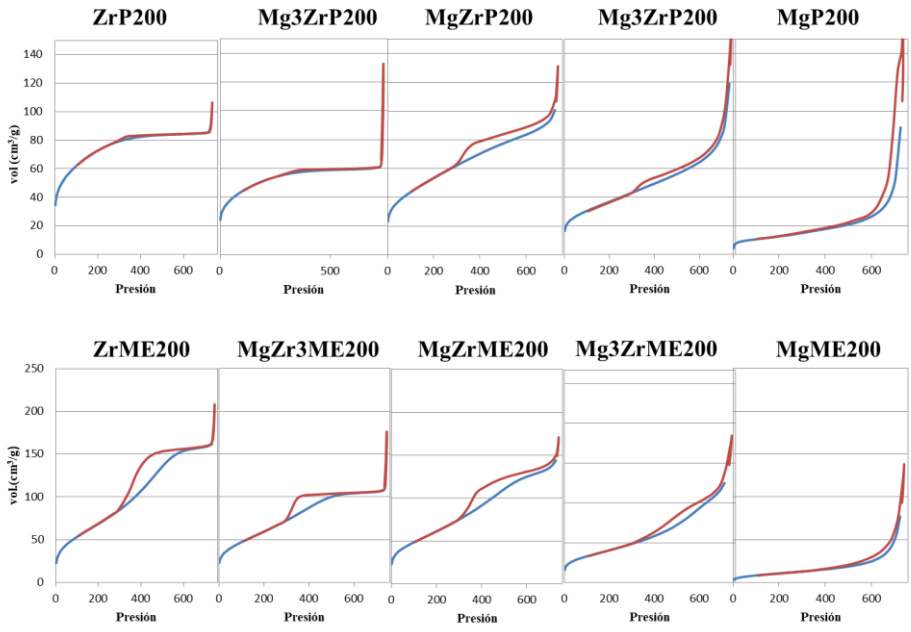

Supplementary Figure S2: Nitrogen adsorption-desorption isotherms corresponding to the solids of both SG and ME series.

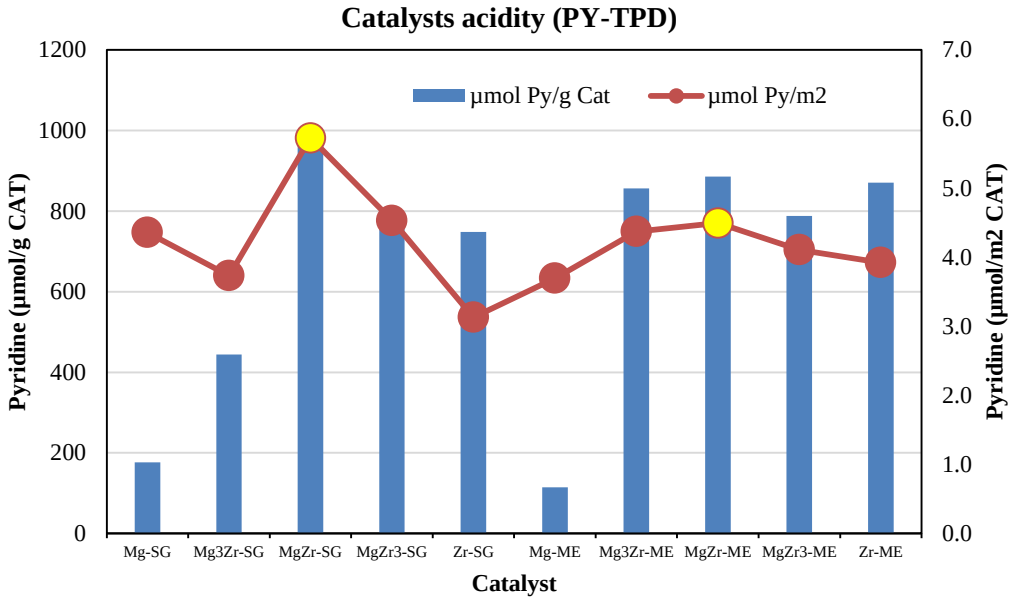

Supplementary Figure S3: Catalysts acidity determined from temperature programmed desorption of pre-adsorbed pyridine (µmol PY/g CAT and µmol PY/m^2 CAT).

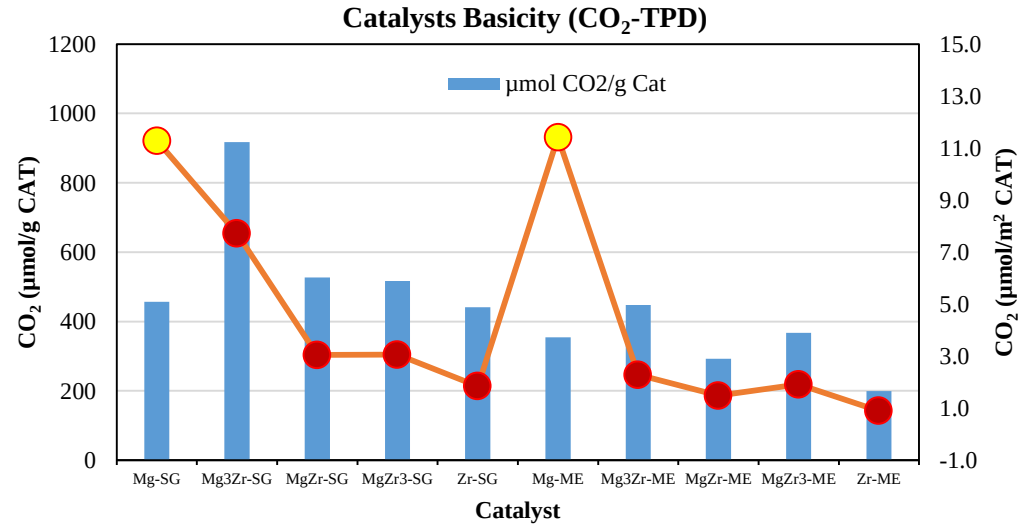

Supplementary Figure S4: Catalysts basicity determined from temperature programmed desorption of pre-adsorbed carbon dioxide (µmol CO_2/g and µmol CO_2/m^2).

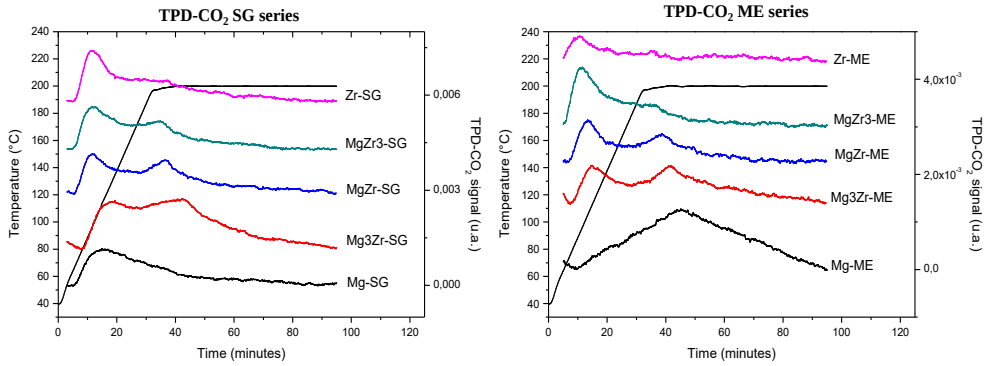

Supplementary Figure S5: Temperature-programmed desorption profiles of pre-adsorbed carbon dioxide obtained for the catalysts synthesized in this work.

Acknowledgements

The authors are thankful to Ramon Areces Foundation for financial support. The scientific support from the Central Service for Research Support (SCAI) at the University of Cordoba was also acknowledged

References

1. Field, C.B.; Campbell, J.E.; Lobell, D.B. Biomass energy: the scale of the potential resource. *Trends in Ecology & Evolution* **2008**, *23*, 65-72, doi:10.1016/j.tree.2007.12.001.
2. Gallezot, P. Conversion of biomass to selected chemical products. *Chemical Society Reviews* **2012**, *41*, 1538-1558, doi:10.1039/c1cs15147a.
3. Zhang, J.; Zhuang, J.; Lin, L.; Liu, S.; Zhang, Z. Conversion of D-xylose into furfural with mesoporous molecular sieve MCM-41 as catalyst and butanol as the extraction phase. *Biomass & Bioenergy* **2012**, *39*, 73-77, doi:10.1016/j.biombioe.2010.07.028.
4. Sairanen, E.; Karinen, R.; Lehtonen, J. Comparison of solid acid-catalyzed and autocatalyzed C5 and C6 sugar dehydration reactions with water as a

solvent. *Catalysis Letters* **2014**, *144*, 1839-1850, doi:10.1007/s10562-014-1350-1.

5. Sheldon, R.A. Green and sustainable manufacture of chemicals from biomass: state of the art. *Green Chemistry* **2014**, *16*, 950-963, doi:10.1039/c3gc41935e.
6. Bozell, J.J.; Petersen, G.R. Technology development for the production of biobased products from biorefinery carbohydrates-the US Department of Energy's "Top 10" revisited. *Green Chemistry* **2010**, *12*, 539-554, doi:10.1039/b922014c.
7. Dutta, S.; De, S.; Saha, B.; Alam, M.I. Advances in conversion of hemicellulosic biomass to furfural and upgrading to biofuels. *Catalysis Science & Technology* **2012**, *2*, 2025-2036, doi:10.1039/c2cy20235b.
8. Barrett, C.J.; Chheda, J.N.; Huber, G.W.; Dumesic, J.A. Single-reactor process for sequential aldol-condensation and hydrogenation of biomass-derived compounds in water. *Applied Catalysis B: Environmental* **2006**, *66*, 111-118, doi:10.1016/j.apcatb.2006.03.001
9. Chheda, J.N.; Dumesic, J.A. An overview of dehydration, aldol-condensation and hydrogenation processes for production of liquid alkanes from biomass-derived carbohydrates. *Catalysis Today* **2007**, *123*, 59-70, doi:10.1016/j.cattod.2006.12.006.
10. Corma, A.; de la Torre, O.; Renz, M. High-Quality Diesel from Hexose- and Pentose-Derived Biomass Platform Molecules. *ChemSusChem* **2011**, *4*, 1574-1577, doi:10.1002/cssc.201100296.
11. Dautzenberg, G.; Gerhardt, M.; Kamm, B. Bio based fuels and fuel additives from lignocellulose feedstock via the production of levulinic acid and furfural. *Holzforschung* **2011**, *65*, 439-451, doi:10.1515/hf.2011.081.
12. Yan, K.; Liu, Y.; Lu, Y.; Chai, J.; Sun, L. Catalytic application of layered double hydroxide-derived catalysts for the conversion of biomass-dderived

molecules. *Catalysis Science & Technology* **2017**, *7*, 1622-1645, doi:10.1039/c7cy00274b.

13. Carrasco, F. Production of furfural by dilute-acid hydrolysis of wood: methods for calculating furfural yield. *Wood and Fiber Science* **1993**, *25*, 91-102.
14. Faba, L.; Diaz, E.; Ordonez, S. One-pot Aldol Condensation and Hydrodeoxygenation of Biomass-derived Carbonyl Compounds for Biodiesel Synthesis. *ChemSusChem* **2014**, *7*, 2816-2820, doi:10.1002/cssc.201402236.
15. Lucas, N.; Kokate, G.; Nagpure, A.; Chilukuri, S. Dehydration of fructose to 5-hydroxymethyl furfural over ordered AlSBA-15 catalysts. *Microporous and Mesoporous Materials* **2013**, *181*, 38-46, doi:10.1016/j.micromeso.2013.07.015.
16. Grande, P.M.; Bergs, C.; de Maria, P.D. Chemo-enzymatic conversion of glucose into 5-hydroxymethylfurfural in seawater. *ChemSusChem* **2012**, *5*, 1203-1206, doi:10.1002/cssc.201200065.
17. Dee, S.J.; Bell, A.T. A Study of the acid-catalyzed hydrolysis of cellulose dissolved in ionic liquids and the factors influencing the dehydration of glucose and the formation of humins. *ChemSusChem* **2011**, *4*, 1166-1173, doi:10.1002/cssc.201000426.
18. Karinen, R.; Vilonen, K.; Niemela, M. Biorefining: heterogeneously catalyzed reactions of carbohydrates for the production of furfural and hydroxymethylfurfural. *ChemSusChem* **2011**, *4*, 1002-1016, doi:10.1002/cssc.201000375.
19. Campos Molina, M.J.; Mariscal, R.; Ojeda, M.; Lopez Granados, M. Cyclopentyl methyl ether: a green co-solvent for the selective dehydration of lignocellulosic pentoses to furfural. *Bioresource Technology* **2012**, *126*, 321-327, doi:10.1016/j.biortech.2012.09.049.

20. Delbecq, F.; Wang, Y.; Len, C. Various carbohydrate precursors dehydration to 5-HMF in an acidic biphasic system under microwave heating using betaine as a co-catalyst. *Molecular Catalysis* **2017**, *434*, 80-85, doi:10.1016/j.mcat.2017.02.037.
21. Le Guenic, S.; Delbecq, F.; Ceballos, C.; Len, C. Microwave-assisted dehydration of D-xylose into furfural by diluted inexpensive inorganic salts solution in a biphasic system. *Journal of Molecular Catalysis a-Chemical* **2015**, *410*, 1-7, doi:10.1016/j.molcata.2015.08.019.
22. Hua, D.-R.; Wu, Y.-L.; Liu, Y.-F.; Chen, Y.; Yang, M.-D.; Lu, X.-N.; Li, J. Preparation of furfural and reaction kinetics of xylose dehydration to furfural in high-temperature water. *Petroleum Science* **2016**, *13*, 167-172, doi:10.1007/s12182-015-0069-y.
23. Hu, X.; Westerhof, R.J.M.; Dong, D.; Wu, L.; Li, C.-Z. Acid-catalyzed conversion of xylose in 20 solvents: insight into interactions of the solvents with xylose, furfural, and the acid catalyst. *ACS Sustainable Chemistry & Engineering* **2014**, *2*, 2562-2575, doi:10.1021/sc5004659.
24. Sievers, C.; Musin, I.; Marzialetti, T.; Olarte, M.B.V.; Agrawal, P.K.; Jones, C.W. Acid-catalyzed conversion of sugars and furfurals in an ionic-liquid phase. *ChemSusChem* **2009**, *2*, 665-671, doi:10.1002/cssc.200900092.
25. Kim, Y.C.; Lee, H.S. Selective synthesis of furfural from xylose with supercritical carbon dioxide and solid acid catalyst. *Journal of Industrial and Engineering Chemistry* **2001**, *7*, 424-429.
26. Climent, M.J.; Corma, A.; Iborra, S. Heterogeneous catalysts for the one-pot synthesis of chemicals and fine chemicals. *Chemical Reviews* **2011**, *111*, 1072-1133, doi:10.1021/cr1002084.
27. Aramendia, M.A.; Borau, V.; Jimenez, C.; Marinas, J.M.; Romero, F.J.; Navio, J.A.; Barrios, J. Modification of the activity of $Mg_3(PO_4)_2$ in the

gas-phase conversion of cyclohexanol by addition of sodium-carbonate. *Journal of Catalysis* **1995**, *157*, 97-108, doi:10.1006/jcat.1995.1271.

28. Stefanic, G.; Music, S.; Popovic, S.; Sekulic, A. FT-IR and laser Raman spectroscopic investigation of the formation and stability of low temperature t-ZrO_2. *Journal of Molecular Structure* **1997**, *408-409*, 391-394, doi:10.1016/s0022-2860(96)09549-x.
29. Miñambres, J.F.; Marinas, A.; Marinas, J.M.; Urbano, F.J. Activity and deactivation of catalysts based on zirconium oxide modified with metal chlorides in the MPV reduction of crotonaldehyde. *Applied Catalysis B: Environmental* **2013**, *140–141*, 386-395, doi:http://dx.doi.org/10.1016/j.apcatb.2013.04.036.
30. Aramendia, M.A.; Borau, V.; Jimenez, C.; Marinas, J.M.; Porras, A.; Urbano, F.J. Synthesis and characterization of ZrO_2 as an acid-base catalyst: dehydration-dehydrogenation of propan-2-ol. *Journal of the Chemical Society - Faraday Transactions* **1997**, *93*, 1431-1438, doi:10.1039/A606813H.
31. Aramendia, M.A.; Borau, V.; Garcia, I.M.; Jimenez, C.; Marinas, A.; Marinas, J.M.; Porras, A.; Urbano, F.J. Comparison of different organic test reaction over acid-base catalysts. *Applied Catalysis A: General* **1999**, *184*, 115-125, doi:10.1016/s0926-860x(99)00096-4
32. Aramendia, M.A.; Borau, V.; Jimenez, C.; Marinas, A.; Marinas, J.M.; Ruiz, J.R.; Urbano, F.J. Magnesium-containing mixed oxides as basic catalysts: base characterization by carbon dioxide TPD-MS and test reactions. *Journal of Molecular Catalysis A: Chemical* **2004**, *218*, 81-90, doi:10.1016/j.molcata.2004.04.006.
33. Yan, K.; Wu, X.; An, X.; Xie, X. Facile synthesis of reusable coal-hydrotalcite catalyst for dehydration of biomass-derived fructose into platform chemical 5-hydroxymethylfurfural. *Chemical Engineering Communications* **2014**, *201*, 456-465, doi:10.1080/00986445.2013.775646.

34. Haffad, D.; Chambellan, A.; Lavalley, J.C. Propan-2-ol transformation on simple metal oxides TiO_2, ZrO_2 and CeO_2. *Journal of Molecular Catalysis A: Chemical* **2001**, *168*, 153-164, doi:10.1016/s1381-1169(00)00516-1.
35. Marinas, A.; Marinas, J.M.; Aramendia, M.A.; Urbano, F.J. Heterogeneous catalysis on basic sites in organic chemistry. En *New Developments in Catalysis Research*, Bevy, L.P., Ed. Nova Science: New York, 2005; pág. 85-127.

Capítulo IV.

Resultados y discusión (Paper 2)

CHAPTER IV. RESULTS AND DISCUSSION: ALDOL CONDENSATION OF FURFURAL WITH ACETONE OVER Mg/Al MIXED OXIDES. INFLUENCE OF WATER AND SYNTHESIS METHOD

PAPER 2

Aldol condensation of furfural with acetone over Mg/Al mixed oxides. Influence of water and synthesis method

Almudena Parejas, Daniel Cosano, Jesús Hidalgo-Carrillo, José Rafael Ruiz, Alberto Marinas, César Jiménez-Sanchidrían and Francisco J. Urbano*

Departamento de Química Orgánica, Instituto Universitario de Investigación en Química Fina y Nanoquímica IUIQFN, Universidad de Córdoba, Campus de Rabanales, Edificio Marie Curie, E-14071 Córdoba, España

* Correspondence: jesus.hidalgo@uco.es, Tel.: +34957218638.

Published in *Catalysis* **2019**, 9, 203; doi: 10.3390/catal9020203.

Abstract

Aldol condensation of furfural and acetone (an important initial step to obtain diesel from biomass) was studied over MgAl mixed oxides. The influence of the utilization of microwaves and/or a surfactant (Pluronic 123) during the synthesis as well as the use of water (either pre-hydrating the solids before catalytic studies or in water/toluene mixtures as the reaction medium) is discussed. The combined use of Pluronic 123 and microwaves led to solids with bigger pore sizes, exhibiting lower basicity and higher acidity than the conventional synthetic method, thus resulting in an increase in the yield of the desired product of condensation, comprising two molecules of furfural and one of acetone (F2Ac). As for the influence of water, re-hydration of the mixed oxides was detrimental to activity, probably as a result of the partial blocking (solvation) of active sites. On the contrary, the increase in water percentage in the reaction medium resulted in higher conversions, though selectivity to F2Ac decreased. The weakening of the C=O bond of furfural in the presence of water as well as the higher solubility of the first condensation product (FAc) in toluene, as compared to water, could account for that. A 44.5% yield of F2Ac (66% conversion) after 16 h was obtained with the most active solid, which maintained the activity for three consecutive reactions.

Keywords: aldol condensation; biomass valorization; Mg/Al mixed oxides; surfactant; microwaves; influence of water.

IV.1. Introduction

Fossil fuel depletion and environmental concern have boosted the search for renewable energies, one of the possible sources being biomass [1,2]. Furfural is a so-called platform molecule from biomass obtained through xylose dehydration [3] and can be transformed into a wide range of chemicals via hydrogenation, oxidation, decarbonylation, nitration, or condensation processes, just to cite some of them [4]. For instance, aldol condensation and subsequent hydrogenation and hydrodeoxygenation can lead to liquid hydrocarbons for use as diesel [5].

Aldol condensation is a well-known C-C bond formation process which can occur in acidic or basic sites, the latter being more frequently reported in the literature [6-15]. It requires the existence of a reactive hydrogen in alpha position, with respect to a carbonyl compound able to form an enol, which reacts with another carbonyl compound, and after dehydration, yields a conjugated enone. Focusing on aldol condensation between furfural and acetone (Figure 1), it can initially lead to 4-(2-furanyl)-3-buten-2-one (FAc), a subsequent aldol condensation with another furfural molecule, forming 1,5-bis-(2-furanyl)-1,4-pentadien-3-one (F2Ac) (Figure 1a) [16,17]. Some side reactions include acetone self-condensation to form diacetone-alcohol and mesityl oxide (Figure 1b), condensation between FAc and acetone (Figure 1c), and multiple aldol condensations between different carbonyl compounds, thus forming polymers [18,19] (Figure 1d).

Aldol condensations have been traditionally performed in organic media, using base catalysts such as sodium or calcium hydroxides. Nevertheless, the existence of corrosion problems and the difficult reutilization have led to the use of some other base heterogeneous catalysts, such as hydrotalcites and hydrotalcite-derived mixed oxides [20,21], amorphous

aluminophosphate [15], and diamine-functionalized MCM-41[22], just to cite some examples.

In the present work, different AlMg mixed oxides were obtained through calcination of layered double hydroxides (LDHs) and tested for aldol condensation with acetone to form F2Ac. The influence on the catalytic results of two synthetic variables (conventional or microwave heating with the presence or absence of Pluronic 123 as the surfactant) was explored. Furthermore, the effect of water (either pre-hydrating the solids before catalytic studies or in water/toluene mixtures as the reaction medium) is discussed.

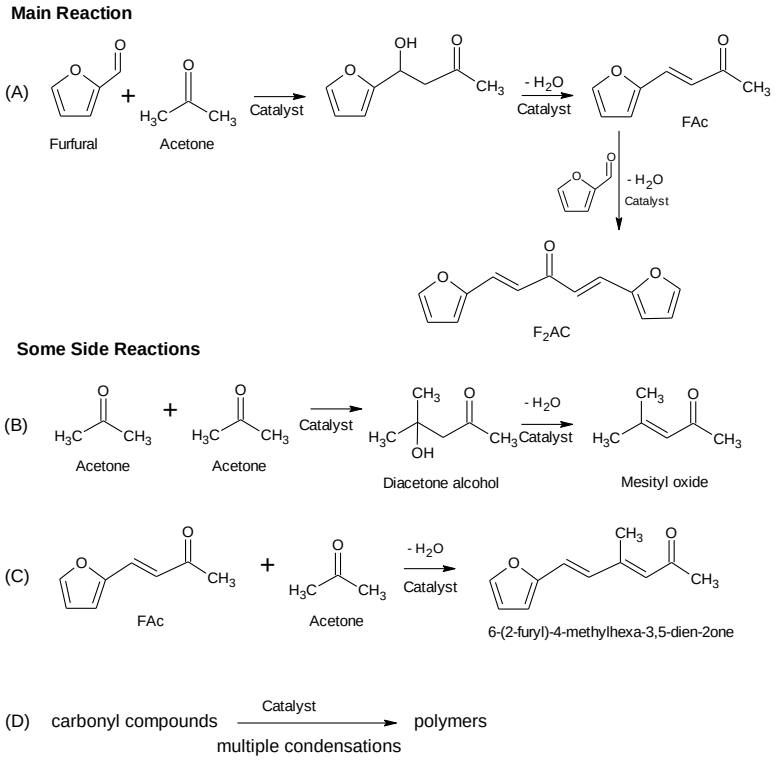

Figure 1. Reaction scheme for aldol condensation of furfural and acetone. Some side reactions have also been included. (**a**) aldol condensation between furfural and acetone, (**b**) acetone self-condensation, (**c**) condensation between FAc and acetone and (**d**) multiple aldol condensations between different carbonyl compounds.

IV.2. Results and Discussion

IV.2.1. Textural, Structural and Acid- Base Characterization of the Solids

X-ray diffractograms of uncalcined and calcined hydrotalcites are shown in Figure 2. As can be seen, uncalcined solids exhibit a typical hydrotalcite crystallinity profile (JCPDS 22-700), with symmetric reflections at 2θ = 11°, 22°, 36°, 37°, 45°, 60°, and 62°. Therefore, sharper peaks corresponded to (003), (006), (010), and (013) reflections, whereas broader signals were obtained for (009), (015), and (016) reflections, all of them representative of layered materials. As for calcined solids (Figure 2b), diffraction patterns are very similar to each other, exhibiting (111), (200), and (220) reflections ascribed to periclase. In a previous paper, Aramendia et al. [23], using ^{27}Al NMR-MAS, demonstrated that the coordination of Al^{3+} changed from octahedral to tetrahedral upon calcination of hydrotalcites, Al^{3+} ions thus isomorphically substituting Mg^{2+} ions, forming MgAlOx periclase.

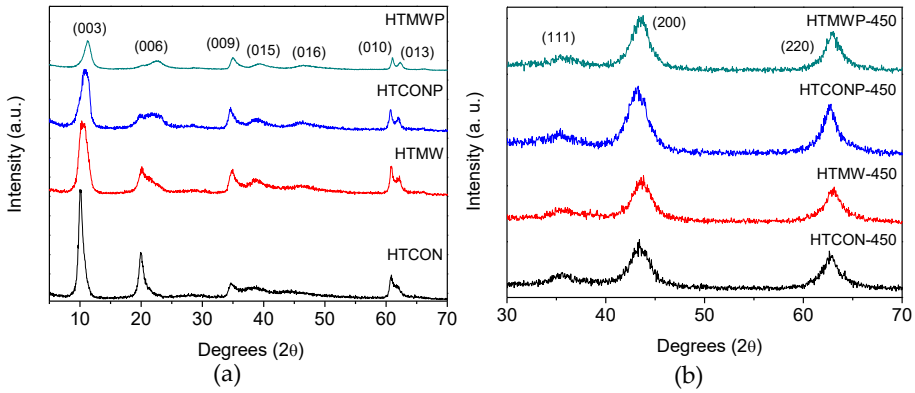

Figure 2. X-ray diffractograms of the different solids synthesized in the present work. (**a**) Uncalcined solids. (**b**) Solids calcined at 450 ºC.

Thermal stability of hydrotalcites was determined by TG-DTA (Figure 3). In all cases, weight loss percentage is in the 42–45% range (Figure 3a). HTCON and HTMW thermogravimetric profiles are consistent with those

reported in the literature for hydrotalcites [24,25]. Therefore, two main weight losses are observed. The first one at 100–200 ºC is ascribed to the loss of intercalated water molecules, whereas nitrate coming from both the precursor and hydroxyl groups can account for the second loss at higher temperatures (250–500 ºC). For the solids synthesized using the surfactant (HTCONP and HTMWP), the second weight loss seems to be produced quicker (i.e., at lower temperatures), thus suggesting that for those systems, re-structuration to form periclase is somehow favored by Pluronic 123. Heat flow profiles (Figure 3b) seem to confirm this hypothesis, the exothermal peak centered at 450 °C in HTCON and HTMW being shifted to lower temperatures (300–350 ºC) for HTCONP and HTMWP.

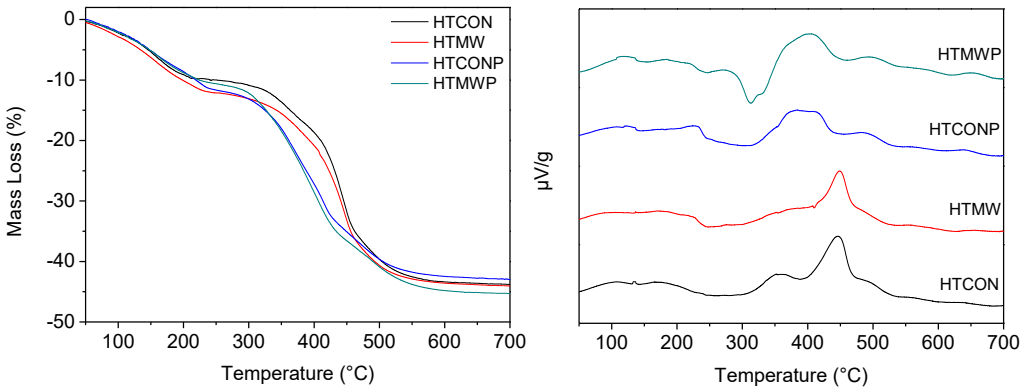

Figure 3. TG analyses (**a**) and heat flow (**b**) of hydrotalcites.

Raman spectra of uncalcined solids (i.e., hydrotalcites) are represented in Figure 4. The band appearing at 557 cm^{-1} can be assigned to vibrations of brucite-like octahedral layers, Al-O-Mg, which are present in all Mg-Al hydrotalcites [26]. Moreover, the spectra also exhibit bands at 710 and 1055 cm^{-1}, corresponding to nitrate vibrations [27] and bands at ca. 3500 cm^{-1}, due to surface hydroxyl groups. In the case of HTCONP and HTMWP solids, there are also some intense bands of C-H stretching Pluronic 123 at 2986, 2941, and 2933 cm^{-1} [28].

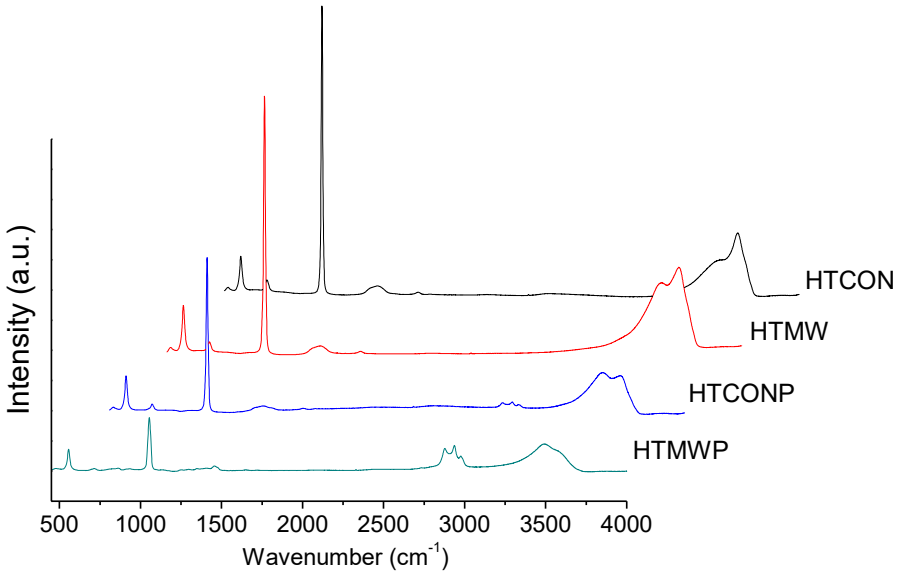

Figure 4. Raman spectra of the uncalcined solids (hydrotalcites).

N_2 adsorption–desorption isotherms of calcined solids are shown in Figure 5. In all cases, type IV isotherms corresponding to mesoporous materials were obtained. BET surface areas, pore volume and average pore diameter values are given in Table 1. With regards to the BET areas, they are in the 160–210 $m^2 \cdot g^{-1}$ range, the highest value corresponding to HTCONP-450. Modification of conventional synthesis by using microwave irradiation and/or in the presence of the surfactant (Pluronic 123) led in all cases to an increase in BET area. Solids that aged under microwave irradiation exhibit smaller pore diameters than their conventionally-heated counterparts (compare HTMW-450 vs. HTCON-450 or HTMWP-450 vs. HTCONP-450). Systems synthesized in the presence of the surfactant present bigger pores (compare HTCONP-450 vs. HTCON-450 and HTMWP-450 vs. HTMW-450). Therefore, the effect of microwaves and the presence of a surfactant on pore volume is the opposite. However, if both variables are changed simultaneously, the influence of the surfactant is more important, thus resulting in the pore diameter increasing

(compare HTCON-450 and HTMWP-450 with pore diameters of 6.8 and 8.4 nm, respectively).

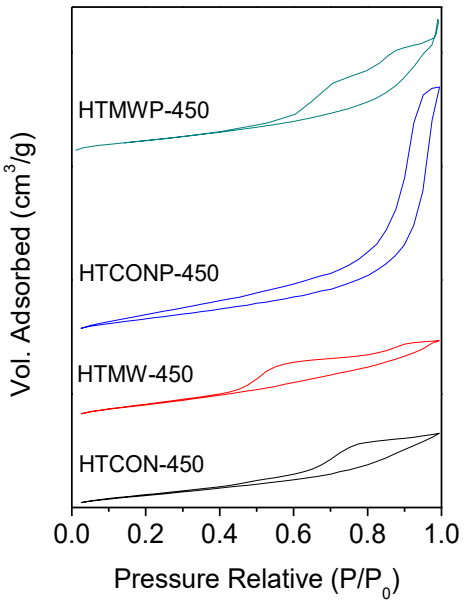

Figure 5. Nitrogen adsorption-desorption isotherms corresponding to the mixed oxides.

Table 1. Summary of the main features of the mixed oxides synthesis in this work.

Catalyst	Textural properties			Base sites (CO_2-TPD) (µmol/g)	Acid sites (Py-TPD) (µmol/g)	Mg/Al Ratio	
	S_{BET} (m^2/g)	V_p (cm^3/g)	D_p (nm)			Nominal	XRF
HTCON-450	160	0.26	6.8	1105	871	2.00	2.01
HTMW-450	201	0.29	4.2	880	1030	2.00	1.94
HTCONP-450	210	0.86	16.6	932	960	2.00	2.04
HTMWP-450	183	0.40	8.4	775	1124	2.00	1.97

X-Ray fluorescence results (Table 1) evidenced a good incorporation of Mg and Al to the solids, with Mg/Al ratios very similar to the nominal value (Mg/Al = 2).

Base characterization of the solids was performed using thermal programmed desorption of pre-adsorbed CO_2 (CO_2-TPD) and the results are given in Tables 1 and 2, and in Figure 6. In all cases, signals were deconvoluted in peaks, which, depending on the desorption temperature, were ascribed to weak (80–200 ºC), medium (200–300 ºC), or strong (>300 ºC) basic sites, respectively. Taking HTCON-450 as the reference, the use of microwave irradiation and/or the presence of the surfactant in the synthesis results in a drop in total basicity. Interestingly, as far as the base site distribution is concerned, the effect of microwave irradiation, the presence of the surfactant, or both variables simultaneously considered is different. Therefore, in the absence of Pluronic 123, microwave irradiation does not vary base site distribution. On the contrary, the presence of Pluronic 123 results in an increase in the strong base sites' percentage, to the detriment of weak ones. Finally, simultaneous use of microwaves and Pluronic 123 leads to an increase in the percentage of weak base sites.

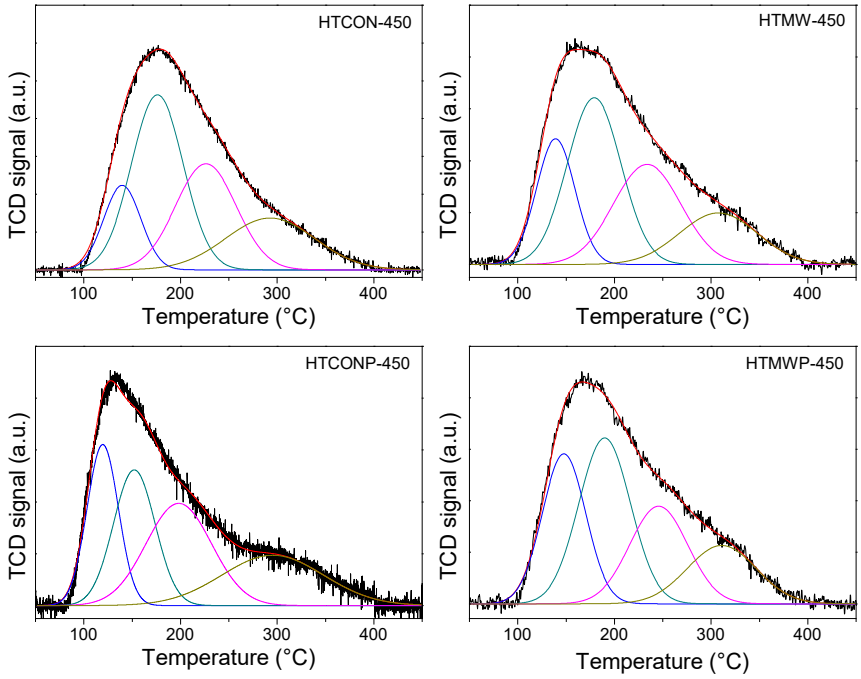

Figure 6. Temperature-programmed desorption profiles of CO_2 for the mixed oxides synthesized in this work.

Table 2. Base site distribution of the solids expressed as μmol CO_2/g. Values in brackets represent the percentage of the total basicity.

	Base sites distribution, μmol CO_2/g		
Catalyst	**Weak (80–200 ºC)**	**Medium (200–300 ºC)**	**Strong (>300 ºC)**
HTCON-450	580.34 (52.53%)	304.89 (27.60%)	219.51 (19.87%)
HTMW-450	468.05 (53.20%)	241.95 (27.50%)	169.80 (19.30%)
HTCONP-450	428.62 (45.97%)	276.64 (29.67%)	227.13 (24.36%)
HTMWP-450	470.96 (60.80%)	177.38 (22.90%)	126.26 (16.30%)

Acid characterization of the solids was performed by thermal programmed desorption of pre-adsorbed pyridine (Py-TPD), results being given in Tables 1 and 3, and in Figure 7. Taking HTCON-450 as the reference, contrary to basicity, total acidity increases when the solids are synthesized utilizing a microwave and/or in the presence of Pluronic 123. Furthermore, with regards to acid site distribution, only microwave irradiation has some effect (acid strength decreases), whereas the presence of Pluronic 123, either under conventional heating or microwave irradiation, does not vary acid site distribution.

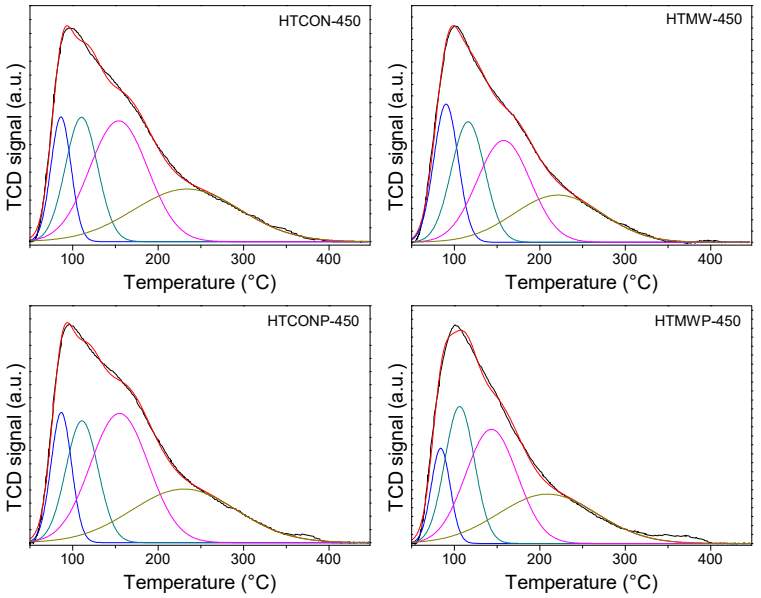

Figure 7. Temperature-programmed desorption profiles of pyridine for the mixed oxides synthesized in this work.

Table 3. Base site distribution of the solids expressed as μmol Py/g. Values in brackets represent the percentage of the total basicity.

	Acid site distribution, μmol Py/g		
Catalyst	**Weak (80–200 ºC)**	**Medium (200–300 ºC)**	**Strong (>300 ºC)**
HTCON-450	296.36 (34.01%)	320.14 (36.74%)	254.88 (29.25%)
HTMW-450	447.56 (43.44%)	329.59 (31.99%)	253.14 (24.57%)
HTCONP-450	320.58 (33.39%)	365.71 (38.09%)	273.82 (28.52%)
HTMWP-450	397.24 (35.33%)	398.70 (35.46%)	328.43 (29.21%)

All in all, microwave irradiation and/or the use of Pluronic 123 as the surfactant result in an increase in total acidity and a decrease in total basicity together with an increase in BET areas.

IV.2.2.Catalytic Activity

The solid synthesized under conventional heating and in the absence of the surfactant (HTCON-450) was used as the reference material in order to study the influence of reaction temperature and the presence of water in the reaction medium on catalytic activity.

IV.2.2.1. Influence of Reaction Temperature

Table 4 summarizes catalytic results obtained for t = 3 h at different temperatures. From that table, it is evident that the increase in temperature results in the increase in conversion, whereas selectivity to F2Ac, the desired product, hardly changes. Therefore, from then on, 100 °C was selected as the reaction temperature.

Table 4. Aldol condensation of furfural and acetone on HTCON-450: Influence of temperature on catalytic activity. Reaction conditions: Reactor pressurized to 5 bar with N_2; 10 mmol of furfural, 20 mmol acetone, 20 mL toluene, and 400 mg catalyst, t=3h.

Temperature (°C)	Conv. (%)	Sel. FAc (%)	Sel. F2Ac (%)	Yield FAc (%)	Yield F2Ac (%)
60	3.8	45.5	54.5	1.7	2.1
80	14.4	50.3	49.7	7.3	7.2
100	35.0	42.5	57.6	14.8	20.1

IV.2.2.2. Influence of Water

Two different approaches were made to study the influence of water on catalytic activity of HTCON-450. On the one hand, the solid was re-hydrated using a N_2 flow saturated in water. On the other hand, reactions were performed in water/toluene mixtures (0%, 5%, 10%, 50%). Regarding the former approach (Table 5), the pretreatment of HTCON-450 with a flow of nitrogen saturated in water results in a drop in conversion (35.0% and 23.7% for HTCON-450 and HTCON-450-rehydrated, respectively, at t = 3 h), whereas selectivity values to F2Ac are quite similar. This suggests that rehydration results in the elimination of active sites to a certain extent, which could be ascribed to solvation. Results obtained for the uncalcined HTCON solid (which exhibits very low catalytic activity) are also given for the sake of comparison.

Table 5. Aldol condensation of furfural and acetone on HTCON-450: Influence of calcination and rehydration of the solid. Reaction conditions: Reactor pressurized to 5 bar with N_2; 10 mmol of furfural, 20 mmol acetone , 20 mL toluene, and 400 mg catalyst, t=3h, 100 ºC.

Catalyst	Conv. (%)	Sel. FAc (%)	Sel. F2Ac (%)	Yield FAc (%)	Yield F2Ac (%)
HTCON	0.7	85.0	14.9	0.6	0.1
HTCON-450	35.0	42.5	57.6	14.8	20.1
HTCON-450-rehidrated	23.7	40.1	59.8	9.5	14.2

Table 6 summarizes the results obtained for the study conducted using different water/toluene ratios as the reaction medium. As can be seen, the higher the percentage of water, the higher the conversion, but in general, the lower the selectivity to the desired product, F2Ac. In a previous paper [29] on chemoselective hydrogenation of alpha,beta-unsaturated carbonyl compounds, our research group found evidence by Raman spectroscopy that water interacted with the carbonyl group and made the double bond weaker and thus more reactive (carbonyl band shifted to lower wavelength values). The same could occur in the C=O group in furfural and account for its higher conversion in the presence of water. With regards to the change in selectivity, one should consider that we are working in a biphasic media and thus the catalyst hydrophilic character, as well as the relative solubility of reactants and products both in toluene and water, is important. Active sites in the catalyst will probably interact better with water than with toluene. Furfural is partially soluble in water (50–100 $mg \cdot mL^{-1}$). Its condensation with one molecule of acetone will produce FAc, whose solubility in water is much lower (1–10 $mg \cdot mL^{-1}$). Therefore, once formed, FAc will pass to the organic phase (toluene) and will not be able to undergo subsequent condensation with another acetone molecule to produce F2Ac. This results in the increase in selectivity to FAc and probably in conversion, since FAc is retired of the aqueous phase as the reaction proceeds. All in all, the highest yield to F2Ac, the desired product, is achieved with pure toluene. Therefore, this reaction medium was selected for subsequent studies on other catalysts.

Table 6. Aldol condensation of furfural and acetone on HTCON-450: Influence of the presence of water in water/toluene mixtures. Reaction conditions: Reactor pressurized to 5 bar with N_2; 10 mmol of furfural, 20 mmol acetone , 20 mL (toluene+water) and 400 mg catalyst, t=3h, 100 ºC.

Water (%)	Conv. (%)	Sel. FAc (%)	Sel. F2Ac (%)	Yield FAc (%)	Yield F2Ac (%)
0	35.0	42.5	57.6	14.8	20.1
5	37.6	60.8	39.2	22.9	14.7
10	53.2	70.3	29.6	37.4	15.8
50	80.4	88.1	11.9	70.8	9.6

IV.2.3.Catalytic Activity of the Other Mixed Oxides

Once pure toluene and 100 ºC had been selected as the reaction conditions for aldol condensation of furfural and acetone in order to obtain F2Ac, the study was extended to the other mixed oxides. Reactions were conducted at 3 h and 16 h, the main catalytic results being summarized in Table 7.

A first conclusion from that table is that the lowest conversion values correspond to HTMW-450. It is important to note that this solid was the one exhibiting the lowest pore diameter (4.2 nm, Table 1), which could account for that. Focusing on the other solids, the highest conversion value at 3 h is achieved for HTCON-450, whereas as the reaction proceeds, the rate is higher for the systems synthesized using Pluronic 123, which together with their higher selectivity to F2Ac results in F2Ac yields of 24.6%, 28.3%, and 44.5% for HTCON-450, HTCONP-450, and HTMWP-450, respectively, at t = 16 h. As evidenced by thermal-programmed desorption of pyridine and CO_2, the use of microwave irradiation and/or the presence of Pluronic 123 in the reaction medium during the synthesis resulted in an increase in total acidity and a decrease in total basicity. In a previous paper, Climent et al. [15] described the cooperative effect of weak acid and base sites of an amorphous aluminophosphate in aldol condensation, thus resulting in higher selectivities

than those presented by stronger acid or base catalysts. This effect together with the increase in pore size could explain the higher yields obtained for the solids synthesized using the surfactant.

Table 7. Results obtained for aldol condensation of furfural and acetone on the different solids. Reaction conditions: Reactor pressurized to 5 bar with N_2; 10 mmol of furfural, 20 mmol acetone, 20 mL toluene and 400 mg catalyst, 100 ºC .

Time (h)	Catalyst	Conv. (%)	Sel. FAc (%)	Sel. F2Ac (%)	Yield FAc (%)	Yield F2Ac (%)
3	HTCON-450	35.0	42.5	57.6	14.8	20.1
	HTMW-450	19.5	63.2	36.8	12.3	7.2
	HTCONP-450	28.4	47.6	52.4	13.5	14.9
	HTMWP-450	32.9	32.9	67.1	10.8	22.1
16	HTCON-450	46.9	47.6	52.4	22.4	24.6
	HTMW-450	27.4	42.9	57.1	11.8	15.7
	HTCONP-450	45.2	37.4	62.6	18.9	28.3
	HTMWP-450	66.2	32.8	67.2	21.7	44.5

IV.2.4.Reutilization of HTCON-450 and HTMWP-450

Finally, some reutilization studies were conducted on HTCON-450 and HTMWP-450 solids, results being summarized in Table 8. In all cases, the Mg/Al ratio of the solids was quite similar to the nominal value (Mg/Al = 2). Moreover, after the reactions, the reaction medium was analyzed by inductively coupled plasma mass spectrometry (ICP-MS). No Mg or Al was detected which is evidence of the stability of the solids, which do not undergo leaching.

Table 8. Results obtained for reutilization studies. Reaction conditions: Reactor pressurized to 5 bar with N_2; 10 mmol of furfural, 20 mmol acetone, 20 mL toluene and 400 mg catalyst, 100 ºC.

Catalyst	Conv. (%)	Sel. FAc (%)	Sel. F2Ac (%)	Yield FAc (%)	Yield F2Ac (%)	Mg/Al ratio (XRF)
HTCON-450	35.0	42.5	57.6	14.8	20.1	2.01
HTCON-450-R	37.4	41.2	58.8	15.4	22.0	2.03
HTMWP-450	32.9	32.9	67.1	10.8	22.1	1.97
HTMWP-450-R	31.1	41.5	58.5	12.9	18.2	1.98
HTMWP-450-R2	34.4	43.5	56.5	15.0	19.4	2.02

As far as the catalytic activity is concerned, neither HTCON-450 nor HTMWP-450 exhibited any remarkable deactivation keeping F2Ac yield in the ca. 20% order after three hours. In the case of the most active solid at long reaction times (HTMWP-450), its activity and selectivity only decreased slightly (from 67.1 to 58.5%) after three consecutive uses.

IV. 3. Materials and Methods

Hydrotalcites were synthesized by a co-precipitation method, starting from two solutions containing 0.2 mol $Mg(NO_3)_2 \cdot 6H_2O$ and 0.1 mol $Al(NO_3)_3 \cdot 9H_2O$ in 25 mL deionized water, respectively (Mg/Al = 2). The mixture was slowly added to a pH 10 aqueous solution under continuous stirring and an inert atmosphere (N_2), with temperature maintained at 60 ºC. During precipitation, the pH value was maintained, adding NaOH 1M. The suspension was divided into four portions for further treatment. One part was kept under conventional heating at 80 ºC for 24 h, followed by filtration and washing with deionized water, thus obtaining the solid called HTCON. A second portion was aged under microwave heating at 80 ºC for 1 h, thus leading, after filtration and washing, to the solid termed as HTMW. A flexiWave platform for microwave synthesis (22 V, 50 Hz) with an IR temperature sensor (p/n IRT0500) was used. The other two portions were

submitted to the same conventional or microwave heating while performing the synthesis in the presence of surfactant Pluronic 123 (2% by weight), thus leading to the solids named HTCONP and HTMWP, respectively. Finally, all four solids were calcined at 450 ºC in the air for 8 h (1 ºC·min^{-1} ramp). Nomenclature of these solids include the suffix 450, referring to calcination temperature (HTCON-450, HTMW-450, HTCONP-450, and HTMWP-450). Subsequent treatment of HTCON-450 for 2 h at 450 ºC in the presence of a N_2 flow (50 mL·min^{-1}) saturated in water at 20 ºC led to a solid called HTCON-450-rehydrated.

A Setaram SetSys 12 instrument (SETARAM Instrumentation, Caluire - France) was used for thermogravimetric analyses (TGA). Experiments were performed on 20 mg samples placed in an alumina crucible and heated in the 30–600 ºC range (10 ºC·min^{-1}, 50 mL·min^{-1} air stream).

Textural properties (BET surface area, cumulative pore volume, and average pore diameter) were measured in a Micromeritics ASAP-2010 instrument (Micromeritics, Norcross, USA.). Samples were heated at 120 ºC and degassed to 0.1 Pa before measurement.

The measure of magnesium or aluminium leaching (presence in filtered reaction medium) was performed by inductively coupled plasma mass spectrometry (ICP-MS) on a Perkin–Elmer ELAN DRC-e instrument.

The Mg/Al ratio of solids was measured by X-ray fluorescence (XRF) spectroscopy (Rigaku ZSK PrimusIV wavelength X-ray spectrometer (Rigaku, The Woodlands, USA). Further details are given elsewhere [30].

Raman spectra were recorded on a Renishaw spectrometer (InVia Raman Microscope, Renishaw, Gloucestershire, UK), equipped with a Leica microscope with various lenses, monochromators, filters, and a CCD detector.

Spectra were recorded over the 150–4000 cm^{-1} range, using green laser light excitation (532 nm) and gathering 32 scans.

X-ray diffraction (XRD) analysis was performed on a Siemens D-5000 diffractometer (Bruker Corporation, Billerica, U.S.A.) using CuKα radiation over the range 5–80º.

Surface acidity of samples was measured by thermal programmed desorption of pre-adsorbed pyridine (Py-TPD) using TC detection. Samples (30 mg) were cleaned by heating to 450 ºC (10 ºC·min^{-1} ramp) under He flow (75 mL·min^{-1}) and then cooled down to 50 ºC. The catalysts were subsequently saturated with pyridine for 30 min, cleaned for 60 min with He and TPD monitored from 50 to 450 ºC (10 ºC·min^{-1}), the final temperature being held for 45 min.

Surface basicity of the catalysts was determined on a Micromeritics Autochem II instrument by thermal programmed desorption of pre-absorbed CO_2 (CO_2-TPD) with TCD detection. Samples (100 mg) were cleaned in an Air stream (20 mL·min^{-1} Ar, heating at 450 ºC at a rate of 10 ºC·min^{-1} for 60 min and then cooled down to 40 ºC). Then, solids were saturated with CO_2 (5% CO_2/Ar flow at 20 mL·min^{-1} for 60 min), physisorbed CO_2 removed with Ar flow (20 mL·min^{-1} for 30 min) and TPD monitored from 50 to 450 ºC (5 ºC·min^{-1}), the final temperature being held for 60 min.

The solids were tested for aldol condensation of furfural using a Berghof HR-100 stainless steel high-pressure autoclave equipped with a 75 mL PTFE insert vessel. Under standard conditions, 10 mmol of furfural, 20 mmol acetone, 20 mL toluene, and a 400 mg catalyst were introduced in the vessel. Reactor was purged with nitrogen and pressurized to 5 bar of N_2. The reaction temperature was set to 100 ºC and started by switching on the stirring at 750

rpm. To stop the reaction, the vessel was submerged in an ice bath. The choice of toluene as the organic medium was motivated by a previous paper [3] on xylose dehydration to furfural where toluene was found to give the highest yield to furfural. The final strategy would be to make the one-pot transformation of xylose to furfural and then F2Ac.

Experiments to evaluate the influence of the presence of water in the reaction medium were conducted varying the water/toluene ratio (0%, 5%, 10%, and 50% volume) while keeping the total solvent volume constant (20 mL).

Once the reactions were finished, the products were analyzed by gas chromatography (Agilent 7890) with a flame ionization detector (GC-FID), using a Supelco Nukol^{TM} capillary column. In the case of using biphasic media (toluene/water mixtures), products were extracted from the aqueous phase with dichloromethane before GC-FID analysis. Quantification of furfural and condensation products was performed using the appropriate calibration curves. In all cases, mass balance considering unreacted furfural, FAc, and F2Ac was over 95%.

For reutilization experiments, after the reaction, the solids were filtered, washed with ethanol, and dried at 100 °C, followed by calcination at 450 °C under the same conditions as described in the synthesis. Nomenclature of reused catalysts include the suffix R (one reuse) or R2 (two reuses).

Furfural conversion and FAc and F2Ac selectivity were defined by Equations (1)–(3):

$$\text{Furfural conversion (\%)}: \frac{\text{initial furfural concentration - final furfural concentration}}{\text{initial furfural concentration}} \text{ x } 100 \quad (1)$$

$$\text{FAc selectivity (\%)}: \frac{\text{FAc concentration}}{\text{FAc concentration} + 2\cdot \text{F2Ac concentration}} \text{ x } 100 \quad (2)$$

$$\text{F2Ac selectivity (\%)}: \frac{2 \cdot \text{F2Ac concentration}}{\text{FAc concentration} + 2 \cdot \text{F2Ac concentration}} \text{ x } 100 \quad (3)$$

IV.4. Conclusions

The synthesis of hydrotalcites in the presence of Pluronic 123 led, after calcination, to MgAl mixed oxides with bigger pore sizes than untreated solids. On the other hand, microwave irradiation led to smaller pore sizes as compared to conventional thermal treatment. As far as acid–base characteristics are concerned, the use of both microwave irradiation and Pluronic 123 during the synthesis resulted in a decrease of total basicity and an increase in total acidity.

Rehydration of mixed oxides by treating them with a nitrogen flow saturated with water led to solids exhibiting lower catalytic activity in aldol condensation of furfural, probably as a result of the partial blocking (solvation) of active sites. By contrast, the increase in the percentage of water in water/toluene biphasic media resulted in an increase in conversion values, though selectivity to FAc also increased at the expense of the desired product F2Ac. A plausible explanation is that water weakens the C=O bond in furfural, thus favoring its transformation. Moreover, once FAc is produced, its higher solubility in toluene, as compared to water, favors its transfer to the organic medium, thus avoiding its subsequent reaction with another furfural molecule to yield F2Ac. The fact that the produced FAc is retired to the organic phase could also account for the observed increase in conversion.

A comparison of catalytic activity of the reference material (HTCON-450) with that of the other solids allows us to conclude that the use of Pluronic 123 during synthesis (especially in combination with microwave irradiation) resulted in solids exhibiting higher F2Ac yields at long reaction times. This could be the result of the combination of two factors: The above-mentioned

larger pore size achieved with the surfactant and the increase in total acidity which could favor aldol condensation.

HTMWP-450 exhibited a good stability without any significant loss of activity after three uses.

Funding

This research was funded by Ramón Areces Foundation.

Acknowledgements

The scientific support from the Central Service for Research Support (SCAI) at the University of Cordoba is acknowledged.

References

1. Field, C.B.; Campbell, J.E.; Lobell, D.B. Biomass energy: the scale of the potential resource. *Trends in Ecology & Evolution* **2008**, *23*, 65-72, doi:10.1016/j.tree.2007.12.001.
2. Chheda, J.N.; Huber, G.W.; Dumesic, J.A. Liquid-phase catalytic processing of biomass-derived oxygenated hydrocarbons to fuels and chemicals. *Angewandte Chemie-International Edition* **2007**, *46*, 7164-7183, doi:10.1002/anie.200604274.
3. Parejas, A.; Montes, V.; Hidalgo-Carrillo, J.; Sanchez-Lopez, E.; Marinas, A.; Urbano, F.J. Microemulsion and sol-gel synthesized ZrO_2-MgO catalysts for the liquid-phase dehydration of xylose to furfural. *Molecules* **2017**, *22*, doi:10.3390/molecules22122257.

4. Sheldon, R.A. Green and sustainable manufacture of chemicals from biomass: state of the art. *Green Chemistry* **2014**, *16*, 950-963, doi:10.1039/c3gc41935e.
5. O'Neill, R.E.; Vanoye, L.; De Bellefon, C.; Aiouache, F. Aldol-condensation of furfural by activated dolomite catalyst. *Applied Catalysis B: Environmental* **2014**, *144*, 46-56, doi:10.1016/j.apcatb.2013.07.006.
6. Smolakova, L.; Frolich, K.; Kocik, J.; Kikhtyanin, O.; Capek, L. Surface properties of hydrotalcite-based zn(mg)al oxides and their catalytic activity in aldol condensation of furfural with acetone. *Industrial & Engineering Chemistry Research* **2017**, *56*, 4638-4648, doi:10.1021/acs.iecr.6b04927.
7. Faba, L.; Diaz, E.; Ordonez, S. Aqueous-phase furfural-acetone aldol condensation over basic mixed oxides. *Applied Catalysis B: Environmental* **2012**, *113*, 201-211, doi:10.1016/j.apcatb.2011.11.039.
8. Chheda, J.N.; Dumesic, J.A. An overview of dehydration, aldol-condensation and hydrogenation processes for production of liquid alkanes from biomass-derived carbohydrates. *Catalysis Today* **2007**, *123*, 59-70, doi:10.1016/j.cattod.2006.12.006.
9. Climent, M.J.; Corma, A.; Iborra, S. Conversion of biomass platform molecules into fuel additives and liquid hydrocarbon fuels. *Green Chemistry* **2014**, *16*, 516-547, doi:10.1039/c3gc41492b.
10. Shen, W.Q.; Tompsett, G.A.; Hammond, K.D.; Xing, R.; Dogan, F.; Grey, C.P.; Conner, W.C.; Auerbach, S.M.; Huber, G.W. Liquid phase aldol condensation reactions with MgO-ZrO_2 and shape-selective nitrogen-substituted NaY. *Applied Catalysis A: General* **2011**, *392*, 57-68, doi:10.1016/j.apcata.2010.10.023.
11. Cota, I.; Ramirez, E.; Medina, F.; Sueiras, J.E.; Layrac, G.; Tichit, D. New synthesis route of hydrocalumite-type materials and their application as basic catalysts for aldol condensation. *Applied Clay Science* **2010**, *50*, 498-502, doi:10.1016/j.clay.2010.09.019.

12. West, R.M.; Liu, Z.Y.; Peter, M.; Gaertner, C.A.; Dumesic, J.A. Carbon-carbon bond formation for biomass-derived furfurals and ketones by aldol condensation in a biphasic system. *Journal of Molecular Catalysis A: Chemical* **2008**, *296*, 18-27, doi:10.1016/j.molcata.2008.09.001.
13. Resasco, D.E.; Sitthisa, S.; Faria, J.; Prasomsri, T.; Ruiz, A.M.P. Furfurals as chemical platform forbiofuels production. En *Heterogeneous Catalysis in Biomass to Chemicals and Fuels*, Kubičková, D; Kubička, D. Editores, Research Signpost, 2011.
14. Bao, Q.; Qi, H.; Zhang, C.; Ning, C.; Zhang, Y.; Jiang, Y.; Wu, Y.; Gui, W.; Wang, Z. Highly Catalytic activity of Ba/γ-Ti-Al_2O_3 catalyst for aldol condensation of methyl acetate with formaldehyde. *Catalysis Letters* **2018**, *148*, 3402-3412, doi:10.1007/s10562-018-2535-9.
15. Climent, M.J.; Corma, A.; Fornes, V.; Guil-Lopez, R.; Iborra, S. Aldol condensations on solid catalysts: A cooperative effect between weak acid and base sites. *Advanced Synthesis & Catalysis* **2002**, *344*, 1090-1096, doi:10.1002/1615-4169(200212)344:10<1090::aid-adsc1090>3.0.co;2-x.
16. Fakhfakh, N.; Cognet, P.; Cabassud, M.; Lucchese, Y.; Rios, M.D.D.L. Stoichio-kinetic modeling and optimization of chemical synthesis: Application to the aldolic condensation of furfural on acetone. *Chemical Engineering and Processing* **2008**, *47*, 349-362, doi:10.1016/j.cep.2007.01.015.
17. Xing, R.; Subrahmanyam, A.V.; Olcay, H.; Qi, W.; van Walsum, G.P.; Pendse, H.; Huber, G.W. Production of jet and diesel fuel range alkanes from waste hemicellulose-derived aqueous solutions. *Green Chemistry* **2010**, *12*, 1933-1946, doi:10.1039/c0gc00263a.
18. Patel, A.A.; Patel, S.R. Synthesis and characterization of furfural acetone polymers. *European Polymer Journal* **1983**, *19*, 231-234, doi:10.1016/0014-3057(83)90132-5.

19. Gandini, A.; Belgacem, M.N. Furans in polymer chemistry. *Progress in Polymer Science* **1997**, *22*, 1203-1379, doi:10.1016/s0079-6700(97)00004-x.
20. Hora, L.; Kelbichova, V.; Kikhtyanin, O.; Bortnovskiy, O.; Kubicka, D. Aldol condensation of furfural and acetone over Mg-Al layered double hydroxides and mixed oxides. *Catalysis Today* **2014**, *223*, 138-147, doi:10.1016/j.cattod.2013.09.022.
21. Ordonez, S.; Diaz, E.; Leon, M.; Faba, L. Hydrotalcite-derived mixed oxides as catalysts for different C-C bond formation reactions from bioorganic materials. *Catalysis Today* **2011**, *167*, 71-76, doi:10.1016/j.cattod.2010.11.056.
22. Choudary, B.M.; Kantam, M.L.; Sreekanth, P.; Bandopadhyay, T.; Figueras, F.; Tuel, A. Knoevenagel and aldol condensations catalysed by a new diamino-functionalised mesoporous material. *Journal of Molecular Catalysis A: Chemical* **1999**, *142*, 361-365, doi:10.1016/s1381-1169(98)00301-x.
23. Aramendia, M.A.; Aviles, Y.; Borau, V.; Luque, J.M.; Marinas, J.M.; Ruiz, J.R.; Urbano, F.J. Thermal decomposition of Mg/Al and Mg/Ga layered-double hydroxides: a spectroscopic study. *Journal of Materials Chemistry* **1999**, *9*, 1603-1607, doi:10.1039/a900535h.
24. Morato, A.; Alonso, C.; Medina, F.; Cesteros, Y.; Salagre, P.; Sueiras, J.E.; Tichit, D.; Coq, B. Palladium hydrotalcites as precursors for the catalytic hydroconversion of CCl_2F_2 (CFC-12) and $CHClF_2$ (HCFC-22). *Applied Catalysis B: Environmental* **2001**, *32*, 167-179, doi:10.1016/s0926-3373(01)00140-0.
25. Xu, C.; Gao, Y.; Liu, X.; Xin, R.; Wang, Z. Hydrotalcite reconstructed by in situ rehydration as a highly active solid base catalyst and its application in aldol condensations. *RSC Advances* **2013**, *3*, 793-801, doi:10.1039/c2ra21762g.

26. Frost, R.L.; Palmer, S.J.; Theiss, F. Synthesis and Raman spectroscopic characterisation of hydrotalcites based on the formula $Ca_6Al_2(CO_3)(OH)_{16}\cdot 4H_2O$. *Journal of Raman Spectroscopy* **2010**, *42*, 1163-1167, doi:10.1002/jrs.2827.
27. Frost, R.L.; Erickson, K.L.; Kloprogge, T.J. Vibrational spectroscopic study of the nitrate containing hydrotalcite mbobomkulite. *Spectrochimica Acta Part A: Molecular and Biomolecular Spectroscopy* **2005**, *61*, 2919-2925, doi:10.1016/j.saa.2004.11.002.
28. Pirouzmand, M.; Seyed-Rasulzade, S.K.; Nikzad-Kojanag, B. Effect of Preparation Methods and Pluronic Template on the Catalytic Activity of Ca/SBA-15. *Iranian Journal of Chemistry & Chemical Engineering-International English Edition* **2018**, *37*, 53-60.
29. Hidalgo-Carrillo, J.; Marinas, A.; Marinas, J.M.; Delgado, J.J.; Raya-Miranda, R.; Urbano, F.J. Water as solvent in the liquid-phase selective hydrogenation of crotonaldehyde to crotyl alcohol over Pt/ZnO: A factorial design approach. *Applied Catalysis B: Environmental* **2014**, *154*, 369-378, doi:10.1016/j.apcatb.2014.02.023.
30. Cosano, D.; Esquivel, D.; Mateos, L.D.; Quesada, F.; Jimenez-Sanchidrian, C.; Rafael Ruiz, J. Spectroscopic analysis of corrosion products in a bronze cauldron from the Late Iberian Iron Age. *Spectrochimica Acta Part A: Molecular and Biomolecular Spectroscopy* **2018**, *205*, 489-496, doi:10.1016/j.saa.2018.07.072.

Capítulo V.

Resultados y discusión (Paper 3)

CHAPTER V. RESULTS AND DISCUSSION: MPV REDUCTION OF FURFURAL TO FURFURYL ALCOHOL ON Mg, Zr, Ti, Zr-Ti AND Mg-Ti SOLIDS: INFLUENCE OF ACID-BASE PROPERTIES

PAPER 3

MPV reduction of furfural to furfuryl alcohol on Mg, Zr, Ti, Zr-Ti and Mg-Ti solids: influence of acid-base properties

*Jesús Hidalgo-Carrillo, Almudena Parejas, Manuel Cuesta-Rioboo, Alberto Marinas * and Francisco José Urbano*

Departamento de Química Orgánica, Instituto Universitario de Investigación en Química Fina y Nanoquímica IUIQFN, Universidad de Córdoba, Campus de Rabanales, Edificio Marie Curie, E-14071 Córdoba, Spain.

* Correspondence: alberto.marinas@uco.es, Tel.: +34957218622.

Published in *Catalysts* **2018**, *8*, 539; https://doi.org/10.3390/catal8110539

Abstract

Meerwein-Ponndorf-Verley (MPV) reaction is an environmentally-friendly process consisting in the reduction of a carbonyl compound through hydrogen transfer from a secondary alcohol. This work deals with MPV reduction of furfural to furfuryl alcohol on different ZrO_x, MgO_x, TiO_x and Mg-Ti as well as Zr-Ti mixed systems. The solids were synthesized through the sol-gel process and subsequently calcined at 200 ºC. Characterization was performed using a wide range of techniques: ICP-MS, N_2 adsorption-desorption isotherms, EDX, TGA-DTA, XRD, XPS, TEM, TPD of preadsorbed pyridine (acidity) and CO_2 (basicity), DRIFT of adsorbed pyridine and methylbutynol (MBOH) test reaction. ZrO_x showed the highest conversion and selectivity values which was attributed to the existence of acid-base pair sites (as evidenced by MBOH test reaction) whereas the introduction of titanium resulted in the drop of both conversion and selectivity, probably due to the increase in Brönsted-type acidity. As for MgO_x, it had a predominantly basic character and thus led to the production of the condensation product of one molecule of furfural and one molecule of acetone, thus resulting in a lower selectivity to furfuryl alcohol. TiO_x solid was found to be mainly acidic exhibiting both Lewis and Brönsted acid sites. The presence of the latter could account for the lower selectivity to furfuryl alcohol. All in all, results seem to suggest that MPV reaction is favored on Lewis acid sites and especially on acid-base pair sites. The process was accelerated under microwave irradiation.

Keywords: furfural; MPV reaction; acid-base characterization; methylbutynol test reaction

V.1. Introduction

The transformation of natural residues from agriculture into platform molecules is one of the promising research lines to obtain high added value chemical products [1,2]. One of those platform molecules is furfural [3] which can be obtained from lignocellulose [4]. It contains an aromatic ring and an aldehyde group which makes it a versatile molecule to obtain a wide range of chemical compounds [5], one of the most important ones being furfuryl alcohol. This alcohol is widely used in the production of thermostatic resins, rubbers, fibers, adhesives and some fine chemicals [5-7]. Furfuryl alcohol is produced by furfural hydrogenation mainly. Approximately 60% of the furfural produced is used to synthesize furfuryl alcohol. The catalytic liquid phase hydrogenation of furfural to produce furfuryl alcohol has been extensively investigated in the presence of catalysts based on Ni, Co, Cu, Pt and Pd [8-12]. Cu-Cr based catalysts are commonly used in the industry, but environmentally-friendlier catalysts are required. The transformation of furfural to furfuryl alcohol can also be carried out through the hydrogen transfer from a donor, typically secondary alcohols such as 2-propanol, using the so-called Meerwein-Ponndorf-Verley (MPV) process [13].This reaction involves the formation of a six-membered ring transition state in which both the reducing alcohol and the carbonyl compound are coordinated to the metal center (Lewis site) [14]. The assistance of the basic sites has also been proposed for the formation of the six-membered ring [15].

A wide range of heterogeneous catalysts has been described for MPV process such as zirconia [16,17], mesoporous silica [18,19], zeolites [20] or alumina [21,22].

In previous papers our research group described that zirconium gels calcined at low temperatures (ca. 200 ºC) were quite selective to the

corresponding unsaturated alcohol [16,17] in the MPV process. In the present work, different gels calcined at 200 ºC consisting of pure ZrO_x, TiO_x and MgO_x or mixed Mg-Ti and Zr-Ti solids were synthesized and tested in the MPV reduction of furfural to furfuryl alcohol to try and cast further light on the nature of the active sites responsible for the desired catalytic activity. The possibility of carrying out the reaction with microwave-assisted heating is also evaluated.

V.2. Results and Discussion

V.2.1. Textural, Structural, and Acid–Base Characterization of the Solids

The Brunnauer–Emmett–Teller (BET) surface areas as well as Mg/Ti and Zr/Ti atomic ratios (both nominal and experimental) of the synthesized solids are depicted in Table1. The highest BET areas (in the 219–263 m^2/g range) corresponded to solids consisting of Zr and/or Ti, whereas lower values were found for the systems containing magnesium (42–81 m^2/g). In regard to the chemical composition, experimental results were in general quite similar to the nominal values and was thus evidence of a good precipitation of the metals during the synthesis.

Table 1. Brunnauer–Emmett–Teller (BET) surface area and atomic composition (nominal and experimental) of the different solids synthesized in the present study.

Catalyst	BET Surface area (m^2/g)	M/Ti Ratio (M= Zr or Mg)		
		Nominal	ICP-MS	XPS
ZrO_x	221	-	-	-
Zr3Ti1	251	3.0	2.43	2.29
ZrTi	263	1.0	0.78	1.03
Zr1Ti3	219	0.33	0.34	0.45
TiO_x	232	-	-	-
Mg1Ti3	42	0.33	0.45	0.39
MgTi	81	1.0	1.06	0.62
Mg3Ti1	68	3.0	3.02	3.5
MgO_x	66	-	-	-

The TGA-DTA profiles of the different solids are shown in Figures 1 and 2 (Zr–Ti and Mg–Ti solids, respectively). The ZrO_x heat flow profile (Figure 1B) exhibited two main peaks centered at ca. 104 ºC and 436 ºC, respectively. The first endothermal peak corresponded to the loss of water whereas the second peak was the so-called glow exotherm attributed to the crystallization of zirconia [17,23]. For Zr–Ti mixed systems, the glow-exotherm was shifted to higher temperatures (450–466 ºC) which suggests that titanium retards zirconium crystallization. In the case of MgO_x solids (Figure 2B), the heat flow profile exhibited two main endothermal peaks centered at ca. 117 ºC and 385 ºC. The latter peak was assigned to the transformation of $Mg(OH)_2$ into MgO [24]. For Mg–Ti solids, the presence of titanium seemed to favor such a transformation as evidenced by the shift of the peak to lower temperatures (in the 318–357 ºC range).

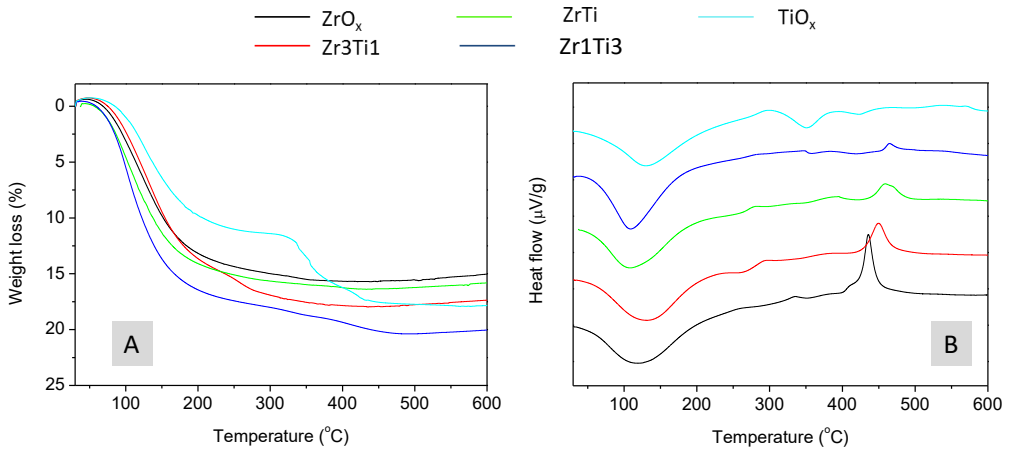

Figure 1. TG-DTA profiles of the precursor gels of the catalysts based on ZrO_x and TiO_x. Weight loss **(A)** and heat flow **(B)** profiles.

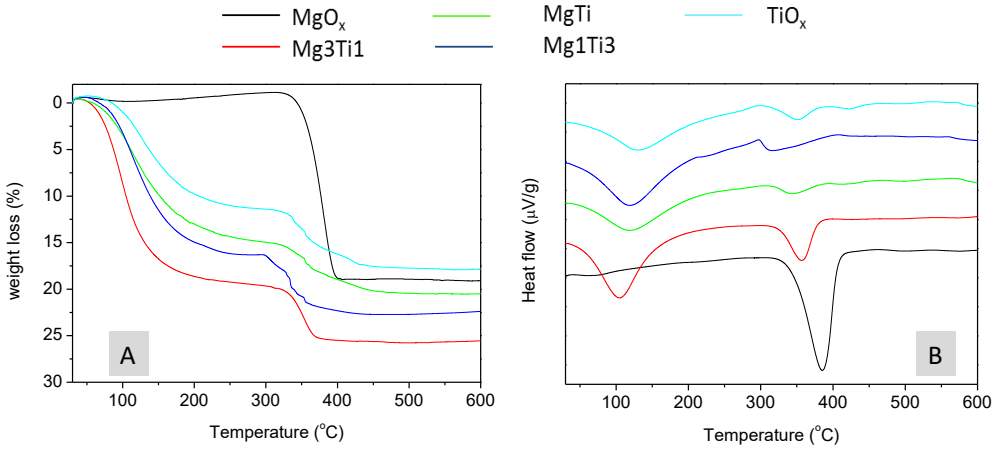

Figure 2. TG-DTA profiles of the precursor gels of catalysts based on MgO_x and TiO_x. Weight loss **(A)** and heat flow **(B)** profiles.

X-ray diffractograms of Zr-containing solids (Figure 3) showed evidence of their amorphous character, which was consistent with the TGA-DTA profiles; crystallization occurred at temperatures above 300 ºC. In the case of MgO_x (Figure 3B), there were some peaks present due to the $Mg(OH)_2$ brookite structure. Those peaks were also evident in Mg3Ti1 solid whereas higher titanium contents resulted in the disappearance of brookite signals and the appearance of some new signals which could be assigned to MgO5Ti2 pseudobrookite.

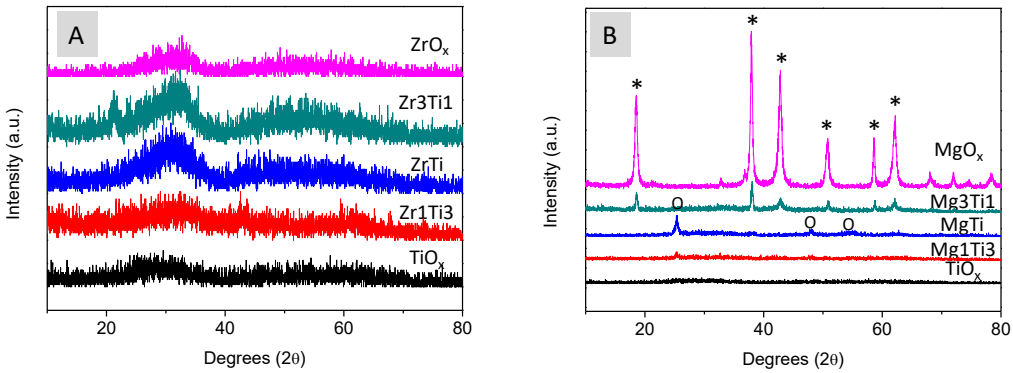

Figure 3. X-ray diffractograms of the different solids synthesized in the present work. Zr-Ti solids **(A)** and Mg-Ti systems **(B)**. The corresponding pure compounds have also been included for the sake of comparison. * and ° denote brookite and pseudobrookite phases, respectively.

Transmission electron microscopy (TEM) images of all the samples are represented in Figure 4. As can be seen in the central part of Figure 4, MgO_x, ZrO_x and TiO_x exhibited quite different textures which allowed us to distinguish them in mixed solids.

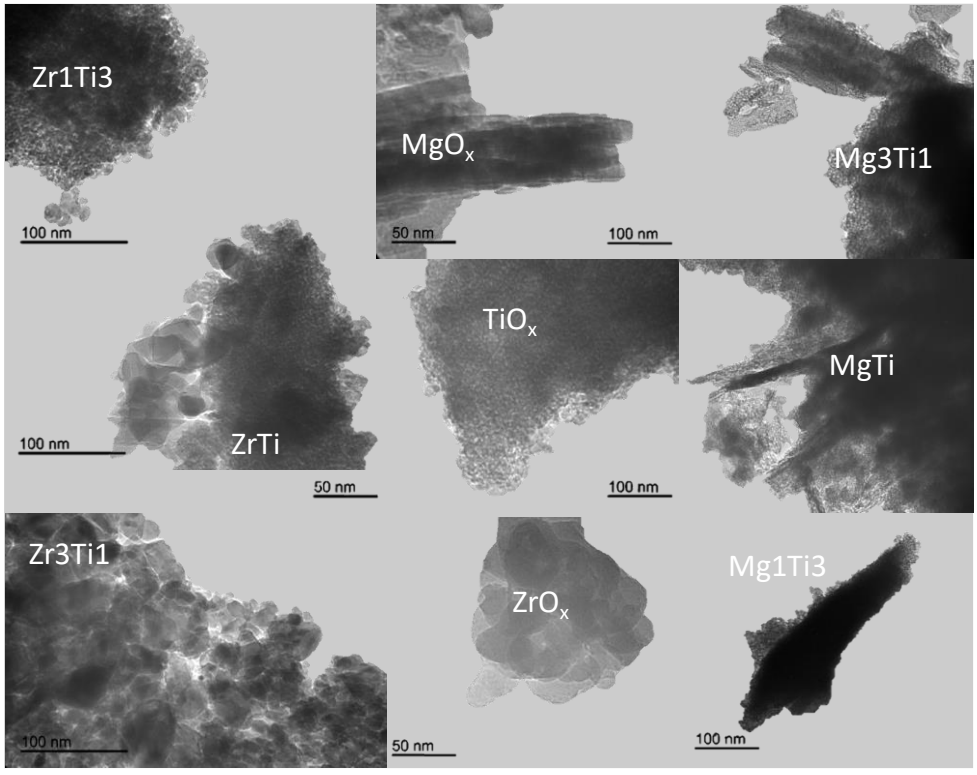

Figure 4. Transmission electron microscopy (TEM) images of the different solids.

X-ray photoelectron spectroscopy (XPS) profiles of Mg–Ti solids are represented in Figure 5. The signal for Mg1 in MgO_x presented two types of magnesium atoms. Moreover, as titanium content increased, there was a shift of signals to higher binding energies (from 1303.0 to 1303.8 eV for MgO_x and Mg1Ti3, respectively). A similar trend was observed for the Ti(2p) signal, and the Ti2p3/2 signal shifted, in this case, to lower binding energies in the presence of magnesium (Ti2p3/2 signal at 458.4 and 458.1 eV for TiO_x and Ti3Mg1, respectively). These results suggest the existence of some Mg–Ti interaction in Mg–Ti solids.

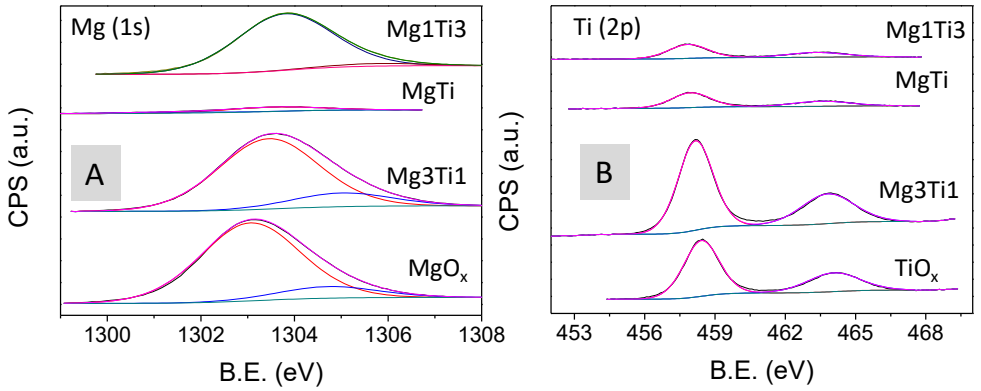

Figure 5. X-ray photoelectron spectroscopy (XPS) profiles of Mg(1s) **(A)** and Ti (2p) **(B)** in Mg–Ti solids.

As far as the Zr–Ti XPS profiles were concerned (Figure 6), there was suggestion of some Zr–Ti interaction as evidenced by the Zr3d and Ti2p signals shifting to higher and lower binding energy values, respectively, as the Ti content increased.

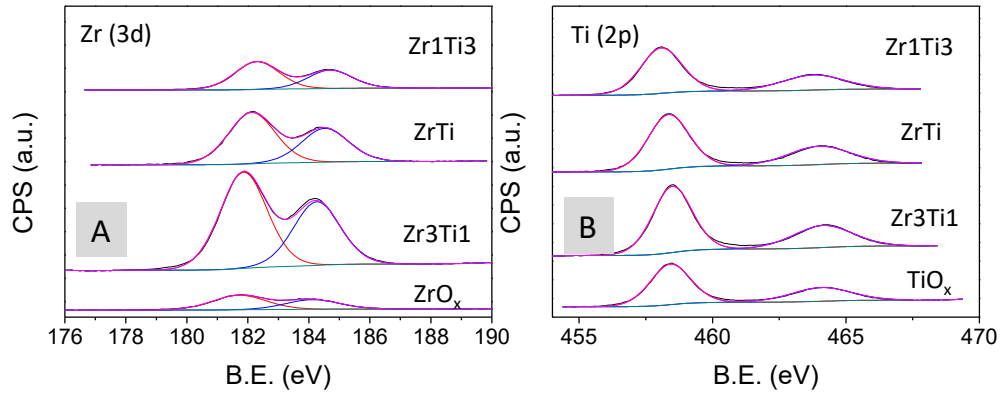

Figure 6. XPS profiles of Zr(3d) **(A)** and Ti (2p) **(B)** in Zr–Ti solids.

Surface acid–base characterization of the solids was carried out by TPD of pre-adsorbed CO_2 (basicity) and pyridine (acidity), and the main results are summarized in Table 2. As can be seen, ZrO_x exhibited a good balance between acid and basic sites (CO_2/py = 1.09), TiO_x was mainly acidic (CO_2/Py = 0.57) and MgO_x was a predominantly basic solid (CO_2/py = 3.39). As for the corresponding mixed solids, they all had an acid–base characteristic between the corresponding pure solids.

Table 2. Acid–base characteristics of the solids as determined by CO_2-TPD and Py-TPD, respectively.

Catalyst	μmol CO_2/g	μmol Py/g	CO_2/Py
ZrO_x	774	707	1.09
Zr3Ti1	728	753	0.97
ZrTi	658	921	0.71
Zr1Ti3	460	635	0.72
TiO_x	371	650	0.57
Mg1Ti3	508	622	0.82
MgTi	1126	616	1.83
Mg3Ti1	1142	354	3.22
MgO_x	1096	323	3.39

Complementary acid–base results could be obtained using the methylbutynol test reaction (Figure 7) which allow us to distinguish between acid, base, and acid–base pair sites.

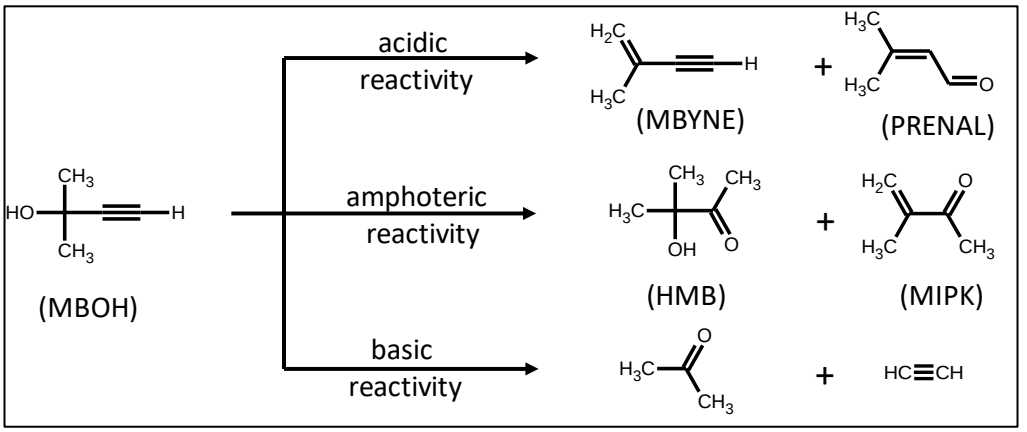

Figure 7. Overall reaction scheme as proposed by Lauron-Pernot et al. [25]. MBOH, 2-methyl-3-butyn-2-ol; MBYNE, 3-methyl-3-buten-1-yne; PRENAL, 3-methyl-2-buten-1-al; HMB, 3-hydroxy-3-methyl-2-butatone; MIPK, 3-methyl-3-buten-2-one.

As can be seen in Table 3, the methylbutynol (MBOH) test reaction confirmed the results found in the TPD studies of pre-adsorbed CO_2 and pyridine. Therefore, MgO_x mainly yielded acetone and acetylene (basic reactivity, 96.2% selectivity), TiO_x was mainly acidic (73.1% selectivity), and ZrO_x was predominantly amphoteric (53.4%) and mainly yielded 3-methyl-3-buten-2-one (MIPK). This was evidence for the presence of acid–base pair sites in ZrO_x.

Table 3. MBOH reaction. Comparison between selectivities of the pure oxides. The reaction conditions were as follows: microcatalytic pulse reactor; 20 mg catalyst, 200 ºC, methylbutynol (MBOH) pulses of 0.5 µL (see experimental section).

Catalyst	Conversion (%)	S_{basic} (%)	S_{acid} (%)	$S_{amphoteric}$ (%)
MgO_x	5.6	96.2	3.8	0
TiO_x	1.0	12.3	73.1	14.6
ZrO_x	1.0	26.3	20.3	53.4

Further diffuse reflectance infrared Fourier transform (DRIFT) pyridine studies were performed on Zr–Ti solids to distinguish between Lewis and Brönsted acid sites (Figure 8). Peaks observed at 1443 and 1603 cm^{-1} were attributed to the presence of pyridine adsorbed on Lewis acid sites, whereas the band at ca. 1486 cm^{-1} could be due to adsorbed pyridine on both Lewis and

Brönsted sites [26]. The signal at ca. 1534 cm^{-1} corresponded to pyridine on Brönsted acid sites [27]. An estimation of the Lewis/Brönsted acid site ratio can be made by integrating signals using the molar extinction coefficients [28]. Therefore, Lewis/Brönsted values of 15.4 and 4.9 could be obtained for ZrO_x and TiO_x, respectively.

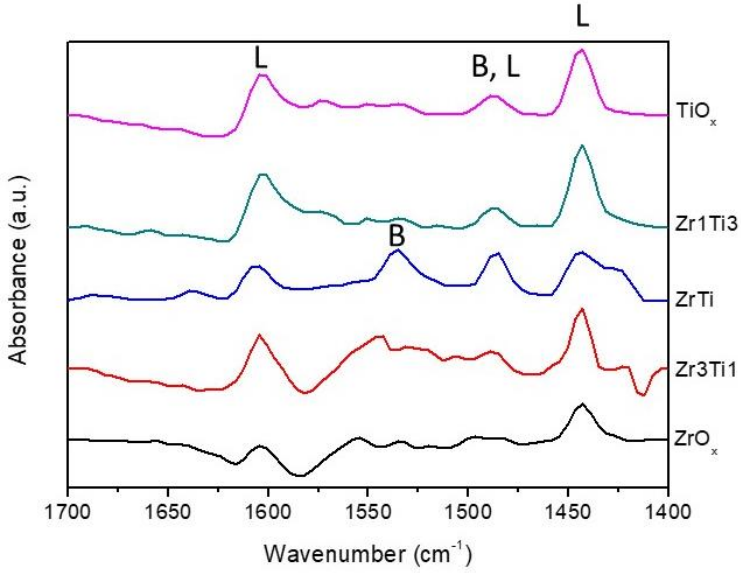

Figure 8. Diffuse reflectance infrared Fourier transform (DRIFT) studies of pyridine chemisorbed on the Zr–Ti solids. B and L stand for Brönsted and Lewis acid sites, respectively.

All in all, the acid–base studies indicated that MgO_x was mainly basic, ZrO_x was amphoteric, and TiO_x was acidic. Moreover, the highest Lewis/Brönsted site ratio corresponded to ZrO_x solids.

V.2.2. Catalytic Activity in Furfural Hydrogenation into Furfuryl Alcohol

The solids were then tested for liquid-phase MPV reduction of furfural to furfuryl alcohol (FUOL) using propan-2-ol as the hydrogen donor. The main results are summarized in Table 4.

Table 4. Results obtained for experiments under conventional (t = 20 h) and microwave (t = 2 h) heating on the different solids expressed in terms of conversion, selectivity to furfuryl alcohol (FUOL), and FUOL yield. The reaction conditions were as follows: 100 ºC, molar propan-2-ol/furfural ratio of 10.8, and furfural/catalyst weight ratio of 5.8. Maximum microwave power was set at 300 W.

Catalyst	Conventional heating			Microwave heating		
	Conv. (%)	Selec. FUOL (%)	Yield FUOL (%)	Conv. (%)	Selec. FUOL (%)	Yield FUOL (%)
ZrO_x	50.1	90.4	45.3	27.6	96.8	26.7
Zr3Ti1	42.9	88.2	37.8	19.8	97.9	19.4
ZrTi	30.2	79.0	23.9	20.9	75.2	15.7
Zr1Ti3	22.3	80.5	18.0	17.1	79.5	13.6
TiO_x	16.2	68.7	11.1	7.4	53.5	4.0
Mg1Ti3	11.6	35.4	4.1	7.2	31.5	2.3
MgTi	13.4	46.6	6.3	8.6	47.8	3.1
Mg3Ti1	15.8	48.0	7.6	7.4	46.0	3.4
MgO_x	15.2	56.0	8.5	7.9	57.8	4.6

Firstly, the solids were tested under conventional heating. As can be seen, ZrO_x was the most active solid, followed by TiO_x and MgO_x. Both conversion and selectivity to furfuryl alcohol dropped upon the introduction of titanium in Zr–Ti and Mg–Ti solids. This seems to indicate that the interaction evidenced by XPS (and also suggested by TGA-DTA profiles) is detrimental to activity. In the case of MgO_x, the main by-product was the condensation product between one molecule of furfural and one molecule of acetone. Microwave heating was also tested, and results for t = 2 h are given in Table 4. The reactions were indeed accelerated under microwave irradiation. For instance, for t = 2 h, conversions of 6.5% (not shown) and 27.6% as well as selectivities of 97.0 and 96.8% to furfuryl alcohol were achieved on ZrO_x under conventional and microwave heating, respectively. The results under microwave irradiation confirmed the observed activity trend in experiments under conventional heating.

The higher selectivity values (over 90%) found for ZrO_x could be ascribed to the existence of acid–base pair sites. As suggested by Komanoya et al. [29], there would be a synergistic effect of acid–base pair sites: base sites could activate methylene groups in propan-2-ol bonded to Lewis sites. A tentative reaction mechanism on those acid–base pair sites is presented in Figure 9. The better catalytic performance of ZrO_x as compared to TiO_x could also be explained as the result of Lewis sites being more active than Brönsted sites in the MPV reaction [30,31].

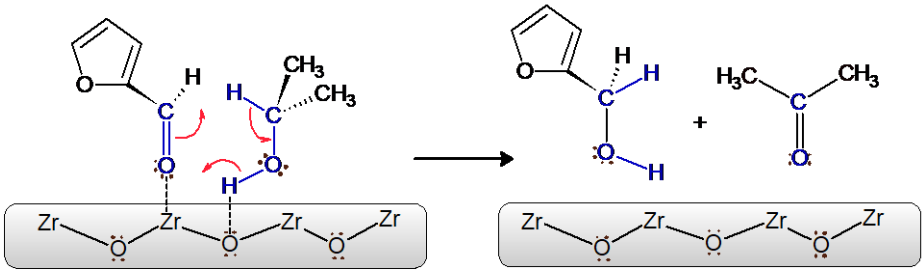

Figure 9. Suggested mechanism for furfural hydrogenation into furfuryl alcohol on acid–base pair sites in ZrOx through transfer hydrogenation from propan-2-ol.

V.3. Materials and Methods

For the synthesis of the catalysts, the following compounds were used: aqueous solutions of ammonium hydroxide (5 N) (Fluka 318620-2L, Honeywell, Bucharest, Romania) and hydrochloric acid (1 M) (Fluka 318949-2L); propan-2-ol (Sigma-Aldrich 190764-2.5L, Merck KGaA, Darmstadt, Germany); hydrated zirconium(IV) oxynitrate (Sigma-Aldrich 346462, Merck KGaA, Darmstadt, Germany); magnesium nitrate hexahydrate (Sigma-Aldrich 237175-1KG, Merck KGaA, Darmstadt, Germany); and titanium isopropoxide (Sigma-Aldrich 20527-3, Merck KGaA, Darmstadt, Germany).

The synthesis of the catalysts was carried out by the sol–gel method [32], following previous studies in our research group [17,33-35].

Two types of mixed systems were synthesized: titanium gels with magnesium and titanium gels with zirconium, with different (Mg or Zr)/Ti molar ratios (0%, 25%, 50%, 75%, and 100%). The syntheses were carried out at a constant pH of 10 with magnetic stirring at 700 rpm. The pH was kept constant using a pump (Atlas syringe pump, Syrris, (Hertfordshire, UK), which added 5 N ammonium hydroxide or 1 M hydrochloric acid throughout the synthesis process. The precipitate was filtered, washed with water, dried at 120 ºC overnight, and calcined at 200 ºC for 8 h. After calcination, the catalysts were sieved (0.149 μm). The nomenclature of the solids was as follows: TiO_x, ZrO_x, and MgO_x for solids based on pure titanium, zirconium, and magnesium gels, respectively. For mixtures of gels, the nomenclature included the symbol of the metals followed by a number referring to their atomic ratio in the mixture. For instance, Mg3Ti1 indicates a magnesium–titanium system containing 75% Mg and 25% Ti (i.e., Mg/Ti atomic ratio of 3).

Thermogravimetric analyses (TGA) were performed on a Setaram SetSys 12 instrument (Caluire, France). A 20 mg amount of sample (precursor gels of the catalysts) was placed in an alumina crucible and heated at temperatures ranging from 30 to 600 ºC (heating rate of 10 ºC/min) under a synthetic air stream (50 mL/min) in order to measure weight loss, heat flow, and derivative weight loss.

X-ray photoelectron spectroscopy (XPS) data were recorded at the Central Service for Research Support (SCAI) of the University of Córdoba on 4 mm × 4 mm pellets of 0.5 mm thickness that were obtained by gently pressing the powered materials. The samples were outgassed to a pressure below about 2×10^{-8} Torr at 150 ºC in the instrument pre-chamber to remove chemisorbed volatile species. The main chamber of the Leibold-Heraeus LHS10 spectrometer used, which is capable of operating down to less than 2×10^{-9} Torr, was equipped with a EA-200MCD hemispherical electron analyzer with a

dual X-ray source using Al Kα (hυ = 1486.6 eV) at 120 W and 30 mA. C (1 s) was used as the energy reference (284.6 eV).

Transmission electron microscopy (TEM) images were obtained at the Central Service for Research Support (SCAI) of the University of Córdoba using a JEOL JEM 1400 microscope available at SCAI. The samples were mounted on 3 mm holey carbon copper grids.

X-ray patterns of the samples in the 10−80º (2θ) range were registered in a D8 Advanced Diffractometer (Bruker AXS) equipped with a Lynxeye detector.

Surface areas of solids were obtained from nitrogen adsorption-desorption isotherms obtained at liquid nitrogen temperature on a Micromeritics ASAP-2010 instrument following the Brunnauer–Emmett–Teller (BET) method. All samples were degassed to 0.1 Pa at 120 ºC before measurement.

Surface basicity of the catalysts was determined on a Micromeritics Autochem II instrument by thermal programmed desorption of pre-absorbed CO_2 (TPD-CO_2) with TCD detection. An amount of 100 mg of each catalyst was loaded into a reactor of 10 mm ID and placed in a furnace. Solids were cleaned with an Ar stream (20 mL/min) by heating to 200 ºC at a rate of 10 ºC/min for 60 min and then cooled down to 40 ºC. At that temperature, the catalysts were saturated with the probe molecule using 5% CO_2/Ar flow at 20 mL/min for 60 min. After saturation, physisorbed CO_2 was removed by a flowing Ar stream for 30 min (20 mL/min). Then, the temperature-programmed desorption of chemisorbed CO_2 was carried out by ramping the temperature from 40 to 200 ºC (heating rate 5 ºC/min) and holding the final temperature for

60 min. The amount of CO_2 adsorbed was determined from a calibration graph constructed from the injection of variable volumes of 5% CO_2/Ar.

The surface acidity of the catalysts was determined by thermal programmed desorption of pre-adsorbed pyridine (TPD-PY) with TCD detection. A 30 mg amount of sample was introduced in a 10 mm ID reactor that was placed inside an oven. The solids were cleaned under a He flow (75 mL/min) by heating to 200 ºC at a rate of 10 ºC/min and then cooled down to 50 ºC. At that temperature, the solids were exposed for 30 min to a pyridine-saturated He flow. After saturation, physisorbed pyridine was removed by flowing a pure He stream for 60 min (75 mL/min). Then, the temperature-programmed desorption of chemisorbed pyridine was carried out by ramping the temperature from 50 to 200 ºC (heating rate 10 ºC/min) and holding the final temperature for 30 min. Desorbed pyridine was quantified against a calibration graph constructed from variable volumes of pyridine injected.

Complementary studies using diffuse reflectance infrared Fourier transform (DRIFT) spectra of adsorbed pyridine were carried out on a FTIR instrument (Bomem MB-3000, ABB Corporate, Zurich, Switzerland) equipped with an "environmental chamber" (Spectra Tech, Jefferson Court, Oak Ridge, TN, USA) placed in a diffuse reflectance attachment (Spectra Tech, Collector). A resolution of 8 cm^{-1} was used with 256 scans averaged to obtain a spectrum from 4000 to 400 cm^{-1}. In each measurement, the reference was the same sample after heating at 150 ºC. Pyridine adsorption was carried out at 150 ºC for 45 min to allow the saturation of the catalyst surface. The physisorbed pyridine was then cleaned with a N_2 flow (50 mL/min) and its spectrum was registered.

The MBOH test reaction was carried out as described elsewhere [36]. A microcatalytic pulse reactor (1/8 in i.d. quartz tubular reactor) was placed in the

injection port of a gas chromatograph (GC System 7890A, Agilent Technologies, Santa Clara, CA, USA). The reactor was packed with alternating layers of quartz wool with the catalyst (20 mg) placed between them. Prior to each run, the catalyst was pre-treated in the reactor at 200 ºC for 2 h under nitrogen (75 mL/min). MBOH pulses of 0.5 µL were then carried out.

The MPV reaction of furfural was carried out under conventional heating in a Carousel 12 Plus™ Reaction Station, Discovery Technologies, and reactions under microwaves were carried out in a CEM-DISCOVER apparatus with PC control. In both cases, temperature was 100 ºC. Maximum microwave power was set at 300 W. The reactions by conventional heating were carried out with 100 mg of catalyst, 5 mL of propan-2-ol, and 0.5 mL of furfural over 20 h, the reactions in the microwave oven kept the same catalyst, propan-2-ol, and furfural ratios at a volume of reaction of 2 mL with a reaction time of 2 h. Analysis of reaction products was carried out by gas chromatography (GC-FID System 7890A, Agilent Technologies, equipped with a HP-5 chromatographic column) using the corresponding calibration graphs.

V.4. Conclusions

Several solids consisting of pure magnesium, zirconium, titanium, and mixed magnesium–titanium as well as zirconium–titanium gels were obtained through the sol–gel process and calcined at 200 ºC. The presence of titanium retarded the crystallization of zirconium oxide whereas transformation of $Mg(OH)_2$ into MgO was favored in the presence of titanium. XPS results also suggested the existence of some Mg–Ti and Zr–Ti interaction in mixed gels. In regard to the acid–base properties as determined from the TPD of pre-adsorbed pyridine and CO_2, the ZrO_x system exhibited a good balance between acid and base sites, whereas TiO_x and MgO_x were predominantly acidic and basic,

respectively. The MBOH test reaction evidenced the presence of acid–base pair sites in ZrO_x, and pyridine DRIFT studies showed that acid sites in ZrO_x were mainly of the Lewis type whereas both Brönsted and Lewis sites were present in TiO_x and Zr–Ti mixed solids. The most active and selective catalyst in the MPV reduction of furfural to furfuryl alcohol was ZrO_x whereas both parameters decreased in Zr–Ti solids as the titanium content increased. These results suggest that acid–base pair sites are particularly active in MPV reduction and that Lewis acid sites are more active than Brönsted acid ones. The same reactivity order was found for the reactions under microwave irradiation which led to an acceleration of the process as compared to conventional heating.

Funding

This research was funded by the Ramón Areces Foundation.

Acknowledgments

The scientific support from the Central Service for Research Support (SCAI) at the University of Cordoba is acknowledged.

References

1. Chheda, J.N.; Huber, G.W.; Dumesic, J.A. Liquid-phase catalytic processing of biomass-derived oxygenated hydrocarbons to fuels and chemicals. *Angewandte Chemie-International Edition* **2007**, *46*, 7164-7183, doi:10.1002/anie.200604274.
2. Turhollow, A.; Perlack, R.; Eaton, L.; Langholtz, M.; Brandt, C.; Downing, M.; Wright, L.; Skog, K.; Hellwinckel, C.; Stokes, B., et al. The updated

billion-ton resource assessment. *Biomass & Bioenergy* **2014**, *70*, 149-164, doi:10.1016/j.biombioe.2014.09.007.

3. Bozell, J.J.; Petersen, G.R. Technology development for the production of biobased products from biorefinery carbohydrates-the US Department of Energy's "Top 10" revisited. *Green Chemistry* **2010**, *12*, 539-554, doi:10.1039/b922014c.
4. Mamman, A.S.; Lee, J.M.; Kim, Y.C.; Hwang, I.T.; Park, N.J.; Hwang, Y.K.; Chang, J.S.; Hwang, J.S. Furfural: hemicellulose/xylosederived biochemical. *Biofuels Bioproducts & Biorefining-Biofpr* **2008**, *2*, 438-454, doi:10.1002/bbb.95.
5. Chatterjee, C.; Pong, F.; Sen, A. Chemical conversion pathways for carbohydrates. *Green Chemistry* **2015**, *17*, 40-71, doi:10.1039/c4gc01062k.
6. Corma, A.; Iborra, S.; Velty, A. Chemical routes for the transformation of biomass into chemicals. *Chemical Reviews* **2007**, *107*, 2411-2502, doi:10.1021/cr050989d.
7. Bauer, K.; Garbe, D.; Surburg, H. *Common Fragrance and Flavour Materials. Preparation, Properties and Uses*; VCH Verlagsgesellschaft mbH: Weinheim, Germany,1985.
8. Liu, H.; Huang, Z.; Zhao, F.; Cui, F.; Li, X.; Xia, C.; Chen, J. Efficient hydrogenolysis of biomass-derived furfuryl alcohol to 1,2-and 1,5-pentanediols over a non-precious Cu-$Mg_3AlO_{4.5}$ bifunctional catalyst. *Catalysis Science & Technology* **2016**, *6*, 668-671, doi:10.1039/c5cy01442e.
9. Rao, R.; Dandekar, A.; Baker, R.T.K.; Vannice, M.A. Properties of copper chromite catalysts in hydrogenation reactions. *Journal of Catalysis* **1997**, *171*, 406-419, doi:10.1006/jcat.1997.1832.
10. Sang, S.; Wang, Y.; Zhu, W.; Xiao, G. Selective hydrogenation of furfuryl alcohol to tetrahydrofurfuryl alcohol over Ni/γ-Al_2O_3 catalysts. *Research*

on Chemical Intermediates **2017**, *43*, 1179-1195, doi:10.1007/s11164-016-2691-8.

11. Taylor, M.J.; Durndell, L.J.; Isaacs, M.A.; Parlett, C.M.A.; Wilson, K.; Lee, A.F.; Kyriakou, G. Highly selective hydrogenation of furfural over supported Pt nanoparticles under mild conditions. *Applied Catalysis B: Environmental* **2016**, *180*, 580-585, doi:10.1016/j.apcatb.2015.07.006.
12. Thompson, S.T.; Lamb, H.H. Palladium-rhenium catalysts for selective hydrogenation of furfural: evidence for an optimum surface composition. *ACS Catalysis* **2016**, *6*, 7438-7447, doi:10.1021/acscatal.6b01398.
13. Meerwein, H.; Schmidt, R. Ein neues verfahren zur reduktion von aldehyden und ketonen. *Justus Liebigs Annalen der Chemie* **1925**, doi:10.1002/jlac.19254440112.
14. Ooi, T.; Ichikawa, H.; Maruoka, K. Practical approach to the Meerwein-Ponndorf-Verley reduction of carbonyl substrates with new aluminum catalysts. *Angewandte Chemie-International Edition* **2001**, *40*, 3610-3612, doi:10.1002/1521-3773(20011001)40:19<3610::aid-anie3610>3.0.co;2-l.
15. Ivanov, V.A.; Bachelier, J.; Audry, F.; Lavalley, J.C. Study of the Meerwein-Pondorff-Verley reaction between ethanol and acetone on various metal-oxides. *Journal of Molecular Catalysis* **1994**, *91*, 45-59, doi:10.1016/0304-5102(94)00017-4.
16. Montes, V.; Miñambres, J.F.; Khalilov, A.N.; Boutonnet, M.; Marinas, J.M.; Urbano, F.J.; Maharramov, A.M.; Marinas, A. Chemoselective hydrogenation of furfural to furfuryl alcohol on ZrO_2 systems synthesized through the microemulsion method. *Catalysis Today* **2018**, *306*, 89-95, doi:https://doi.org/10.1016/j.cattod.2017.05.022.
17. Axpuac, S.; Aramendía, M.A.; Hidalgo-Carrillo, J.; Marinas, A.; Marinas, J.M.; Montes-Jiménez, V.; Urbano, F.J.; Borau, V. Study of structure-performance relationships in Meerwein-Ponndorf-Verley reduction of

crotonaldehyde on several magnesium and zirconium-based systems. *Catalysis Today* **2012**, *187*, 183-190, doi:10.1016/j.cattod.2011.10.004.

18. Antunes, M.M.; Lima, S.; Neves, P.; Magalhaes, A.L.; Fazio, E.; Neri, F.; Pereira, M.T.; Silva, A.F.; Silva, C.M.; Rocha, S.M., et al. Integrated reduction and acid-catalysed conversion of furfural in alcohol medium using Zr,Al-containing ordered micro/mesoporous silicates. *Applied Catalysis B: Environmental* **2016**, *182*, 485-503, doi:10.1016/j.apcatb.2015.09.053.
19. Iglesias, J.; Antonio Melero, J.; Morales, G.; Moreno, J.; Segura, Y.; Paniagua, M.; Cambra, A.; Hernandez, B. Zr-SBA-15 lewis acid catalyst: activity in Meerwein Ponndorf Verley reduction. *Catalysts* **2015**, *5*, 1911-1927, doi:10.3390/catal5041911.
20. Iglesias, J.; Melero, J.A.; Morales, G.; Paniagua, M.; Hernandez, B. Dehydration of xylose to furfural in alcohol media in the presence of solid acid catalysts. *ChemCatChem* **2016**, *8*, 2089-2099, doi:10.1002/cctc.201600292.
21. Kim, M.S.; Simanjuntak, F.S.H.; Lim, S.; Jae, J.; Ha, J.-M.; Lee, H. Synthesis of alumina–carbon composite material for the catalytic conversion of furfural to furfuryl alcohol. **2017**, *52*, 59-65, doi:10.1016/j.jiec.2017.03.024.
22. Lopez-Asensio, R.; Cecilia, J.A.; Jimenez-Gomez, C.P.; Garcia-Sancho, C.; Moreno-Tost, R.; Maireles-Torres, P. Selective production of furfuryl alcohol from furfural by catalytic transfer hydrogenation over commercial aluminas. *Applied Catalysis A: General* **2018**, *556*, 1-9, doi:10.1016/j.apcata.2018.02.022.
23. Stefanic, G.; Music, S.; Popovic, S.; Sekulic, A. FT-IR and laser Raman spectroscopic investigation of the formation and stability of low temperature t-ZrO_2. *Journal of Molecular Structure* **1997**, *408-409*, 391-394, doi:10.1016/S0022-2860(96)09549-X.

24. Formosa, J.; Chimenos, J.M.; Lacasta, A.M.; Haurie, L. Thermal study of low-grade magnesium hydroxide used as fire retardant and in passive fire protection. *Thermochimica Acta* **2011**, *515*, 43-50, doi:10.1016/j.tca.2010.12.018.
25. Lauronpernot, H.; Luck, F.; Popa, J.M. Methylbutynol: a new and simple diagnostic-tool for acidic and basic sites of solids. *Applied Catalysis* **1991**, *78*, 213-225, doi:10.1016/0166-9834(91)80107-8.
26. Osman, A.I.; Abu-Dahrieh, J.K.; Rooney, D.W.; Halawy, S.A.; Mohamed, A.M.; Abdelkader, A. Effect of precursor on the performance of alumina for the dehydration of methanol to dimethyl ether. *Applied Catalysis B: Environmental* **2012**, *127*, 307-315, doi:10.1016/j.apcatb.2012.08.033.
27. Lu, J.; Kosuda, K.M.; Van Duyne, R.P.; Stair, P.C. Surface Acidity and properties of TiO_2/SiO_2 catalysts prepared by atomic layer deposition: uv-visible diffuse reflectance, DRIFTS, and visible Raman spectroscopy studies. *Journal of Physical Chemistry C* **2009**, *113*, 12412-12418, doi:10.1021/jp902200c.
28. Emeis, C.A. Determination of integrated molar extinction coefficients for infrared-absorption bands of pyridine adsorbed on solid acid catalysts. *Journal of Catalysis* **1993**, *141*, 347-354, doi:10.1006/jcat.1993.1145.
29. Komanoya, T.; Nakajima, K.; Kitano, M.; Hara, M. Synergistic catalysis by lewis acid and base sites on ZrO_2 for Meerwein-Ponndorf-Verley reduction. *Journal of Physical Chemistry C* **2015**, *119*, 26540-26546, doi:10.1021/acs.jpcc.5b08355.
30. Gao, Z.-K.; Hong, Y.-C.; Hu, Z.; Xu, B.-Q. Transfer hydrogenation of cinnamaldehyde with 2-propanol on Al_2O_3 and SiO_2-Al_2O_3 catalysts: role of lewis and bronsted acidic sites. *Catalysis Science & Technology* **2017**, *7*, 4511-4519, doi:10.1039/c7cy01569k.
31. Minambres, J.F.; Aramendia, M.A.; Marinas, A.; Marinas, J.M.; Urbano, F.J. Liquid and gas-phase Meerwein-Ponndorf-Verley reduction of

crotonaldehyde on ZrO_2 catalysts modified with Al_2O_3, Ga_2O_3 and In_2O_3. *Journal of Molecular Catalysis A: Chemical* **2011**, *338*, 121-129, doi:10.1016/j.molcata.2011.02.005.

32. Debecker, D.P.; Mutin, P.H. Non-hydrolytic sol-gel routes to heterogeneous catalysts. *Chemical Society Reviews* **2012**, *41*, 3624-3650, doi:10.1039/c2cs15330k.
33. Miñambres, J.F.; Marinas, A.; Marinas, J.M.; Urbano, F.J. Activity and deactivation of catalysts based on zirconium oxide modified with metal chlorides in the MPV reduction of crotonaldehyde. *Applied Catalysis B: Environmental* **2013**, *140–141*, 386-395, doi:http://dx.doi.org/10.1016/j.apcatb.2013.04.036.
34. Minambres, J.F.; Marinas, A.; Marinas, J.M.; Urbano, F.J. Chemoselective crotonaldehyde hydrogen transfer reduction over pure and supported metal nitrates. *Journal of Catalysis* **2012**, *295*, 242-253, doi:10.1016/j.jcat.2012.08.013.
35. Aramendia, M.A.; Borau, V.; Jimenez, C.; Marinas, J.M.; Ruiz, J.R.; Urbano, F.J. Influence of the preparation method on the structural and surface properties of various magnesium oxides and their catalytic activity in the Meerwein-Ponndorf-Verley reaction. *Applied Catalysis A: General* **2003**, *244*, 207-215, doi:10.1016/s0926-860x(02)00213-2.
36. Aramendia, M.A.; Borau, V.; Garcia, I.M.; Jimenez, C.; Marinas, A.; Marinas, J.M.; Porras, A.; Urbano, F.J. Comparison of different organic test reaction over acid-base catalysts. *Applied Catalysis A: General* **1999**, *184*, 115-125, doi:10.1016/S0926-860X(99)00096-4.

Capítulo VI.

Conclusiones/Conclusions

Conclusiones

A continuación se detallarán las conclusiones más relevantes obtenidas de cada uno de los artículos publicados, que han aportado resultados a la presente memoria de Tesis Doctoral.

Artículo 1 "Microemulsion and sol-gel synthesized ZrO_2-MgO catalysts for the liquid-phase dehydration of xylose to furfural"

En esta trabajo se prepararon dos series de catalizadores mediante el método sol-gel y un procedimiento sintético de microemulsión (SG y ME, respectivamente). Cada serie incluye sólidos puros de Mg y Zr, así como óxidos mixtos de Mg-Zr con un contenido atómico nominal de Zr del 25%, 50% y 75%. El sólido MgZr-SG presentó la mayor acidez superficial, mientras que el Mg3Zr-SG mostró la mayor basicidad superficial entre los sistemas mixtos. En cuanto a la deshidratación de la xilosa, el uso de tolueno como disolvente orgánico en la mezcla de reacción bifásica (agua/tolueno) conduce a un mejor rendimiento del furfural que el uso de butan-1-ol, lo que puede deberse a la mayor capacidad de extracción del furfural por parte del tolueno, evitando así la formación de huminas que tienen lugar principalmente en la fase acuosa.

El rendimiento a furfural aumenta con el contenido de Zr del catalizador y, por lo tanto, los catalizadores constituidos por ZrO_2 puro son los más adecuados para llevar a cabo el proceso (conversión del 98%, rendimiento del 40%, tras 24 horas), aunque los sólidos mixtos de MgZr también podrían ser adecuados para procesos generales con etapas de reacción adicionales que precisen tanto de centros ácidos como de básicos.

Artículo 2 "Aldol condensation of furfural with acetone over Mg/Al mixed oxides. Influence of water and synthesis method"

En este trabajo se han sintetizado cuatro óxidos mixtos de Mg/Al mediante el método de co-precipitación con modificaciones durante la síntesis como el empleo del calentamiento convencional o microondas y la presencia o ausencia de Pluronic 123. Se observó, a partir de los difractogramas de rayos X, que todos los sólidos calcinados presentaban las reflexiones típicas de la periclasa $MgAlO_x$. Las isotermas de los sólidos fueron tipo IV y aquellos que sufrieron alguna modificación en la síntesis (microondas y/o surfactante) mostraron un aumento en el área BET. Además, al utilizar el calentamiento por microondas y/o Pluronic 123, los sólidos presentaron una disminución en la basicidad total y un aumento en la acidez total.

Cuando los sólidos fueron probados en la reacción de condensación aldólica del furfural con acetona durante 3h, el valor más alto de conversión obtenido (35,0%), fue cuando se utilizó el sólido HTCON-450 (calentamiento convencional, sin surfactante). Mientras que cuando el tiempo aumenta, hasta las 16h, los sólidos que fueron sintetizados con Pluronic 123 consiguieron valores de rendimiento a 1,5-bis-(2-furanil)-1,4-pentadien-3-ona más altos, sobresaliendo el sólido HTMWP-450 (sintetizado en microondas) con un valor de rendimiento del 44,5%. Así, se puede concluir que la presencia de ambas modificaciones en la síntesis de los sólidos, calentamiento por microondas y Pluronic 123, favorecen la transformación del furfural al producto de interés, lo que podría ser debido al aumento del tamaño de poro y el aumento de la acidez total producido en los sólidos. Respecto a la influencia del agua, se ha observado cómo los sólidos que sufrieron una rehidratación previa a la reacción presentaron una peor actividad, probablemente debido a la solvatación de los centros activos. Mientras que, por el contrario, el aumento del porcentaje de agua añadido al medio de reacción (agua/tolueno) consiguió un aumento en la

conversión de furfural, pero una disminución de la selectividad a 1,5-bis-(2-furanil)-1,4-pentadien-3-ona. Una posible explicación es que el agua debilita el enlace C=O del furfural favoreciendo su transformación, pero al mismo tiempo el primer producto de condensación del furfural con una molécula de acetona (FAc, 4-(2-furanil)-3-buten-2-ona) es retirado de la fase orgánica una vez formado, dada su mayor solubilidad en agua, por lo que no puede reaccionar con otra molécula de furfural y originar el producto deseado (F_2Ac).

Artículo 3 "MPV reduction of furfural to furfuryl alcohol on Mg, Zr, Ti, Zr-Ti, and Mg-Ti solids: influence of acid-base properties"

- En este trabajo se sintetizaron catalizadores a base de MgO_x, ZrO_x y TiO_x puros, así como los sistemas mixtos Mg-Ti y Zr-Ti mediante el método sol-gel. Los sólidos fueron caracterizados, obteniéndose valores de superficies específicas (S_{BET}) de 219-263 m^2/g en aquellos que contienen Zr y/o Ti, mientras que para los sólidos compuestos por Mg fueron de 42-81 m^2/g. Comparando los perfiles termogravimétricos obtenidos, se pudo observar cómo la presencia de titanio retarda la cristalización del ZrO_2, pero favorece la transformación de $Mg(OH)_2$ a MgO. Los sólidos fueron probados en la reacción de reducción de MPV del furfural a alcohol furfurílico bajo calentamiento convencional y por microondas. Cuando se emplea el primer tipo de calentamiento, analizando los sólidos puros, el ZrO_x demostró ser el más activo, con un 90,4 % de selectividad a alcohol furfurílico (a 50.1% conversión, t=20h), seguido del TiO_x, con un 68,7% (16.2% conv.), y el MgO_x con un 56% (15.2% conv). Por otro lado, en los sólidos mixtos, la selectividad obtenida a alcohol furfurílico disminuye con el contenido en titanio. Cuando se emplea el calentamiento por microondas, las actividades catalíticas aumentaron (conversiones del orden de 4 veces mayores respecto al calentamiento convencional), manteniendo las selectividades en valores similares o superiores,

como el caso del catalizador ZrO_x, con el que se obtuvo un 96,8% de selectividad a alcohol furfurílico, a 27.6% de conversión (t=2h).

La reacción test del metilbutinol (MBOH) evidenció la presencia de pares de centros ácido-base en el ZrO_x, y los estudios DRIFT con piridina mostraron que los centros ácidos del ZrO_x eran principalmente de Lewis mientras que los sitios de Brönsted y Lewis estaban presentes en los sólidos mixtos de TiO_x y Zr-Ti. El catalizador más activo y selectivo en la reducción de MPV de furfural a alcohol furfurílico fue el ZrO_x, mientras que ambos parámetros disminuyeron en los sólidos de Zr-Ti a medida que aumentaba el contenido de titanio. Estos resultados sugieren que pares ácido-base son particularmente activos en la reducción de MPV y que los sitios de ácidos de Lewis son más activos que los de Brönsted.

Conclusions

The most relevant conclusions drawn from each of the papers published as a result of this Doctoral Thesis are detailed below.

Paper 1 "Microemulsion and sol-gels synthesized ZrO_2-MgO catalysts for the liquid-phase dehydration of xylose to furfural"

In this paper, two series of catalysts were prepared by sol-gel and microemulsion synthetic procedures (SG and ME series, respectively). Each series includes both pure Mg and Zr solids as well as Mg-Zr mixed solids with 25%, 50% and 75% atomic nominal Zr content. The MgZr-SG solid presented the highest surface acidity while the Mg3Zr-SG exhibited the highest surface basicity among mixed systems. As for xylose dehydration, the use of toluene as organic solvent in the biphasic reaction mixture (toluene/water) led to higher furfural yields than the use of butan-1-ol which could be associated with the ability of toluene to extract the furfural formed, thus avoiding the formation of humins that takes place mainly in the aqueous phase.

The yield to furfural increases with the Zr content of the catalysts and, therefore, the catalysts constituted by pure ZrO_2 are the most suitable to carry out the process (98% conversion, 40% yield, 24h), although MgZr mixed solids could also be suitable for overall processes with additional reaction steps requiring both acid and basic sites.

Paper 2 "Aldol condensation of furfural with acetone over Mg/Al mixed oxides. Influence of water and synthesis method"

In this paper, four Mg/Al mixed oxides were synthesized by co-precipitation synthetic procedure with two synthetic variables: conventional or microwave heating with the presence or in the absence of Pluronic 123. All

XRD diffractograms of the calcined solids exhibited the typical reflections ascribed to periclase $MgAlO_x$. Moreover, isotherms were type IV and the solids with modification of conventional synthesis (use of microwaves and/or surfactant) led to an increase in BET area. Furthermore, microwave irradiation and/or the use of Pluronic 123 resulted in a decrease in total basicity and an increase in total acidity.

When the solids were tested for aldol condensation with acetone for 3h, the highest conversion value (35.0%) was achieved for HTCON-450 (Conventional heating, no surfactant). For longer reaction times (16h), the yield obtained to 1,5-bis-(2-furanyl)-1,4-pentadien-3-one on the systems synthesized using Pluronic 123 is higher, the best results (44.5% yield) being obtained for HTMWP-450 (synthesized using microwaves). Therefore, it can be concluded that the combined use of Pluronic 123 and microwaves in the reaction medium during the synthesis improves the transformation of furfural to desired product of condensation. The increase in pore size and total acidity could account for that. As for the influence of water, re-hydration of the solid prior to catalytic test was detrimental to activity, probably as a result of the solvation of active sites. On the contrary, the increase in water percentage in the reaction medium (water/toluene) resulted in higher furfural conversions, though selectivity to 1,5-bis-(2-furanyl)-1,4-pentadien-3-one decreased. A plausible explanation is that water weakens the C=O bond in furfural, this favoring its transformation. However, at the same time the first condensation product with one molecule of acetone (FAc, 4-(2-furanyl)-3-buten-2-one) is retired from the aqueous phase once formed, due to its higher solubility in water, thus avoiding its subsequent reaction with another furfural molecule to obtain the desired product (F_2Ac).

Paper 3 "MPV reduction of furfural to furfuryl alcohol on Mg, Zr, Ti, Zr-Ti, and Mg-Ti solids: influence of acid-base properties"

In this paper, several catalysts consisting of pure MgO_x, ZrO_x and TiO_x, as well as Mg-Ti and Zr-Ti mixed systems, were synthesized by the sol-gel method. BET surface values are in the 219-263 m^2/g range for the solids consisting of Zr and/or Ti, whereas for the solids containing Mg are in the 42-81 m^2/g range. Thermogravimetric profiles evidenced that the presence of titanium retards ZrO_2 crystallization but favors the transformation of $Mg(OH)_2$ to MgO. The solids were tested in the MPV reduction of furfural to furfuryl alcohol under conventional and microwave heating. When the solids were tested under conventional heating, ZrO_x was the most active, (selectivity to furfuryl alcohol of 90.4% at 50.1% conversion, t=20h), followed by TiO_x (68.7% selectivity, 16.2% conversion) and MgO_x (56.0% selectivity, 15.2% conversion). The selectivity to furfuryl alcohol dropped upon the introduction of titanium in the mixed systems. When the microwave heating was tested, catalytic activities increased (conversions 4 times higher than the conventional heating), while the selectivity values were similar or higher; for instance, conversion of 27.6% and selectivity to furfuryl alcohol of 96.8% was achieved on ZrO_x.

The methylbutynol (MBOH) test reaction evidenced the presence of acid-base pair sites in ZrO_x, and pyridine DRIFT studies showed that acid sites in ZrO_x were mainly of the Lewis type whereas both Brönsted and Lewis sites were present in TiO_x and Zr-Ti mixed solids. The most active and selective catalysts in the MPV reduction of furfural to furfuryl alcohol was ZrO_x whereas both parameters decreased in Zr-Ti solids as the titanium content increased. These results suggest that acid-base pair sites are particularly active in MPV reduction and that Lewis acid sites are more active than Brönsted ones.

Indicios de calidad

Clave	Artículo
Título	Microemulsion and sol-gel synthesized ZrO_2-MgO catalysts for the liquid-phase dehydration of xylose to furfural.
Autores	A. Parejas, V. Montes, J. Hidalgo-Carrillo, E. Sánchez-López, A. Marinas, F.J. Urbano.
Nombre de la revista	Molecules
Año, volumen, página	2017, 22, 257
Editorial	MDPI
Revista incluida en el Journal Citation Reports (JCR)	Sí
Índice de impacto (2017)	3.098
Categorías	Biochemistry & Molecular biology; Chemistry, Multidisciplinary.
Lugar que ocupa la revista en las categorías (2017)	131/293; 68/171 (respectivamente).
Cuartil	Q2

Clave	Artículo
Título	Aldol condensation of furfural with acetone over Mg/Al mixed oxides. Influence of water and synthesis method.
Autores	A. Parejas, D.Cosano, J. Hidalgo-Carrillo, J. R. Ruiz, A. Marinas, C. Jiménez-Sanchidrián, F.J. Urbano.
Nombre de la revista	Catalysts
Año, volumen, página	2019, 9, 203
Editorial	MDPI
Revista incluida en el Journal Citation Reports (JCR)	Sí
Índice de impacto (2017)	3.465
Categorías	Chemistry, Physical
Lugar que ocupa la revista en las categorías (2017)	55/147
Cuartil	Q2

Clave	Artículo
Título	MPV reduction of furfural to furfuryl alcohol on Mg, Zr, Ti, Zr-Ti, and Mg-Ti solids: influence of acid-base properties.
Autores	J. Hidalgo-Carrillo, A. Parejas, M. J. Cuesta-Rioboo, A. Marinas, F.J. Urbano.
Nombre de la revista	Catalysts
Año, volumen, página	2018, 8, 539
Editorial	MDPI
Revista incluida en el Journal Citation Reports (JCR)	Sí
Índice de impacto (2017)	3.465
Categorías	Chemistry, Physical
Lugar que ocupa la revista en las categorías (2017)	55/147
Cuartil	Q2

Anexo I.

Materiales y métodos

ANEXO I. MATERIALES Y MÉTODOS

AI.1. Preámbulo

En el presente capítulo se describen brevemente las diferentes estrategias de síntesis empleadas para la obtención de los sólidos, las técnicas de caracterización utilizadas y los diferentes montajes experimentales donde se han llevado a cabo las diversas reacciones estudiadas en la presente memoria de Tesis Doctoral.

Los sólidos sintetizados han sido caracterizados empleando varias técnicas instrumentales como la microscopía electrónica de barrido (SEM/EDX) y de transmisión (TEM), el análisis termogravimétrico y térmico diferencial (ATG-ATD), la porosimetría de adsorción-desorción de nitrógeno, la espectroscopía fotoelectrónica de rayos X (XPS), la termodesorción programada de piridina y de CO_2 (TPD-Py y CO_2), la reacción modelo de 2-propanol, la difracción de rayos X (DRX), la espectrometría de masas con fuente de plasma de acoplamiento inductivo (ICP-MS), la fluorescencia de rayos X (FRX), la espectroscopía infrarroja de reflectancia difusa con transformada de Fourier (DRIFT) de piridina, la espectroscopía Raman y la reacción modelo del metilbutinol (MBOH).

La actividad catalítica de los sólidos sintetizados se ha estudiado empleando un multi-reactor, un reactor a presión y un microondas. Posteriormente los productos de reacción obtenidos han sido determinados por un cromatógrafo de gases con detector de ionización de llama (GC-FID) y/o un cromatógrafo de líquidos de alta presión equipado con un detector de índice de refracción (HPLC-RID). La identidad de los productos fue confirmada por espectrometría de masas.

AI.2. Síntesis de Catalizadores

Existe una amplia variedad de técnicas que se pueden emplear para la síntesis de catalizadores como: el método de deposición-precipitación [1], intercambio iónico [2], fotodeposición [3], método de microemulsión [4], método de sol-gel [5], etc. Todas tienen como objetivo obtener un sólido que combine diferentes propiedades como: actividad, selectividad, vida útil, baja toxicidad, fácil regeneración y bajo coste [6].

En esta memoria de Tesis Doctoral han sido sintetizados varios tipos de catalizadores empleando diferentes métodos de síntesis que serán explicados a continuación.

AI.2.1. Método de sol-gel

El método de sol-gel está ampliamente descrito en bibliografía y permite la síntesis de materiales amorfos o policristalinos de forma relativamente sencilla [7-9].

Durante este método se produce la transformación de una solución precursora en un sólido hidratado, el cual mediante un tratamiento térmico se transformará eventualmente en un óxido [10,11]. Los cuatros pasos principales de este método son:

- Formación de un hidrogel: la disolución precursora que contiene el metal se mezcla con un hidróxido, siendo NH_4OH en nuestro caso, para dar lugar al hidróxido correspondiente.

$$M^+ + NH_4OH \rightarrow M\text{-}OH$$

- Envejecimiento: tienen lugar las etapas de nucleación y crecimiento mientras que la mezcla obtenida se deja reaccionando un tiempo determinado.
- Eliminación del disolvente: el gel obtenido en la etapa anterior se filtra, obteniendo así, un precipitado que se secará en una estufa.
- Tratamiento térmico: una vez secado el sólido, se calcina aportándole estabilidad y evitándose su posible rehidratación.

A partir del método de sol-gel se sintetizaron: el óxido de magnesio, el óxido de zirconio, el óxido de titanio y sus correspondientes óxidos mixtos Mg-Ti, Zr-Ti y Mg-Zr. Para ello, se emplearon disoluciones precursoras con un contenido de 0, 25, 75 y 100% molar en Mg o Zr (se escoge el primer metal del óxido mixto) dependiendo del óxido mixto (el resto a 100% es el otro metal del óxido mixto).

Metodología experimental

Los diferentes óxidos se sintetizaron siguiendo el esquema de la Figura AI.1, comenzando por la preparación de una disolución precursora 0,4 M de $Mg(NO_3)_2 \cdot H_2O$, $ZrO(NO_3)_2 \cdot xH_2O$, $Ti[OCH(CH_3)_2]_4$ o mezclas de éstos

dependiendo de la composición de los sólidos. Las disoluciones precursoras de los diferentes óxidos fueron preparadas en agua Milli-Q, a excepción de aquellos que contenían titanio que fueron preparados en propan-2-ol. En un reactor de síntesis de 1L, se adicionaron 400 mL de agua milli-Q a pH 10. Seguidamente, mediante un perfusor se agregaron, gota a gota, 50 mL de la disolución precursora previamente preparada, a una velocidad de 0,56 mL/min. El proceso tuvo lugar bajo agitación magnética a 700 rpm y a pH 10. Con la ayuda de una bomba se pudo mantener el pH constante adicionando, según demanda, NH_4OH 5 N o HCl 0,2 M. A continuación, se dejó envejecer una noche manteniéndose la agitación. Después, se filtró a vacío, obteniéndose un precipitado, el cual se secó en estufa a 120 ºC durante 24 h. Luego, el sólido se pre-molió y se calcinó a 200 ºC con un flujo de aire, durante 6 h. Finalmente se molió y se tamizó a 0,149 mm.

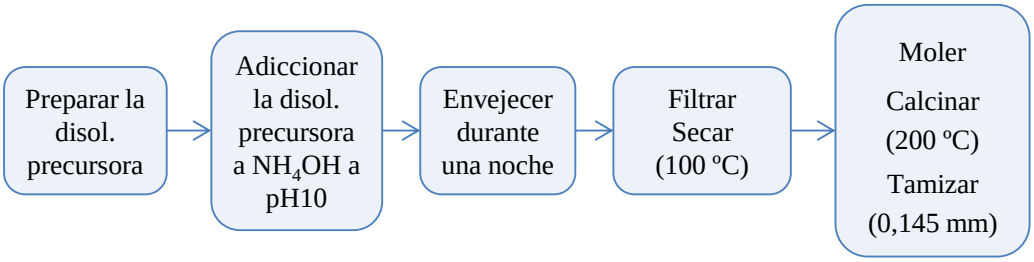

Figura AI.1. Esquema de las etapas seguidas para la síntesis de los catalizadores por el método de sol-gel.

AI.2.2. Método de microemulsión

El método de microemulsión presenta una amplia variedad de aplicaciones, permitiendo generar micelas en una fase continua y pudiendo actuar como nano-reactores en los que se sintetizará el sólido.

La microemulsión está compuesta por una combinación de agua, aceite, surfactante y cosurfactante. Se trata de una solución ópticamente isotrópica y termodinámicamente estable, mostrándose como una solución homogénea a escala macroscópica [12].

Dependiendo de la relación interna de los componentes de la microemulsión, se puede distinguir entre microemulsión *o/w (oil/water)* y *w/o (water/oil)* (Figura AI.2). El primer tipo de microemulsión dará lugar a la formación de una micela, cuyo contenido interno se compone de pequeñas gotas de aceite dispersas en una fase continua de agua. En el segundo tipo, se formará una micela reversa donde pequeñas gotas de agua se encuentran en una fase continua de aceite (es el tipo de microemulsión empleada en los sólidos del Capítulo 3 de esta memoria de Tesis Doctoral). El tamaño de las gotas formadas varía de 10 a 100 nm [13] dependiendo del tipo de surfactante empleado, fuerza iónica, agente precipitante, pH, tipo de aceite, etc.

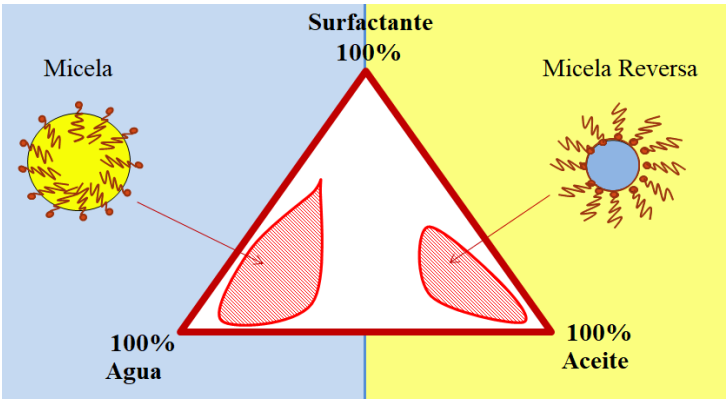

Figura AI.2. Diagrama de fases, mostrándose el tipo de microemulsión según la proporción de sus componentes.

El bromuro de hexadeciltrimetilamonio (CTAB) fue el surfactante empleado en esta síntesis. Presenta una naturaleza anfifílica, es miscible en una mezcla de hidrocarburos/agua y además, debido a que las orientaciones de las moléculas que lo componen no son aleatorias permite la formación de agregados esféricos [14].

El butan-1-ol fue utilizado como cosurfactante, actuando como "espaciador electronegativo" y minimizando así, las repulsiones entre las cabezas positivamente cargadas del surfactante.

A partir del método de microemulsión se sintetizaron el óxido de magnesio, el óxido de zirconio y sus correspondientes óxidos mixtos Mg-Zr. Para ello, se utilizaron disoluciones precursoras con un contenido de 0, 25, 75 y 100% molar en Mg (el resto a 100% es Zr).

Metodología experimental

Previo a las síntesis de los diferentes óxidos por el método de microemulsión, se llevaron a cabo varios ensayos para comprobar la estabilidad de la microemulsión.

Para ello se mezcló una cantidad conocida de surfactante y fase continua (en concreto, 20% y 80%, respectivamente, se trata de las zonas donde comúnmente es estable el sistema) obteniéndose una mezcla turbia. Luego, mediante pesada, se añadió una cantidad conocida de fase acuosa (las disoluciones precursoras anteriormente preparadas en el método de sol-gel) hasta que la mezcla se tornó transparente. Éste es considerado el mínimo necesario de fase acuosa para que se produzca la microemulsión. Después se añadió más cantidad de fase acuosa hasta que la mezcla se tornó turbia, conociéndose así, el límite máximo de fase acuosa que es capaz de admitir la mezcla. Una vez conocida la cantidad de fase acuosa que se puede añadir a la mezcla, se calcula el porcentaje límite de cada componente para que la microemulsión sea estable.

Con los datos que se obtuvieron, se eligió un punto intermedio, incluyendo el posible error experimental. En la Tabla AI.1, se muestra la receta que se siguió para la síntesis de los catalizados [15].

Tabla AI.1. Receta expresada en porcentaje en peso de la cantidad de cada componente de la mezcla.

Fase	Componente	Composición (% en peso)
Aceite	Iso-octano	53
Surfactante	CTAB	15
Cosurfactante	Butan-1-ol	12
Agua	ME1: disolución 0,4M de los precursores. ME2: disolución de NH_4OH	20

Conocida la receta a seguir, se siguieron las etapas que aparecen en la Figura AI.3 para sintetizar los diferentes sólidos. Se comenzó preparando en dos recipientes, la ME1 con la disolución 0,4 M de los precursores y la ME2 con la disolución de NH_4OH. Posteriormente, se adicionó la ME1 sobre ME2, mediante goteo. Luego, se dejó envejecer durante una noche, estando ambos recipientes en todo momento bajo agitación constante. Posteriormente, se filtró el sólido y se lavó 5 veces con 80 mL de una mezcla cloroformo/etanol (50/50) (v/v), para así, poder eliminar posibles restos de surfactante y aceite. Después al igual que en la síntesis por el método de sol-gel, se secó el sólido, se calcinó y se tamizó.

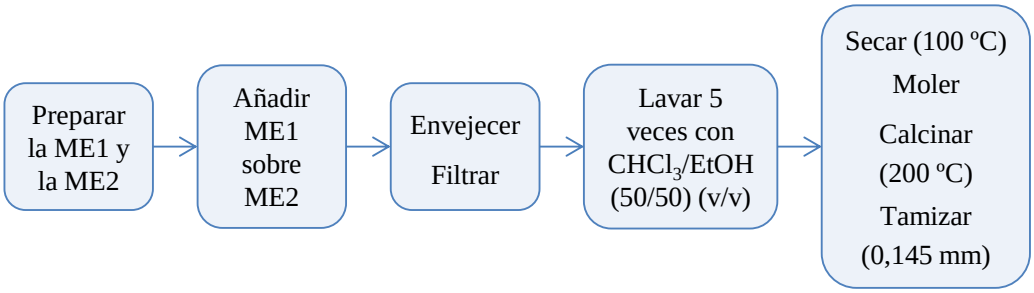

Figura AI.3. Esquema de las etapas seguidas para la síntesis de los catalizadores por el método de microemulsión.

AI.2.3. Método de co-precipitación

En el método de co-precipitación se produce la precipitación simultánea de un componente normalmente soluble con un macro-componente de la misma

solución para la formación de cristales mixtos [16]. Existen tres mecanismos principales de co-precipitación: inclusión, oclusión y adsorción.

- Una inclusión ocurre cuando la impureza es incorporada a la estructura cristalina, provocando un defecto cristalográfico.
- Una oclusión ocurre cuando la impureza es adsorbida durante el paso de crecimiento dando lugar a la formación de imperfecciones en el cristal.
- Una adsorción ocurre cuando una impureza está débilmente unida a la superficie del precipitado, debido a que la adsorción ha tenido lugar después de que el precipitado se hubiese formado o separado [17].

A partir del método de co-precipitación se sintetizaron los óxidos mixtos laminares de Mg/Al, modificando dos variables durante la síntesis (calentamiento convencional o microondas con la presencia o ausencia de Pluronic 123 como surfactante).

Metodología experimental

Para llevarlo a cabo se siguieron las etapas que aparecen en la Figura AI.4, comenzando por la adicción de dos disoluciones, cuyo contenido fue 0,2 moles de $Mg(NO_3)_3 \cdot 6H_2O$ y 0,1 moles de $Al(NO_3)_3 \cdot 9H_2O$ (relación molar Mg/Al=2), en 25 mL de agua Milli-Q. La mezcla se añadió lentamente a una disolución a pH 10, a una temperatura de 60 ºC, con agitación continua y atmósfera inerte. El pH se mantuvo constante mediante la adicción necesaria de NaOH 1 M. Posteriormente, la mezcla obtenida se separó en dos fracciones. La primera se mantuvo durante 24 h a 80 ºC, luego se filtró y lavó con agua Milli-Q. La otra se envejeció mediante un tratamiento asistido por microondas durante 1h a 80 ºC bajo agitación magnética. Estos dos procesos de síntesis fueron repetidos, pero en presencia de una agente surfactante, como el Pluronic

123 al 2% en peso. Por último, todos los sólidos fueron calcinados a 450 ºC en aire, con un gradiente térmico de 1 ºC·min^{-1} durante 8h.

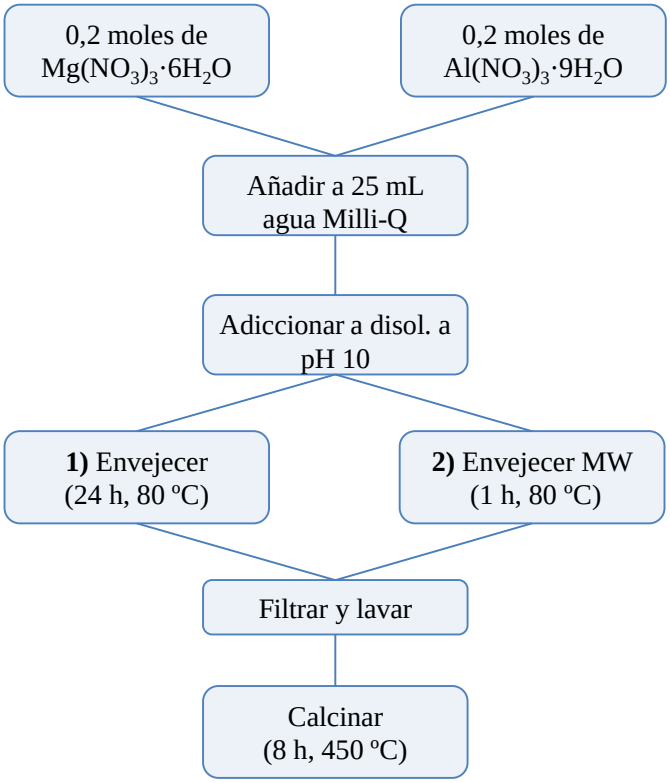

Figura AI.4. Esquema de las etapas seguidas para la síntesis de los catalizadores por el método de co-precipitacion. Siendo: la etapa **1)** cuando se produce el envejecimiento mediante calentamiento convencional y, la etapa **2)** cuando se produce el envejecimiento mediante calentamiento por microondas. Caso de producirse la adición de Pluronic 123 se lleva a cabo al inicio de la síntesis.

AI.3. Técnicas de Caracterización

Seguidamente se describen las técnicas de caracterización que se han empleado y que han aportado información relacionada con la estabilidad térmica, textural, morfología, estructura y composición de los sólidos sintetizados. Así como las características ácido-básicas superficiales.

AI.3.1. Microscopía electrónica de barrido/Espectroscopía de energía dispersiva de Rayos X (SEM-EDX)

A partir de la microscopía electrónica de barrido se puede obtener información sobre la naturaleza de los sólidos, como su morfología, composición, tamaño, grado de interacción entre diferentes fases, etc., resultando de gran utilidad para correlacionarla con el comportamiento catalítico de los diferentes catalizadores. Es capaz de proporcionar hasta 200.000 aumentos y producir imágenes tridimensionales realistas de la superficie del objeto.

La técnica consiste en hacer incidir un haz de electrones, manejado a través de lentes electromagnéticas, sobre la superficie de una muestra situada en

una columna de alto vacío. Al incidir este haz de electrones se producirán varios fenómenos como emisión de electrones secundarios, electrones Auger, rayos X, entre otros, siendo estos últimos los más comunes. En la Figura AI.5. se representa un esquema de las interacciones producidas al incidir sobre la muestra el haz de electrones.

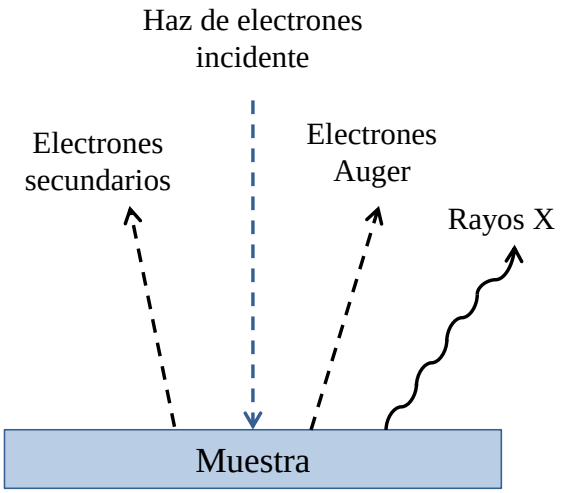

Figura AI.5. Esquema de las interacciones producidas al incidir sobre la muestra el haz de electrones.

Los **electrones secundarios** son de muy baja intensidad y se producen cuando un electrón del haz de electrones pasa muy cerca del núcleo de un átomo del sólido, proporcionando energía a uno o varios de los electrones interiores para ser emitidos fuera del sólido. Posteriormente con la ayuda de un detector apropiado, se registra esta interacción producida, contando el número de electrones secundarios de baja energía que son emitidos por cada punto de la superficie, formándose la imagen del sólido [18].

Los **electrones Auger o retrodispersados** se producen cuando un electrón del haz incide frontalmente con el núcleo de un átomo de la muestra, reflejándose en sentido contrario fuera del sólido. La intensidad de la emisión dependerá del número atómico del sólido [19].

Los **rayos X** son emitidos cuando los electrones del haz incidente excitan los átomos de la muestra y provocan su emisión. Esta energía puede ser medida por la espectroscopia de energía dispersiva de rayos X (EDX), pudiéndose determinar la composición elemental del sólido, a partir de la longitud de onda a la que ha sido emitido cada rayo X [18,20,21].

Metodología experimental

El análisis de composición superficial de los sólidos se realizó empleando un microscopio de barrido JEOL, modelo JSM-6300 equipado con un detector de análisis de energía dispersiva de rayos-X. Se trabajó con un voltaje de aceleración de 20 keV y con una resolución de 65 eV. El software permite el análisis cualitativo y semicuantitativo en una línea de barrido.

AI.3.2. Microscopía electrónica de transmisión (TEM)

El microscopio electrónico de transmisión nos permite observar las nanopartículas evitando el empleo de hipótesis físicas y matemáticas. La imagen del TEM ofrece información sobre la morfología del sólido, pudiendo ser medido el diámetro de partículas a partir de programas como "ImageJ" y así, calcular el tamaño de partícula promedio [18].

En la técnica de microscopía electrónica de transmisión (como se observa en la Figura AI.6.), un haz de electrones de 100-200 KeV impacta sobre una muestra muy fina, provocando que una parte de los electrones consigan atravesarla y otros sean dispersados [22]. Los electrones que han atravesado la muestra son recogidos y focalizados por la lente objetivo generando una imagen, la cual posteriormente será ampliada gracias a las lentes proyectoras. La imagen final se proyecta en una pantalla fluorescente [23].

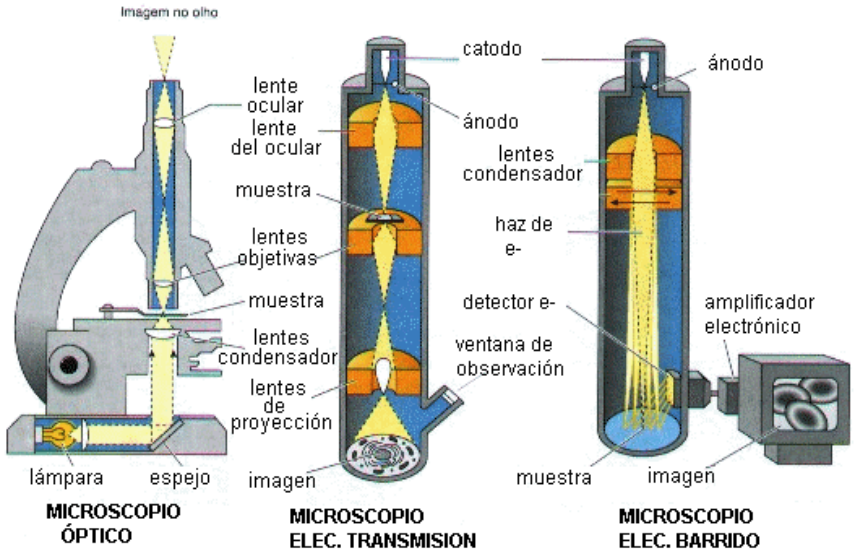

Figura AI.6. Comparación de los componentes del microscopía óptico, microscopio electrónico de transmisión y microscopio electrónico de barrido. Adaptado de [24].

Dependiendo de las características internas de la muestra a analizar, mayor o menor cantidad de electrones, conseguirán atravesarla sin ser desviados. Por ello se obtendrá una imagen con zonas más oscuras y zonas más claras (un menor o mayor número de electrones ha atravesado la muestra, respectivamente).

Metodología experimental

Las imágenes de la microscopía electrónica de transmisión fueron obtenidas empleando un microscopio JEOL JEM 1400. Las muestras se prepararon depositándolas en una rejilla de microscopía de cobre de 3 mm de luz.

AI.3.3. Análisis termogravimétrico y térmico diferencial

El análisis termogravimétrico comprende un conjunto de técnicas que analizan el cambio de comportamiento de una muestra, frente al tiempo o a la temperatura, cuando está siendo sometida a un programa de temperatura en

atmósfera controlada. Ésta puede ser dinámica o estática (los gases más empleados son aire sintético, N_2, Ar y CO_2)

Cuando se desarrolla en función de la temperatura, se trataría de un experimento dinámico, donde la temperatura va aumentando de manera controlada. Normalmente de forma lineal con el tiempo.

Cuando se desarrolla en función del tiempo, se trataría de un proceso estático, en el cual la temperatura se mantiene constante durante todo el experimento [25].

Durante el proceso se pueden detectar procesos de variación de masa de la muestra, cómo adsorción-desorción, descomposición, sublimación, actividad catalítica, entre otros.

En el análisis térmico diferencial se estudia la diferencia de temperatura entre la muestra y un material de referencia, mientras ambos se encuentran expuestos al mismo programa de calentamiento. De esta manera, es posible observar si los procesos de variación de masa que tienen lugar en la muestra son exotérmicos y/o endotérmicos.

Metodología experimental

El análisis termogravimétrico y térmico diferencial de los sólidos se realizó en un instrumento Setaram Setsys 12. En un portamuestras de alúmina se introducen entre 15 y 20 mg de sólido y se calienta a temperaturas de 30 a 600 ºC a una velocidad de 10 ºC/min bajo una corriente de aire sintético (50 mL/min). A los resultados obtenidos por esta técnica se le resta una "línea de base" previamente obtenida a partir de un ensayo en blanco con el portamuestras vacío.

AI.3.4. Porosimetría de adsorción-desorción de nitrógeno

A partir de la técnica de porosimetría de adsorción-desorción de nitrógeno se han podido determinar las propiedades texturales de los sólidos [26], como:

1) Superficie específica, S_{BET} (m^2/g): extensión geométrica de la superficie de las paredes de los poros por gramo de sólido adsorbente.
2) Volumen acumulado de poros, Vp (cm^3/g): volumen total de poros por gramo de adsorbente.
3) Diámetro medio de poro, d_p (nm).
4) Distribución del tamaño de poros, dV_p/dD_p: función distribución $dV_p/dD_p = f(D_p)$.

Estos valores obtenidos a partir de las medidas de adsorción y desorción de gases, dan como resultado una isoterma de adsorción-desorción. La isoterma es una representación donde se relaciona la cantidad de nitrógeno adsorbido por el sólido frente a la presión relativa P/P_0 (siendo P = presión de vapor de equilibrio del adsorbato y P_0 = presión de vapor del adsorbato líquido puro) a temperatura constante. Esta presión relativa se encontrará en un intervalo entre 0 y 1.

Las isotermas se han podido clasificar en seis tipos según la clasificación de la IUPAC. Los primeros cinco tipos (I a V) fueron propuestos originalmente por S. Branauer, L.S. Deming, W.S. Deming y E. Teller (BDDT), posteriormente a esta clasificación fue añadida la isoterma tipo VI (Figura AI.7) [27].

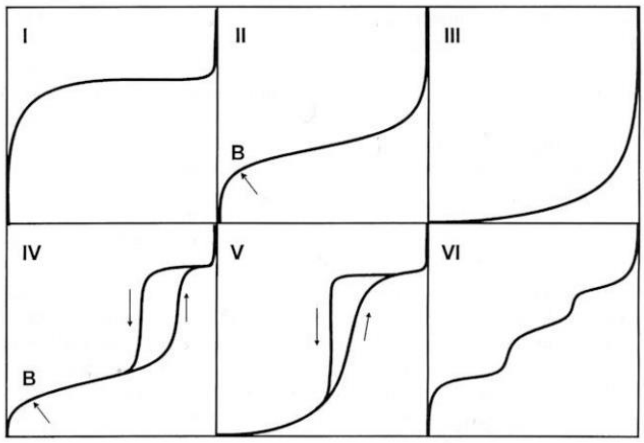

Figura AI.7. Tipos de isotermas de adsorción-desorción según la clasificación de la IUPAC, adaptado de [27].

A continuación se resumen las características de cada una de las isotermas:

– Tipo I: presenta un valor asintótico asociado a la monocapa, es característica de sólidos microporosos con un área superficial pequeña.

– Tipo II: es muy común en sólidos no porosos o materiales macroporosos y representa una adsorción en monocapa-multicapa sin restricción. El punto de inflexión corresponde con el recubrimiento total de la monocapa y el comienzo de la adsorción en multicapa. La ordenada del punto B nos da una estimación de la cantidad de adsorbato requerido para cubrir por unidad de masa, la superficie del sólido con una capa monomolecular (capacidad de monocapa).

– Tipo III: es típica de sistemas donde las interacciones entre el adsorbato y el adsorbente son débiles. No es común encontrarse con este tipo de isotermas.

– Tipo IV: aparece en sólidos mesoporos. A bajos valores de P/P_0, se comporta como la del tipo II, pero para valores más altos la adsorción se incrementa teniendo lugar la condensación capilar de los poros del sólido. Generalmente, presenta ciclo de histéresis asociado a esta condensación.

– Tipo V: es semejante al tipo III, diferenciándose en que la condensación capilar en los poros tiene lugar a mayores valores de P/P_0.

– Tipo VI: representa la adsorción en multicapa sobre una superficie uniforme no porosa. En el caso más sencillo la altura de cada etapa permanece constante para dos o tres capas adsorbidas [28,29].

Conociendo los diferentes tipos de isotermas y su representación se puede conocer:

a) El tipo de material poroso: materiales microporosos (diámetro de poro inferior a 2 nm), mesoporos (diámetro de poro entre 2 y 50 nm) y macroporosos (diámetro de poro mayor de 50 nm) (clasificación según la IUPAC);

b) La naturaleza del proceso de adsorción: en monocapa-multicapa, condensación capilar o adsorción en los microporos.

Para conocer algunas de las propiedades relacionadas con la porosidad de los sólidos se han estudiado numerosos métodos [30]. Entre ellos, destaca el método propuesto por Branuauer, Emmet y Teller "BET" para la obtención de la superficie específica y el método desarrollado por Barrett, Joyner y Halenda "BJH" para la obtención del volumen de los poros presentes en los sólidos, así como su distribución de tamaño de poros. A continuación, dichos métodos se explican con mayor detalle:

– El **método BET** es empleado para la determinación de áreas superficiales [31]. Esta técnica se basa en: que el calor de adsorción de la monocapa es distinto al de las otras capas, pero todas las siguientes capas presentan el mismo calor de adsorción.

Las consideraciones generales de la teoría BET son: no existen sitios preferentes de adsorción; no existen interacciones laterales entre moléculas adsorbidas; y las fuerzas de condensación son activas en al adsorción.

La ecuación BET Ecuación AI.1 en su forma lineal, se expresa como:

$$\frac{P}{V\,(P_0-P)} = \frac{1}{(V_m C)} + \left[\frac{(C-1)}{(V_m C)}\right]\frac{P}{P_0} \qquad \textbf{Ecuación AI.1.}$$

Siendo: V, el volumen de N_2 adsorbido, en condiciones normales, a P_0; V_m, el volumen requerido para cubrir la superficie del adsorbente con una capa monomolecular de adsorbato; P, la presión de equilibrio; P_0, la presión de saturación del adsorbato líquido utilizado; C, una constante relacionada con el calor de adsorción de la primera monocapa.

Para la determinación de V_m se utilizan los volúmenes adsorbidos correspondientes al intervalo de presiones parciales de adsorbato. Representando P / [V (P_0-P)] frente a P/P_0 y a partir de un ajuste lineal se obtienen la pendiente, $(C-1)/(V_m C)$ y la ordenada en el origen, $1/(V_m C)$. Una vez conocido el valor de V_m, se obtiene el área de la superficie (S) del sólido a partir de la Ecuación AI.2.

$$S = \left[\frac{V_m A N}{M}\right] \qquad \textbf{Ecuación AI.2.}$$

Siendo: A el número de Avogadro; N el área ocupada por cada molécula de N_2 adsorbida (0,162 nm^2); y M el volumen molar del gas.

– El **método BJH**, es utilizado para calcular el volumen y la distribución del tamaño de los poros presentes en los sólidos. Este método se basa en la ecuación Kelvin (Ecuación AI.3) y tiene en cuenta los fenómenos de condensación capilar.

$$\ln\left(\frac{P}{P_0}\right) = -\left(\frac{2\gamma\omega_m \cos\theta}{RTr_c}\right) \qquad \textbf{Ecuación AI.3.}$$

Siendo: r_c el radio para poros cilíndricos o la distancia entre láminas para los de tipo rendija; γ la tensión superficial; ω_m el volumen molar; y θ el ángulo de contacto.

Metodología experimental

Las medidas de adsorción-desorción de nitrógeno se han determinado a la temperatura del nitrógeno líquido (-195,8 ºC), en un analizador de superficies Micromeritics ASAP 2010. Primero, los sólidos se someten a un proceso de desgasificación a 120 ºC durante 12 h (evitando posibles gases adsorbidos en la superficie de los sólidos). Posteriormente, se introduce una cantidad conocida de N_2 en un recipiente que contiene el adsorbente y se produce la medición. La isoterma de adsorción se construye punto a punto, introduciendo sucesivas cargas de gas y dejando tiempo suficiente para que se alcance el equilibrio en cada punto.

La superficie específica se ha obtenido mediante el método BET y la distribución de tamaño de poro por el método BJH.

AI.3.5. Espectroscopía fotoelectrónica de rayos X (XPS)

La espectroscopía fotoelectrónica de rayos X, también conocida como espectroscopía electrónica para análisis químico o ESCA, es una técnica de caracterización superficial que permite obtener información, cualitativamente y cuantitativamente, de la superficie de los sólidos o especies químicas. Pudiendo determinar el porcentaje de cada elemento presente, en los primeros 10-12 nm de superficie, exceptuando H y He.

A partir del espectro de XPS se puede más información como: información acerca del entorno molecular (estado oxidación, átomos enlazantes, orbitales moleculares, etc.); información sobre estructuras aromáticas o

insaturadas a partir de las transiciones Π → Π*; información de grupos orgánicos utilizando reacciones de derivatización; perfiles de profundidad de 10 nm no destructivos y destructivos de profundidades de varios cientos de nanómetros; variaciones laterales en la composición de la superficie; etc. [32].

La técnica de espectroscopía fotoelectrónica de rayos X (Figura AI.8) consiste en bombardear la superficie del sólido con radiación de rayos X [33], utilizando como fuentes de excitación las líneas $K\alpha_{1,2}$ de Mg o Al, que poseen energías de 1253,6 y 1486 eV, respectivamente. Como consecuencia de esta irradiación se produce el efecto fotoelectrónico, produciéndose la emisión de los electrones excitados en los orbitales de las capas internas de los átomos irradiados del sólido con una determinada energía cinética para ser expulsados de los átomos, y quedando éstos parcialmente ionizados. Posteriormente, los electrones pasan al analizador de electrones y luego se procede a su lectura en un PC.

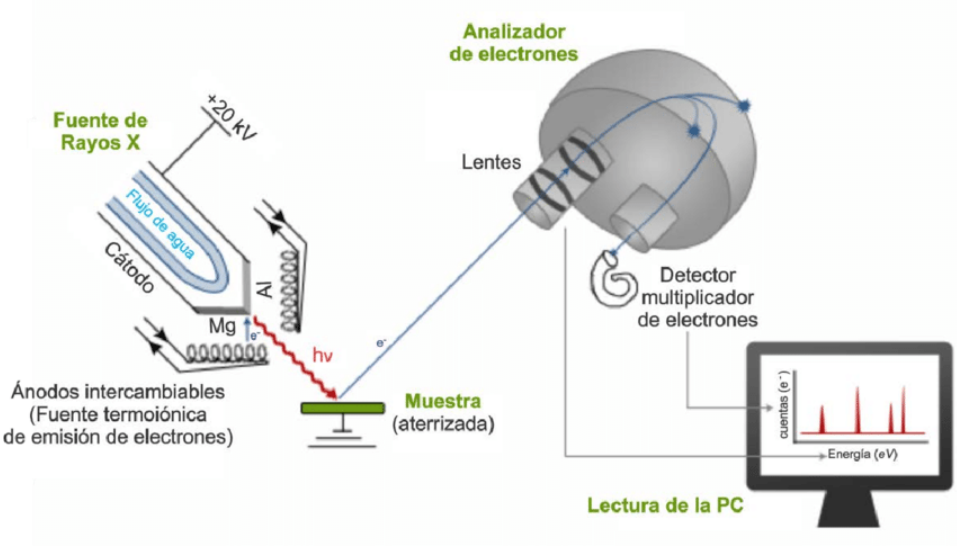

Figura AI.8. Esquema de un equipo de espectroscopía fotoelectrónica de rayos X. Adaptado de J. Vulfrano [34].

La energía cinética se encuentra relacionada con la energía de enlace mediante la Ecuación AI.4, permitiendo la obtención de información acerca de

la naturaleza de los átomos irradiados y de la composición química de la superficie del sólido

$$E_B = h\upsilon - E_K - W \qquad \textbf{Ecuación AI. 4.}$$

Siendo: hυ la energía de los fotones; E_K la energía cinética del fotoelectrón producido; W la función de trabajo del espectrómetro; y E_B la energía de ligadura (parámetro que identifica al electrón de forma específica, en términos del elemento y nivel atómico) [35].

Metodología experimental

Para el análisis de las muestras, se realizan pastillas de los sólidos a analizar. Luego, la pastilla se deposita en una cámara de vacío para eliminar especies volátiles fisisorbidas. Y posteriormente, pasará a una cámara de análisis con una presión residual de $5x10^{-9}$ Pa. Los sólidos se expusieron a una fuente de Al a 120W, 30 mA, con C (1s) como energía de referencia (284.6 eV). El espectrómetro utilizado es un Leibold-Heraeus LHS10, equipado con un analizador electrónico semiesférico EA-200MCD con una fuente de rayos X dual (XR-50, SPECS). Las deconvoluciones de los diferentes espectros XPS se han llevado a cabo mediante un programa informático "Casa XPS" y se ajustan a perfiles simétricos de tipo Gausiano-Lorentziano y la línea de base tipo Shirley.

AI.3.6. Termodesorción programada

La termodesorción programada (TPD) es una técnica que se basa en el fenómeno de quimisorción. Se utiliza para caracterizar diferentes tipos de centros activos superficiales y dependiendo del adsorbato que se emplee, se pueden determinar la densidad y la fortaleza de los centros presentes en los sólidos. Por ejemplo como adsorbatos se pueden emplear: el amoniaco (NH_3) o

piridina (C_5H_5N), moléculas de carácter básico para determinar centros ácidos; o dióxido de carbono (CO_2), una molécula de carácter ácido para determinar centros básicos [36].

En la termodesorción programada, primero se produce la adsorción de un gas sobre una muestra sólida a una temperatura determinada hasta lograr la saturación de la superficie del sólido. Posteriormente, mediante un aumento controlado de la temperatura se producirá la desorción del gas previamente adsorbido. Durante esta etapa, se medirá la evolución del gas desorbido en función de la temperatura o el tiempo, empleando un detector adecuado, como un TCD (detector de conductividad térmica). Por último se obtendrá una curva de desorción, presentando un perfil de tipo gaussiano asimétrico, mostrando un pico máximo de intensidad correspondiente a la temperatura a la que la desorción del gas (adsorbido por la superficie del sólido) es máxima.

Para la caracterización de los sólidos empleados en la presente memoria de Tesis Doctoral, se ha empleado la desorción de piridina a temperatura programada (TPD-Py) y la desorción de dióxido de carbono a temperatura programada (TPD-CO_2).

Metodología experimental

Los perfiles de TPD-Py de los sólidos se obtuvieron en un aparato de la empresa PIK Eng&Tech con detección TCD. En una U de cuarzo se añade 20 mg de sólido, la cual fue colocada en un horno. El primer paso fue realizar un pretratamiento, eliminando la posible agua fisisorbida en el sólido bajo un flujo de helio calentando hasta 200 ºC o 450 ºC (dependiendo del sólido) con un rampa de calentamiento de 10 ºC/min. A continuación, el sólido fue saturado con piridina a 50 ºC durante 30 min. Después de la saturación, la piridina fisisorbida fue eliminada con una corriente de helio, a 50 ºC durante 60 min.

Luego, fue medida la acidez del sólido con una rampa de temperatura de 50 ºC a 200 ºC o 450 ºC (con una rampa de calentamiento de 10 ºC/min), manteniéndose en la temperatura final durante 30 min. La piridina desorbida se cuantificó utilizando una recta de calibrado obtenida a partir de volúmenes variables de piridina inyectada.

Los perfiles de TPD-CO_2 de los sólidos fueron determinados en un instrumento Micromeritics Autochem II (Micromeritics) equipado con un TCD. En cada análisis se ha utilizado una cantidad de 100 mg de cada sólido, añadiéndose en una U de cuarzo colocado en un horno. Al igual que en el TPD-Py, se realizó una etapa de pretratamiento, pero en este caso el sólido fue limpiado bajo una corriente de Ar (20 mL/min). Se calentó hasta 200 ºC o 450 ºC con una rampa de calentamiento de 10 ºC/min durante 60 min, y luego se enfrió hasta 40 ºC. A esa temperatura fueron saturados los sólidos con la molécula sonda, utilizando un flujo de 5% CO_2/Ar a 20 mL/min durante 60 min. Después de la saturación, el CO_2 fisisorbido fue eliminado con una corriente de Ar durante 30 min (20 mL/min). A continuación, fue medida la basicidad con una rampa de temperatura de 40 ºC a 200 ºC o 450 ºC (rampa de calentamiento 10 ºC/min) y mantenida a la temperatura final durante 60 min. La cantidad de CO_2 adsorbido fue determinada utilizando una recta de calibrado construida a partir de volúmenes variables de 5% CO_2/Ar inyectados.

AI.3.7. Reacción modelo del propan-2-ol

La reacción test de transformación del propan-2-ol es un proceso modelo, empleado para conocer los tipos de centros que poseen los sólidos sintetizados, proporcionando información sobre las propiedades ácido-base y/o redox del sólido en función del producto o productos obtenidos.

Los centros ácidos producen propeno (reacción intramolecular) o éter diisopropílico (reacción intermolecular), mientras que los centros básicos, los pares centros ácido-base o de centros básicos con propiedades redox conducen a acetona (reacción de deshidrogenación) [37] como se muestra en la Figura AI.9.

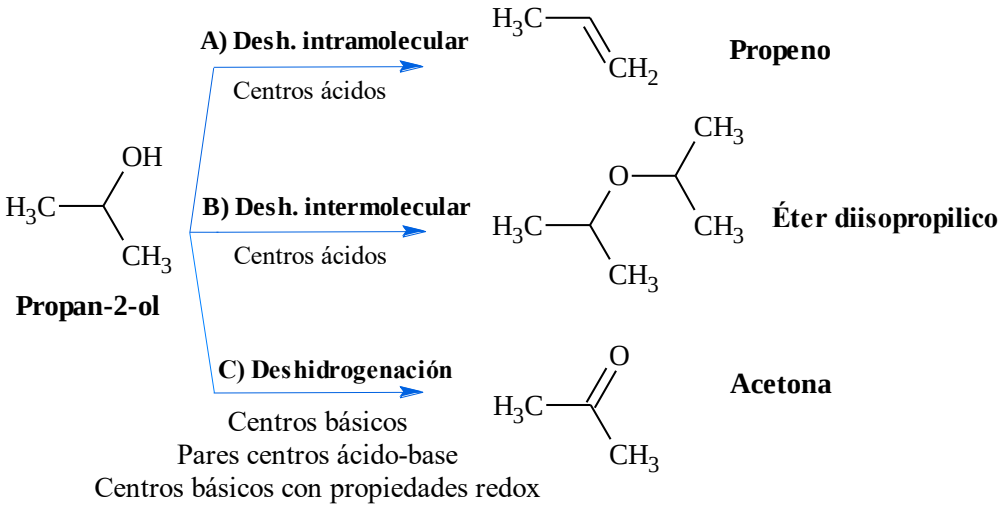

Figura AI.9. Reacción modelo de transformación del propan-2-ol. A) Deshidratación intramolecular; B) Deshidratación intermolecular; y C) Deshidrogenación.

Metodología experimental

La transformación del propan-2-ol en fase gaseosa ha sido llevada a cabo en un reactor de acero inoxidable (1/8 pulgadas O.D.). En el reactor se introdujeron 100 mg de sólido y 1 g de SiO_2 inerte. Antes de la reacción, el sólido fue sometido a un pretratamiento bajo un flujo de N_2 (20 mL/min), mientras que se aumentaba la temperatura hasta 200 ºC (velocidad de calentamiento 2 ºC/min). La reacción se inició introduciendo propan-2-ol con un flujo de N_2, gas portador, de 10 mL/min, a través de un saturador lleno de propan-2-ol a temperatura ambiente. Los análisis de los productos de reacción, así como el propan-2-ol, se llevaron a cabo en línea conectando el efluente a un cromatógrafo de gases (HP 5890 series II) equipado con una columna capilar

Superlcowax-10 (60 m de longitud, 0.25 mm de diámetro interno, 0.25 µm de espesor de película. En la Figura AI.10 se muestra el dispositivo experimental utilizado para llevar a cabo la reacción test.

Figura AI.10. Dispositivo experimental empleado para llevar a cabo la reacción modelo del propan-2-ol.

AI.3.8. Difracción de Rayos X

La difracción de rayos X es una técnica no destructiva empleada para la identificación de fases cristalinas mediante una identificación cualitativa de una amplia gama de materiales como fluidos, minerales, catalizadores, metales, etc., pudiendo llegar a determinar sus propiedades físicas y químicas.

La difracción de rayos X se basa en las interferencias ópticas producidas cuando una radiación monocromática (haz de rayos X) atraviesa una rendija con un espesor que es comparable a la longitud de onda de la radiación. La técnica comienza con la irradiación de la muestra por ese haz de rayos X con una determinada longitud de onda. Posteriormente, se produce la desviación de los fotones del haz incidente en todas las direcciones, siendo sólo una parte la que se produzca a la misma longitud de onda que la radiación incidente, constituyendo la radiación dispersada y originando el fenómeno de difracción (Figura AI.11) [38,39].

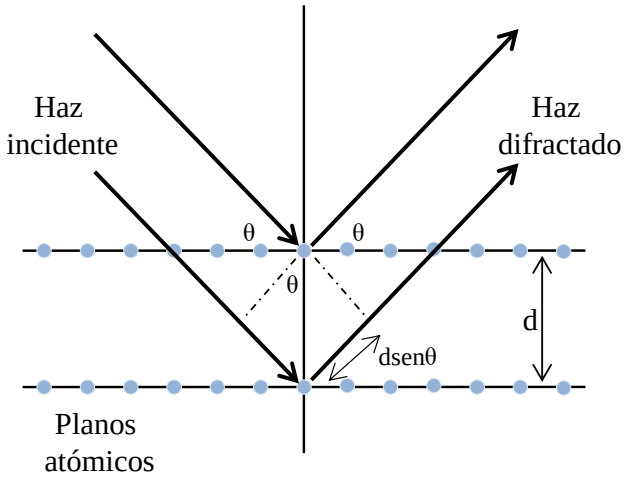

Figura AI.11. Esquema de difracción de rayos X. Adaptada de [40].

El fenómeno de difracción se produce cuando existe una disposición ordenada de átomos y si se cumple la "ecuación de Bragg" (Ecuación AI.5.), cuya condición esencial es que "n" sea un número entero consistente con "senθ" menor o igual que 1. Esta ecuación se basa en la hipótesis de Bragg, que considera la difracción como una reflexión, donde los planos de los átomos son "semi-transparentes", capaces de reflejar y transmitir cada haz de radiación X [41].

$$n \cdot \lambda = 2d \cdot \text{sen}\theta \qquad \textbf{Ecuación AI.5.}$$

Siendo: n número entero; λ la longitud de onda; d espacios interlaminares; θ ángulo de difracción.

A partir de un difractograma de rayos X se obtiene una serie de picos correspondientes a la intensidad en función del ángulo de difracción (2θ), pudiéndose conocer con ellos: la posición, la intensidad (altura o área) y el perfil de los picos [33].

Metodología experimental

La difracción de rayos X se ha llevado a cabo en un difractómetro Siemens D-5000 provisto de un goniómetro. Emplea un filtro de Ni y un

monocromador de grafito. La radiación empleada es la línea K_α del Cu (λ = 1.54 Å) en una rango de 5 a 80º. El voltaje usado es de 40 kV y la intensidad de 30 mA. El sólido en polvo se colocó sobre un portamuestras, presentando una superficie expuesta a la radiación plana y uniforme.

AI.3.9. Espectrometría de masas con fuente de plasma de acoplamiento inductivo "ICP-MS"

La espectrometría de masas con fuente de plasma de acoplamiento inductivo (ICP-MS) es una fuente de ionización a presión atmosférica para la generación de iones, unido a un espectrómetro de masas para así, posteriormente, separar y detectar esos iones.

Su función es proporcionar información multielemental, permitiendo la determinación de elementos traza y sus isótopos. Es posible analizar todos los elementos de la tabla periódica excepto H, He, C, N, O, F, Ne, Cl, S, I, Br y gases nobles [42].

Esta técnica posee grandes ventajas como: una alta precisión, bajos límites de detección y el análisis de una gran cantidad de elementos e isótopos. Algunos de los campos de aplicación más importantes son: agricultura y alimentos; análisis clínico; muestras geológicas; aguas, etc. [43].

Metodología experimental

El análisis semicuantitativo y cuantitativo de metales, así como la medida de lixiviación (obtenido a partir del medio de reacción filtrado) se ha llevado a cabo en un instrumento Perkin-Elmer ELAN DRC-e. Previo al análisis, las muestras fueron tratadas mediante digestión en horno microondas y/o en vaso abierto.

AI.3.10 Fluorescencia de Rayos X

La técnica de fluorescencia de rayos X se trata de una técnica que permite el análisis químico elemental de los elementos comprendidos entre el flúor y el uranio de muestras que se encuentra en estado sólido y líquido. También puede ser empleada para determinar el espesor y la composición de capas y recubrimientos.

Esta técnica espectroscópica emplea la emisión de la radiación X fluorescente o secundaria generada, al ser excitada previamente una muestra con una fuente de radiación X de alta energía o rayos gamma. Esta radiación X incidente expulsa los electrones de las capas interiores del átomo, dejando lugares vacantes que posteriormente serán ocupados por electrones de las capas más externas (como se observa en la Figura AI.12) resultando en un exceso energético que se disipará en forma de radiación fluorescente, comentada anteriormente. Esta radiación emitida estará constituida por energías discretas (K_α y K_β) características de los elementos presentes en la muestra [44].

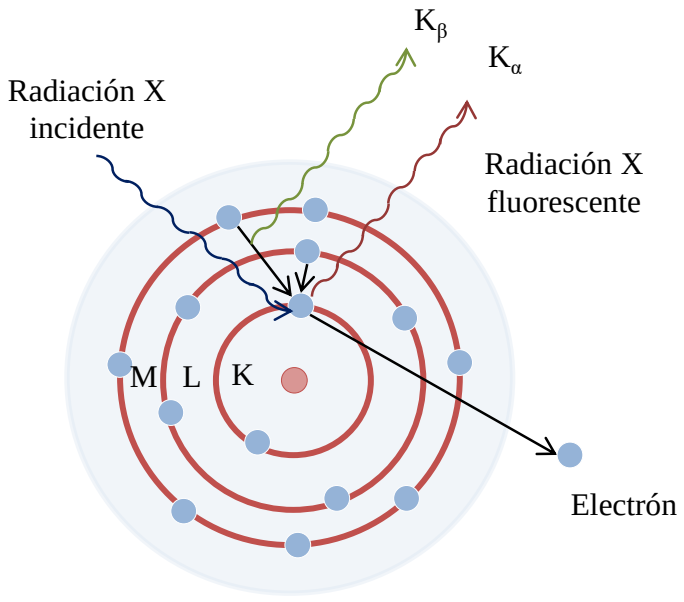

Figura AI.12. Modelo atómico de fluorescencia de rayos X. Adaptado de [45].

Algunas de las ventajas que presenta esta técnica son: es un análisis no destructivo, permite el análisis de los principales elementos presentes en la muestra y de elementos traza; y es posible detectar elementos de Z>11.

Metodología experimental

La fluorescencia de rayos X se ha llevado a cabo en un espectrómetro de rayos X de longitud de onda Rigaku ZSK Priums IV. Está equipado con un tubo de rayos X Rh-target de 3 kW, diez cristales analizadores, un contador proporcional sellado para la detención de elementos ligeros y un contador de centelleo para elementos pesados. Para un escaneo en línea se utilizó un analizador de recubrimiento MAXXI 6 de Hitachi High-Tech Analytical Science. El ángulo de incidencia del haz SR fue 45º y el detector de fluorescencia de energía dispersiva (Röntec) fue colocado en posición normal al haz en el plano horizontal. Para el análisis de la muestras, se realizaron pastillas de los sólidos a analizar [46].

AI.3.11. Espectroscopía Infrarroja de Reflectancia Difusa con Transformada de Fourier de Piridina (DRIFT-Py)

A partir de la espectroscopía infrarroja de reflectancia difusa con transformada de Fourier de piridina se puede diferenciar qué tipos de centros ácidos, Lewis y/o Brönsted, posee el sólido en estudio. La adsorción de la piridina en dichos centros da lugar a la aparición de picos a diferentes números de onda, pudiéndose distinguir ambos tipos de centros.

De manera genérica, en la espectroscopía infrarroja de reflectancia difusa, un haz de infrarrojos incide sobre la muestra, pudiendo interactuar con ella de dos formas: cuando la radiación no penetra la muestra produciéndose la reflexión o múltiples reflexiones en la superficie de la muestra; y cuando la

radiación penetra la muestra, produciéndose la dispersión de la matriz de la muestra, siendo ésta cuando se produce el fenómeno de reflectancia difusa.

En el caso concreto del DRIFT-Py, la piridina es adsorbida por la muestra permitiéndonos distinguir entre centros ácidos Lewis y/o Brönsted, debido a la formación de especies químicas con frecuencias de adsorción diferentes. Si los picos aparecen a 1443 y 1603 cm^{-1} se atribuye a la presencia de piridina adsorbida en centros ácidos Lewis. Cuando la señal aparece a 1486 cm^{-1} es debido a la adsorción en ambos centros Lewis y Brönsted, mientras que cuando aparece a 1534 cm^{-1} corresponde a la presencia de piridina en centros ácidos de Brönsted [47].

Metodología experimental

Los espectros de DRIFT se han llevado a cabo en un instrumento FTIR (Bomem MB-3000) equipado con una "cámara ambiental" (Spectra Tech), colocado en un dispositivo de reflexión difusa (Spectra Tech, Collector). Se empleó una resolución de 8 cm^{-1} con 256 barridos (fueron adiccionados mediante transformadas de Fourier) para obtener un espectro desde 4000 a 400 cm^{-1}. En cada medida, la referencia fue la misma muestra después de ser calentada a 150 ºC. La absorción de la piridina tuvo lugar durante 45 min a 150 ºC, permitiendo la saturación de la superficie del sólido con piridina. La piridina fisisorbida fue posteriormente limpiada con un flujo de N_2 (50 mL/min) y el correspondiente espectro fue registrado.

AI.3.12. Espectroscopía Raman

A partir de la espectroscopía Raman se puede obtener información química y estructural de la muestra a analizar, proporcionando "una huella dactilar" y permitiendo su identificación. Es una técnica que se realiza directamente sobre el material, por lo que las muestras no necesitan ninguna

preparación y no sufrirán ninguna alteración tras el análisis. Además, se pueden analizar materiales en cualquier estado: sólido, líquido o gaseoso [48].

La base del análisis obtenido por esta técnica es el estudio de la luz dispersada por un material al ser incidido sobre él un haz de luz monocromático. Dependiendo de la dispersión que se produzca de la interacción fotón-molécula se puede distinguir entre (Figura AI.13):

- Dispersión Rayleigh: tiene lugar cuando se obtiene un fotón dispersado con la misma frecuencia que el fotón incidente, produciéndose un choque elástico. Por lo que la molécula volverá al mismo nivel de energía que tenía antes de producirse la interacción.
- Dispersión Raman: tiene lugar cuando se obtiene un fotón dispersado con una frecuencia diferente de la del fotón incidente, produciéndose un choque inelástico y una transferencia de energía entre la molécula y el fotón. Dentro de esta interacción se dan dos dispersiones:
    - Dispersión Raman Stokes: tiene lugar cuando el fotón dispersado presenta una frecuencia menor a la del fotón incidente. Se producirá una transferencia de energía del fotón a la molécula, debido a que después de saltar al estado de energía no permitido, volverá a uno permitido pero mayor al que tenía al comienzo.
    - Dispersión Raman anti-Stockes: tiene lugar cuando el fotón dispersado presenta una frecuencia mayor a la del fotón incidente. Esto ocurre porque la molécula se encontraba en un estado vibracional de mayor energía (y no en su estado vibracional fundamental) cuando se produce la interacción de ella con el haz de luz monocromático. Después de la interacción si volverá a su estado vibracional fundamental [48].

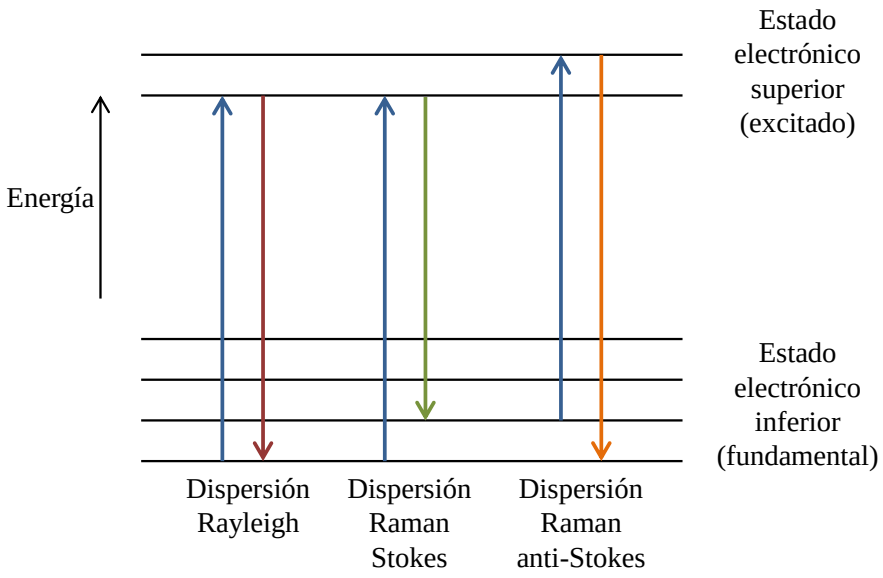

Figura AI. 13. Diagrama energético donde se muestran las diferentes dispersiones producidos entre la interacción fotón-molécula.

Metodología experimental

Los espectros de Raman se han llevado a cabo en un espectrómetro Renishaw (In Via Raman Microscope) equipado con un microscopio Leica con varias lentes, monocromadores, filtros y un detector CCD. Los espectros se midieron en el rango de 150 - 4000 cm^{-1}, utilizando la excitación con luz verde (532 nm) con 32 barridos.

AI.3.13. Reacción modelo del metilbutinol (MBOH)

La reacción modelo del metilbutinol nos permite conocer qué propiedades, ácidas, básicas y/o anfotéricas, poseen los sólidos en estudio, en función de los productos obtenidos.

Dependiendo del tipo de reactividad que se produzca durante la reacción se obtendrán diferentes productos, como se muestra en la Figura AI.14 y se detallan a continuación.

- Reactividad ácida: tiene lugar cuando al reaccionar el metilbutinol con el sólido en estudio se obtienen el 3-metil-3-buten-1-ino y el 3-metil-2-buten-1-al.
- Reactividad anfotérica: tiene lugar cuando al reaccionar el metilbutinol con el sólido en estudio se obtienen el 3-hidroxi-3-metil-2-butanona y el 3-metil-3-buten-2-ona.
- Reactividad básica: tiene lugar cuando al reaccionar el metilbutinol con el sólido en estudio se obtienen la acetona y el etino [49].

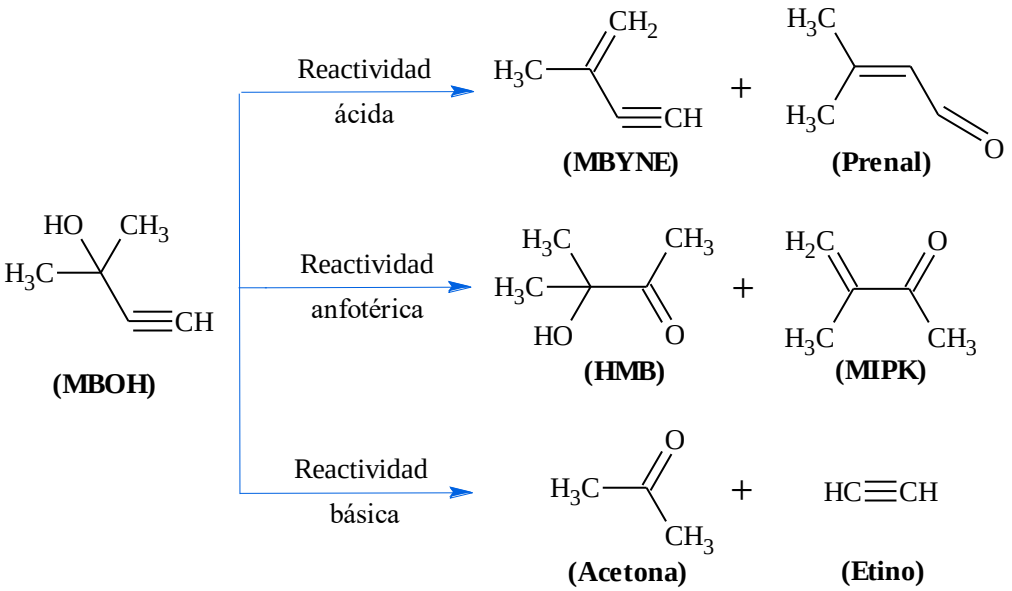

Figura AI.14. Reacción modelo de transformación del metilbutinol propuesta por Lauren-Pernot et al. MBOH, 2-metil-3-butin-2-ol; MBYNE, 3-metil-3-buten-1-ino; Prenal, 3-metil-2-buten-1-al; HMB, 3-hidroxi-3-metil-2-butanona; MIPK, 3-metil-3-buten-2-ona. Adaptado de Lauren-Pernot et al. [50].

Metodología experimental

La transformación del metilbutinol ha sido llevada a cabo en un reactor tubular de cuarzo (1/8 pulgadas O.D.), situado en el puerto de inyección de un cromatógrafo de gases (Agilent 7890) con detector de ionización de llama (CG-FID). En el reactor se introdujeron dos capas de lana de cuarzo y 20 mg de

catalizador entre ellas. Antes de la reacción, el sólido fue sometido a un pretratamiento en el reactor a 200 ºC, durante 2h y bajo un flujo de N_2 (75 mL/min). La reacción tuvo lugar introduciendo pulsos de 0,5µL de metilbutinol con un flujo de N_2 en el cromatógrafo. La cuantificación de los productos de la reacción, así como del metilbutinol, se realizó a partir de sus respectivas rectas de calibrado.

AI.4. Actividad catalítica

AI.4.1. Dispositivos experimentales empleados

Los dispositivos experimentales empleados han sido: un multi-reactor, un reactor a presión y un microondas.

AI.4.1.1. Multi-reactor

Unos de los dispositivos experimentales utilizados fue un multi-reactor Carousel Reaction Station™ (Radley Discovery Technologies) como el que aparece en la Figura AI.15. Se trata de un sistema equipado con doce tubos de vidrio con un volumen de reacción de 1 a 20 mL, provisto de control de temperatura (condición mínima y máxima, -78 y 220 ºC), pudiendo realizar reacciones en una atmósfera inerte y agitación.

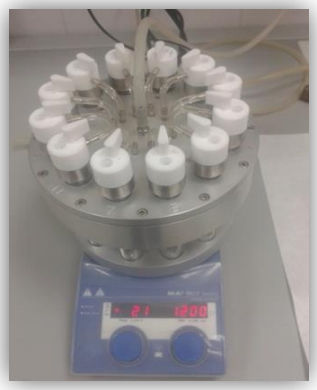

Figura AI.15. Imagen del multi-reactor empleado.

AI.4.1.2. Reactor a presión

El modelo del reactor de alta presión es Berghof HR-100, de acero inoxidable (Berghof Products and Instruments GmbH) como el que aparece en la Figura AI.16 equipado con un recipiente de PTFE de 75 mL de capacidad y un agitador magnético con posibilidad de operar a una presión y temperatura determinada (condiciones máximas 200 bar, 300 ºC, respectivamente).

Figura AI.16. Imagen del reactor a presión modelo Berghof.

AI.4.1.3. Calefacción por microondas

La calefacción por microondas tuvo lugar en un equipo como el que aparece en la Figura AI.17. Se trata de un equipo CEM-DISCOVER controlado por ordenador. Permite un volumen de hasta 80 mL presurizado y una agitación magnética de velocidad variable. La temperatura de reacción es controlada mediante infrarrojo de alta precisión y el enfriamiento se realiza con aire comprimido.

Figura AI.17. Imagen del microondas empleado.

AI.4.2. Identificación y cuantificación de los productos

Para la identificación y cuantificación de los productos obtenidos se filtró cada una de las fases obtenidas con filtros de membrana de nylon de 0.22 µm.

La fase acuosa de la reacción de deshidratación fue analizada por cromatografía líquida de alta presión (Waters 2695 HPLC) con detección de índice de refracción (detector IR) empleando una columna Fortis amino 5 um (250 x 4.6 mm).

Las fases orgánicas de las reacciones de deshidratación y de condensación aldólica fueron analizadas mediante cromatografía de gases

(Agilent 7890) con detector de ionización de llama (GC-FID) equipado con una columna capilar Supelco Nukol^{TM}. Mientras que para el análisis de la fase orgánica obtenida de la reducción MPV se empleó el mismo cromatógrafo de gases pero una columna HP-5.

La cuantificación de los productos se realizó a partir de sus respectivas rectas de calibrado.

AII.5. Referencias

1. You, X.F.; Chen, F.; Zhang, J.L.; Anpo, M. A novel deposition precipitation method for preparation of Ag-loaded titanium dioxide. *Catalysis Letters* **2005**, *102*, 247-250, doi:10.1007/s10562-005-5863-5.
2. Berndt, H.; Lietz, G.; Volter, J. Zinc promoted H-ZSM-5 catalysts for conversion of propane to aromatics .2. Nature of the active sites and their activation. *Applied Catalysis A: General* **1996**, *146*, 365-379, doi:10.1016/s0926-860x(96)00124-x.
3. Aramendia, M.A.; Colmenares, J.C.; Lopez-Fernandez, S.; Marinas, A.; Marinas, J.M.; Urbano, F.J. Screening of different zeolite-based catalysts for gas-phase selective photooxidation of propan-2-ol. *Catalysis Today* **2007**, *129*, 102-109, doi:10.1016/j.cattod.2007.09.005.
4. Malik, M.A.; Wani, M.Y.; Hashim, M.A. Microemulsion method: A novel route to synthesize organic and inorganic nanomaterials. *Arabian Journal of Chemistry* **2012**, *5*, 397-417, doi:10.1016/j.arabjc.2010.09.027.
5. Colmenares, J.C.; Aramendia, M.A.; Marinas, A.; Marinas, J.M.; Urbano, F.J. Synthesis, characterization and photocatalytic activity of different

metal-doped titania systems. *Applied Catalysis A: General* **2006**, *306*, 120-127, doi:10.1016/j.apcata.2006.03.046.

6. Campanati, M.; Fornasari, G.; Vaccari, A. Fundamentals in the preparation of heterogeneous catalysts. *Catalysis Today* **2003**, *77*, 299-314, doi:10.1016/s0920-5861(02)00375-9.
7. Antonelli, D.M.; Ying, J.Y. Synthesis of hexagonally packed mesoporous TiO_2 by a modified sol-gel method. *Angewandte Chemie-International Edition in English* **1995**, *34*, 2014-2017, doi:10.1002/anie.199520141.
8. Schwarz, J.A.; Contescu, C.; Contescu, A. Methods for preparation of catalytic materials. *Chemical Reviews* **1995**, *95*, 477-510, doi:10.1021/cr00035a002.
9. Hector, A.L. Synthesis and processing of silicon nitride and related materials using preceramic polymer and non-oxide sol-gel approaches. *Coordination Chemistry Reviews* **2016**, *323*, 120-137, doi:10.1016/j.ccr.2016.05.009.
10. Cushing, B.L.; Kolesnichenko, V.L.; O'Connor, C.J. Recent advances in the liquid-phase syntheses of inorganic nanoparticles. *Chemical Reviews* **2004**, *104*, 3893-3946, doi:10.1021/cr030027b.
11. Debecker, D.P.; Mutin, P.H. Non-hydrolytic sol-gel routes to heterogeneous catalysts. *Chemical Society Reviews* **2012**, *41*, 3624-3650, doi:10.1039/c2cs15330k.
12. Eriksson, S.; Nylén, U.; Rojas, S.; Boutonnet, M. Preparation of catalysts from microemulsions and their applications in heterogeneous catalysis. *Applied Catalysis A: General* **2004**, *265*, 207-219, doi:10.1016/j.apcata.2004.01.014.
13. Ganguly, A.; Trinh, P.; Ramanujachary, K.V.; Ahmad, T.; Mugweru, A.; Ganguli, A.K. Reverse micellar based synthesis of ultrafine MgO nanoparticles (8–10 nm): Characterization and catalytic properties. *Journal*

of Colloid and Interface Science **2011**, *353*, 137-142, doi:10.1016/j.jcis.2010.09.041.

14. Lisiecki, I.; Pileni, M.P. Synthesis of copper metallic clusters using reverse micelles as microreactors. *Journal of the American Chemical Society* **1993**, *115*, 3887-3896, doi:10.1021/ja00063a006.
15. Svensson, E.E.; Nassos, S.; Boutonnet, M.; Järås, S.G. Microemulsion synthesis of MgO-supported $LaMnO_3$ for catalytic combustion of methane. *Catalysis Today* **2006**, *117*, 484-490, doi:10.1016/j.cattod.2006.06.014.
16. Co-precipitation. Disponible en: http://www.rsc.org/publishing/journals/prospect/ontology.asp?id=CMO:0001690&MSID=c2jm35232j (accesible 06/05/2019).
17. Kolthoff, I.M. "Theory of coprecipitation" the formation and properties of crystalline precipitates. *Journal of Physical Chemistry* **1932**, *36*, 860-881, doi:10.1021/j150333a008.
18. Faraldos, M.; Goberna, C. *Técnicas de Análisis y Caracterización de Materiales*; CSIC Madrid, 2002.
19. Microscopía Electrónica de Barrido-Técnicas-UMA. Disponible en: http://www.scai.uma.es/areas/micr/sem/sem.html (accesible a 06/05/2019).
20. Hernández, F. Historia de la Microscopía Electrónica. *Rev Cost Cienc Méd* **1987**, *8 (4)*.
21. Microscopía Electrónica de Barrido - UNED. Disponible en: https://www2.uned.es/cristamine/mineral/metodos/sem.htm (accesible a 06/05/2019).
22. Microscopía Electrónica de Transmisión. Disponible en: https://sstti.ua.es/es/instrumentacion-cientifica/unidad-de-microscopia/microscopia-electronica-de-transmision.html (accessible a 06/05/2019).

23. Microscopía Electrónica de Transmisión - UNED. Disponible en: https://www2.uned.es/cristamine/mineral/metodos/tem.htm (accesible a 06/05/2019).
24. Microscopía electrónica. Disponible en: https://bioprofe4.blogspot.com/2011/10/microscopia-electronica.html (accesible a 06/05/2019).
25. Coats, A.W.; Redfern, J.P. Thermogravimetric analysis. *Analyst* **1963**, *88*, 906-&, doi:10.1039/an9638800906.
26. Foo, K.Y.; Hameed, B.H. Insights into the modeling of adsorption isotherm systems. *Chemical Engineering Journal* **2010**, *156*, 2-10, doi:10.1016/j.cej.2009.09.013.
27. Adsorción en Sólidos Mesoporosos. Disponible en: http://linux0.unsl.edu.ar/~rlopez/cap3new.pdf (accesible a 06/05/2019).
28. Fenómenos de superficie. Adsorción. Disponible en: http://depa.fquim.unam.mx/amyd/archivero/Unidad3Adsorcion_19664.pdf (accesible a 06/05/2019).
29. Superficies sólidas: adsorción y catálisis heterogénea. Disponible en: https://www.uv.es/tunon/pdf_doc/Superficies_Solidas_A.pdf (accesible a 06/05/2019).
30. Leofanti, G.; Padovan, M.; Tozzola, G.; Venturelli, B. Surface area and pore texture of catalysts. *Catalysis Today* **1998**, *41*, 207-219, doi:10.1016/s0920-5861(98)00050-9.
31. Brunauer, S.; Emmett, P.H.; Teller, E. Adsorption of gases in multimolecular layers. *Journal of the American Chemical Society* **1938**, *60*, 309-319, doi:10.1021/ja01269a023.
32. Hüfner, S. *Photoelectron spectroscopy: principles and applications*; Media, S.S.B., Ed. 2013.
33. Vermúdez-Polonio, J. *Métodos de drifracción de rayos X: principios y aplicaciones*; Pirámide, Ed. 1981.

34. Vulfrano González-Fernández, J. Espectroscopías ópticas y su aplicación para el estudio de nanoestructuras semiconductoras. Universidad autónoma de San Luis Potosí, 2015.
35. Feliu Jr, S. Caracterización química de nanosuperficies. Introducción a la espectroscopía fotoelectrónica de rayos X (XPS). *Técnicas de laboratorio* **2010**, *356*, 838-843.
36. Dabrowski, A. *Applications in Industry*; Elsevier, Ed. 1998.
37. Parejas, A.; Montes, V.; Hidalgo-Carrillo, J.; Sanchez-Lopez, E.; Marinas, A.; Urbano, F.J. Microemulsion and sol-gel synthesized ZrO_2-MgO catalysts for the liquid-phase dehydration of xylose to furfural. *Molecules* **2017**, *22*, doi:10.3390/molecules22122257.
38. Rodríguez, M. *La difracción de los rayos X.*; Editorial Alhambra, 1982.
39. Difracción de rayos X. Disponible en: https://www.upct.es/~minaeees/difraccion_rayosx.pdf (accesible a 06/05/2019).
40. Difracción de Bragg. Disponible en: http://servicios.fis.puc.cl/rayosx/teoria.html (accesible a 06/05/2019).
41. Difracción de Rayos X. Disponible en: https://www.upct.es/~minaeees/difraccion_rayosx.pdf (accesible a 06/05/2019).
42. Thomas, R. *Practical guide to ICP-MS: a tutorial for beginners*; press, C., Ed. 2013.
43. Hill, S.J. *Inductively coupled plasma spectrometry and its applications*; Press, S.S.A., Ed. 1999; pág. 10.
44. Espectroscopía de Fluorescencia de Rayos X. Disponible en: https://sstti.ua.es/es/instrumentacion-cientifica/unidad-de-rayos-x/espectroscopia-de-fluorescencia-de-rayos-x.html (accesible a 06/05/2019).

45. Fluorescencia de Rayos X. Disponible en: https://wpo-altertechnology.com/es/xrf-x-ray-fluorescence-spectroscopy-hi-rel-parts/ (accesible a 06/05/2019).
46. Cosano, D.; Esquivel, D.; Mateos, L.D.; Quesada, F.; Jimenez-Sanchidrian, C.; Rafael Ruiz, J. Spectroscopic analysis of corrosion products in a bronze cauldron from the Late Iberian Iron Age. *Spectrochimica Acta Part A: Molecular and Biomolecular Spectroscopy* **2018**, *205*, 489-496, doi:10.1016/j.saa.2018.07.072.
47. Hidalgo-Carrillo, J.; Parejas, A.; Jorge Cuesta-Rioboo, M.; Marinas, A.; Jose Urbano, F. MPV Reduction of Furfural to Furfuryl Alcohol on Mg, Zr, Ti, Zr-Ti, and Mg-Ti Solids: Influence of Acid-Base Properties. *Catalysts* **2018**, *8*, doi:10.3390/catal8110539.
48. Fundamentos de espectroscopía Raman. Disponible en: https://www.tdx.cat/bitstream/handle/10803/6887/03Rpp03de11.pdf (accesible a 06/05/2019).
49. Aramendia, M.A.; Borau, V.; Garcia, I.M.; Jimenez, C.; Marinas, A.; Marinas, J.M.; Porras, A.; Urbano, F.J. Comparison of different organic test reactions over acid-base catalysts. *Applied Catalysis A: General* **1999**, *184*, 115-125, doi:10.1016/s0926-860x(99)00096-4.
50. Lauron-Pernot, H.; Luck, F.; Popa, J.M. Methylbutynol - a new and simple diagnostic-tool for acidic and basic sites of solids. *Applied Catalysis* **1991**, *78*, 213-225, doi:10.1016/0166-9834(91)80107-8.

Anexo II.

Publicaciones

molecules

MDPI

Article

Microemulsion and Sol-Gel Synthesized ZrO_2-MgO Catalysts for the Liquid-Phase Dehydration of Xylose to Furfural

Almudena Parejas, Vicente Montes, Jesús Hidalgo-Carrillo, Elena Sánchez-López, Alberto Marinas and Francisco J. Urbano *

Department of Organic Chemistry, Institute for Research in Fine Chemistry and Nanochemistry, IUIQFN, Universidad de Córdoba, Campus de Rabanales, Marie Curie Building, E-14014 Córdoba, Spain; q12pabaa@uco.es (A.P.); vicente.montesjimene@ucalgary.ca (V.M.); q12hicaj@uco.es (J.H.-C.); g02saloe@uco.es (E.S.-L.)

* Correspondence: alberto.marinas@uco.es (A.M.); fj.urbano@uco.es (F.J.U.); Tel.: +34-957-218-638

Received: 31 October 2017; Accepted: 12 December 2017; Published: 18 December 2017

Abstract: Two series of catalysts were prepared by sol-gel and microemulsion synthetic procedure (SG and ME, respectively). Each series includes both pure Mg and Zr solids as well as Mg-Zr mixed solids with 25%, 50% and 75% nominal Zr content. The whole set of catalysts was characterized from thermal, structural and surface chemical points of view and subsequently applied to the liquid-phase xylose dehydration to furfural. Reactions were carried out in either a high-pressure autoclave or in an atmospheric pressure multi-reactor under a biphasic (organic/water) reaction mixture. Butan-2-ol and toluene were essayed as organic solvents. Catalysts prepared by microemulsion retained part of the surfactant used in the synthetic procedure, mainly associated with the Zr part of the solid. The MgZr-SG solid presented the highest surface acidity while the Mg3Zr-SG one exhibited the highest surface basicity among mixed systems. Xylose dehydration in the high-pressure system and with toluene/water solvent mixture led to the highest furfural yield. Moreover, the yield of furfural increases with the Zr content of the catalyst. Therefore, the catalysts constituted of pure ZrO_2 (especially Zr-SG) are the most suitable to carry out the process under study although MgZr mixed solids could be also suitable for overall processes with additional reaction steps.

Keywords: xylose dehydration; furfural; MgO-ZrO_2 mixed catalysts; microemulsion synthesis; sol-gel synthesis; solvent effect

1. Introduction

Nowadays, one of the priorities of scientists is the search for alternatives to non-renewable energies. A renewable solution for this challenge is biomass, which can provide both energy [1] and useful chemical compounds for industry [2].

The estimated biomass production is about 10^{11} ton per year whose 60% is terrestrial and 40% aquatic. However, only 3% of the produced biomass is utilized for human-derived applications [3]. Therefore, the transformation of biomass into platform molecules that can be further converted into high-added value chemicals is a hot topic nowadays [4,5].

Biomass is composed by carbohydrates (75%), lignin (20%) and a mixture of triglycerides, proteins and terpenes (5%) [5]. Lignocellulose is the main constituent of plant cell walls whose hydrolysis yields a mixture of C5 and C6 sugars as well as aromatic compounds (lignin). Therefore, valorization of pentoses and hexoses, such as xylose or glucose, is very interesting from the chemical point of view [4].

Furfural is one of the top platform molecules that can be obtained from biomass [6,7] and that is able to be further transformed into a wide range of chemicals by chemo and/or enzymatic

transformations. It is a natural precursor to a range of furan-based chemicals and solvents such as methyltetrahydrofuran, tetrahydrofuran, tetrahydrofurfuryl alcohol and furoic acid, among others. Compounds derived from furfural are used in the pharmaceutical industry, and as plastics, agricultural fungicides or nematocides, lubricants, resins, bleaching agents, food and beverage additives, wood modifiers or book preservatives, among other uses. Moreover, within the last decade the conversion of furfural into diesel by means of a combination of dehydration, aldol condensation and hydrogenation reactions has been described [8–12].

Due to the continuous demand for furfural, the search for alternative synthetic routes or the improvement of the existing ones is still an active research area. The classic industrial furfural production process is based on the treatment of pentose-containing lignocellulosic biomass with mineral acids (H_2SO_4, HCl) [13]. However, mineral acids cause corrosion of the reactors and generate toxic effluents; therefore, the design of active, selective and stable heterogeneous solid acid catalysts is a key point to reduce costs of reactors as well as the environmental impact of the process. An additional effort should be made to improve the process sustainability by designing water resistant and recyclable solid acid catalysts. Furthermore, if a chemical process is to be coupled following the synthesis of furfural in the so-called cascade processes, it may be necessary to synthesize catalysts which, in addition to acidic properties, have a second functionality which may be basic sites (e.g., for condensation reactions) or metal centers (for redox processes) [14].

During the process, due to the high reactivity of furfural molecule, several side reactions such as condensation or acetalyzation can take place leading to hemiacetals and oligomers (humines) [15–17]. Additionally, xylose fragmentation reactions can occur producing acetol, lactic acid, glyceraldehyde, etc. [18]. Water is typically the solvent of choice for sugar transformation reactions due to solubility, economic and environmental aspects. However, water favors the formation of humines thus lowering the selectivity to the desired product. An adequate solvent mixture (biphasic systems) can help to reduce these by-products since formed furfural could be rapidly extracted to a second liquid phase, thus avoiding further transformation [19–21]. Toluene, *n*-butanol or ethyl butyrate [22,23] can be found among the secondary solvents (extracting agents) reported in the literature. Alternative described solutions such as the use of ionic liquids [24] or supercritical carbon dioxide [25] are expensive or technologically demanding.

This piece of research deals with the synthesis and characterization of zirconium/magnesium mixed oxides in order to obtain bifunctional acid/base solids. Two series of catalysts were synthesized using the sol-gel or microemulsion processes (SG and ME series, respectively). The solids were subsequently tested for xylose dehydration to furfural. The final goal was to obtain some robust and water-resistant acid-base catalysts that can be active not only for xylose dehydration to furfural but also able to carry out one-pot or cascade reactions for further transformation of furfural [26].

2. Results

2.1. Catalysts Characterization

Thermogravimetric analysis (TGA) was carried out for the dried gels before thermal treatment at 200 °C, the obtained results being presented in Figure 1. The TGA profiles obtained for both series of solids were quite similar. As for pure systems, the weight loss for both Mg-SG and Mg-ME systems was around 29% with a single weight loss starting at temperatures around 325 °C. This weight loss is consistent with the transformation from $Mg(OH)_2$ to MgO (theoretical weight loss around 31%). For pure Zr-SG and Zr-ME solids a more complex profile was obtained with several weight loss spreading over 100–500 °C temperature range. Overall, the weight loss was 13.9% and 20.8% for Zr-SG and Zr-ME, respectively. Taking into account that the theoretical weight loss associated to the transformation of $ZrO(OH)_2$ into ZrO_2 is around 13%, the weight loss of 20.8% obtained for the Zr-ME gel has to be also ascribed to the burning of the surfactant remaining on the surface of the solid. On the other hand, the fact that the weight loss for Mg-ME and Mg-SG solids is very similar and close

to the theoretical value suggests that no surfactant is remaining on the surface of pure Mg-ME solid. Finally, mixed MgZr solids in both series exhibited an intermediate behavior between both pure Zr and Mg solids.

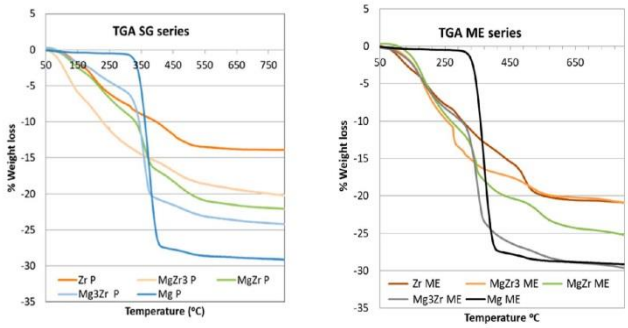

(**a**) (**b**)

Figure 1. Thermogravimetric analysis (TGA) of the dried gels corresponding to both series of solids synthesized: (**a**) Sol-Gel and (**b**) Microemulsion.

Differential thermal analysis (DSC) of the solids is presented in Figure 2 where it can be observed that for pure Mg-based solids there is a single endothermic signal at 375 °C associated to the transition from $Mg(OH)_2$ to MgO [27]. No differences were observed between Mg-SG and Mg-ME solids in DSC profiles, in agreement with the TGA data. On the contrary, Zr-SG and Zr-ME exhibited very different DSC profiles. The first one only presents an exothermic peak (glow exotherm) centered at 450 °C associated to the crystallization of the low-temperature tetragonal metastable phase of ZrO_2 [28]. For mixed solids in the SG series, the glow exotherm is also observed but is weaker and shifted to higher temperatures (up to 650 °C for Mg3Zr-SG), indicating that crystallization is somehow inhibited or retarded in the presence of Mg species [29].

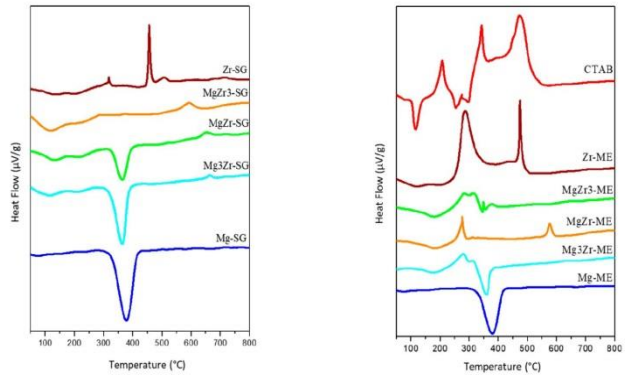

(**a**) (**b**)

Figure 2. Differential thermal analysis (DSC) profiles obtained for the dried gels corresponding to both series of solids synthesized: (**a**) Sol-Gel and (**b**) Microemulsion.

As far as the ME series is concerned, Zr-ME solid presents a DSC profile with two exothermic peaks; the above commented glow exotherm at 475 °C and another one at lower temperature (around 300 °C) associated to the combustion of the organic part of the surfactant remaining on the catalyst surface. This peak is smaller as the magnesium content increases, until complete disappearance for Mg-ME. Again, it seems that the amount of surfactant retained on the surface of the solids is greater for the systems containing the highest Zr content. The DSC profile for pure surfactant, CTAB, is included in Figure 2 for comparison. It is assumed that the CTAB combustion takes place at lower temperatures on the surface of the solids.

As far as the chemical composition of the solids is concerned, it was obtained from SEM-EDX and XPS measurements, the results being presented in Table 1. EDX and XPS atomic concentration values are somehow different to each other and, in this sense, it has to be taken into account that XPS penetration is lower than the EDX one. Therefore, XPS data have to be assumed as a surface composition meanwhile EDX values are associated to bulk chemical composition of the mixed solids. Thus, EDX data indicate that the magnesium content is somehow higher than the nominal value except for the MgZr3-ME solid which is the mixed solid with the lowest magnesium content. It seems that either the precipitation at pH 10 is more efficient for $Mg(OH)_2$ or, more likely, precipitated $ZrO(OH)_2$ species re-dissolve at the precipitating pH.

Table 1. Nominal, EDX and XPS chemical composition (%mol) and textural properties of the catalytic systems synthesized in this work.

	Chemical Composition (Nominal)		Chemical Composition (EDX)		Chemical Composition (XPS)		Surface Area
Catalyst	**Mg**	**Zr**	**Mg**	**Zr**	**Mg**	**Zr**	**BET (m^2/g)**
Mg-SG	100	0.0	100	0.0	100	0.0	41
Mg3Zr-SG	75	25	94.2	5.8	69.4	30.6	119
MgZr-SG	50	50	67.7	32.3	60.3	39.7	173
MgZr3-SG	25	75	32.6	67.4	10.4	89.6	169
Zr-SG	0.0	100	0.0	100	0.0	100	239
Mg-ME	100	0.0	100	0.0	100	0.0	31
Mg3Zr-ME	75	25	90.5	9.5	74.2	25.8	196
MgZr-ME	50	50	70.6	29.4	27.4	72.6	197
MgZr3-ME	25	75	22.2	77.8	3.5	96.5	192
Zr-ME	0.0	100	0.0	100	0.0	100	222

On the other hand, XPS data revealed an opposite behavior, i.e., the Zr content is higher than the nominal value for the mixed solids, except for the MgZr3-ME. This finding implies that ZrO_2 particles are localized on the outer part of the aggregates while the MgO ones are located within the inner part of the agglomerated particles.

SEM-EDX measurements have revealed that in the solids prepared through the microemulsion technique, in spite they were washed 5 times with chloroform/ethanol, a small amount of bromine coming from surfactant molecules was detected on the solids surface (Supplementary Figure S1). In addition, as the zirconium content increases in ME series, the amount of detected Br is higher (from 0.9% for Mg-ME to 4.3% for Zr-ME), thus pointing out the higher affinity of the surfactant for the ZrO_2 particles.

Nitrogen adsorption–desorption isotherms for the solids calcined at 200 °C were obtained (file. Red arrow marks Br signal, Supplementary Figure S2) and the BET surface area presented in Table 1. The largest surface area was obtained for pure Zr-SG solid (239 $m^2 \cdot g^{-1}$) while Zr-ME exhibited a somehow lower surface area (222 $m^2 \cdot g^{-1}$), revealing that the surfactant remaining on the catalyst negatively affects its surface area. On the other hand, pure Mg-SG and Mg-ME solids present the lowest surface area (41 and 31 $m^2 \cdot g^{-1}$ respectively) indicating that the porous structure is still absent on these solids after calcination at 200 °C. As far as the mixed solids are concerned, the higher the Zr

content the higher the surface area. It is, however, relevant to indicate that the Mg3Zr-ME solid with a scarce 9.5% Zr (EDX, Table 1) presents a BET surface area as high as 196 $m^2 \cdot g^{-1}$.

Transmission electron microscopy (TEM) images obtained for the solids are presented in Figures 3–5. Irrespective of the synthetic procedure, pure Zr solids are constituted by agglomerated small particles (2–5 nm) (Figure 3) while pure Mg-SG and Mg-ME solids are based on larger hexagonal particles of around 200 nm in diameter (Figure 4). Moreover, mixed MgZr-SG and MgZr-ME solids are formed by large MgO particles surrounded by small ZrO_2 nanoparticles (Figure 5), in agreement to the higher Zr content observed in the surface XPS measurements (Table 1).

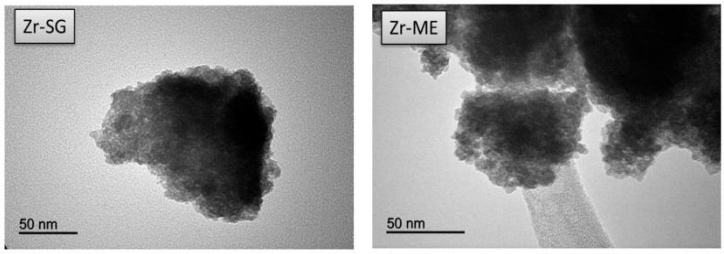

(**a**) (**b**)

Figure 3. TEM images corresponding to pure (**a**) Zr-SG and (**b**) Zr-ME solids.

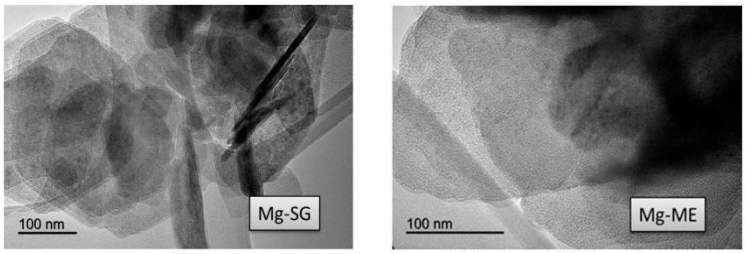

(**a**) (**b**)

Figure 4. TEM images corresponding to pure (**a**) Mg-SG and (**b**) Mg-ME solids.

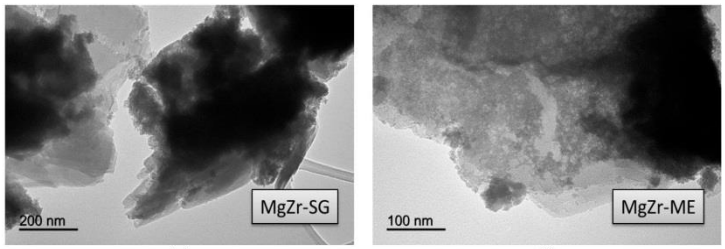

(**a**) (**b**)

Figure 5. TEM images corresponding to **(a)** MgZr-SG and **(b)** MgZr-ME solids.

2.2. Catalysts Surface Acid-Base Properties

Catalysts surface acidity was determined from temperature programmed desorption of pre-adsorbed pyridine (TPD-PY), the results being presented in Table 2 and Supplementary Figure S3. Values obtained for pyridine desorbed per gram of catalyst indicate that, as expected, pure Zr solids are much more acidic than pure Mg ones. Thus, Zr-SG and Zr-ME desorbed 748 and 871 μmol PY/g while Mg-SG and Mg-ME only desorbed 176 and 115 μmol/g, respectively. On the other hand, Mg-Zr mixed solids present a surface acidity in the 444–991 μmol/g range, with some interesting features that will be presented below. First of all, those mixed solids obtained from microemulsion present similar acidity, irrespective of its chemical composition—856, 885 and 788 μmol/g for Mg3Zr-ME, MgZr-ME and MgZr3-ME, respectively, while, on the contrary, sol-gel Mg-Zr mixed solids exhibit large differences in acidity, depending on its chemical composition: 444, 991 and 766 μmol/g for Mg3Zr-ME, MgZr-ME and MgZr3-ME, respectively. As a rule, surface acidity for ME solids is higher than that obtained for SG series. Finally, it is relevant to note that, in both series, the MgZr solids (with the nominal ratio Mg/Zr = 1) are the most acidic among the whole set of synthesized solids with 991 and 885 μmol/g for MgZr-SG and MgZr-ME, respectively. Moreover, the density of surface acid sites is also the highest for MgZr-SG and Mg-Zr-ME solids with 573 and 449 μmol PY/m^2, respectively.

Table 2. Catalysts Surface acid-base properties obtained from temperature programmed desorption of pyridine (TPD-PY) and carbon dioxide (TPD-CO_2) experiments.

Catalyst	Catalyst Acidity (TPD-PY)		Catalysts Basicity (TPD-CO_2)	
	μmol Py/g	μmol Py/m^2	μmol CO_2/g	μmol CO_2/m^2
Mg-SG	176	4.36	457	11.29
Mg3Zr-SG	444	3.73	918	7.71
MgZr-SG	991	5.73	526	3.04
MgZr3-SG	766	4.53	517	3.06
Zr-SG	748	3.13	441	1.84
Mg-ME	115	3.69	354	11.42
Mg3Zr-ME	856	4.37	448	2.28
MgZr-ME	885	4.49	292	1.48
MgZr3-ME	788	4.11	368	1.91
Zr-ME	871	3.92	199	0.90

As far as the surface basicity is concerned, it was determined by means of carbon dioxide temperature programmed desorption, the results being presented in Table 2 and Supplementary Figures S4 and S5. Regarding the TPD profile, all catalysts except Mg-ME exhibited a similar TPD-CO_2 profile with a desorption peak centered at 100 °C and a second, truncated, peak associated to the carbon dioxide desorbed during the isothermal period at 200 °C. The Mg-ME solid, however, only presented an intense second peak while the first one is absent for this catalyst.

As a general rule for the surface basicity per gram of catalyst, ME catalysts present lower basicity than the SG- ones, probably due do the surfactant residues still adsorbed on the catalyst surface. Moreover, it is interesting to point out the low basicity of both pure Mg-SG and Mg-ME solids as compared to the Mg-Zr mixed ones in both series, but especially in the SG-derived catalysts. It has to be assumed that, when calcined at high temperature, MgO is a strongly basic solid that desorbs CO_2 at temperatures higher than 600 °C. Therefore, since our pure Mg-SG and Mg-ME solids were calcined at 200 °C, they do not present the expected basicity for a pure MgO solid.

If surface basicity per square meter is considered (density of surface basic sites), for both series the obtained results indicate that, as a rule, the higher the amount of magnesium in the solid, the higher the surface basicity (Supplementary Figure S4). In this case, surface basic sites density is higher for Mg-SG and Mg-ME dues to the low surface area of theses solids (41 and 31 $m^2 \cdot g^{-1}$, respectively) indicative of a deficient porous structure as a consequence of the low calcination temperature.

Moreover, it is also relevant to indicate that Mg3Zr-SG presents a relatively high basicity (7.7 μmol CO_2/m^2) when compared with the Mg3Zr-ME solid (2.3 μmol CO_2/m^2). For the rest of the catalysts, SG solids exhibit similar surface base properties than their ME counterparts.

In addition to the temperature-programmed desorption experiments, surface acid-base properties of all solids were determined through the gas-phase propan-2-ol decomposition test reaction. This reaction allows us to determine acid and basic properties of the catalysts by analyzing the products distribution formed upon propan-2-ol transformation. When the reaction takes place over acid sites, dehydration products (propene and/or diisopropyl ether) are produced, while if basic or redox sites are involved, acetone and/or diacetone alcohol (resulting from acetone self-condensation) are obtained [30–32]. Since the catalysts were calcined at 200 °C, initially the reaction was carried out at such temperature observing that there was no propan-2-ol conversion. Therefore, 250 °C was selected as reaction temperature obtaining a propan-2-ol conversion in the 1–7% range. No experiments were carried out at higher temperatures in order to avoid further changes in catalysts structure. Figure 6 shows the result obtained for both series of catalysts.

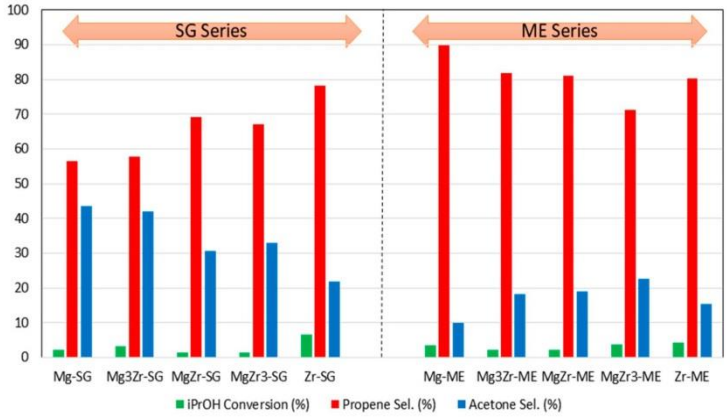

Figure 6. Catalytic activity in the gas-phase propanl-2-ol test reaction for the catalysts prepared in this work. Propan-2-ol conversion and selectivity to propene and acetone obtained at 250 °C.

Despite the low conversion levels obtained, some interesting conclusions could be drawn from these experiments. First of all, for both series of catalysts, pure Zr-SG and Zr-ME catalysts exhibited the highest propan-2-ol conversion with 6.6 and 4.2%, respectively. Pure Mg and mixed Mg-Zr catalysts presented a catalytic conversion in the 1–4% range, irrespective of its composition and synthetic procedure.

The results concerning the selectivity to propene, formed over acid sites, or to acetone, formed over basic ones, seem to be more relevant. Thus, although propene is the major reaction product for all solids with selectivity in the 56–90% range, there are, however, significant differences. In general, in agreement with the TPD-PY results presented above (Table 2 and Supplementary Figure S3), selectivity to propene is higher for the ME- than for the SG series. In this line, the catalysts exhibiting the highest propene selectivity of the whole set of catalysts was Mg-ME (90% selectivity), an unexpected result since this solid was the less acidic (from TPD-PY, Table 2). Probably, the remaining surfactant on the surface of the solids in the ME series accounts for this unexpected result. As for the SG series, propene selectivity results are somehow in good agreement with the TPD-PY data. Thus, pure Zr-SG catalyst presented a 78% selectivity to propene followed by MgZr-SG and MgZr3-SG solids with 69% and

67% selectivity respectively. These were also the most acidic catalysts in the SG series from pyridine temperature-programmed desorption experiments.

On the other hand, as far as the selectivity to basic site-derived products is concerned, SG series gives the best results for the selectivity to acetone (22–44% sel.), being the solids with the highest magnesium content those giving the highest values: Mg-SG and Mg3Zr-SG with 44% and 42% sel., respectively. These results agree with catalyst basicity (TPD-CO_2, Table 2) where Mg-SG and especially Mg3Zr-SG present the highest basicity among the SG series catalysts. In contrast, for the catalysts corresponding to the ME series, the selectivity to acetone is in the range of 10–23%, even for those solids constituted mostly by Mg species (Mg-ME, 10% sel. to acetone). This fact, together with the unexpectedly high propene selectivity shown by the ME series catalysts, seems to indicate that surfactant molecules still remaining on the catalyst surface after calcination at 200 °C affect its surface chemical properties.

2.3. Catalytic Activity

The above described catalysts were tested in the liquid-phase xylose dehydration to furfural in either a high-pressure autoclave or in an atmospheric pressure multi-reactor. The reaction medium in both cases was a biphasic system consisting of an organic/water (1:1 v/v) mixture, butan-1-ol or toluene being used as the organic solvent. The selected reaction temperature was 150 °C. An initial set of reactions was performed to select the most appropriate reaction system to maximize the furfural yield. Figure 7 shows the catalytic activity obtained for both series of catalysts in a butan-1-ol/water biphasic mixture in a multi-reactor and high-pressure autoclave reactors after 24 h of reaction.

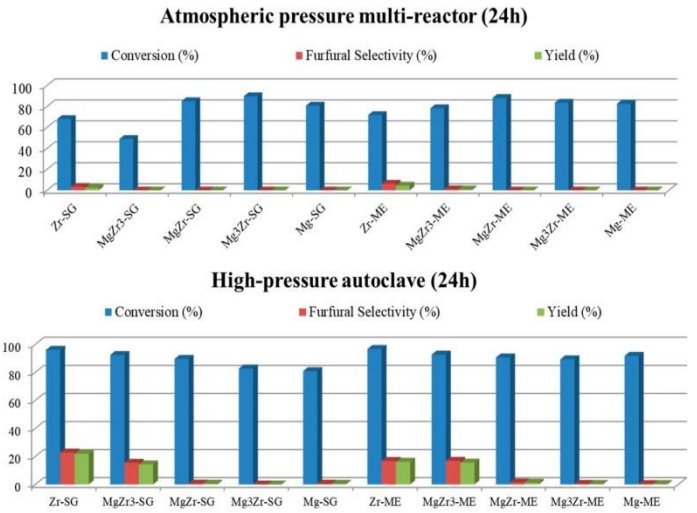

Figure 7. Catalytic activity for both series of catalysts in xylose dehydration in an atmospheric pressure multi-reactor (**upper**) and a high-pressure autoclave (**lower**) in a butan-1-ol/water biphasic media at 150 °C. Xylose conversion and furfural selectivity and yield.

As can be observed in both reaction systems, xylose conversion is higher than 50%, being in most cases close to 90–100%. However, in spite of the above-described high xylose conversion, the selectivity for furfural is quite low (less than 25% at the best). Moreover, as a general trend, xylose conversion as well as furfural selectivity obtained in the high-pressure autoclave are both higher than those obtained

in the multi-reactor system. Focusing on the autoclave reactions, Zr-SG and Zr-ME (pure zirconia solids) presented 23% and 17% selectivity to furfural, followed by MgZr3-SG and MgZr3-ME catalysts with 16% selectivity in both cases. As could be expected, the higher the zirconium content, the higher the dehydrating activity for the catalysts.

Based on the above-presented results, additional experiments were carried out with the high-pressure autoclave in order to increase the selectivity to furfural. Therefore, toluene was essayed as organic solvent in the biphasic reaction media, the obtained results being presented in Figure 8. The general trend observed in toluene/water medium is similar to that already reported by using butan-1-ol/water, that is, xylose conversions higher than 90% but, in this case, selectivity values to furfural practically doubled those obtained for the butan-1-ol/water mixture. Thus, Zr-SG presents a 41% selectivity to furfural, followed by Zr-ME (32% sel.), MgZr3-ME (29% sel.) and MgZr3-SG (17% sel.). The rest of the catalysts presented furfural selectivity lower than 5%.

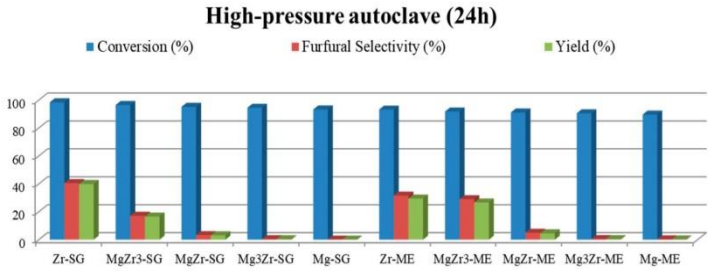

Figure 8. Catalytic activity for both series of catalysts in xylose dehydration in a high-pressure autoclave in a toluene/water biphasic media at 150 °C. Xylose conversion and furfural selectivity and yield.

According to Hu et al. [23] ,with aromatic solvents, the formation of furfural from xylose is quick but so is its degradation. Therefore, additional experiments were carried out at shorter reaction times (3 and 5 h) to analyze the influence of reaction time on both xylose conversion and furfural selectivity (Figure 9). Surprisingly, after 3 h of reaction xylose conversion was already higher than 80% indicating that xylose was converted at the very beginning of the reaction process. Moreover, furfural selectivity obtained at shorter reaction time was lower than that reported at 24 h suggesting that xylose was converted to partially dehydrated intermediates during the initial stages of the process. It is interesting to note here that the transformation of xylose into furfural implies the loss of 3 water molecules and, therefore, longer reaction times facilitate furfural formation.

Since the time dependence of xylose conversion and furfural selectivity are opposite, it seems to be relevant to focus the discussion on the yield to furfural for all reaction times and catalytic systems. Moreover, as discussed above, the higher the zirconium content in the catalysts the better the furfural yield achieved. To illustrate this, Figure 10 presents the yield to furfural as a function of zirconium content for all reaction times essayed. It can be observed that irrespective of the reaction time, the yield to furfural depends mainly on the Zr content on the catalyst, being Zr-SG the solid yielding 40% to furfural as the better value after 24 h of reaction. Zr-ME (29% yield), MgZr3-ME (27%) and MgZr3-SG (17%) catalysts showed a reasonably high yield to furfural. On the contrary, solids with high proportion of Mg yielded low amounts of furfural.

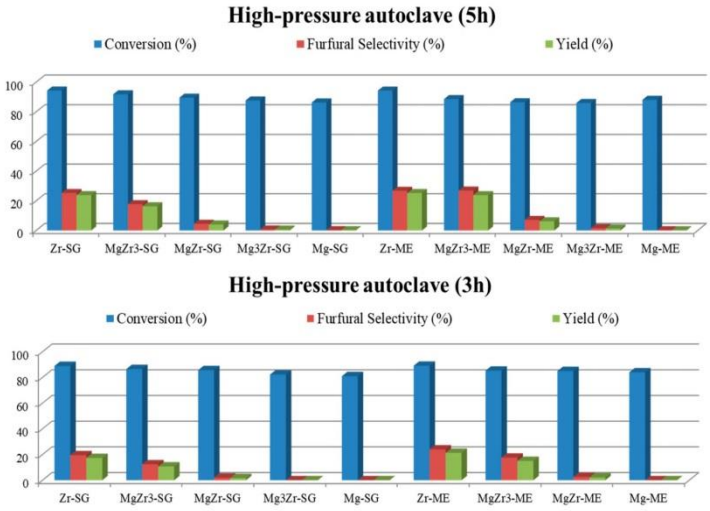

Figure 9. Catalytic activity in xylose dehydration in a high-pressure autoclave in a toluene/water biphasic media at 3 and 5 h of reaction, and 150 °C.

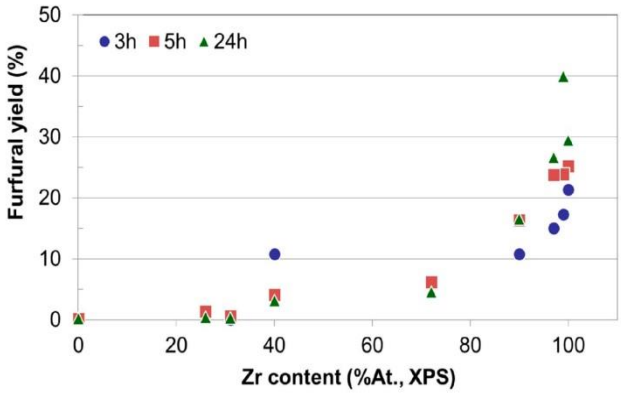

Figure 10. Furfural yield in xylose dehydration as a function of zirconium content (XPS) obtained after 3, 5 and 24 h of reaction at 150 °C in toluene/water reaction medium.

The results described above point out that the Zr sites are responsible for the dehydration of xylose to furfural, whereas the Mg related sites are not active at this point. However, in order to extend the scope of the research to cascade (one-pot) reactions, where both acid and base sites are needed, MgZr3 and MgZr catalysts may be interesting solids. Catalysts based on pure MgO, however, appear to be unsuitable for a reaction sequence including a dehydration step, as might reasonably be expected.

Finally, additional experiments were designed to rule out any homogeneous catalytic process due to the possibly lixiviated zirconium species under hydrothermal reaction conditions. Thus, Zr-SG catalyst was added to toluene/water (without xylose) solution and put under reaction condition

(6 bar initial N_2 pressure, 150 °C) for 5 h. Then, the solid was removed by vacuum filtration and the appropriate amount of xylose was added to the filtrated, and put again under reaction conditions for another 5 h of reaction. The xylose conversion obtained in this experiment was similar to that obtained in blank experiments, without any catalyst (less than 7%).

Additional experiments were carried out to verify the recyclability of our catalysts. Several reactions were performed using the MgZr3-SG catalyst; the reactions were stopped after 3 h and the catalyst was recovered by vacuum filtration, washed with distilled water, dried in an oven at 110 °C overnight and calcined at 200 °C before being re-tested in a new reaction.

Figure 11 shows the results obtained after two reuses of the MgZr3-SG catalyst. With regard to the conversion of xylose (87% conversion in the first reaction), the conversion fell to 81% (a reduction of 7%) while after the second reuse, the conversion obtained was 78%, which represents a reduction of 10% with respect to the initial one. On the contrary, during the reuse tests, the selectivity to furfural increases slightly from the initial 12% to the 17–18% obtained in the reuses and, therefore, the furfural yield increases from 11 to 14%.

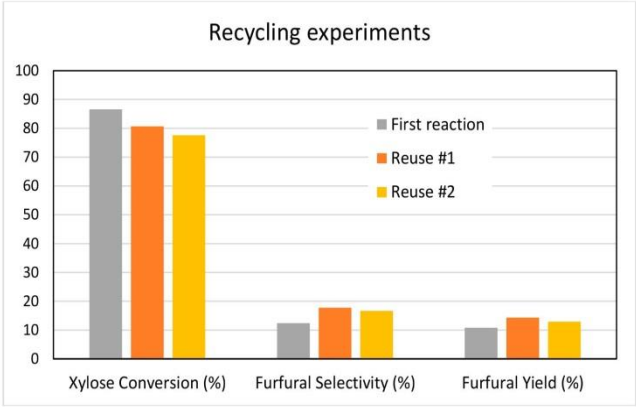

Figure 11. Conversion, selectivity and yield to furfural obtained during the dehydration of xylose on MgZr3-SG catalyst and two subsequent reuses. Reaction conditions: 0.1 g of catalyst, 20 mL of biphasic reaction mixture (water / toluene), 150 °C, 3 h reaction.

In line with the reuse experiments, after 3 h of reaction on MgZr3-SG catalyst, the aqueous phase of the reaction medium was analyzed by ICP-MS to verify the existence of leaching of the component species of the catalyst.

Results indicated the existence of magnesium at a level of 500 ppm while detected amount of zirconium was less than 20 ppb. According to the EDX composition of MgZr3-SG catalyst (Table 1), MgO molar content in the solid was 32.6% and, therefore, 65% of magnesium species were leached to the liquid-phase. However, zirconium species were resistant to leaching under reaction conditions.

In any case, as reported above, the loss in catalytic activity after the first reuse was only of 7%, while furfural selectivity slightly increases. These results support the conclusion that ZrO_2 is the catalytically active component of the mixed catalyst.

3. Discussion

Two series of catalysts were prepared by sol-gel (SG series) and microemulsion (ME series) synthetic procedure. Each series includes both pure Mg and Zr solids as well as Mg-Zr mixed solids with 25%, 50% and 75% nominal Zr content.

Thermal TGA-DSC experiments carried out to the precursor ME-derived gels of the solids indicate that although the precipitated solid was washed five times with a mixture of chloroform/ethanol, part of the surfactant is retained on the surface of the solid. Moreover, results indicate that the surfactant is retained mainly on the Zr component of the solids, as confirmed by the detection of Br from the surfactant by SEM-EDX.

Due to the low calcination temperature (200 °C), the porous structure of pure MgO-based catalysts has not been adequately developed as evidenced by the low surface area of the Mg-SG and Mg-ME catalysts. This lack of porous structure is reflected in the low surface basicity of these solids. In addition, the catalysts synthesized by ME retain surfactant in their structure which makes them less basic. TEM micrographs indicate that pure Zr-based catalysts are formed by agglomerated of small particles (2–5 nm) while pure Mg-SG and Mg-ME solids are based on larger hexagonal particles of around 200 nm in diameter. In addition, mixed Mg-Zr solids are formed by large MgO particles surrounded by small ZrO_2 nanoparticles.

In terms of acidity, it is possible that Bromide, coming from the surfactant, is adsorbed on the solids creating Lewis acid sites responsible for relatively higher acidity in the solids of the ME series than in those of the series SG.

The above results clearly indicate that the ME series catalysts retain surfactant adsorbed on their surface after calcination at 200 °C which determines their surface chemical properties. In any case, the catalyst MgZr-SG has the best surface acidic properties, either per gram or per square meter of catalyst. As far as basicity is concerned, the solid with the most promising basic properties is Mg3Zr-SG, although MgZr-SG also shows interesting basic surface properties.

These results are reflected in the propan-2-ol decomposition test reaction since the Mg3Zr-SG catalyst exhibits comparable selectivities to propene and acetone, as a consequence of equilibrium balance between surface acid and basic properties.

The synthesized catalysts were tested for the xylose dehydration reaction in two different reaction systems (high-pressure autoclave and atmospheric-pressure multi-reactor) and using different reaction mixtures (solvents). For both reaction systems and using butan-1-ol/water as solvent, the obtained xylose conversions after 24 h of reaction were high, although the furfural selectivity obtained was quite low (less than 25% sel.). In any case, the yields to furfural were higher in the high-pressure autoclave, so the multi-reactor at atmospheric pressure was ruled out for further testing. Similar yields were reported in the literature for monosaccharides dehydration on acid-base heterogeneous catalysts such as CoAl-hydrotalcite (22% yield to hydroxymethylfurfural) [33].

As regards the solvent effect, the change from butan-1-ol to toluene as the organic solvent in the biphasic reaction mixture led to better yields to furfural after 24 h of reaction. According to the literature, compared with water, alcohols can promote the formation of furfural and slow down its degradation at prolonged reaction times. Moreover, when using aromatics as organic solvent, the formation of furfural is quick but so is the degradation of furfural due to the aprotic properties of these solvents [23]. This behavior is, however, contrary to that observed in our case since with toluene better yield to furfural is obtained as compared to butan-1-ol (Zr-SG, toluene/water, 24 h, 40% yield vs. Zr-SG, butan-2-ol/water, 24 h, 22% yield). This could be due to the fact that toluene is a good organic solvent that can extract furfural as it is formed, thus avoiding the formation of humins which takes place mainly in the aqueous phase [23].

Additional tests conducted with toluene/water at shorter reaction times (3 and 5 h) still led to high xylose conversions but associated with even lower furfural selectivities. This behavior could be associated with a rapid dehydration of xylose to partially dehydrated intermediates which, along the reaction course, slowly culminate in the formation of furfural.

When we study the influence of the catalyst on the yield to furfural it is observed that the higher the zirconium content, the higher the dehydrating activity for the catalysts. That is, irrespective of the reaction time, the yield to furfural depends on the Zr content on the catalyst, while, on the contrary, solids with high proportion of Mg yielded low amounts of furfural (0% yield for Mg-SG and Mg-ME catalysts).

Finally, the reuse experiments of the catalysts, together with the analysis of leached species, indicated that while ZrO_2 component is practically not leached, a large part of the MgO component of the solids is leached to the reaction medium under the hydrothermal reaction conditions. However, this only implies a slight reduction in the conversion of xylose because, as mentioned, it is the ZrO_2 component that is responsible for the catalytic activity of the MgO-ZrO_2 mixed oxides.

All in all, from the point of view of the xylose dehydration to furfural, the catalysts constituted by pure ZrO_2 (especially Zr-SG) are the most suitable to carry out the process under study.

However, if a second process that occurs with the participation of surface basic sites is to be coupled to it in the so-called one-pot or cascade reactions, the MgZr mixed solids could be suitable for the overall process. Thus, the MgZr-SG and MgZr3-SG catalysts present a balance of acid and base centers that could be adequate for this type of processes. Leaching of the MgO component, however, is an issue that has to be solved in order to carry out the process in an effective way.

Finally, although some catalysts of the series ME present results that could be interesting, the problems associated to the surfactant that remains adsorbed on them seem to advise its use in more complex processes.

4. Materials and Methods

4.1. Materials

Chloroform anhydrous ≥99% (ref. 288306), 2,2,4-trimethylpentane anhydrous 99.8% (ref. 360066), hexadecyltrimethylammonium bromide ≥98% (CTAB) (ref. H5882), butan-1-ol ≥99% (ref. B7906), ethanol (ref. 652261), zirconium (IV) oxynitrate hydrate (ref. 346462), magnesium nitrate hexahydrate (ref. 203696), D-(+)-xylose ≥99% (ref. X1500) and toluene (ref. 244511) were purchased from Sigma-Aldrich (Merck KGaA, Darmstadt, Germany). Ammonium hydroxide solution 5.0 N (ref. 318612) and hydrochloric acid solution 1.0 M (ref. 318949) were obtained from Honeywell Fluka (Honeywell, Bucharest, Romania). MilliQ water was used for preparation of the aqueous solutions.

4.2. Catalysts Synthesis

Pure MgO and ZrO_2 as well as several mixed MgO-ZrO_2 systems (in an atomic Mg:Zr nominal ratio of 75:25, 50:50 and 25:75) were synthesized through both microemulsion (ME series) and sol-gel (SG series) methods. In both synthetic methods, magnesium and zirconyl nitrates were used as the precursors and aqueous NH_4OH (pH 10) as precipitating agent.

4.2.1. Sol-Gel Method

MgO was prepared from a 0.4 M aqueous solution of magnesium nitrate hexahydrate which was introduced at controlled rate (0.56 mL/min) into a reactor containing 0.4 L of ammonium hydroxide solution at pH 10. The process was carried out under magnetic stirring (700 rpm) and maintaining the initial pH level of 10 with help of a Syrris Atlas pump (Syrris Ltd., Hertfordshire, UK) that introduced NH_4OH 5 N or HCl 0.2 M as needed. The gel was aged for 24 h and the precipitate was then vacuum filtered and washed with water to obtain a white solid which was dried overnight at 120 °C. The dried solid was calcined at 200 °C for 6 h under air flow. Finally, the solid was ground and sieved (0.149 µm light sieve). Similar procedure was followed for the rest of catalysts in the SG series just adjusting the appropriate amounts of magnesium and zirconium precursors to obtain solids with Mg:Zr atomic ratio of 100:0 (Mg-SG), 75:25 (Mg3Zr-SG), 50:50 (MgZr-SG), 25:75 (MgZr3-SG) and 0:100 (Zr-SG).

4.2.2. Microemulsion Method

As for the solids prepared through microemulsion technique (ME series), two different microemulsions were prepared to include Mg and Zr precursors (ME1) and the precipitating agent, NH_4OH (ME2). Under optimized conditions, the composition of microemulsions was: 2,2,4-trimethylpentane anhydrous (oil, 53 wt %), hexadecyltrimethylammonium bromide (surfactant, 15 wt %), 1-butanol (co-surfactant, 12 wt %) and 0.4 M aqueous solution of Mg and Zr precursors (ME1) or NH_4OH aqueous solutions of pH = 10 (ME2) (20 wt %).

As a standard procedure ME1 was slowly added to ME2 under constant stirring (700 rpm) and the resulting mixture aged overnight under stirring. The white precipitate was then filtered and washed five times with 80 mL of a chloroform/ethanol mixture (1:1 v/v) to remove surfactant and oil remaining on the solid surface. The solid was dried, calcined and sieved in a similar way to the SG series. Catalysts in the ME series were prepared just adjusting the appropriate amounts of magnesium and zirconium precursors to obtain solids with Mg:Zr atomic ratio of 100:0 (Mg-ME), 75:25 (Mg3Zr-ME), 50:50 (MgZr-ME), 25:75 (MgZr3-ME) and 0:100 (Zr-ME).

4.3. Catalysts Characterization

Both series of catalysts were thoroughly characterized from textural, structural and chemical point of view.

Thermogravimetric analyses (TGA) were performed on a Setaram SetSys 12 instrument (Caluire, France). An amount of 20 mg of sample was placed in an alumina crucible and heated at temperatures ranging from 30 to 600 °C (heating rate of 10 °C·min^{-1}) under synthetic air stream (50 mL·min^{-1}) in order to measure weight loss, heat flow and derivative weight loss.

Surface areas of solids were obtained from nitrogen adsorption-desorption isotherms obtained at liquid nitrogen temperature on a Micromeritics ASAP-2010 instrument, following the Brunnauer-Emmett-Teller (BET) method. All samples were degassed to 0.1 Pa at 120 °C before measurement.

Scanning electron microscopy (SEM-EDX) measurements were obtained on a JEOL JSM-6300 scanning electron microscope (Jeol, Tokyo, Japan) equipped with an energy-dispersive X-ray (EDX) detector (Oxford Instruments, Abingdon, United Kingdom), available at the Central Service for Research Support (SCAI) of the University of Córdoba. It was operated at an acceleration voltage of 20 keV with a resolution of 65 eV. Transmission electron microscopy (TEM) images were obtained at the Central Service for Research Support (SCAI) of the University of Córdoba using a JEOL JEM 1400 microscope (Jeol, Tokyo, Japan). All samples were mounted on 3 mm holey carbon copper grids.

X-ray photoelectron spectroscopy (XPS) data were recorded at the Central Service for Research Support (SCAI) of the University of Córdoba on 4 mm × 4 mm pellets, 0.5 mm thick that were obtained by gently pressing the powered materials. Samples were outgassed to a pressure below about 2 × 10^{-8} Torr at 150 °C in the instrument pre-chamber to remove chemisorbed volatile species. The main chamber of the Leibold-Heraeus LHS10 spectrometer used (Leibold, Cologne, Germany), capable of operating down to less than 2 × 10^{-9} Torr, was equipped with a EA-200MCD hemispherical electron analyzer with a dual X-ray source using Al Kα (hυ = 1486.6 eV) at 120 W and 30 mA. C (1s) was used as energy reference (284.6 eV).

Surface acidity of the catalysts was determined by thermal programmed desorption of pre-absorbed pyridine (TPD-PY) with TCD detection. An amount of 20 mg of sample was introduced in a 10 mm ID reactor that was placed inside an oven. Solids were cleaned under He flow (75 mL·min^{-1}) by heating to 200 °C at a rate of 10 °C min^{-1} and then cooled down to 50 °C. At that temperature, the solids were exposed for 30 min to a pyridine saturated Helium flow. After saturation, physisorbed pyridine was removed by flowing a pure He stream for 60 min (75 mL·min^{-1}). Then, the temperature-programmed desorption of chemisorbed pyridine was carried out by ramping the temperature from 50 to 200 °C (heating rate 10 °C·min^{-1}) and holding the final temperature for

30 min. Desorbed pyridine was quantified against a calibration graph constructed from variable volumes of pyridine injected.

Surface basicity of the catalysts was determined on a Micromeritics Autochem II instrument (Micromeritics, Norcross, GA, USA) by thermal programmed desorption of pre-absorbed CO_2 (TPD-CO_2) with TCD detection. An amount of 100 mg of each catalyst was loaded into a reactor 10 mm ID and placed in a furnace. Solids were cleaned with an Ar stream (20 mL·min^{-1}) by heating to 200 °C at a rate of 10 °C·min^{-1} for 60 min and then cooled down to 40 °C. At that temperature, the catalysts were saturated with the probe molecule, using 5%CO_2/Ar flow at 20 mL·min^{-1} for 60 min. After saturation, physisorbed CO_2 was removed by flowing Ar stream for 30 min (20 mL·min^{-1}). Then, the temperature-programmed desorption of chemisorbed CO_2 was carried out by ramping the temperature from 40 to 200 °C (heating rate 5 °C·min^{-1}) and holding the final temperature for 60 min. The amount of CO_2 adsorbed was determined from a calibration graph constructed from the injection of variable volumes of 5%CO_2/Ar.

Propan-2-ol transformation test reaction was also used to confirm the surface chemical properties of the prepared catalysts. This reaction, widely described as a model process, can provide valuable information on surface acid-base properties of the catalyst as a function of its products distribution: surface acid sites yield propene or diisopropyl ether while basic or redox properties lead to acetone [30–32,34,35].

The gas-phase propan-2-ol transformation was carried out in a stainless-steel reactor (1/8 inch OD) that was loaded with 100 mg of catalyst and 1 g of inert SiO_2. Prior to the reaction, the catalyst was cleaned with a N_2 flow (20 mL·min^{-1}) while increasing the temperature until 200 °C (rate, 2 °C·min^{-1}). The reaction was started by introducing propan-2-ol by passing a nitrogen flow of 10 mL·min^{-1} through a saturator filled with propan-2-ol at room temperature. Analyses were carried out on-line by connecting the effluent to a gas chromatograph (HP 5890 series II) equipped with a capillary column Supelcowax-10 (60 m long, 0.25 mm ID, 0.25 μm film thickness).

4.4. Catalytic Tests

The solids were tested for dehydration of xylose to furfural using a biphasic reaction medium on two different reaction systems.

4.4.1. Multi-Reactor under Conventional Thermal Heating

A Carousel 12 Reaction StationTM multi-reactor (Radley Discovery Technologies, Essex, UK) furnished with twelve reaction glass tubes with a maximum reaction volume of 20 mL. The reaction mixture consisted of 75 mg xylose, 6 mL milliQ water, 6 mL organic solvent (1-butanol or toluene) and 30 mg catalyst. The reaction mixture was purged with N_2 before reaction to work under controlled atmosphere. Temperature and stirring rate were adjusted at 150 °C and 750 rpm, respectively, and the reaction time extended to 24 h. The upper part of the reaction tubes was always refrigerated at 5 °C thus preventing loss of the reaction mixture by evaporation.

4.4.2. High-Pressure Autoclave

A Berghof HR-100 stainless steel high-pressure autoclave (Berghof Products and Instruments GmbH, Eningen, Germany) equipped with a 75 mL PTFE insert vessel was also used in xylose dehydration to furfural. Under standard conditions, 250 mg xylose, 10 mL milliQ water, 10 mL organic solvent (1-butanol or toluene) and 100 mg catalyst were introduced in the vessel (i.e., same substrate/catalyst ratio as in multi-reactor). Reactor was purged with nitrogen and pressurized to 5 bar of N_2. The reaction temperature was set to 150 °C and the reaction started by switching on the stirring at 750 rpm. Reaction was stopped by introducing the vessel in an ice bath at selected times (3, 5 and 24 h).

4.4.3. Product Analysis

Once finished the reactions, the aqueous and organic phases were separated by centrifugation and filtered through a nylon syringe filter (0.22 μm). The aqueous phase was analysed by high-performance liquid chromatography (Water 2695 HPLC) with refraction index detection (IR detector) on a Fortis amino 5 μm (250 × 4.6 mm) column. 5 mM of H_2SO_4 was employed as the eluent with a 0.7 μL/min flow rate at 50 °C. The volume of injection was 5 μL. The organic phase was analysed by gas chromatography (Agilent 7890, Santa Clara, CA, USA) with flame ionization detector (GC-FID) using a Supelco Nukol™ capillary column. No xylose was detected in the organic phase and furfural detected in the aqueous phase was negligible. Quantification of xylose and furfural was performed using the appropriate calibration curves.

Blank experiments (without catalyst) were carried for both reaction systems being the xylose conversion obtained less than 7% at the best.

Xylose conversion and furfural selectivity and yield were defined by Equations (1)–(3):

$$\text{Xylose conversion } (\%) = \frac{initial\ xylose\ cncentration - final\ xylose\ cncentration}{initial\ xylose\ cncentration} \times 100 \quad (1)$$

$$\text{Furfural selectivity } (\%) = \frac{furfural\ cncentration}{initial\ xylose\ cncentration - final\ xylose\ cncentration} \times 100 \quad (2)$$

$$\text{Furfural yield } (\%) = \frac{furfural\ cncentration}{initial\ xylose\ cncentration} \times 100 \quad (3)$$

5. Conclusions

Two series of catalysts were prepared (by sol-gel and microemulsion synthetic procedures), characterized and applied to the liquid-phase xylose dehydration to furfural. Catalysts prepared by microemulsion retained part of the surfactant used in the synthetic procedure, mainly associated to the Zr part of the solid.

As for xylose dehydration, the use of toluene as organic solvent in the biphasic reaction mixture (toluene/water) leads to better performance to furfural than the use of alcohols (1-butanol) which is associated with the ability of toluene to extract the furfural formed, thus avoiding the formation of humins that take place mainly in the aqueous phase.

The yield to furfural increases with the Zr content of the catalyst and, therefore, the catalysts constituted by pure ZrO_2 (especially Zr-SG) are the most suitable to carry out the process (98% conversion, 40% yield, 24 h). The results described above point out that the Zr sites are responsible for the dehydration of xylose to furfural, whereas the Mg related sites are not active at this point.

The reuse experiments of the catalysts, together with the analysis of leached species, indicated that while ZrO_2 component is practically not leached, a large part of the MgO component of the solids is leached to the reaction medium under the hydrothermal reaction conditions. However, this only implies a slight reduction in the conversion of xylose because, as mentioned, it is the ZrO_2 component that is responsible for the catalytic activity of the MgO-ZrO_2 mixed oxides.

Supplementary Materials: The following are available online: Supplementary Figure S1: SEM-EDX measurements for the MgZr-ME catalysts, including EDX profiles for the whole image area. Inserts correspond to the chemical composition associated to EDX profile. Red arrow marks Br signal, Supplementary Figure S2: Nitrogen adsorption-desorption isotherms corresponding to the solids synthesized in both SG and ME series, Supplementary Figure S3: Catalysts acidity determined from temperature programmed desorption of pre-adsorbed pyridine (μmol PY/g CAT and μmol PY/m^2 CAT), Supplementary Figure S4: Catalysts basicity determined from temperature programmed desorption of pre-adsorbed carbon dioxide (μmol CO_2/g CAT and μmol CO_2/m^2 CAT), Supplementary Figure S5: Temperature-programmed desorption profiles of pre-adsorbed carbon dioxide obtained for the catalysts synthesized in this work.

Acknowledgments: The authors are thankful to Ramon Areces Foundation for financial support. The scientific support from the Central Service for Research Support (SCAI) at the University of Cordoba was also acknowledged.

Author Contributions: A.M. and F.J.U. conceived and designed the experiments; A.P. performed the experiments; A.P., V.M., J.H.-C. and E.S.-L. analyzed the data; A.P., A.M. and F.J.U. wrote the paper.

Conflicts of Interest: The authors declare no conflict of interest. The founding sponsors had no role in the design of the study; in the collection, analyses, or interpretation of data; in the writing of the manuscript, and in the decision to publish the results.

References

1. Field, C.B.; Campbell, J.E.; Lobell, D.B. Biomass energy: The scale of the potential resource. *Trends Ecol. Evol.* **2008**, *23*, 65–72. [CrossRef] [PubMed]
2. Gallezot, P. Conversion of biomass to selected chemical products. *Chem. Soc. Rev.* **2012**, *41*, 1538–1558. [CrossRef] [PubMed]
3. Zhang, J.; Zhuang, J.; Lin, L.; Liu, S.; Zhang, Z. Conversion of D-xylose into furfural with mesoporous molecular sieve MCM-41 as catalyst and butanol as the extraction phase. *Biomass Bioenergy* **2012**, *39*, 73–77. [CrossRef]
4. Sairanen, E.; Karinen, R.; Lehtonen, J. Comparison of Solid Acid-Catalyzed and Autocatalyzed C5 and C6 Sugar Dehydration Reactions with Water as a Solvent. *Catal. Lett.* **2014**, *144*, 1839–1850. [CrossRef]
5. Sheldon, R.A. Green and sustainable manufacture of chemicals from biomass: State of the art. *Green Chem.* **2014**, *16*, 950–963. [CrossRef]
6. Bozell, J.J.; Petersen, G.R. Technology development for the production of biobased products from biorefinery carbohydrates-the US Department of Energy's "Top 10" revisited. *Green Chem.* **2010**, *12*, 539–554. [CrossRef]
7. Dutta, S.; De, S.; Saha, B.; Alam, M.I. Advances in conversion of hemicellulosic biomass to furfural and upgrading to biofuels. *Catal. Sci. Technol.* **2012**, *2*, 2025–2036. [CrossRef]
8. Barrett, C.J.; Chheda, J.N.; Huber, G.W.; Dumesic, J.A. Single-reactor process for sequential aldol-condensation and hydrogenation of biomass-derived compounds in water. *Appl. Catal. B Environ.* **2006**, *66*, 111–118. [CrossRef]
9. Chheda, J.N.; Dumesic, J.A. An overview of dehydration, aldol-condensation and hydrogenation processes for production of liquid alkanes from biomass-derived carbohydrates. *Catal. Today* **2007**, *123*, 59–70. [CrossRef]
10. Corma, A.; de la Torre, O.; Renz, M. High-Quality Diesel from Hexose- and Pentose-Derived Biomass Platform Molecules. *ChemSusChem* **2011**, *4*, 1574–1577. [CrossRef] [PubMed]
11. Dautzenberg, G.; Gerhardt, M.; Kamm, B. Bio based fuels and fuel additives from lignocellulose feedstock via the production of levulinic acid and furfural. *Holzforschung* **2011**, *65*, 439–451. [CrossRef]
12. Yan, K.; Liu, Y.; Lu, Y.; Chai, J.; Sun, L. Catalytic application of layered double hydroxide-derived catalysts for the conversion of biomass-dderived molecules. *Catal. Sci. Technol.* **2017**, *7*, 1622–1645. [CrossRef]
13. Carrasco, F. Production of furfural by dilute-acid hydrolysis of wood—Methods for calculating furfural yield. *Wood Fiber Sci.* **1993**, *25*, 91–102.
14. Faba, L.; Diaz, E.; Ordonez, S. One-pot Aldol Condensation and Hydrodeoxygenation of Biomass-derived Carbonyl Compounds for Biodiesel Synthesis. *ChemSusChem* **2014**, *7*, 2816–2820. [CrossRef] [PubMed]
15. Lucas, N.; Kokate, G.; Nagpure, A.; Chilukuri, S. Dehydration of fructose to 5-hydroxymethyl furfural over ordered AlSBA-15 catalysts. *Microporous Mesoporous Mater.* **2013**, *181*, 38–46. [CrossRef]
16. Grande, P.M.; Bergs, C.; de Maria, P.D. Chemo-Enzymatic Conversion of Glucose into 5-Hydroxymethylfurfural in Seawater. *ChemSusChem* **2012**, *5*, 1203–1206. [CrossRef] [PubMed]
17. Dee, S.J.; Bell, A.T. A Study of the Acid-Catalyzed Hydrolysis of Cellulose Dissolved in Ionic Liquids and the Factors Influencing the Dehydration of Glucose and the Formation of Humins. *ChemSusChem* **2011**, *4*, 1166–1173. [CrossRef] [PubMed]
18. Karinen, R.; Vilonen, K.; Niemela, M. Biorefining: Heterogeneously Catalyzed Reactions of Carbohydrates for the Production of Furfural and Hydroxymethylfurfural. *ChemSusChem* **2011**, *4*, 1002–1016. [CrossRef] [PubMed]
19. Campos Molina, M.J.; Mariscal, R.; Ojeda, M.; Lopez Granados, M. Cyclopentyl methyl ether: A green co-solvent for the selective dehydration of lignocellulosic pentoses to furfural. *Bioresour. Technol.* **2012**, *126*, 321–327. [CrossRef] [PubMed]

20. Delbecq, F.; Wang, Y.; Len, C. Various carbohydrate precursors dehydration to 5-HMF in an acidic biphasic system under microwave heating using betaine as a co-catalyst. *Mol. Catal.* **2017**, *434*, 80–85. [CrossRef]
21. Le Guenic, S.; Delbecq, F.; Ceballos, C.; Len, C. Microwave-assisted dehydration of D-xylose into furfural by diluted inexpensive inorganic salts solution in a biphasic system. *J. Mol. Catal. Chem.* **2015**, *410*, 1–7. [CrossRef]
22. Hua, D.-R.; Wu, Y.-L.; Liu, Y.-F.; Chen, Y.; Yang, M.-D.; Lu, X.-N.; Li, J. Preparation of furfural and reaction kinetics of xylose dehydration to furfural in high-temperature water. *Pet. Sci.* **2016**, *13*, 167–172. [CrossRef]
23. Hu, X.; Westerhof, R.J.M.; Dong, D.; Wu, L.; Li, C.-Z. Acid-Catalyzed Conversion of Xylose in 20 Solvents: Insight into Interactions of the Solvents with Xylose, Furfural, and the Acid Catalyst. *ACS Sustain. Chem. Eng.* **2014**, *2*, 2562–2575. [CrossRef]
24. Sievers, C.; Musin, I.; Marzialetti, T.; Olarte, M.B.V.; Agrawal, P.K.; Jones, C.W. Acid-Catalyzed Conversion of Sugars and Furfurals in an Ionic-Liquid Phase. *ChemSusChem* **2009**, *2*, 665–671. [CrossRef] [PubMed]
25. Kim, Y.C.; Lee, H.S. Selective synthesis of furfural from xylose with supercritical carbon dioxide and solid acid catalyst. *J. Ind. Eng. Chem.* **2001**, *7*, 424–429.
26. Climent, M.J.; Corma, A.; Iborra, S. Heterogeneous Catalysts for the One-Pot Synthesis of Chemicals and Fine Chemicals. *Chem. Rev.* **2011**, *111*, 1072–1133. [CrossRef] [PubMed]
27. Aramendia, M.A.; Borau, V.; Jimenez, C.; Marinas, J.M.; Romero, F.J.; Navio, J.A.; Barrios, J. Modification of the activity of $Mg_3(PO_4)_2$ in the gas-phase conversion of cyclohexanol by addition of sodium-carbonate. *J. Catal.* **1995**, *157*, 97–108. [CrossRef]
28. Stefanic, G.; Music, S.; Popovic, S.; Sekulic, A. FT-IR and laser Raman spectroscopic investigation of the formation and stability of low temperature t-ZrO_2. *J. Mol. Struct.* **1997**, *408*, 391–394. [CrossRef]
29. Minambres, J.F.; Marinas, A.; Marinas, J.M.; Urbano, F.J. Activity and deactivation of catalysts based on zirconium oxide modified with metal chlorides in the MPV reduction of crotonaldehyde. *Appl. Catal. B Environ.* **2013**, *140*, 386–395. [CrossRef]
30. Aramendia, M.A.; Borau, V.; Jimenez, C.; Marinas, J.M.; Porras, A.; Urbano, F.J. Synthesis and characterization of ZrO_2 as an acid-base catalyst: Dehydration-dehydrogenation of propan-2-ol. *J. Chem. Soc. Faraday Trans.* **1997**, *93*, 1431–1438. [CrossRef]
31. Aramendia, M.A.; Borau, V.; Garcia, I.M.; Jimenez, C.; Marinas, A.; Marinas, J.M.; Porras, A.; Urbano, F.J. Comparison of Different Organic Test Reaction over Acid-Base Catalysts. *Appl. Catal. A Gen.* **1999**, *184*, 115–125. [CrossRef]
32. Aramendia, M.A.; Borau, V.; Jimenez, C.; Marinas, A.; Marinas, J.M.; Ruiz, J.R.; Urbano, F.J. Magnesium-containing mixed oxides as basic catalysts: Base characterization by carbon dioxide TPD-MS and test reactions. *J. Mol. Catal. A Chem.* **2004**, *218*, 81–90. [CrossRef]
33. Yan, K.; Wu, X.; An, X.; Xie, X. Facile Synthesis of Reusable CoAl-Hydrotalcite Catalyst for Dehydration of Biomass-Derived Fructose into Platform Chemical 5-Hydroxymethylfurfural. *Chem. Eng. Commun.* **2014**, *201*, 456–465. [CrossRef]
34. Haffad, D.; Chambellan, A.; Lavalley, J.C. Propan-2-ol transformation on simple metal oxides TiO_2, ZrO_2 and CeO_2. *J. Mol. Catal. A: Chem.* **2001**, *168*, 153–164. [CrossRef]
35. Marinas, A.; Marinas, J.M.; Aramendia, M.A.; Urbano, F.J. Heterogeneous catalysis on basic sites in organic chemistry. In *New Developments in Catalysis Research*; Bevy, L.P., Ed.; Nova Science: New York, NY, USA, 2005; pp. 85–127.

Sample Availability: Samples of the catalysts are available from the authors.

© 2017 by the authors. Licensee MDPI, Basel, Switzerland. This article is an open access article distributed under the terms and conditions of the Creative Commons Attribution (CC BY) license (http://creativecommons.org/licenses/by/4.0/).

catalysts

MDPI

Article

Aldol Condensation of Furfural with Acetone Over Mg/Al Mixed Oxides. Influence of Water and Synthesis Method

Almudena Parejas, Daniel Cosano, Jesús Hidalgo-Carrillo *, José Rafael Ruiz, Alberto Marinas, César Jiménez-Sanchidrián and Francisco J. Urbano

Departamento de Química Orgánica, Instituto Universitario de Investigación en Química Fina y Nanoquímica IUIQFN, Universidad de Córdoba, Campus de Rabanales, Edificio Marie Curie, E-14071 Córdoba, Spain; q12pabaa@uco.es (A.P.); q92cohid@uco.es (D.C.); qo1ruarj@uco.es (J.R.R.); alberto.marinas@uco.es (A.M.); qo1jisac@uco.es (C.J.-S.); fj.urbano@uco.es (F.J.U.)

* Correspondence: jesus.hidalgo@uco.es; Tel.:+34-957-218-638

Received: 23 January 2019; Accepted: 20 February 2019; Published: 23 February 2019

check for updates

Abstract: Aldol condensation of furfural and acetone (an important initial step to obtain diesel from biomass) was studied over MgAl mixed oxides. The influence of the utilization of microwaves and/or a surfactant (Pluronic 123) during the synthesis as well as the use of water (either pre-hydrating the solids before catalytic studies or in water/toluene mixtures as the reaction medium) is discussed. The combined use of Pluronic 123 and microwaves led to solids with bigger pore sizes, exhibiting lower basicity and higher acidity than the conventional synthetic method, thus resulting in an increase in the yield of the desired product of condensation, comprising two molecules of furfural and one of acetone (F2Ac). As for the influence of water, re-hydration of the mixed oxides was detrimental to activity, probably as a result of the partial blocking (solvation) of active sites. On the contrary, the increase in water percentage in the reaction medium resulted in higher conversions, though selectivity to F2Ac decreased. The weakening of the C=O bond of furfural in the presence of water as well as the higher solubility of the first condensation product (FAc) in toluene, as compared to water, could account for that. A 44.5% yield of F2Ac (66% conversion) after 16 h was obtained with the most active solid, which maintained the activity for three consecutive reactions.

Keywords: aldol condensation; biomass valorization; Mg/Al mixed oxides; surfactant; microwaves; influence of water

1. Introduction

Fossil fuel depletion and environmental concern have boosted the search for renewable energies, one of the possible sources being biomass [1,2]. Furfural is a so-called platform molecule from biomass obtained through xylose dehydration [3,4] and can be transformed into a wide range of chemicals via hydrogenation, oxidation, decarbonylation, nitration, or condensation processes, just to cite some of them [5]. For instance, aldol condensation and subsequent hydrogenation and hydrodeoxygenation can lead to liquid hydrocarbons for use as diesel [6–8].

Aldol condensation is a well-known C–C bond formation process which can occur in acidic or basic sites, the latter being more frequently reported in the literature [6–15]. It requires the existence of a reactive hydrogen in alpha position, with respect to a carbonyl compound able to form an enol, which reacts with another carbonyl compound, and after dehydration, yields a conjugated enone. Focusing on aldol condensation between furfural and acetone (Figure 1), it can initially lead to 4-(2-furanyl)-3-buten-2-one (FAc), a subsequent aldol condensation with another furfural molecule, forming 1,5-bis-(2-furanyl)-1,4-pentadien-3-one (F2Ac) (Figure 1a) [16,17]. Some side reactions include

acetone self-condensation to form diacetone-alcohol and mesityl oxide (Figure 1b), condensation between FAc and acetone (Figure 1c), and multiple aldol condensations between different carbonyl compounds, thus forming polymers [18,19] (Figure 1d).

Aldol condensations have been traditionally performed in organic media, using base catalysts such as sodium or calcium hydroxides. Nevertheless, the existence of corrosion problems and the difficult reutilization have led to the use of some other base heterogeneous catalysts, such as hydrotalcites and hydrotalcite-derived mixed oxides [20,21], amorphous aluminophosphate [15], and diamine-functionalized MCM-41 [22], just to cite some examples.

In the present work, different AlMg mixed oxides were obtained through calcination of layered double hydroxides (LDHs) and tested for aldol condensation with acetone to form F2Ac. The influence on the catalytic results of two synthetic variables (conventional or microwave heating with the presence or absence of Pluronic 123 as the surfactant) was explored. Furthermore, the effect of water (either pre-hydrating the solids before catalytic studies or in water/toluene mixtures as the reaction medium) is discussed.

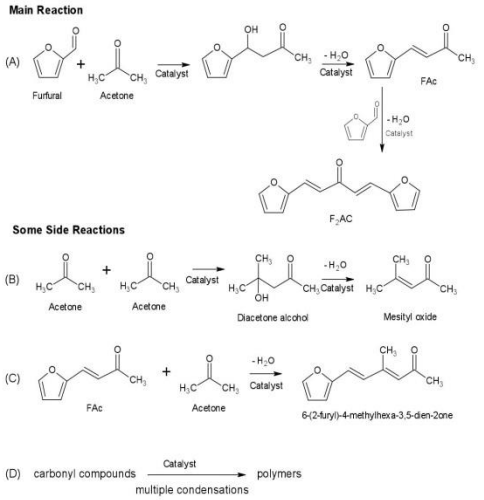

Figure 1. Reaction scheme for aldol condensation of furfural and acetone. Some side reactions have also been included. (**A**) aldol condensation between furfural and acetone, (**B**) acetone self-condensation, (**C**) condensation between FAc and acetone and (**D**) multiple aldol condensations between different carbonyl compounds.

2. Results and Discussion

2.1. Textural, Structural and Acid–Base Characterization of the Solids

X-ray diffractograms of uncalcined and calcined hydrotalcites are shown in Figure 2. As can be seen, uncalcined solids exhibit a typical hydrotalcite crystallinity profile (JCPDS 22-700), with symmetric reflections at 2θ = 11°, 22°, 36°, 37°, 45°, 60°, and 62°. Therefore, sharper peaks corresponded to (003), (006), (010), and (013) reflections, whereas broader signals were obtained for (009), (015), and (016) reflections, all of them representative of layered materials. As for calcined solids (Figure 2b), diffraction patterns are very similar to each other, exhibiting (111), (200), and (220) reflections ascribed to periclase. In a previous paper, Aramendia et al. [23], using ^{27}Al NMR-MAS,

demonstrated that the coordination of Al^{3+} changed from octahedral to tetrahedral upon calcination of hydrotalcites, Al^{3+} ions thus isomorphically substituting Mg^{2+} ions, forming MgAlOx periclase.

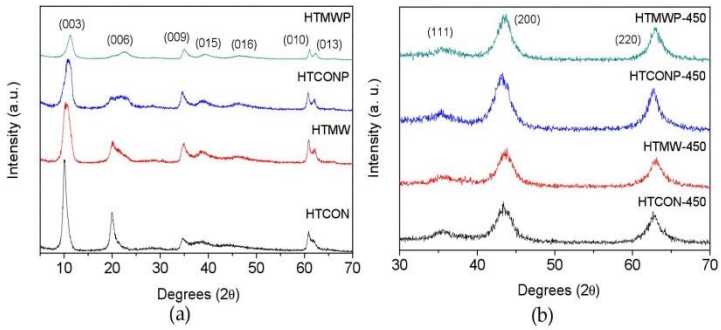

Figure 2. X-ray diffractograms of the different solids synthesized in the present work. (**a**) Uncalcined solids. (**b**) Solids calcined at 450 °C.

Thermal stability of hydrotalcites was determined by TG-DTA (Figure 3). In all cases, weight loss percentage is in the 42–45% range (Figure 3a). HTCON and HTMW thermogravimetric profiles are consistent with those reported in the literature for hydrotalcites [24,25]. Therefore, two main weight losses are observed. The first one at 100–200 °C is ascribed to the loss of intercalated water molecules, whereas nitrate coming from both the precursor and hydroxyl groups can account for the second loss at higher temperatures (250–500 °C). For the solids synthesized using the surfactant (HTCONP and HTMWP), the second weight loss seems to be produced quicker (i.e., at lower temperatures), thus suggesting that for those systems, re-structuration to form periclase is somehow favored by Pluronic 123. Heat flow profiles (Figure 3b) seem to confirm this hypothesis, the exothermal peak centered at 450 °C in HTCON and HTMW being shifted to lower temperatures (300–350 °C) for HTCONP and HTMWP.

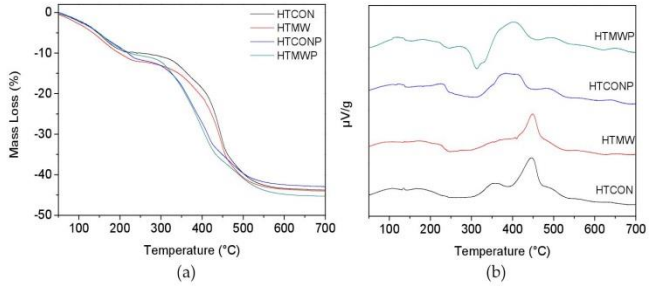

Figure 3. TG analyses (**a**) and heat flow (**b**) of hydrotalcites.

Raman spectra of uncalcined solids (i.e., hydrotalcites) are represented in Figure 4. The band appearing at 557 cm^{-1} can be assigned to vibrations of brucite-like octahedral layers, Al-O-Mg, which are present in all Mg-Al hydrotalcites [26]. Moreover, the spectra also exhibit bands at 710 and 1055 cm^{-1}, corresponding to nitrate vibrations [27] and bands at ca. 3500 cm^{-1}, due to surface hydroxyl groups. In the case of HTCONP and HTMWP solids, there are also some intense bands of C-H stretching Pluronic 123 at 2986, 2941, and 2933 cm^{-1} [28].

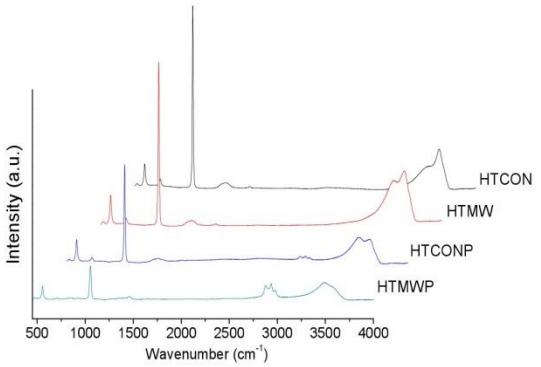

Figure 4. Raman spectra of the uncalcined solids (hydrotalcites).

N_2 adsorption–desorption isotherms of calcined solids are shown in Figure 5. In all cases, type IV isotherms corresponding to mesoporous materials were obtained. BET surface areas, pore volume and average pore diameter values are given in Table 1. With regards to the BET areas, they are in the 160–210 $m^2 \cdot g^{-1}$ range, the highest value corresponding to HTCONP-450. Modification of conventional synthesis by using microwave irradiation and/or in the presence of the surfactant (Pluronic 123) led in all cases to an increase in BET area. Solids that aged under microwave irradiation exhibit smaller pore diameters than their conventionally-heated counterparts (compare HTMW-450 vs. HTCON-450 or HTMWP-450 vs. HTCONP-450). Systems synthesized in the presence of the surfactant present bigger pores (compare HTCONP-450 vs. HTCON-450 and HTMWP-450 vs. HTMW-450). Therefore, the effect of microwaves and the presence of a surfactant on pore volume is the opposite. However, if both variables are changed simultaneously, the influence of the surfactant is more important, thus resulting in the pore diameter increasing (compare HTCON-450 and HTMWP-450 with pore diameters of 6.8 and 8.4 nm, respectively).

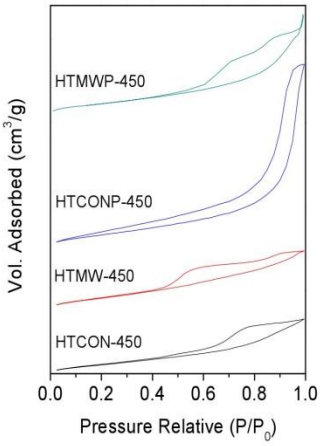

Figure 5. Nitrogen adsorption–desorption isotherms corresponding to the mixed oxides.

Table 1. Summary of the main features of the mixed oxides synthesized in this work.

Catalyst	Textural Properties			Base Sites (CO_2-TPD) (μmol/g)	Acid Sites (Py-TPD) (μmol/g)	Mg/Al Ratio	
	S_{BET} (m^2/g)	V_p (cm^3/g)	D_p (nm)			Nominal	XRF
HTCON-450	160	0.26	6.8	1105	871	2.00	2.01
HTMW-450	201	0.29	4.2	880	1030	2.00	1.94
HTCONP-450	210	0.86	16.6	932	960	2.00	2.04
HTMWP-450	183	0.40	8.4	775	1124	2.00	1.97

X-Ray fluorescence results (Table 1) evidenced a good incorporation of Mg and Al to the solids, with Mg/Al ratios very similar to the nominal value (Mg/Al = 2).

Base characterization of the solids was performed using thermal programmed desorption of pre-adsorbed CO_2 (CO_2-TPD) and the results are given in Tables 1 and 2, and in Figure 6. In all cases, signals were deconvoluted in peaks, which, depending on the desorption temperature, were ascribed to weak (80–200 °C), medium (200–300 °C), or strong (>300 °C) basic sites, respectively. Taking HTCON-450 as the reference, the use of microwave irradiation and/or the presence of the surfactant in the synthesis results in a drop in total basicity. Interestingly, as far as the base site distribution is concerned, the effect of microwave irradiation, the presence of the surfactant, or both variables simultaneously considered is different. Therefore, in the absence of Pluronic 123, microwave irradiation does not vary base site distribution. On the contrary, the presence of Pluronic 123 results in an increase in the strong base sites' percentage, to the detriment of weak ones. Finally, simultaneous use of microwaves and Pluronic 123 leads to an increase in the percentage of weak base sites.

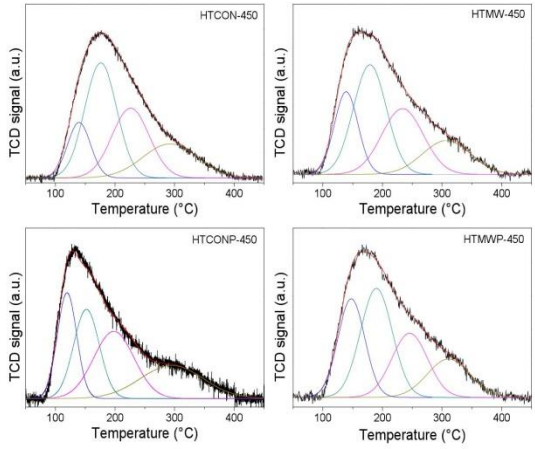

Figure 6. Temperature-programmed desorption profiles of CO_2 for the mixed oxides synthesized in this work.

Table 2. Base site distribution of the solids expressed as μmol CO_2/g. Values in brackets represent the percentage of the total basicity.

Catalyst	Base Sites Distribution, μmol CO_2/g		
	Weak (80–200 °C)	Medium (200–300 °C)	Strong (>300 °C)
HTCON-450	580.34 (52.53%)	304.89 (27.60%)	219.51 (19.87%)
HTMW-450	468.05 (53.20%)	241.95 (27.50%)	169.80 (19.30%)
HTCONP-450	428.62 (45.97%)	276.64 (29.67%)	227.13 (24.36%)
HTMWP-450	470.96 (60.80%)	177.38 (22.90%)	126.26 (16.30%)

Acid characterization of the solids was performed by thermal programmed desorption of pre-adsorbed pyridine (Py-TPD), results being given in Tables 1 and 3, and in Figure 7. Taking HTCON-450 as the reference, contrary to basicity, total acidity increases when the solids are synthesized utilizing a microwave and/or in the presence of Pluronic 123. Furthermore, with regards to acid site distribution, only microwave irradiation has some effect (acid strength decreases), whereas the presence of Pluronic 123, either under conventional heating or microwave irradiation, does not vary acid site distribution.

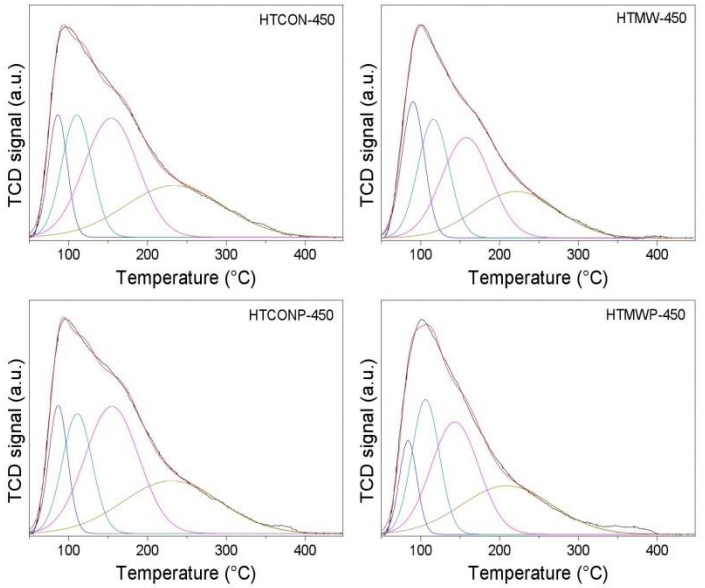

Figure 7. Temperature-programmed desorption profiles of pyridine for the solids synthesized in this work.

Table 3. Acid site distribution of the solids expressed as μmol Py/g. Values in brackets represent the percentage of the total basicity.

Catalyst	Acid Site Distribution, μmol Py/g		
	Weak (80–200 °C)	Medium (200–300 °C)	Strong (>300 °C)
HTCON-450	296.36 (34.01%)	320.14 (36.74%)	254.88 (29.25%)
HTMW-450	447.56 (43.44%)	329.59 (31.99%)	253.14 (24.57%)
HTCONP-450	320.58 (33.39%)	365.71 (38.09%)	273.82 (28.52%)
HTMWP-450	397.24 (35.33%)	398.70 (35.46%)	328.43 (29.21%)

All in all, microwave irradiation and/or the use of Pluronic 123 as the surfactant result in an increase in total acidity and a decrease in total basicity together with an increase in BET areas.

2.2. Catalytic Activity

The solid synthesized under conventional heating and in the absence of the surfactant (HTCON-450) was used as the reference material in order to study the influence of reaction temperature and the presence of water in the reaction medium on catalytic activity.

2.2.1. Influence of Reaction Temperature

Table 4 summarizes catalytic results obtained for t = 3 h at different temperatures. From that table, it is evident that the increase in temperature results in the increase in conversion, whereas selectivity to F2Ac, the desired product, hardly changes. Therefore, from then on, 100 °C was selected as the reaction temperature.

Table 4. Aldol condensation of furfural and acetone on HTCON-450: Influence of temperature on catalytic activity. Reaction conditions: Reactor pressurized to 5 bar with N_2; 10 mmol of furfural, 20 mmol acetone, 20 mL toluene, and 400 mg catalyst, t = 3 h.

Temperature (°C)	Conv. (%)	Sel. FAc (%)	Sel. F2Ac (%)	Yield FAc (%)	Yield F2Ac (%)
60	3.8	45.5	54.5	1.7	2.1
80	14.4	50.3	49.7	7.3	7.2
100	35.0	42.5	57.6	14.8	20.1

2.2.2. Influence of Water

Two different approaches were made to study the influence of water on catalytic activity of HTCON-450. On the one hand, the solid was re-hydrated using a N_2 flow saturated in water. On the other hand, reactions were performed in water/toluene mixtures (0%, 5%, 10%, 50%). Regarding the former approach (Table 5), the pretreatment of HTCON-450 with a flow of nitrogen saturated in water results in a drop in conversion (35.0% and 23.7% for HTCON-450 and HTCON-450-rehydrated, respectively, at t = 3 h), whereas selectivity values to F2Ac are quite similar. This suggests that rehydration results in the elimination of active sites to a certain extent, which could be ascribed to solvation. Results obtained for the uncalcined HTCON solid (which exhibits very low catalytic activity) are also given for the sake of comparison.

Table 5. Aldol condensation of furfural and acetone on HTCON-450: Influence of calcination and rehydration of the solid. Reaction conditions: Reactor pressurized to 5 bar with N_2; 10 mmol of furfural, 20 mmol acetone, 20 mL toluene, and 400 mg catalyst, t = 3 h, 100 °C.

Catalyst	Conv. (%)	Sel. FAc (%)	Sel. F2Ac (%)	Yield FAc (%)	Yield F2Ac (%)
HTCON	0.7	85.0	14.9	0.6	0.1
HTCON-450	35.0	42.5	57.6	14.8	20.1
HTCON-450-rehidrated	23.7	40.1	59.8	9.5	14.2

Table 6 summarizes the results obtained for the study conducted using different water/toluene ratios as the reaction medium. As can be seen, the higher the percentage of water, the higher the conversion, but in general, the lower the selectivity to the desired product, F2Ac. In a previous paper [29] on chemoselective hydrogenation of alpha,beta-unsaturated carbonyl compounds, our research group found evidence by Raman spectroscopy that water interacted with the carbonyl group and made the double bond weaker and thus more reactive (carbonyl band shifted to lower wavelength values). The same could occur in the C=O group in furfural and account for its higher conversion in the presence of water. With regards to the change in selectivity, one should consider that we are working in a biphasic media and thus the catalyst hydrophilic character, as well as the relative solubility of reactants and products both in toluene and water, is important. Active sites in the catalyst will probably interact better with water than with toluene. Furfural is partially soluble in water (50–100 $mg \cdot mL^{-1}$). Its condensation with one molecule of acetone will produce FAc, whose solubility in water is much lower (1–10 $mg \cdot mL^{-1}$). Therefore, once formed, FAc will pass to the organic phase (toluene) and will not be able to undergo subsequent condensation with another acetone molecule to produce F2Ac. This results in the increase in selectivity to FAc and probably in conversion, since FAc is retired of the aqueous phase as the reaction proceeds. All in all, the highest yield to F2Ac, the desired product, is

achieved with pure toluene. Therefore, this reaction medium was selected for subsequent studies on other catalysts.

Table 6. Aldol condensation of furfural and acetone on HTCON-450: Influence of the presence of water in water/toluene mixtures. Reaction conditions: Reactor pressurized to 5 bar with N_2; 10 mmol of furfural, 20 mmol acetone, 20 mL (toluene + water) and 400 mg catalyst, t = 3 h, 100 °C.

Water (%)	Conv. (%)	Sel. FAc (%)	Sel. F2Ac (%)	Yield FAc (%)	Yield F2Ac (%)
0	35.0	42.5	57.6	14.8	20.1
5	37.6	60.8	39.2	22.9	14.7
10	53.2	70.3	29.6	37.4	15.8
50	80.4	88.1	11.9	70.8	9.6

2.3. Catalytic Activity of the Other Mixed Oxides

Once pure toluene and 100 °C had been selected as the reaction conditions for aldol condensation of furfural and acetone in order to obtain F2Ac, the study was extended to the other mixed oxides. Reactions were conducted at 3 h and 16 h, the main catalytic results being summarized in Table 7.

A first conclusion from that table is that the lowest conversion values correspond to HTMW-450. It is important to note that this solid was the one exhibiting the lowest pore diameter (4.2 nm, Table 1), which could account for that. Focusing on the other solids, the highest conversion value at 3 h is achieved for HTCON-450, whereas as the reaction proceeds, the rate is higher for the systems synthesized using Pluronic 123, which together with their higher selectivity to F2Ac results in F2Ac yields of 24.6%, 28.3%, and 44.5% for HTCON-450, HTCONP-450, and HTMWP-450, respectively, at t = 16 h. As evidenced by thermal-programmed desorption of pyridine and CO_2, the use of microwave irradiation and/or the presence of Pluronic 123 in the reaction medium during the synthesis resulted in an increase in total acidity and a decrease in total basicity. In a previous paper, Climent et al. [15] described the cooperative effect of weak acid and base sites of an amorphous aluminophosphate in aldol condensation, thus resulting in higher selectivities than those presented by stronger acid or base catalysts. This effect together with the increase in pore size could explain the higher yields obtained for the solids synthesized using the surfactant.

Table 7. Results obtained for aldol condensation of furfural and acetone on the different solids. Reaction conditions: Reactor pressurized to 5 bar with N_2; 10 mmol of furfural, 20 mmol acetone, 20 mL toluene and 400 mg catalyst, 100 °C.

Time (h)	Catalyst	Conv. (%)	Sel. FAc (%)	Sel. F2Ac (%)	Yield FAc (%)	Yield F2Ac (%)
3	HTCON-450	35.0	42.5	57.6	14.8	20.1
	HTMW-450	19.5	63.2	36.8	12.3	7.2
	HTCONP-450	28.4	47.6	52.4	13.5	14.9
	HTMWP-450	32.9	32.9	67.1	10.8	22.1
16	HTCON-450	46.9	47.6	52.4	22.4	24.6
	HTMW-450	27.4	42.9	57.1	11.8	15.7
	HTCONP-450	45.2	37.4	62.6	18.9	28.3
	HTMWP-450	66.2	32.8	67.2	21.7	44.5

2.4. Reutilization of HTCON-450 and HTMWP-450

Finally, some reutilization studies were conducted on HTCON-450 and HTMWP-450 solids, results being summarized in Table 8. In all cases, the Mg/Al ratio of the solids was quite similar to the nominal value (Mg/Al = 2). Moreover, after the reactions, the reaction medium was analyzed by inductively coupled plasma mass spectrometry (ICP-MS). No Mg or Al was detected which is evidence of the stability of the solids, which do not undergo leaching.

Table 8. Results obtained for reutilization studies. Reaction conditions: Reactor pressurized to 5 bar with N_2; 10 mmol of furfural, 20 mmol acetone, 20 mL toluene and 400 mg catalyst, 100 °C.

Catalyst	Conv. (%)	Sel. FAc (%)	Sel. F2Ac (%)	Yield FAc (%)	Yield F2Ac (%)	Mg/Al Ratio (XRF)
HTCON-450	35.0	42.5	57.6	14.8	20.1	2.01
HTCON-450-R	37.4	41.2	58.8	15.4	22.0	2.03
HTMWP-450	32.9	32.9	67.1	10.8	22.1	1.97
HTMWP-450-R	31.1	41.5	58.5	12.9	18.2	1.98
HTMWP-450-R2	34.4	43.5	56.5	15.0	19.4	2.02

As far as the catalytic activity is concerned, neither HTCON-450 nor HTMWP-450 exhibited any remarkable deactivation keeping F2Ac yield in the ca. 20% order after three hours. In the case of the most active solid at long reaction times (HTMWP-450), its activity and selectivity only decreased slightly (from 67.1 to 58.5%) after three consecutive uses.

3. Materials and Methods

Hydrotalcites were synthesized by a co-precipitation method, starting from two solutions containing 0.2 mol $Mg(NO_3)_2{\cdot}6H_2O$ and 0.1 mol $Al(NO_3)_3{\cdot}9H_2O$ in 25 mL deionized water, respectively (Mg/Al = 2). The mixture was slowly added to a pH 10 aqueous solution under continuous stirring and an inert atmosphere (N_2), with temperature maintained at 60 °C. During precipitation, the pH value was maintained, adding NaOH 1M. The suspension was divided into four portions for further treatment. One part was kept under conventional heating at 80 °C for 24 h, followed by filtration and washing with deionized water, thus obtaining the solid called HTCON. A second portion was aged under microwave heating at 80 °C for 1 h, thus leading, after filtration and washing, to the solid termed as HTMW. A flexiWave platform for microwave synthesis (22 V, 50 Hz) with an IR temperature sensor (p/n IRT0500) was used. The other two portions were submitted to the same conventional or microwave heating while performing the synthesis in the presence of surfactant Pluronic 123 (2% by weight), thus leading to the solids named HTCONP and HTMWP, respectively. Finally, all four solids were calcined at 450 °C in the air for 8 h (1 °C·min^{-1} ramp). Nomenclature of these solids include the suffix 450, referring to calcination temperature (HTCON-450, HTMW-450, HTCONP-450, and HTMWP-450). Subsequent treatment of HTCON-450 for 2 h at 450 °C in the presence of a N_2 flow (50 mL·min^{-1}) saturated in water at 20 °C led to a solid called HTCON-450-rehydrated.

A Setaram SetSys 12 instrument (SETARAM Instrumentation, Caluire, France) was used for thermogravimetric analyses (TGA). Experiments were performed on 20 mg samples placed in an alumina crucible and heated in the 30–600 °C range (10 °C·min^{-1}, 50 mL·min^{-1} air stream).

Textural properties (BET surface area, cumulative pore volume, and average pore diameter) were measured in a Micromeritics ASAP-2010 instrument (Micromeritics, Norcross, GA, USA.). Samples were heated at 120 °C and degassed to 0.1 Pa before measurement.

The measure of magnesium or aluminium leaching (presence in filtered reaction medium) was performed by inductively coupled plasma mass spectrometry (ICP-MS) on a Perkin–Elmer ELAN DRC-e instrument.

The Mg/Al ratio of solids was measured by X-ray fluorescence (XRF) spectroscopy (Rigaku ZSK PrimusIV wavelength X-ray spectrometer (Rigaku, The Woodlands, TX, USA). Further details are given elsewhere [30].

Raman spectra were recorded on a Renishaw spectrometer (InVia Raman Microscope, Renishaw, Gloucestershire, UK), equipped with a Leica microscope with various lenses, monochromators, filters, and a CCD detector. Spectra were recorded over the 150–4000 cm^{-1} range, using green laser light excitation (532 nm) and gathering 32 scans.

X-ray diffraction (XRD) analysis was performed on a Siemens D-5000 diffractometer (Bruker Corporation, Billerica, MA, USA) using CuKα radiation over the range 5–80°.

Surface acidity of samples was measured by thermal programmed desorption of pre-adsorbed pyridine (Py-TPD) using TC detection. Samples (30 mg) were cleaned by heating to 450 °C (10 °C·min^{-1}

ramp) under He flow (75 mL·min^{-1}) and then cooled down to 50 °C. The catalysts were subsequently saturated with pyridine for 30 min, cleaned for 60 min with He and TPD monitored from 50 to 450 °C (10 °C·min^{-1}), the final temperature being held for 45 min.

Surface basicity of the catalysts was determined on a Micromeritics Autochem II instrument by thermal programmed desorption of pre-absorbed CO_2 (CO_2-TPD) with TCD detection. Samples (100 mg) were cleaned in an Air stream (20 mL·min^{-1} Ar, heating at 450 °C at a rate of 10 °C·min^{-1} for 60 min and then cooled down to 40 °C). Then, solids were saturated with CO_2 (5% CO_2/Ar flow at 20 mL·min^{-1} for 60 min), physisorbed CO_2 removed with Ar flow (20 mL·min^{-1} for 30min) and TPD monitored from 50 to 450 °C (5 °C·min^{-1}), the final temperature being held for 60 min.

The solids were tested for aldol condensation of furfural using a Berghof HR-100 stainless steel high-pressure autoclave equipped with a 75 mL PTFE insert vessel. Under standard conditions, 10 mmol of furfural, 20 mmol acetone, 20 mL toluene, and a 400 mg catalyst were introduced in the vessel. Reactor was purged with nitrogen and pressurized to 5 bar of N_2. The reaction temperature was set to 100 °C and started by switching on the stirring at 750 rpm. To stop the reaction, the vessel was submerged in an ice bath. The choice of toluene as the organic medium was motivated by a previous paper [3] on xylose dehydration to furfural where toluene was found to give the highest yield to furfural. The final strategy would be to make the one-pot transformation of xylose to furfural and then F2Ac.

Experiments to evaluate the influence of the presence of water in the reaction medium were conducted varying the water/toluene ratio (0%, 5%, 10%, and 50% volume) while keeping the total solvent volume constant (20 mL).

Once the reactions were finished, the products were analyzed by gas chromatography (Agilent 7890) with a flame ionization detector (GC-FID), using a Supelco Nukol™ capillary column. In the case of using biphasic media (toluene/water mixtures), products were extracted from the aqueous phase with dichloromethane before GC-FID analysis. Quantification of furfural and condensation products was performed using the appropriate calibration curves. In all cases, mass balance considering unreacted furfural, FAc, and F2Ac was over 95%.

For reutilization experiments, after the reaction, the solids were filtered, washed with ethanol, and dried at 100 °C, followed by calcination at 450 °C under the same conditions as described in the synthesis. Nomenclature of reused catalysts include the suffix R (one reuse) or R2 (two reuses).

Furfural conversion and FAc and F2Ac selectivity were defined by Equations (1)–(3):

$$\text{Furfural conversion } (\%): \frac{\text{initial furfural concentration} - \text{final furfural concentration}}{\text{initial furfural concentration}} \times 100 \quad (1)$$

$$\text{FAc selectivity } (\%): \frac{\text{FAc concentration}}{\text{FAc concentration} + 2 \cdot \text{F2Ac concentration}} \times 100 \quad (2)$$

$$\text{F2Ac selectivity } (\%): \frac{2 \cdot \text{F2Ac concentration}}{\text{FAc concentration} + 2 \cdot \text{F2Ac concentration}} \times 100 \quad (3)$$

4. Conclusions

The synthesis of hydrotalcites in the presence of Pluronic 123 led, after calcination, to MgAl mixed oxides with bigger pore sizes than untreated solids. On the other hand, microwave irradiation led to smaller pore sizes as compared to conventional thermal treatment. As far as acid–base characteristics are concerned, the use of both microwave irradiation and Pluronic 123 during the synthesis resulted in a decrease of total basicity and an increase in total acidity.

Rehydration of mixed oxides by treating them with a nitrogen flow saturated with water led to solids exhibiting lower catalytic activity in aldol condensation of furfural, probably as a result of the partial blocking (solvation) of active sites. By contrast, the increase in the percentage of water in water/toluene biphasic media resulted in an increase in conversion values, though selectivity to FAc also increased at the expense of the desired product F2Ac. A plausible explanation is that

water weakens the C=O bond in furfural, thus favoring its transformation. Moreover, once FAc is produced, its higher solubility in toluene, as compared to water, favors its transfer to the organic medium, thus avoiding its subsequent reaction with another furfural molecule to yield F2Ac. The fact that the produced FAc is retired to the organic phase could also account for the observed increase in conversion.

A comparison of catalytic activity of the reference material (HTCON-450) with that of the other solids allows us to conclude that the use of Pluronic 123 during synthesis (especially in combination with microwave irradiation) resulted in solids exhibiting higher F2Ac yields at long reaction times. This could be the result of the combination of two factors: The above-mentioned larger pore size achieved with the surfactant and the increase in total acidity which could favor aldol condensation.

HTMWP-450 exhibited a good stability without any significant loss of activity after three uses.

Author Contributions: Conceptualization, C.J.-S. and F.J.U.; methodology, A.M. and J.R.R.; validation, F.J.U., J.R.R. and J.H.-C.; formal analysis, A.M. and J.R.R.; investigation, A.P. and D.C.; data curation, A.M., J.H.-C. and A.P.; writing—original draft preparation, A.P. and D.C.; writing—review and editing, J.H.-C and A.M.; supervision, C.J.-S. and F.J.U.

Funding: This research was funded by Ramón Areces Foundation.

Acknowledgments: The scientific support from the Central Service for Research Support (SCAI) at the University of Cordoba is acknowledged.

Conflicts of Interest: The authors declare no conflict of interest.

References

1. Field, C.B.; Campbell, J.E.; Lobell, D.B. Biomass energy: The scale of the potential resource. *Trends Ecol. Evol.* **2008**, *23*, 65–72. [CrossRef] [PubMed]
2. Chheda, J.N.; Huber, G.W.; Dumesic, J.A. Liquid-phase catalytic processing of biomass-derived oxygenated hydrocarbons to fuels and chemicals. *Angew. Chem. Int. Ed.* **2007**, *46*, 7164–7183. [CrossRef] [PubMed]
3. Parejas, A.; Montes, V.; Hidalgo-Carrillo, J.; Sanchez-Lopez, E.; Marinas, A.; Urbano, F.J. Microemulsion and Sol-Gel Synthesized ZrO2-MgO Catalysts for the Liquid-Phase Dehydration of Xylose to Furfural. *Molecules* **2017**, *22*, 2257. [CrossRef] [PubMed]
4. Sheldon, R.A. Green and sustainable manufacture of chemicals from biomass: State of the art. *Green Chem.* **2014**, *16*, 950–963. [CrossRef]
5. O'Neill, R.E.; Vanoye, L.; De Bellefon, C.; Aiouache, F. Aldol-condensation of furfural by activated dolomite catalyst. *Appl. Catal. B Environ.* **2014**, *144*, 46–56. [CrossRef]
6. Smolakova, L.; Frolich, K.; Kocik, J.; Kikhtyanin, O.; Capek, L. Surface Properties of Hydrotalcite-Based Zn(Mg)Al Oxides and Their Catalytic Activity in Aldol Condensation of Furfural with Acetone. *Ind. Eng. Chem. Res.* **2017**, *56*, 4638–4648. [CrossRef]
7. Faba, L.; Díaz, E.; Ordóñez, S. Aqueous-phase furfural-acetone aldol condensation over mixed oxides. *Appl. Catal. B Environ.* **2012**, *113–114*, 201–211. [CrossRef]
8. Chheda, J.N.; Dumesic, J.A. An overview of dehydration, aldol-condensation and hydrogenation processes for production of liquid alkanes from biomass-derived carbohydrates. *Catal. Today* **2007**, *123*, 59–70. [CrossRef]
9. Climent, M.J.; Corma, A.; Iborra, S. Conversion of biomass platform molecules into fuel additives and liquid hydrocarbon fuels. *Green Chem.* **2014**, *16*, 516–547. [CrossRef]
10. Shen, W.Q.; Tompsett, G.A.; Hammond, K.D.; Xing, R.; Dogan, F.; Grey, C.P.; Conner, W.C.; Auerbach, S.M.; Huber, G.W. Liquid phase aldol condensation reactions with MgO-ZrO2 and shape-selective nitrogen-substituted NaY. *Appl. Catal. A Gener.* **2011**, *392*, 57–68. [CrossRef]
11. Cota, I.; Ramirez, E.; Medina, F.; Sueiras, J.E.; Layrac, G.; Tichit, D. New synthesis route of hydrocalumite-type materials and their application as basic catalysts for aldol condensation. *Appl. Clay Sci.* **2010**, *50*, 498–502. [CrossRef]
12. West, R.M.; Liu, Z.Y.; Peter, M.; Gaertner, C.A.; Dumesic, J.A. Carbon-carbon bond formation for biomass-derived furfurals and ketones by aldol condensation in a biphasic system. *J. Mol. Catal. A Chem.* **2008**, *296*, 18–27. [CrossRef]

13. Daniel, E.; Resasco, S.S.; Faria, J.; Prasomsri, T.; Ruiz, A.M.P. Furfurals as chemical platform forbiofuels production. In *Heterogeneous Catalysis in Biomass to Chemicals and Fuels*; D.K.A.I., Ed.; Stanford Court: Irvine, CA, USA, 2011.
14. Bao, Q.; Qi, H.; Zhang, C.; Ning, C.; Zhang, Y.; Wu, Y.; Gui, W.; Wang, Z. Highly Catalytic Activity of Ba/γ-Ti–Al2O3 Catalyst for Aldol Condensation of Methyl Acetate with Formaldehyde. *Catal. Lett.* **2018**, *148*, 3402–3412. [CrossRef]
15. Climent, M.J.; Corma, A.; Fornés, V.; Guil-Lopez, R.; Iborra, S. Aldol condensations on solid catalysts: A cooperative effect between weak acid and base catalysts. *Adv. Synth. Catal.* **2002**, *344*, 1090–1096. [CrossRef]
16. Fakhfakh, N.; Cognet, P.; Cabassud, M.; Lucchese, Y.; Rios, M.D.D.L. Stoichio-kinetic modeling and optimization of chemical synthesis: Application to the aldolic condensation of furfural on acetone. *Chem. Eng. Process.* **2008**, *47*, 349–362. [CrossRef]
17. Xing, R.; Subrahmanyam, A.V.; Olcay, H.; Qi, W.; van Walsum, G.P.; Pendse, H.; Huber, G.W. Production of jet and diesel fuel range alkanes from waste hemicellulose-derived aqueous solutions. *Green Chem.* **2010**, *12*, 1933–1946. [CrossRef]
18. Patel, A.A.; Patel, S.R. Synthesis and characterization of furfural-acetone polymers. *Eur. Polym. J.* **1983**, *19*, 231–234. [CrossRef]
19. Gandini, A.; Belgacem, M.N. Furans in polymer chemistry. *Prog. Polym. Sci.* **1997**, *22*, 1203–1379. [CrossRef]
20. Hora, L.; Kelbichova, V.; Kikhtyanin, O.; Bortnovskiy, O.; Kubicka, D. Aldol condensation of furfural and acetone over Mg-Al layered double hydroxides and mixed oxides. *Catal. Today* **2014**, *223*, 138–147. [CrossRef]
21. Ordonez, S.; Diaz, E.; Leon, M.; Faba, L. Hydrotalcite-derived mixed oxides as catalysts for different C-C bond formation reactions from bioorganic materials. *Catal. Today* **2011**, *167*, 71–76. [CrossRef]
22. Choudary, B.M.; Kantam, M.L.; Sreekanth, P.; Bandopadhyay, T.; Figueras, F.; Tuel, A. Knoevenagel and aldol condensations catalysed by a new diamino-functionalised mesoporous material. *J. Mol. Cataly. A Chem.* **1999**, *142*, 361–365. [CrossRef]
23. Aramendia, M.A.; Aviles, Y.; Borau, V.; Luque, J.M.; Marinas, J.M.; Ruiz, J.R.; Urbano, F.J. Thermal decomposition of Mg Al and Mg Ga layered-double hydroxides: A spectroscopic study. *J. Mater. Chem.* **1999**, *9*, 1603–1607. [CrossRef]
24. Morato, A.; Alonso, C.; Medina, F.; Cesteros, Y.; Salagre, P.; Sueiras, J.E.; Tichit, D.; Coq, B. Palladium hydrotalcites as precursors for the catalytic hydroconversion of CCl2F2 (CFC-12) and CHClF2 (HCFC-22). *Appl. Catal. B Environ.* **2001**, *32*, 167–179. [CrossRef]
25. Xu, C.; Gao, Y.; Liu, X.; Xin, R.; Wang, Z. Hydrotalcite reconstructed by in situ rehydration as a highly active solid base catalyst and its application in aldol condensations. *RSC Adv.* **2013**, *3*, 793–801. [CrossRef]
26. Frost, R.L.; Palmer, S.J.; Theiss, F. Synthesis and Raman spectroscopic characterisation of hydrotalcites based on the formula $Ca_6Al_2(CO_3)(OH)_{16}{\cdot}4H_2O$. *J. Raman Spectrosc.* **2010**, *42*, 1163–1167. [CrossRef]
27. Frost, R.L.; Erickson, K.L. Vibrational spectroscopic study of the nitrate containing hydrotalcite Mbobomkulite, Spectrochim. *Acta Part A* **2005**, *61*, 2919–2925. [CrossRef] [PubMed]
28. Mahtab, P.; Seyed-Rasulzade, S.K.; Nikzad-Kojanag, B. Effect of Preparation Methods and Pluronic Template on the Catalytic Activity of Ca/SBA-15. *Iran. J. Chem. Chem. Eng.* **2018**, *37*, 53–60.
29. Hidalgo-Carrillo, J.; Marinas, A.; Marinas, J.M.; Delgado, J.J.; Raya-Miranda, R.; Urbano, F.J. Water as solvent in the liquid-phase selective hydrogenation of crotonaldehyde to crotyl alcohol over Pt/ZnO: A factorial design approach. *Appl. Catal. B Environ.* **2014**, *154*, 369–378. [CrossRef]
30. Cosano, D.; Esquivel, D.; Mateos, L.D.; Quesada, E.; Jiménez-Sanchidrián, C.; Ruiz, J.R. Spectroscopic analysis of corrosion products in a bronze cauldron from the Late Iberian Iron Age. *Spectrochim. Acta Part A Mol. Biomol. Spectrosc.* **2018**, *205*, 489–496. [CrossRef] [PubMed]

© 2019 by the authors. Licensee MDPI, Basel, Switzerland. This article is an open access article distributed under the terms and conditions of the Creative Commons Attribution (CC BY) license (http://creativecommons.org/licenses/by/4.0/).

catalysts

MDPI

Article

MPV Reduction of Furfural to Furfuryl Alcohol on Mg, Zr, Ti, Zr–Ti, and Mg–Ti Solids: Influence of Acid–Base Properties

Jesús Hidalgo-Carrillo, Almudena Parejas, Manuel Jorge Cuesta-Rioboo, Alberto Marinas * and Francisco José Urbano

Departamento de Química Orgánica, Instituto Universitario de Investigación en Química Fina y Nanoquímica IUIQFN, Universidad de Córdoba, Campus de Rabanales, Edificio Marie Curie, E-14071 Córdoba, Spain; yimo@hotmail.com (J.H.-C.); q12pabaa@uco.es (A.P.); qo2maara@uco.es (M.J.C.-R.); qo1urnaf@uco.es (F.J.U.)
* Correspondence: alberto.marinas@uco.es; Tel.: +34-957-218-622

Received: 1 October 2018; Accepted: 9 November 2018; Published: 13 November 2018

Abstract: The Meerwein–Ponndorf–Verley (MPV) reaction is an environmentally-friendly process consisting of the reduction of a carbonyl compound through hydrogen transfer from a secondary alcohol. This work deals with MPV reduction of furfural to furfuryl alcohol on different ZrO_x, MgO_x, TiO_x, and Mg–Ti, as well as Zr–Ti mixed systems. The solids were synthesized through the sol–gel process and subsequently calcined at 200 °C. Characterization was performed using a wide range of techniques: ICP-MS, N_2 adsorption-desorption isotherms, EDX, TGA-DTA, XRD, XPS, TEM, TPD of pre-adsorbed pyridine (acidity) and CO_2 (basicity), DRIFT of adsorbed pyridine, and methylbutynol (MBOH) test reaction. ZrO_x showed the highest conversion and selectivity values, which was attributed to the existence of acid–base pair sites (as evidenced by the MBOH test reaction), whereas the introduction of titanium resulted in the drop of both conversion and selectivity probably due to the increase in Brönsted-type acidity. As for MgO_x, it had a predominantly basic character that led to the production of the condensation product of one molecule of furfural and one molecule of acetone, and thus resulted in a lower selectivity to furfuryl alcohol. The TiO_x solid was found to be mainly acidic and exhibited both Lewis and Brönsted acid sites. The presence of the latter could account for the lower selectivity to furfuryl alcohol. All in all, these results seemed to suggest that the MPV reaction is favored on Lewis acid sites and especially on acid–base pair sites. The process was accelerated under microwave irradiation.

Keywords: furfural; MPV reaction; acid–base characterization; methylbutynol test reaction

1. Introduction

The transformation of natural residues from agriculture into platform molecules is one of the promising research lines in obtaining high added value chemical products [1,2]. One of those platform molecules is furfural [3], which can be obtained from lignocellulose [4]. It contains an aromatic ring and an aldehyde group which makes it a versatile molecule to obtain a wide range of chemical compounds [5], and one of the most important ones is furfuryl alcohol. This alcohol is widely used in the production of thermostatic resins, rubbers, fibers, adhesives, and some fine chemicals [5–7]. Furfuryl alcohol is mainly produced by furfural hydrogenation. Approximately 60% of the furfural produced is used to synthesize furfuryl alcohol. The catalytic liquid-phase hydrogenation of furfural to produce furfuryl alcohol has been extensively investigated in the presence of catalysts based on Ni, Co, Cu, Pt, and Pd [8–12]. Cu–Cr-based catalysts are commonly used in the industry, but environmentally friendlier catalysts are required. The transformation of furfural to furfuryl alcohol can also be carried

out through the hydrogen transfer from a donor, which are typically secondary alcohols such as propan-2-ol, using the so-called Meerwein–Ponndorf–Verley (MPV) process [13]. This reaction involves the formation of a six-membered ring transition state in which both the reducing alcohol and the carbonyl compound are coordinated to the metal center (Lewis site) [14]. The assistance of the basic sites has also been proposed for the formation of the six-membered ring [15].

A wide range of heterogeneous catalysts has been described for the MPV process such as zirconia [16,17], mesoporous silica [18,19], zeolites [20], and alumina [21,22].

In previous papers, our research group described that zirconium gels calcined at low temperatures (ca. 200 °C) were quite selective to the corresponding unsaturated alcohol [16,17] in the MPV process. In the present work, different gels consisting of pure ZrO_x, TiO_x, and MgO_x, or mixed Mg–Ti and Zr–Ti solids and calcined at 200 °C were synthesized and tested in the MPV reduction of furfural to furfuryl alcohol to try and cast further light on the nature of the active sites responsible for the desired catalytic activity. The possibility of carrying out the reaction with microwave-assisted heating was also evaluated.

2. Results and Discussion

2.1. Textural, Structural, and Acid–Base Characterization of the Solids

The Brunnauer–Emmett–Teller (BET) surface areas as well as Mg/Ti and Zr/Ti atomic ratios (both nominal and experimental) of the synthesized solids are depicted in Table 1. The highest BET areas (in the 219–263 m^2/g range) corresponded to solids consisting of Zr and/or Ti, whereas lower values were found for the systems containing magnesium (42–81 m^2/g). In regard to the chemical composition, experimental results were in general quite similar to the nominal values and was thus evidence of a good precipitation of the metals during the synthesis.

Table 1. Brunnauer–Emmett–Teller (BET) surface area and atomic composition (nominal and experimental) of the different solids synthesized in the present study.

Catalyst	BET Surface Area (m^2/g)	M/Ti Ratio (M = Zr or Mg)		
		Nominal	ICP-MS	XPS
ZrO_x	221	-	-	-
Zr3Ti1	251	3.0	2.43	2.29
ZrTi	263	1.0	0.78	1.03
Zr1Ti3	219	0.33	0.34	0.45
TiO_x	232	-	-	-
Mg1Ti3	42	0.33	0.45	0.39
MgTi	81	1.0	1.06	0.62
Mg3Ti1	68	3.0	3.02	3.5
MgO_x	66	-	-	-

The TGA-DTA profiles of the different solids are shown in Figures 1 and 2 (Zr–Ti and Mg–Ti solids, respectively). The ZrO_x heat flow profile (Figure 1B) exhibited two main peaks centered at ca. 104 °C and 436 °C, respectively. The first endothermal peak corresponded to the loss of water whereas the second peak was the so-called glow exotherm attributed to the crystallization of zirconia [17,23]. For Zr–Ti mixed systems, the glow-exotherm was shifted to higher temperatures (450–466 °C) which suggests that titanium retards zirconium crystallization. In the case of MgO_x solids (Figure 2B), the heat flow profile exhibited two main endothermal peaks centered at ca. 117 °C and 385 °C. The latter peak was assigned to the transformation of $Mg(OH)_2$ into MgO [24]. For Mg–Ti solids, the presence of titanium seemed to favor such a transformation as evidenced by the shift of the peak to lower temperatures (in the 318–357 °C range).

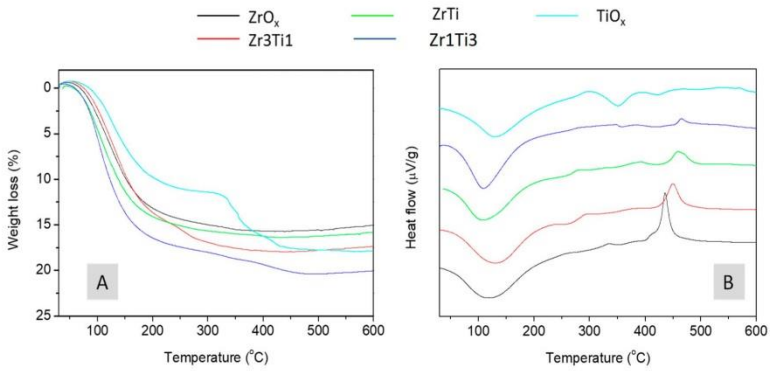

Figure 1. TG-DTA profiles of the precursor gels of the catalysts based on ZrO_x and TiO_x. Weight loss (**A**) and heat flow (**B**) profiles.

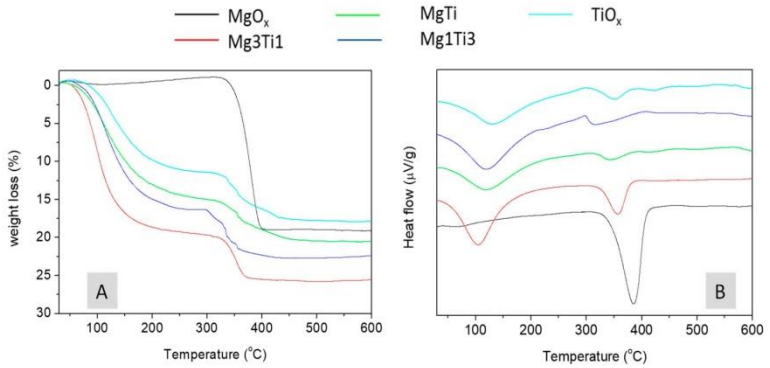

Figure 2. TG-DTA profiles of the precursor gels of catalysts based on MgO_x and TiO_x. Weight loss (**A**) and heat flow (**B**) profiles.

X-ray diffractograms of Zr-containing solids (Figure 3) showed evidence of their amorphous character, which was consistent with the TGA-DTA profiles; crystallization occurred at temperatures above 300 °C. In the case of MgO_x (Figure 3B), there were some peaks present due to the $Mg(OH)_2$ brookite structure. Those peaks were also evident in Mg3Ti1 solid whereas higher titanium contents resulted in the disappearance of brookite signals and the appearance of some new signals which could be assigned to MgO5Ti2 pseudobrookite.

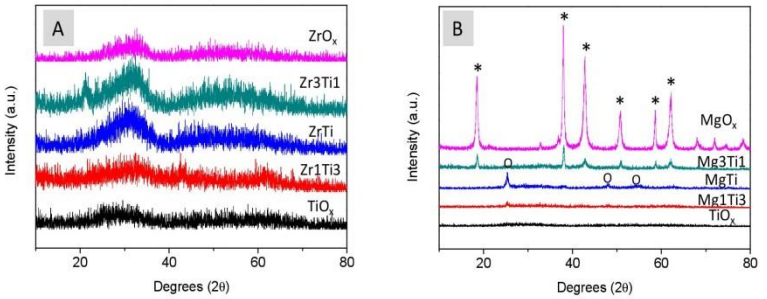

Figure 3. X-ray diffractograms of the different solids synthesized in the present work. Zr-Ti solids (**A**) and Mg-Ti systems (**B**). The corresponding pure compounds have also been included for the sake of comparison. * and ○ denote brookite and pseudobrookite phases, respectively.

Transmission electron microscopy (TEM) images of all the samples are represented in Figure 4. As can be seen in the central part of Figure 4, MgO_x, ZrO_x, and TiO_x exhibited quite different textures which allowed us to distinguish them in mixed solids.

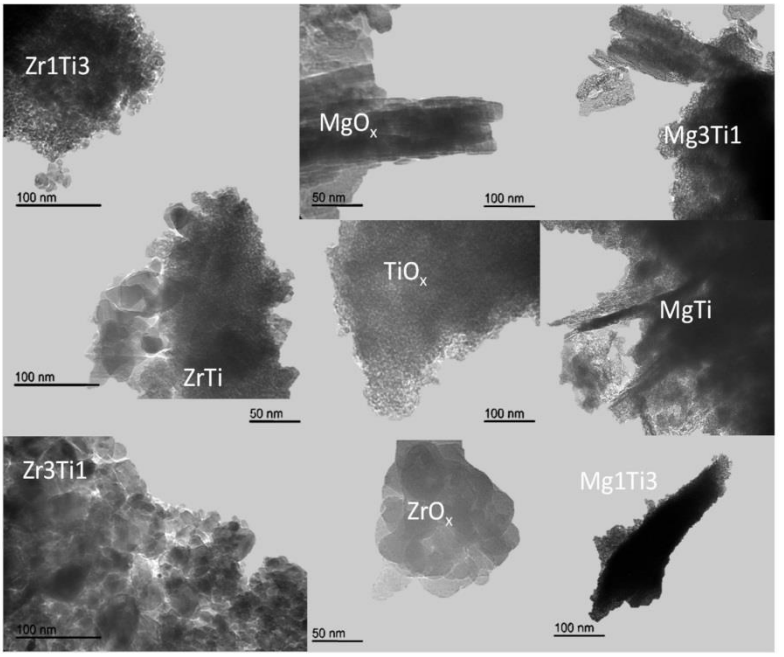

Figure 4. Transmission electron microscopy (TEM) images of the different solids.

X-ray photoelectron spectroscopy (XPS) profiles of Mg–Ti solids are represented in Figure 5. The signal for Mg1 in MgO_x presented two types of magnesium atoms. Moreover, as titanium content increased, there was a shift of signals to higher binding energies (from 1303.0 to 1303.8 eV for MgO_x

and Mg1Ti3, respectively). A similar trend was observed for the Ti(2p) signal, and the Ti2p3/2 signal shifted, in this case, to lower binding energies in the presence of magnesium (Ti2p3/2 signal at 458.4 and 458.1 eV for TiO_x and Ti3Mg1, respectively). These results suggest the existence of some Mg–Ti interaction in Mg–Ti solids.

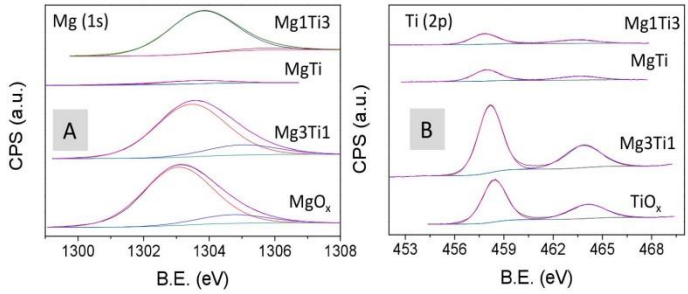

Figure 5. X-ray photoelectron spectroscopy (XPS) profiles of Mg(1s) (**A**) and Ti (2p) (**B**) in Mg–Ti solids.

As far as the Zr–Ti XPS profiles were concerned (Figure 6), there was suggestion of some Zr–Ti interaction as evidenced by the Zr3d and Ti2p signals shifting to higher and lower binding energy values, respectively, as the Ti content increased.

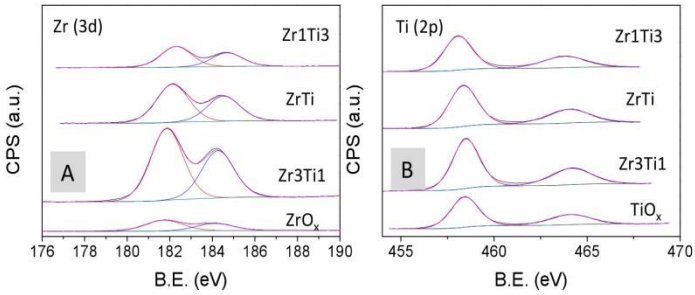

Figure 6. XPS profiles of Zr(3d) (**A**) and Ti (2p) (**B**) in Zr–Ti solids.

Surface acid–base characterization of the solids was carried out by TPD of pre-adsorbed CO_2 (basicity) and pyridine (acidity), and the main results are summarized in Table 2. As can be seen, ZrO_x exhibited a good balance between acid and basic sites (CO_2/py = 1.09), TiO_x was mainly acidic (CO_2/Py = 0.57) and MgO_x was a predominantly basic solid (CO_2/py = 3.39). As for the corresponding mixed solids, they all had an acid–base characteristic between the corresponding pure solids.

Table 2. Acid–base characteristics of the solids as determined by CO_2-TPD and Py-TPD, respectively.

Catalyst	µmol CO_2/g	µmol Py/g	CO_2/Py
ZrO_x	774	707	1.09
Zr3Ti1	728	753	0.97
ZrTi	658	921	0.71
Zr1Ti3	460	635	0.72
TiO_x	371	650	0.57
Mg1Ti3	508	622	0.82
MgTi	1126	616	1.83
Mg3Ti1	1142	354	3.22
MgO_x	1096	323	3.39

Complementary acid–base results could be obtained using the methylbutynol test reaction (Figure 7) which allow us to distinguish between acid, base, and acid–base pair sites.

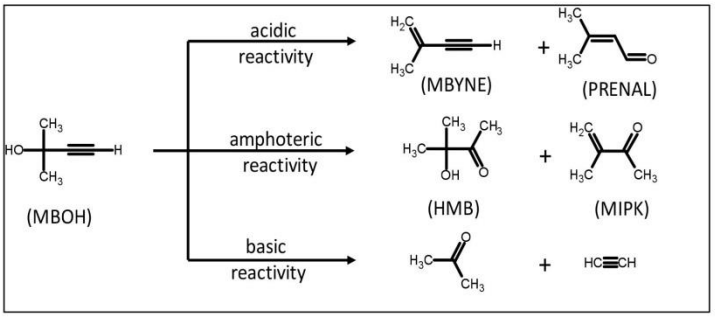

Figure 7. Overall reaction scheme as proposed by Lauron-Pernot et al. [25]. MBOH, 2-methyl-3-butyn-2-ol; MBYNE, 3-methyl-3-buten-1-yne; PRENAL, 3-methyl-2-buten-1-al; HMB, 3-hydroxy-3-methyl-2-butatone; MIPK, 3-methyl-3-buten-2-one.

As can be seen in Table 3, the methylbutynol (MBOH) test reaction confirmed the results found in the TPD studies of pre-adsorbed CO_2 and pyridine. Therefore, MgO_x mainly yielded acetone and acetylene (basic reactivity, 96.2% selectivity), TiO_x was mainly acidic (73.1% selectivity), and ZrO_x was predominantly amphoteric (53.4%) and mainly yielded 3-methyl-3-buten-2-one (MIPK). This was evidence for the presence of acid–base pair sites in ZrO_x.

Table 3. MBOH reaction. Comparison between selectivities of the pure oxides. The reaction conditions were as follows: microcatalytic pulse reactor; 20 mg catalyst, 200 °C, methylbutynol (MBOH) pulses of 0.5 µL (see experimental section).

Catalyst	Conversion (%)	S_{basic} (%)	S_{acid} (%)	$S_{amphoteric}$ (%)
MgO_x	5.6	96.2	3.8	0
TiO_x	1.0	12.3	73.1	14.6
ZrO_x	1.0	26.3	20.3	53.4

Further diffuse reflectance infrared Fourier transform (DRIFT) pyridine studies were performed on Zr–Ti solids to distinguish between Lewis and Brönsted acid sites (Figure 8). Peaks observed at 1443 and 1603 cm^{-1} were attributed to the presence of pyridine adsorbed on Lewis acid sites, whereas the band at ca. 1486 cm^{-1} could be due to adsorbed pyridine on both Lewis and Brönsted sites [26]. The signal at ca. 1534 cm^{-1} corresponded to pyridine on Brönsted acid sites [27]. An estimation

of the Lewis/Brönsted acid site ratio can be made by integrating signals using the molar extinction coefficients [28]. Therefore, Lewis/Brönsted values of 15.4 and 4.9 could be obtained for ZrO_x and TiO_x, respectively.

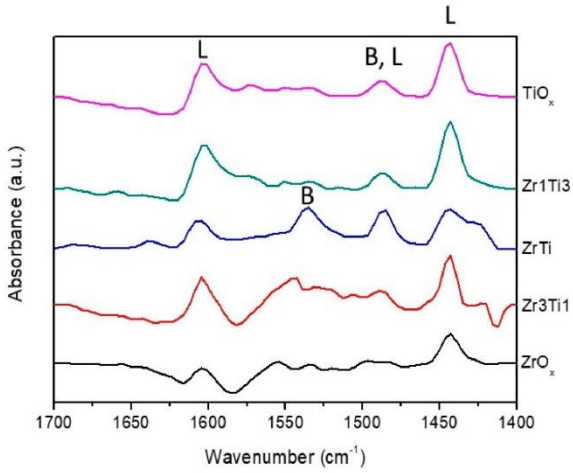

Figure 8. Diffuse reflectance infrared Fourier transform (DRIFT) studies of pyridine chemisorbed on the Zr–Ti solids. B and L stand for Brönsted and Lewis acid sites, respectively.

All in all, the acid–base studies indicated that MgO_x was mainly basic, ZrO_x was amphoteric, and TiO_x was acidic. Moreover, the highest Lewis/Brönsted site ratio corresponded to ZrO_x solids.

2.2. *Catalytic Activity in Furfural Hydrogenation into Furfuryl Alcohol*

The solids were then tested for liquid-phase MPV reduction of furfural to furfuryl alcohol (FUOL) using propan-2-ol as the hydrogen donor. The main results are summarized in Table 4.

Table 4. Results obtained for experiments under conventional (t = 20 h) and microwave (t = 2 h) heating on the different solids expressed in terms of conversion, selectivity to furfuryl alcohol (FUOL), and FUOL yield. The reaction conditions were as follows: 100 °C, molar propan-2-ol/furfural ratio of 10.8, and furfural/catalyst weight ratio of 5.8. Maximum microwave power was set at 300 W.

Catalyst	Conventional Heating			Microwave Heating		
	Conversion (%)	Selectivity FUOL (%)	Yield FUOL (%)	Conversion (%)	Selectivity FUOL (%)	Yield FUOL (%)
ZrO_x	50.1	90.4	45.3	27.6	96.8	26.7
Zr3Ti1	42.9	88.2	37.8	19.8	97.9	19.4
ZrTi	30.2	79.0	23.9	20.9	75.2	15.7
Zr1Ti3	22.3	80.5	18.0	17.1	79.5	13.6
TiO_x	16.2	68.7	11.1	7.4	53.5	4.0
Mg1Ti3	11.6	35.4	4.1	7.2	31.5	2.3
MgTi	13.4	46.6	6.3	8.6	47.8	3.1
Mg3Ti1	15.8	48.0	7.6	7.4	46.0	3.4
MgO_x	15.2	56.0	8.5	7.9	57.8	4.6

Firstly, the solids were tested under conventional heating. As can be seen, ZrO_x was the most active solid, followed by TiO_x and MgO_x. Both conversion and selectivity to furfuryl alcohol

dropped upon the introduction of titanium in Zr–Ti and Mg–Ti solids. This seems to indicate that the interaction evidenced by XPS (and also suggested by TGA-DTA profiles) is detrimental to activity. In the case of MgO_x, the main by-product was the condensation product between one molecule of furfural and one molecule of acetone. Microwave heating was also tested, and results for t = 2 h are given in Table 4. The reactions were indeed accelerated under microwave irradiation. For instance, for t = 2 h, conversions of 6.5% (not shown) and 27.6% as well as selectivities of 97.0 and 96.8% to furfuryl alcohol were achieved on ZrO_x under conventional and microwave heating, respectively. The results under microwave irradiation confirmed the observed activity trend in experiments under conventional heating.

The higher selectivity values (over 90%) found for ZrO_x could be ascribed to the existence of acid–base pair sites. As suggested by Komanoya et al. [29], there would be a synergistic effect of acid–base pair sites: base sites could activate methylene groups in propan-2-ol bonded to Lewis sites. A tentative reaction mechanism on those acid–base pair sites is presented in Figure 9. The better catalytic performance of ZrO_x as compared to TiO_x could also be explained as the result of Lewis sites being more active than Brönsted sites in the MPV reaction [30,31].

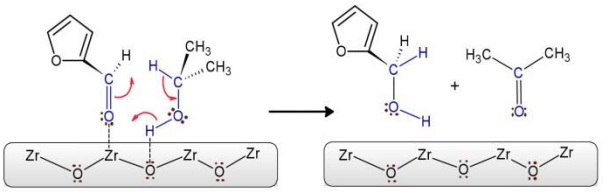

Figure 9. Suggested mechanism for furfural hydrogenation into furfuryl alcohol on acid–base pair sites in ZrO_x through transfer hydrogenation from propan-2-ol.

3. Materials and Methods

For the synthesis of the catalysts, the following compounds were used: aqueous solutions of ammonium hydroxide (5 N) (Fluka 318620-2L, Honeywell, Bucharest, Romania) and hydrochloric acid (1 M) (Fluka 318949-2L); propan-2-ol (Sigma-Aldrich 190764-2.5L, Merck KGaA, Darmstadt, Germany); hydrated zirconium(IV) oxynitrate (Sigma-Aldrich 346462, Merck KGaA, Darmstadt, Germany); magnesium nitrate hexahydrate (Sigma-Aldrich 237175-1KG, Merck KGaA, Darmstadt, Germany); and titanium isopropoxide (Sigma-Aldrich 20527-3, Merck KGaA, Darmstadt, Germany).

The synthesis of the catalysts was carried out by the sol–gel method [32], following previous studies in our research group [17,33–35].

Two types of mixed systems were synthesized: titanium gels with magnesium and titanium gels with zirconium, with different (Mg or Zr)/Ti molar ratios (0%, 25%, 50%, 75%, and 100%). The syntheses were carried out at a constant pH of 10 with magnetic stirring at 700 rpm. The pH was kept constant using a pump (Atlas syringe pump, Syrris, (Hertfordshire, UK), which added 5 N ammonium hydroxide or 1 M hydrochloric acid throughout the synthesis process. The precipitate was filtered, washed with water, dried at 120 °C overnight, and calcined at 200 °C for 8 h. After calcination, the catalysts were sieved (0.149 μm). The nomenclature of the solids was as follows: TiO_x, ZrO_x, and MgO_x for solids based on pure titanium, zirconium, and magnesium gels, respectively. For mixtures of gels, the nomenclature included the symbol of the metals followed by a number referring to their atomic ratio in the mixture. For instance, Mg3Ti1 indicates a magnesium–titanium system containing 75% Mg and 25% Ti (i.e., Mg/Ti atomic ratio of 3).

Thermogravimetric analyses (TGA) were performed on a Setaram SetSys 12 instrument (Caluire, France). A 20 mg amount of sample (precursor gels of the catalysts) was placed in an alumina crucible and heated at temperatures ranging from 30 to 600 °C (heating rate of 10 °C/min) under a synthetic air stream (50 mL/min) in order to measure weight loss, heat flow, and derivative weight loss.

X-ray photoelectron spectroscopy (XPS) data were recorded at the Central Service for Research Support (SCAI) of the University of Córdoba on 4 mm × 4 mm pellets of 0.5 mm thickness that were obtained by gently pressing the powered materials. The samples were outgassed to a pressure below about 2×10^{-8} Torr at 150 °C in the instrument pre-chamber to remove chemisorbed volatile species. The main chamber of the Leibold-Heraeus LHS10 spectrometer used, which is capable of operating down to less than 2×10^{-9} Torr, was equipped with a EA-200MCD hemispherical electron analyzer with a dual X-ray source using Al Kα (hυ = 1486.6 eV) at 120 W and 30 mA. C (1 s) was used as the energy reference (284.6 eV).

Transmission electron microscopy (TEM) images were obtained at the Central Service for Research Support (SCAI) of the University of Córdoba using a JEOL JEM 1400 microscope available at SCAI. The samples were mounted on 3 mm holey carbon copper grids.

X-ray patterns of the samples in the 10−80° (2θ) range was registered in a D8 Advanced Diffractometer (Bruker AXS) equipped with a Lynxeye detector.

Surface areas of solids were obtained from nitrogen adsorption-desorption isotherms obtained at liquid nitrogen temperature on a Micromeritics ASAP-2010 instrument following the Brunnauer–Emmett–Teller (BET) method. All samples were degassed to 0.1 Pa at 120 °C before measurement.

Surface basicity of the catalysts was determined on a Micromeritics Autochem II instrument by thermal programmed desorption of pre-absorbed CO_2 (TPD-CO_2) with TCD detection. An amount of 100 mg of each catalyst was loaded into a reactor of 10 mm ID and placed in a furnace. Solids were cleaned with an Ar stream (20 mL/min) by heating to 200 °C at a rate of 10 °C/min for 60 min and then cooled down to 40 °C. At that temperature, the catalysts were saturated with the probe molecule using 5% CO_2/Ar flow at 20 mL/min for 60 min. After saturation, physisorbed CO_2 was removed by a flowing Ar stream for 30 min (20 mL/min). Then, the temperature-programmed desorption of chemisorbed CO_2 was carried out by ramping the temperature from 40 to 200 °C (heating rate 5 °C/min) and holding the final temperature for 60 min. The amount of CO_2 adsorbed was determined from a calibration graph constructed from the injection of variable volumes of 5% CO_2/Ar.

The surface acidity of the catalysts was determined by thermal programmed desorption of pre-adsorbed pyridine (TPD-PY) with TCD detection. A 30 mg amount of sample was introduced in a 10 mm ID reactor that was placed inside an oven. The solids were cleaned under a He flow (75 mL/min) by heating to 200 °C at a rate of 10 °C/min and then cooled down to 50 °C. At that temperature, the solids were exposed for 30 min to a pyridine-saturated He flow. After saturation, physisorbed pyridine was removed by flowing a pure He stream for 60 min (75 mL/min). Then, the temperature-programmed desorption of chemisorbed pyridine was carried out by ramping the temperature from 50 to 200 °C (heating rate 10 °C/min) and holding the final temperature for 30 min. Desorbed pyridine was quantified against a calibration graph constructed from variable volumes of pyridine injected.

Complementary studies using diffuse reflectance infrared Fourier transform (DRIFT) spectra of adsorbed pyridine were carried out on a FTIR instrument (Bomem MB-3000, ABB Corporate, Zurich, Switzerland) equipped with an "environmental chamber" (Spectra Tech, Jefferson Court, Oak Ridge, TN, USA) placed in a diffuse reflectance attachment (Spectra Tech, Collector). A resolution of 8 cm^{-1} was used with 256 scans averaged to obtain a spectrum from 4000 to 400 cm^{-1}. In each measurement, the reference was the same sample after heating at 150 °C. Pyridine adsorption was carried out at 150 °C for 45 min to allow the saturation of the catalyst surface. The physisorbed pyridine was then cleaned with a N_2 flow (50 mL/min) and its spectrum was registered.

The MBOH test reaction was carried out as described elsewhere [36]. A microcatalytic pulse reactor (1/8 in i.d. quartz tubular reactor) was placed in the injection port of a gas chromatograph (GC System 7890A, Agilent Technologies, Santa Clara, CA, USA). The reactor was packed with alternating layers of quartz wool with the catalyst (20 mg) placed between them. Prior to each run,

the catalyst was pre-treated in the reactor at 200 °C for 2 h under nitrogen (75 mL/min). MBOH pulses of 0.5 µL were then carried out.

The MPV reaction of furfural was carried out under conventional heating in a Carousel 12 Plus™ Reaction Station, Discovery Technologies, and reactions under microwaves were carried out in a CEM-DISCOVER apparatus with PC control. In both cases, temperature was 100 °C. Maximum microwave power was set at 300 W. The reactions by conventional heating were carried out with 100 mg of catalyst, 5 mL of propan-2-ol, and 0.5 mL of furfural over 20 h; the reactions in the microwave oven kept the same catalyst, propan-2-ol, and furfural ratios at a volume of reaction of 2 mL with a reaction time of 2 h. Analysis of reaction products was carried out by gas chromatography (GC-FID System 7890A, Agilent Technologies, equipped with a HP-5 chromatographic column) using the corresponding calibration graphs.

4. Conclusions

Several solids consisting of pure magnesium, zirconium, titanium, and mixed magnesium–titanium as well as zirconium–titanium gels were obtained through the sol–gel process and calcined at 200 °C. The presence of titanium retarded the crystallization of zirconium oxide whereas transformation of $Mg(OH)_2$ into MgO was favored in the presence of titanium. XPS results also suggested the existence of some Mg–Ti and Zr–Ti interaction in mixed gels. In regard to the acid–base properties as determined from the TPD of pre-adsorbed pyridine and CO_2, the ZrO_x system exhibited a good balance between acid and base sites, whereas TiO_x and MgO_x were predominantly acidic and basic, respectively. The MBOH test reaction evidenced the presence of acid–base pair sites in ZrO_x, and pyridine DRIFT studies showed that acid sites in ZrO_x were mainly of the Lewis type whereas both Brönsted and Lewis sites were present in TiO_x and Zr–Ti mixed solids. The most active and selective catalyst in the MPV reduction of furfural to furfuryl alcohol was ZrO_x whereas both parameters decreased in Zr–Ti solids as the titanium content increased. These results suggest that acid–base pair sites are particularly active in MPV reduction and that Lewis acid sites are more active than Brönsted acid ones. The same reactivity order was found for the reactions under microwave irradiation which led to an acceleration of the process as compared to conventional heating.

Author Contributions: A.M., J.H.-C. and F.J.U. conceived and designed the experiments; J.H.-C., A.P. and M.J.C.-R. performed the experiments; J.H.-C., A.P. and M.J.C.-R. analyzed the data; J.H.-C., A.M. and F.J.U. wrote the paper.

Funding: This research was funded by the Ramón Areces Foundation.

Acknowledgments: The scientific support from the Central Service for Research Support (SCAI) at the University of Cordoba is acknowledged.

Conflicts of Interest: The authors declare no conflict of interest.

References

1. Chheda, J.N.; Huber, G.W.; Dumesic, J.A. Liquid-phase catalytic processing of biomass-derived oxygenated hydrocarbons to fuels and chemicals. *Angew. Chem. Int. Ed.* **2007**, *46*, 7164–7183. [CrossRef] [PubMed]
2. Turhollow, A.; Perlack, R.; Eaton, L.; Langholtz, M.; Brandt, C.; Downing, M.; Wright, L.; Skog, K.; Hellwinckel, C.; Stokes, B.; et al. The updated billion-ton resource assessment. *Biomass Bioenergy* **2014**, *70*, 149–164. [CrossRef]
3. Bozell, J.J.; Petersen, G.R. Technology development for the production of biobased products from biorefinery carbohydrates-the US Department of Energy's "Top 10" revisited. *Green Chem.* **2010**, *12*, 539–554. [CrossRef]
4. Mamman, A.S.; Lee, J.-M.; Kim, Y.-C.; Hwang, I.T.; Park, N.-J.; Hwang, Y.K.; Chang, J.-S.; Hwang, J.-S. Furfural: Hemicellulose/xylosederived biochemical. *Biofuels Bioprod. Biorefin.* **2008**, *2*, 438–454. [CrossRef]
5. Chatterjee, C.; Pong, F.; Sen, A. Chemical conversion pathways for carbohydrates. *Green Chem.* **2015**, *17*, 40–71. [CrossRef]
6. Corma, A.; Iborra, S.; Velty, A. Chemical Routes for the Transformation of Biomass into Chemicals. *Chem. Rev.* **2007**, *107*, 2411–2502. [CrossRef] [PubMed]

7. Rothe, M.; Bauer, K.; Garbe, D. *Common Fragrance and Flavour Materials. Preparation, Properties and Uses*; VCH Verlagsgesellschaft mbH: Weinheim, Germany, 1985.
8. Liu, H.; Huang, Z.; Zhao, F.; Cui, F.; Li, X.; Xia, C.; Chen, J. Efficient hydrogenolysis of biomass-derived furfuryl alcohol to 1,2-and 1,5-pentanediols over a non-precious Cu-$Mg_3AlO_{4.5}$ bifunctional catalyst. *Catal. Sci. Technol.* **2016**, *6*, 668–671. [CrossRef]
9. Rao, R.; Dandekar, A.; Baker, R.T.K.; Vannice, M.A. Properties of Copper Chromite Catalysts in Hydrogenation Reactions. *J. Catal.* **1997**, *171*, 406–419. [CrossRef]
10. Sang, S.; Wang, Y.; Zhu, W.; Xiao, G. Selective hydrogenation of furfuryl alcohol to tetrahydrofurfuryl alcohol over Ni/γ-Al_2O_3 catalysts. *Res. Chem. Intermed.* **2017**, *43*, 1179–1195. [CrossRef]
11. Taylor, M.J.; Durndell, L.J.; Isaacs, M.A.; Parlett, C.M.A.; Wilson, K.; Lee, A.F.; Kyriakou, G. Highly selective hydrogenation of furfural over supported Pt nanoparticles under mild conditions. *Appl. Catal. B Environ.* **2016**, *180*, 580–585. [CrossRef]
12. Thompson, S.T.; Lamb, H.H. Palladium–Rhenium Catalysts for Selective Hydrogenation of Furfural: Evidence for an Optimum Surface Composition. *ACS Catal.* **2016**, *6*, 7438–7447. [CrossRef]
13. Meerwein, H.; Schmidt, R. Ein neues Verfahren zur Reduktion von Aldehyden und Ketonen. *Justus Liebigs Annalen der Chemie* **1925**, *444*, 221–238. [CrossRef]
14. Ooi, T.; Ichikawa, H.; Maruoka, K. Practical Approach to the Meerwein–Ponndorf–Verley Reduction of Carbonyl Substrates with New Aluminum Catalysts. *Angew. Chem.* **2001**, *113*, 3722–3724. [CrossRef]
15. Ivanov, V.; Bachelier, J.; Audry, F.; Lavalley, J.C. Study of the Meerwein-Pondorff-Verley Reaction Between Ethanol and Acetone on Various Metal-Oxides. *J. Mol. Catal.* **1994**, *91*, 45–59. [CrossRef]
16. Montes, V.; Miñambres, J.F.; Khalilov, A.N.; Boutonnet, M.; Marinas, J.M.; Urbano, F.J.; Maharramov, A.M.; Marinas, A. Chemoselective hydrogenation of furfural to furfuryl alcohol on ZrO_2 systems synthesized through the microemulsion method. *Catal. Today* **2018**, *306*, 89–95. [CrossRef]
17. Axpuac, S.; Aramendía, M.A.; Hidalgo-Carrillo, J.; Marinas, A.; Marinas, J.M.; Montes-Jiménez, V.; Urbano, F.J.; Borau, V. Study of structure-performance relationships in Meerwein-Ponndorf-Verley reduction of crotonaldehyde on several magnesium and zirconium-based systems. *Catal. Today* **2012**, *187*, 183–190. [CrossRef]
18. Antunes, M.M.; Lima, S.; Neves, P.; Magalhães, A.L.; Fazio, E.; Neri, F.; Pereira, M.T.; Silva, A.F.; Silva, C.M.; Rocha, S.M.; et al. Integrated reduction and acid-catalysed conversion of furfural in alcohol medium using Zr,Al-containing ordered micro/mesoporous silicates. *Appl. Catal. B Environ* **2016**, *182*, 485–503. [CrossRef]
19. Iglesias, J.; Melero, J.A.; Morales, G.; Moreno, J.; Segura, Y.; Paniagua, M.; Cambra, A.; Hernandez, B. Zr-SBA-15 Lewis Acid Catalyst: Activity in Meerwein Ponndorf Verley Reduction. *Catalysts* **2015**, *5*, 1911–1927. [CrossRef]
20. Iglesias, J.; Melero, J.A.; Morales, G.; Paniagua, M.; Hernández, B. Dehydration of Xylose to Furfural in Alcohol Media in the Presence of Solid Acid Catalysts. *ChemCatChem* **2016**, *8*, 2089–2099. [CrossRef]
21. Kim, M.S.; Simanjuntak, F.S.H.; Lim, S.; Jae, J.; Ha, J.-M.; Lee, H. Synthesis of alumina–carbon composite material for the catalytic conversion of furfural to furfuryl alcohol. *J. Ind. Eng. Chem.* **2017**, *52*, 59–65. [CrossRef]
22. Lopez-Asensio, R.; Cecilia, J.A.; Jimenez-Gomez, C.P.; Garcia-Sancho, C.; Moreno-Tost, R.; Maireles-Torres, P. Selective production of furfuryl alcohol from furfural by catalytic transfer hydrogenation over commercial aluminas. *Appl. Catal. A Gen.* **2018**, *556*, 1–9. [CrossRef]
23. Stefanic, G.; Music, S.; Popovic, S.; Sekulic, A. FT-IR and laser Raman spectroscopic investigation of the formation and stability of low temperature t-ZrO_2. *J. Mol. Struct.* **1997**, *408–409*, 391–394. [CrossRef]
24. Formosa, J.; Chimenos, J.M.; Lacasta, A.M.; Haurie, L. Thermal study of low-grade magnesium hydroxide used as fire retardant and in passive fire protection. *Thermochim. Acta* **2011**, *515*, 43–50. [CrossRef]
25. Lauron-Pernot, H.; Luck, F.; Popa, J.M. Methylbutynol: A new and simple diagnostic tool for acidic and basic sites of solids. *Appl. Catal.* **1991**, *78*, 213. [CrossRef]
26. Osman, A.I.; Abu-Dahrieh, J.K.; Rooney, D.W.; Halawy, S.A.; Mohamed, M.A.; Abdelkader, A. Effect of precursor on the performance of alumina for the dehydration of methanol to dimethyl ether. *Appl. Catal. B Environ.* **2012**, *127*, 307–315. [CrossRef]
27. Lu, J.; Kosuda, K.M.; Van Duyne, R.P.; Stair, P.C. Surface Acidity and Properties of TiO_2/SiO_2 Catalysts Prepared by Atomic Layer Deposition: UV-visible Diffuse Reflectance, DRIFTS, and Visible Raman Spectroscopy Studies. *J. Phys. Chem. C* **2009**, *113*, 12412–12418. [CrossRef]

28. Emeis, C.A. Determination of Integrated Molar Extinction Coefficients for Infrared Absorption Bands of Pyridine Adsorbed on solid Acid Catalysts. *J. Catal.* **1993**, *141*, 347–354. [CrossRef]
29. Komanoya, T.; Nakajima, K.; Kitano, M.; Hara, M. Synergistic Catalysis by Lewis Acid and Base Sites on ZrO_2 for Meerwein-Ponndorf-Verley Reduction. *J. Phys. Chem. C* **2015**, *119*, 26540–26546. [CrossRef]
30. Guo, Z.-K.; Hong, Y.-C.; Xu, B.-Q. Transfer hydrogenation of cinnamaldehyde with 2-propanol on Al_2O_3 and SiO_2-Al_2O_3 catalysts: Role of Lewis and Brönsted acidic sites. *Catal. Sci. Technol.* **2017**, *7*, 4511–4519. [CrossRef]
31. Miñambres, J.F.; Aramendía, M.A.; Marinas, A.; Marinas, J.M.; Urbano, F.J. Liquid and gas-phase Meerwein–Ponndorf–Verley reduction of crotonaldehyde on ZrO_2 catalysts modified with Al_2O_3, Ga_2O_3 and In_2O_3. *J. Mol. Catal. A Chem.* **2011**, *338*, 121–129. [CrossRef]
32. Debecker, D.P.; Mutin, P.H. Non-hydrolytic sol-gel routes to heterogeneous catalysts. *Chem. Soc. Rev.* **2012**, *41*, 3624–3650. [CrossRef] [PubMed]
33. Minambres, J.F.; Marinas, A.; Marinas, J.M.; Urbano, F.J. Activity and deactivation of catalysts based on zirconium oxide modified with metal chlorides in the MPV reduction of crotonaldehyde. *Appl. Catal. B Environ.* **2013**, *140*, 386–395. [CrossRef]
34. Minambres, J.F.; Marinas, A.; Marinas, J.M.; Urbano, F.J. Chemoselective crotonaldehyde hydrogen transfer reduction over pure and supported metal nitrates. *J. Catal.* **2012**, *295*, 242–253. [CrossRef]
35. Aramendia, M.A.; Borau, V.; Jimenez, C.; Marinas, J.M.; Ruiz, J.R.; Urbano, F.J. Influence of the preparation method on the structural and surface properties of various magnesium oxides and their catalytic activity in the Meerwein-Ponndorf-Verley reaction. *Appl. Catal. A Gen.* **2003**, *244*, 207–215. [CrossRef]
36. Aramendia, M.A.; Borau, V.; Garcia, I.M.; Jimenez, C.; Marinas, A.; Marinas, J.M.; Porras, A.; Urbano, F.J. Comparison of Different Organic Test Reaction over Acid-Base Catalysts. *Appl. Catal. A Gen.* **1999**, *184*, 115–125. [CrossRef]

© 2018 by the authors. Licensee MDPI, Basel, Switzerland. This article is an open access article distributed under the terms and conditions of the Creative Commons Attribution (CC BY) license (http://creativecommons.org/licenses/by/4.0/).